TopFuel

REACTOR FUEL PERFORMANCE 2012

Transactions

Manchester, United Kingdom
2 - 6 September 2012

TopFuel 2012 Gold Sponsor

Westinghouse

EUROPEAN NUCLEAR SOCIETY

ENS CONFERENCE

organised in cooperation with:

AMERICAN NUCLEAR SOCIETY

ATOMIC ENERGY SOCIETY OF JAPAN

CNS

IAEA
International Atomic Energy Agency

AEN NEA

European Nuclear Society
Rue Belliard 65
1040 Brussels, Belgium
Phone + 32 2 505 30 54
Fax +32 2 502 39 02
E-mail ens@euronuclear.org
Internet www.euronuclear.org

ISBN 978-92-95064-16-4

These transactions contain all contributions submitted by 7 September 2012.

Operation and Experience

CHANGES OF PLUTONIUM DISTRIBUTION AND FISSION GAS RELEASE IN IRRADIATED MOX FUEL	Nakae, N. (1); Baba, T. (1); Kamimura, K. (1); Verwerft, M. (2); Jutier, F. (2); Iwafuchi, J. (3); Kobayashi, Y. (3); Shikakura, S. (3) 1 - Japan Nuclear Energy safety Organization, Japan 2 - Studiecentrum voor Kernenergie / Centre d'Etude de l'Energie Nucléaire, Belgium 3 - PESCO Co., Ltd., Japan
POST SEISMIC EVALUATION FOR WESTINGHOUSE DESIGN FUEL IN US	Jiang, J. X. (1); Bradfute, J. L. (1); Karoutas, Z. E. (1) 1 - Westinghouse Electric Company, United States
FISSION GAS RELEASE OF MOX IRRADIATED TO HIGH BURNUP	Nakae, N. (1); Miura, H. (1); Akiyama, H. (1); Baba, T. (1); Kamimura, K. (1); Kurematsu, S. (2); Kosaka, Y. (2); Yoshino, A. (3); Kitagawa, T. (3) 1 - Japan Nuclear Energy Safety Organization, Japan 2 - Nuclear Development Corporation, Japan 3 - Mitsubishi Nuvlear Fuel Co., Ltd., Japan
ANALYSIS OF FISSION GAS IN ADVANCED GAS COOLED REACTOR FUEL	Barker, M. (1); Adam, M. (1); Foster, A. (1); Gonzales, M. (1); Graves, N. (1); Morgan, S. (1); Robinson, I. (1); Rutherford, N. (1); Ball, J. (2); Levy, M. (2) 1 - The UK's National Nuclear Laboratory Ltd, United Kingdom 2 - EDF Energy Nuclear Generation Ltd, United Kingdom
STUDY OF FISSION GAS BEHAVIOUR AND FUEL RESTRUCTURATION IN IRRADIATED (U,GD)O2 FUEL	Delorme, R. (1); Valot, C. (1); Carlot, G. (1); Sabathier, C. (1); Martin, P. (1); Fayette, L. (1); Pujol, X. (1); Pasquet, B. (1); Bienvenu, P. (1); Roure, I. (1); Lamontagne, J. (1); Blay, T. (1); Trillon, G. (2); Auret, V. (3); Bouffard, S. (4) 1 - CEA, DEN, Département d'Etudes des Combustibles, France 2 - AREVA/NP SAS, France 3 - EDF-DIN/SEPTEN, France 4 - CIMAP, CEA-CNRS-ENSICAEN-UCBN, France
AREVA PRODUCT EXPERIENCE IN SUPPORT OF EPR FUEL DESIGN	Teboul, N. (1); Gentet, G. (1); Hintergraeber, C. (2); Wiltz, C. (3) 1 - AREVA, AREVA NP SAS, France 2 - AREVA, AREVA NP GmbH, Germany 3 - AREVA, AREVA NP , United States
ATOMIC DIFFUSIVITY MEASUREMENT OF XENON GAS IN VARIOUS TYPES OF FUELS WITH LOW BURNUP BY POST-IRRADIATION ANNEALING TEST	Kim, H. (1); Park, K. (2); Kim, K.-S. (1); Na, S.-H. (1); Kang, K.-H. (1); Kim, D.-J. (1); Lee, J.-W. (1); Ahn, S.-B. (1) 1 - Korea Atomic Energy Research Institute, Daejeon, Korea, Republic of 2 - Dept. of Nuclear Eng., Kyunghee University, Kiheong, Yongin, Kyunggi, Korea, Republic of
POST-IRRADIATION EXAMINATION OF HIGH BURNUP FUEL RODS IN VANDELLOS II	Arana, I. (1); Muñoz-Reja, C. (1); Doncel, N. (1); Culebras, F. (2) 1 - ENUSA Industrias Avanzadas, S.A, Spain 2 - Asociación Nuclear Ascó-Vandellós II, Spain
SUCCESSFUL HIGH BURNUP IRRADIATION CAMPAIGN OF THE GE14 LUAS AT TVO'S OL1 REACTOR: INSPECTION RESULTS AND ASSESSMENTS	Dunavant, R. (1); Jahingir, M. (1); Schneider, R. (1); Doncell, N. (2); Muñoz-Reja, C. (2); Knuutila, A. (3); Ranta-Puska, K. (3) 1 - Global Nuclear Fuel-Americas, United States 2 - ENUSA Industrias Avanzadas, Spain 3 - Teollisuuden Voima Oyj, Finland
IN-CORE FUEL MANAGEMENT WITH MIXED FUEL ASSEMBLIES FOR BELGIAN NUCLEAR POWER PLANTS	Druenne, H. (1); Zhang, J. (1); Flachet, F. (2) 1 - Tractebel Engineering (GDF SUEZ), Belgium 2 - Electrabel (GDF SUEZ), Belgium
POST-IRRADIATION EXAMINATIONS ON AGR FUEL PINS IN STUDSVIK	Källström, R. (1); Karlsson, J. (1); Johansson, H. (1); Levy, M. (2); Minay, J. (2); Barker, M. (3); Gonzales, M. (3) 1 - Studsvik Nuclear AB, Sweden 2 - EDF Energy, United Kingdom 3 - National Nuclear Laboratory, United Kingdom

PERFORMANCE OF AN UPDATED CELL FRICTION METHODOLOGY	Cantonwine, P. (1); Karve, A. (1); Thomas, M. (1); Galloway, G. (1) 1 - Global Nuclear Fuels, United States
INVESTIGATION OF BWR FUEL FAILURES	Lutz, D. (1); Lin, Y.-P. (1); Schneider, R. (1); Yeager, H. (1); Kucuk, A. (2); Cheng, B. (2); Lemons, J. (3); Nesmith, K. (3) 1 - Global Nuclear Fuel - Americas, United States 2 - Electric Power Research Institute, United States 3 - Tennessee Valley Authority, United States
REVISED INDUSTRY GUIDANCE ON LIGHT WATER REACTOR FUEL SURVEILLANCE AND INSPECTION	Daum, R. (1); Mader, E. (1); Armstrong, E. (2); Smith, F. (3) 1 - Electric Power Research Institute, United States 2 - Finetech, Inc., United States 3 - Entergy Corporation, United States
FUEL INSPECTIONS AND THE ROOT CAUSES STUDY	Mala, M. (1); Mikus, J. (1); Miklos, M. (1) 1 - CV Rez Ltd, Czech Republic
NEW CORES ON BASE COATED PARTICLES FOR POWER WATER REACTORS (PWR-CP)	Grishanin, E. I. (1); Alekseev, P. N. (1); Semchenkov, Y. M. (1); Kucharkin, N. E. (1) 1 - National Research Center "Kurchatov Institute", Russian Federation
REDUCTION OF FUEL ASSEMBLY BOW WITH THE RFA FUEL	Aulló, M. (1); Aleshin, Y. (2); Messier, J. (3) 1 - ENUSA Industrias Avanzadas, S.A., Spain 2 - Westinghouse Electric Company, United States 3 - Electricité de France, France
WESTINGHOUSE FUEL DESIGNS AND PERFORMANCE OVERVIEW	Bradfute, J. (1); Chapin, D. (1); Reparaz, A. (1); Quecedo, M. (2); Munoz, C. (2) 1 - Westinghouse Electric Company, United States 2 - ENUSA, Spain

Operation and Experience

CHANGES OF PLUTONIUM DISTRIBUTION AND FISSION GAS RELEASE IN IRRADIATED MOX FUEL

N. NAKAE, T. BABA, K. KAMIMURA
Nuclear Energy System Safety Division, Japan Nuclear Energy Safety Organization
Toranomon Towers Office, 4-1-26, Toranomon, Minato-ku, Tokyo, 105-0001, Japan

F. JUTIER, M. VERWERFT
Studiecentrum voor Kernenergie / Centre d'Etude de l'Energie Nucleaire, Boeretang 200, B-2400 MOL, Belgium

J. IWAFUCHI, Y. KOBAYASHI, S. SHIKAKURA
PESCO Co., LTD.
2-5-12, Higashi-shimbashi, Minato-ku Tokyo, 105-0021, Japan

ABSTRACT

Japan Nuclear Energy Safety Organization (JNES) has conducted an irradiation experiment on MOX having high plutonium content of 14.3 wt% under the collaboration with Studiecentrum voor Kernenergie / Centre d'Etude de l'Energie Nucléaire (SCK/CEN) and post irradiation examination results have been obtained. Among them, changes in the plutonium distribution and the fission gas release behavior are presented in this paper. In order to examine the changes in the plutonium distribution and the fission gas release behavior, Electron Probe Micro-Analysis (EPMA), focusing on the elements U, Pu, O, Cs, Xe, and Nd, has been done at different radial positions of irradiated MOX fuel pellets. High plutonium enriched zones (Pu spot) in fresh MOX pellet tends to be surrounded by intermediate enriched zones. This means that fission is limited within Pu spots at the early stage of irradiation, and that fission expands to the surrounding area of the Pu spot. Fission gas atoms confined in Pu spot might have the possibility to release from the Pu spot to its surroundings due to the formation of paths for fission gas release. A certain relationship between the pellet microstructure changes and fission gas release can be speculated from the EPMA results obtained here.

1. Introduction

A lot of Uranium Plutonium Mixed Oxide (MOX) irradiation tests have been carried out in some countries. [1-10] Plutonium content of MOX in these irradiation tests is less than 7 %. However, plutonium content tends to be increased since plutonium isotopic composition becomes higher with the plutonium recovered from spent higher burnup UO_2 fuel in current LWR. [11] Thus, it is necessary to investigate the irradiation behavior of MOX having high plutonium content. Japan Nuclear Energy Safety Organization (JNES) has conducted irradiation experiment on MOX having high plutonium content of 14.3 wt% under the collaboration with the Studiecentrum voor Kernenergie / Centre d'Etude de l'Energie Nucléaire (SCK/CEN). One of the interesting characteristics of MOX is the plutonium distribution in the pellet which changes during irradiation due to the inter-diffusion of uranium and plutonium

depending on the temperature at each radial position, and certainly contributes to fission gas release. Fission gas release is one of the most important issues since released fission gases induce significant increase of the rod internal gas pressure and reduction of gap conductance. It certainly causes high stress on cladding and expansion of radial gap, then an increase of fuel temperature which also induce an additional fission gas release. This kind of irradiation behavior tends to lead to the loss of fuel integrity. Therefore, the changes of the plutonium distribution and the related fission gas release on irradiated MOX with high plutonium content are examined in this study.

2. Experiment

2.1 Fuel specification

MOX was fabricated by Belgonucleaire (BN) using Micronized Masterblend (MIMAS) method. The fabrication data are shown in Tab. 1. Pellet density is slightly lower than that of UO_2 currently used in LWR and plutonium content is high. Cold work stress relieved (CWSR) Zry-4 is used for the cladding tube.

	MOX (MIMAS-AUC) F6673 [*1]
Pellet	
Fabricator	BN
Fabrication method	MIMAS
Puf [*2] content (wt %)	10.1
Put [*2] content (wt %)	14.3
^{235}U enrichment (wt %)	0.404
Diameter (mm)	8.23
Density (%TD)	93.5
Cladding	
Material	Zry-4 CWSR
Outer/inner diameter (mm)	9.64/8.44
Fuel Rod	
Stack length (mm)	1000.75
Filled gas	He
Gas pressure (MPa)	2.1

*1: F6673 is fuel rod used in this paper.
*2: Puf and Put mean fissile plutonium and total plutonium, respectively.

Tab. 1 Fuel specification

2.2 Irradiation condition

Irradiation was carried out in Belgian Reactor 3 (BR-3) from July 1986 to July 1987 for one year and then in BR-2 CALLISTO Loop from April 1997 to August 2001 for about 4 years. A total of 10 irradiation cycles (about 20 days per cycle) were performed during BR-2 irradiation. The BR-2 burnup numbers correspond to the sum of BR-3 and BR-2 irradiation.

F6673	MLHR[*1] (kW/m)	PLHR[*2] (kW/m)	Ave. BU[*3] (GWd/t)	Peak BU (GWd/t)
BR-3 Irradiation	15 - 17	25 - 28	12.5	16.2
BR-2 Irradiation	17 - 20	28 - 33	24.3	35.3

*1: Mean Linear Heat Rate
*2: Peak Linear Heat Rate
*3: Averaged Burnup

Tab. 2 Irradiation conditions

3. Results and Discussion

3.1 Change of plutonium distribution

EPMA is first done on fresh MOX pellet in order to get reference data and on irradiated two samples which are taken from different axial positions of highest and medium linear power levels and these samples are called CT1 and CT2, respectively. The burnups of CT1 and CT2 are 35GWd/t and 25GWd/t, respectively. Plutonium and uranium X-ray mappings are shown in Fig. 1 (a) (Fresh MOX), (b) (Periphery of CT1) and (c) (Center of CT1). In fresh MOX, plutonium enriched zone (Pu spot, medium brown) and uranium enriched zone (U spot, violet) are clearly observed and the periphery of these zones is surrounded by particular enriched zones (yellow and blue). Other parts are covered with intermediate enriched zone (green). It might be pointed out that each zone is clearly divided. In periphery of CT1, Pu spot zone tends to be decreased in size and widely covered with intermediate enriched zone (green). U spot zone still remains and other parts are covered with low plutonium enriched zone (blue). It might be pointed out that inter-diffusion of plutonium and uranium certainly occurs. In center of CT1, the Pu and U spot zones tend to disappear due to active inter-diffusion. Microstructure of center of CT1 shows a well mixing feature.

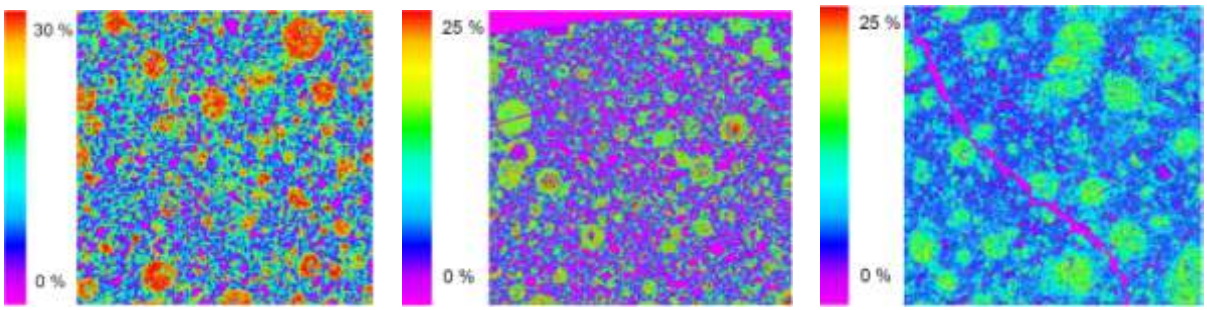

(a) Fresh MOX (b) Periphery of CT1 (c) Center of CT1

Fig. 1 Pu and U X-ray mapping (1x1 mm^2)

In order to evaluate X-ray mapping data quantitatively, the relative Pu content per class is calculated. The relative Pu content per class for CT1 and CT2 are presented in Figs. 2 and 3, respectively. Here the relative Pu content per class is defined as the fraction of plutonium which exists in a zone having a Pu/(U+Pu) value corresponding to an intensity *i*. The histogram is obtained by calculating the ratio of (c_i x f_i) to sum of (c_i x f_i), where c_i is the Pu/(U+Pu) value corresponding to the intensity *i* and f_i is the number of pixels with intensity *i*. As shown here typical plutonium distribution with fresh MIMAS-MOX is composed by two curves. These curves have an intermediate enrichment peak corresponding to region of well mixing of MOX primary blend agglomerates and UO_2 powder (green zone in Fig. 1 (a)) and a high enrichment peak corresponding to region of MOX primary blend agglomerates (medium brown zone in Fig. 1 (a)). The high enriched peak appears at Pu content, (Pu/(U+Pu)), of around 27 wt%, and the intermediate enriched peak at around 14 wt% which corresponds to the total plutonium content of fresh pellet.

The plutonium distribution after irradiation shows a different trend from that of fresh MOX. The two peaks which appeared in fresh MOX tend to be combined. The shape of three curves, which correspond to the periphery of CT1 and to the periphery and the center of CT2, is similar to each other. However, the peak positions exist at plutonium content of about 20 wt% for periphery and center of CT2, and at about 18 wt% for periphery of CT1. This behavior can be explained by inter- diffusion of plutonium and uranium depending on the local temperature. The plutonium content of the peak position becomes low due to the loss of plutonium by fission. Since both burnup and temperature of the center of CT1 are high, the corresponding shape of the curve displays a sharp peak for a plutonium content of about 10 wt%.

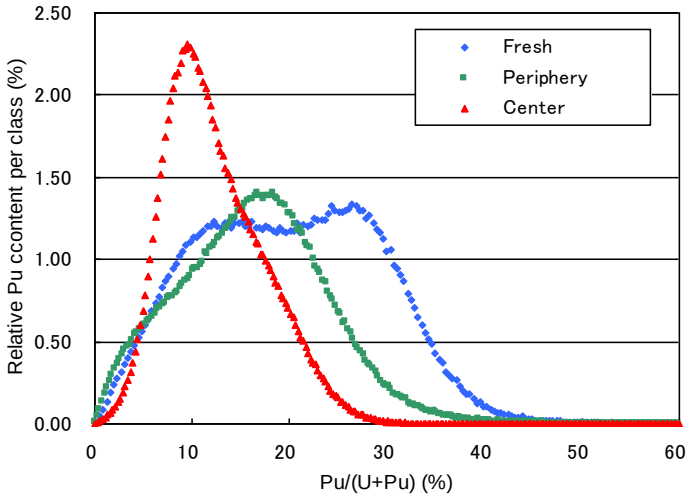

Fig. 2 Relative plutonium content per class for CT1

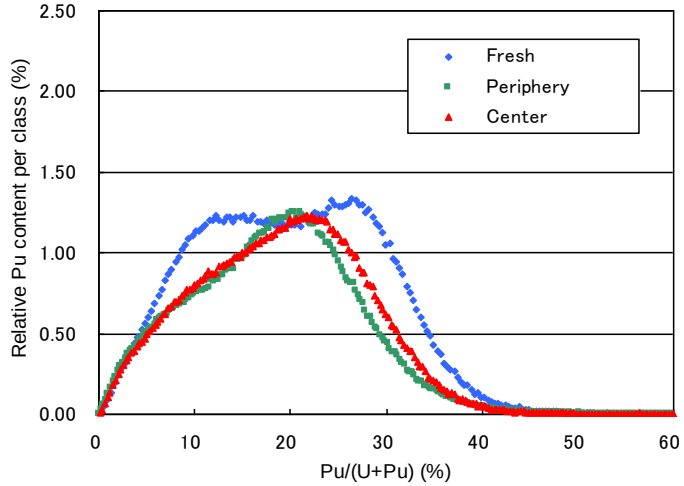

Fig. 3 Relative plutonium content per class for CT2

3.2 Fission gas release

Fission gas release rate of F6673, whose burnups are shown in Tab.2, was measured by a puncture test and gamma spectrometry of ^{85}Kr. The results are 11.1±0.8 % by puncture and 13.1±1.5 % by gamma spectrometry. Fission gas release behavior is examined using the result of radial distribution of Xe/Nd derived from EPMA radial scan as shown in Fig. 4. This figure shows that the onset of Xe release occurs at 0.7 of R/Ro for CT1 and at 0.3-0.4 of R/Ro for CT2. Since EPMA cannot detect Xe in bubble, Xe release behavior cannot be discussed accurately using this result. [12] It is, however, considered that a large amount of Xe is released from pellet and/or trapped in gas bubble in the center region of CT1, and that a small amount of Xe is released and/or trapped in the periphery of CT1.
Fission gas release mechanism has been proposed in the conference of FONTEVRAUD-7 in 2010 and ICAPP 2011. [3, 4] Fission gas atom is generated by fission and it migrates to grain boundary. Gas atom can move easily on grain boundary if there is no gas trapping site such as intergranular pore. Gas atom is usually trapped in intergranular pore and formed fission gas bubble on grain boundary. Fission gas release might occur if the pressure of gas bubble

exceeds the hydrostatic stress due to plenum gas pressure and/or pellet cladding mechanical interaction (PCMI). A large amount of Xe is generated in Pu spot zone and Xe atoms are trapped within intergranular pores and formed into gas bubble. Even if the pressure of the gas bubble becomes high, fission gas release might not be occurred until Pu spot zone disappears. It might be speculated that gas atom escaped from a gas bubble in the Pu spot zone can easily be trapped in an intergranular pore in an area surrounding a Pu spot where there are not a lot of fissions as plutonium content is relatively low.

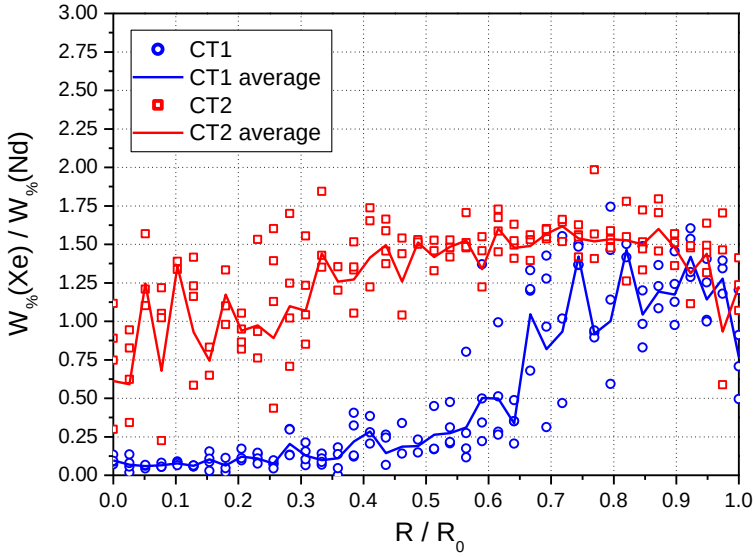

Fig. 4 Radial distribution of Xe/Nd derived from EPMA radial scan for CT1 and CT2

In order to examine the fission gas release from a Pu spot zone, the concentrations of Xe, Cs and Pu obtained by EPMA are shown in Fig. 5.

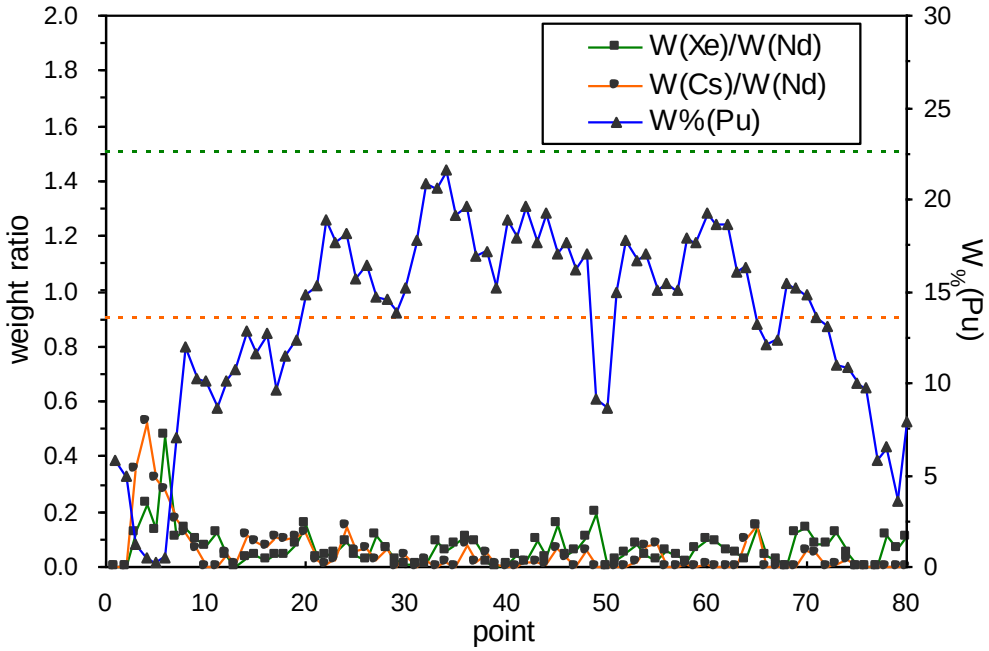

(a) Center of CT1

Fig. 5 Xe/Nd and Cs/Nd ratios and Pu concentration of CT1

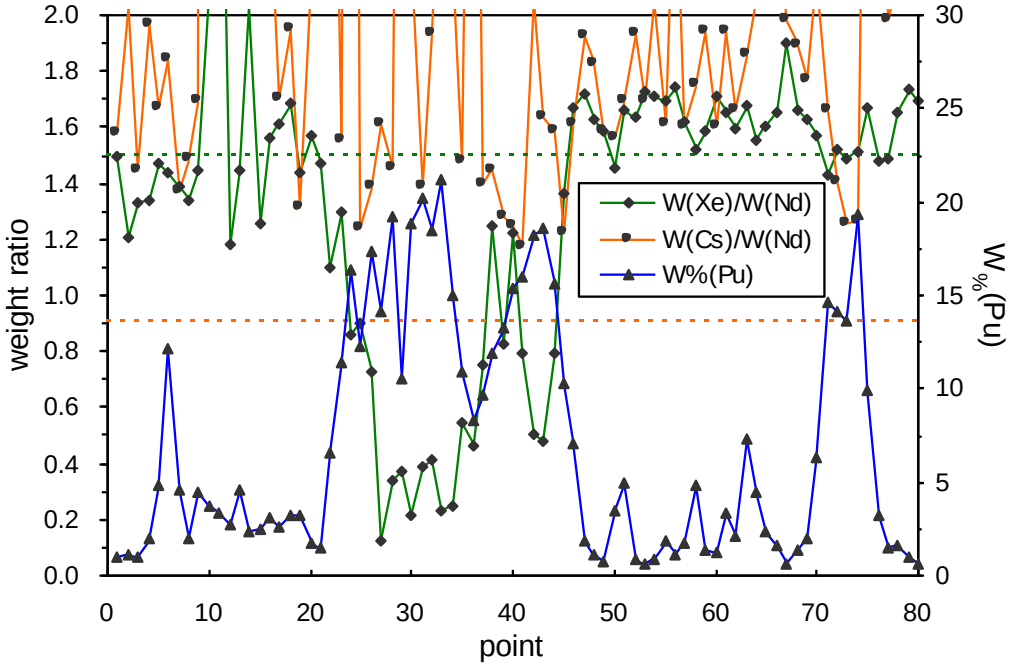

(b) Periphery of CT1

Fig. 5 Xe/Nd and Cs/Nd ratios and Pu concentration of CT1

The weight percentages of Xe, Cs, Nd and Pu are measured by EPMA. The dotted lines of green and medium brown shown in Fig. 5 represent and/or correspond to the amount of Xe and Cs generated by fission. Abscissa axis represents the position where EPMA is carried out and one point corresponds to 1μm. Left hand side vertical axis represents the weight ratios of Xe/Nd and Cs/Nd. Right hand side vertical axis represents weight percentage of plutonium. Connection of closed squares (Fig. 5 (a)) and closed diamonds (Fig. 5 (b)) with green line shows weight ratio of Xe/Nd and connection of closed circles with medium brown line shows weight ratio of Cs/Nd, respectively. Connection of closed triangles with blue line shows weight percentage of Pu.
The Pu spot zone is covered with from the points 10 to 75 in the case of the center of CT1 (Fig. 5 (a)), and from 25 to 45 and 70 to75 in the case of the periphery of CT1 (Fig. 5 (b)). Almost all Xe and Cs are released in the Pu spot zone in the center of CT1. Very little amount of Xe still remains around the points 5, 48 and 78 for center of CT1 where the plutonium content is low. This means that Xe generated in the Pu spot zone can be released to neighboring regions. It is observed in Fig. 5 (b) that Cs accumulates at the periphery of the pellet, and that Xe is released in the Pu spot zone and remains in the non-Pu enriched spot zone. This shows that fission gas release behavior strongly depends on the change of plutonium distribution and the micro-structure of well mixed plutonium and uranium (see Fig. 1 (c)) enhances fission gas release due to the formation of fission gas release paths from intergranular bubbles to the pellet surface.

4. Conclusion

A MOX fuel rod having a high plutonium content of 14.3 wt% has been irradiated in BR-3 and BR-2 CALLISTO Loop. PIE has been done to investigate fission gas release behavior in connection with the microscopic Pu distribution. Fission gas atoms confined in Pu spot zone

are released from the pellet mid radius to the center where the mixing of uranium and plutonium becomes remarkable. It is concluded that fission gas release mechanism has a strong dependence on the microstructure change due to inter-diffusion of uranium and plutonium, and that fission gas release is corresponding with the plutonium homogenization at pellet center.

5. References

[1] N. NAKAE, et al., “Trend in Plutonium Content of MOX in Thermal Reactor Use and Irradiation Behavior of MOX with High Plutonium Content”, 2009 LWR Fuel Performance Meeting, TOP FUEL 2009, 7-9, September, 2009, Paris , France.

[2] N. NAKAE, et al., “Irradiation Behavior of MOX Fuel under High Burnup,” Proceedings of 2010 LWR Fuel Performance/TopFuel/WRFPM, Orlando, Florida, USA, September 26-29, 2010, Paper 007.

[3] N. NAKAE, et al., “STUDY ON IRRADIATION BEHAVIOR OF MOX FUEL USED IN LWR,” Proceedings of International Symposium FONTEVRAUD 7, Avignon, France, September 26-30, 2010, Paper A046-T09.

[4] N. NAKAE, et al., “KINETICS OF GASEOUS ATOMS IN URANIUM PLUTONIUM MIXED OXIDE,” Proceedings of ICAPP 2011, Nice, France, May 2-5, 2011, Paper 11442.

[5] R. J. WHITE, et al., “Measurement and analysis of fission gas release from BNFL’s SBR MOX fuel,” J. Nucl. Mater. **288**, 43-56 (2001).

[6] Y. GUERIN, et al., “Microstructure Evolution and In-reactor Behavior of MOX Fuel,” Proc. of the 2000 International Meeting on LWR Fuel Performance, Park City, USA (2000).

[7] S. A. HODGE, et al., “Irradiation Test of Mixed-Oxide Fuel Prepared with Weapons-derived plutonium,” Proc. of the 2004 International Meeting on LWR Fuel Performance, p. 285, Orlando, USA (2004).

[8] D. BOULANGER, et al., “High Burnup PWR and BWR MOX fuel performance: a review of BELGONUCLEAIRE Recent Experimental programs,” Proc. of the 2004 International Meeting on LWR Fuel Performance, p. 273, Orlando, USA (2004).

[9] F. LEMOINE, “Estimation of the grain boundary gas inventory in MIMAS/AUC MOX fuel and consistency with REP-Na test results,” Proc. of the 2005 International Meeting on LWR Fuel Performance, p. 623, Kyoto, Japan (2005).

[10] P. BLANPAIN, et al., “MOX Fuel performance and Development,” Top Fuel 2001, 4A-2, Stockholm, Sweden (2001).

[11] N. NAKAE, “Management of Plutonium Content based on Reactivity of Each Plutonium Isotope,” J. Nucl. Sci. and Tech., **43**, No. 4, p. 361-366 (2006).

[12] M. VERWERFT, "Multiple voltage electron probe microanalysis of fission gas bubbles in irradiated nuclear fuel", J. Nucl. Mater. **282**, 97-111 (2000).

[13] N. NAKAE, et al., “Fission Gas Release of MOX Irradiated to High Burnup,” TopFuel 2012 A0033 (2012).

POST SEISMIC EVALUATION FOR WESTINGHOUSE DESIGN FUEL IN US

J. X. JIANG, J. L. BRADFUTE and Z. E. KAROUTAS
Westinghouse Electric Company

ABSTRACT

Since the mega-earthquake and tsunami in Japan on March 11, 2011 led to the Fukushima Daiichi reactor accident, nuclear plant safety has been elevated on the world stage. Recently, plants in the Eastern United States have experienced unusual seismic activity. This has resulted in increased interest in the fuel performance during the earthquake. According to the seismic records, the recent U.S. earthquake exceeded some plants operating basis earthquake (OBE) and the design basis earthquake (DBE) limits.

Westinghouse assessed the possibility of fuel assembly (FA) damage based on the actual seismic conditions and determined what actions could be required to resume operation for the beyond design basis ground vibrations. Westinghouse also evaluated the post seismic event for the fuel assembly with or without consideration of a LOCA event.

For the potential new level of operating and design basis earthquakes, Westinghouse evaluated potential impacts if more severe seismic requirements were imposed, including some high seismic regions in United States.

1. Background

1.1 Fukushima Daiichi Nuclear Disaster

On March 11, 2011 a categorised 9.0 M_W earthquake occurred at the northeast coast of Japan. See Figure 1.

Figure 1. Fukushima Daiichi Earthquake

Figure 2. Aftermath of Fukushima Daiichi Nuclear plants

The subsequent destructive tsunami with waves of up to 14 meters (the reactor site were designed for 5.7 m) disabled emergency generators required to cool the reactors.

Over the following three weeks there was evidence of partial nuclear meltdowns. Suspected explosions may have damaged the primary containment vessel and spent fuel pools. See Figure 2.

Since the mega-earthquake and tsunami in Japan, Fukushima Daiichi reactor accident, nuclear plant safety has been elevated on the world stage.

1.2 Earthquake in Eastern U.S.
Recently, plants in eastern United States have experienced unusual seismic activity. On August 23, 2011, a magnitude-5.8 earthquake occurred in Eastern United States. See Figure 3.

The earthquake shut down two reactors. It was the first time that a nuclear reactor in United States was shut down by seismic vibrations. U.S. utilities initially requested Westinghouse support to determine what actions could be required to resume operation for higher-than-expected ground vibrations.

As part of our initial support, Westinghouse (**W**) collected responses from all its functional groups to check:

1. If any groups required to perform evaluations if earthquake was determined to have exceeded the OBE (Operation Basis Earthquake) event.
2. If any groups required to perform evaluations if the earthquake was determined to have exceeded the DBE (Design Basis Earthquake) event.

2. Current Seismic/LOCA Margin for US Plants
A total 41 US plants were reviewed. All the plants satisfied the design criteria of coolable geometry, control rod insertion and fuel rod fragmentation for the seismic/LOCA loads.

The general seismic loads used in the analyses include:

- Operating Basis Earthquake (OBE),
- Design Basis Earthquake (DBE),
- Double Design Earthquake (DDE),
- Safe Shutdown Earthquake (SSE),

For some plants which are close to coasts, severe seismic loads were considered, such as:

- Hosgri fault zone earthquake and
- Long term seismic, etc.

The general LOCA loads used in the analysis include Large Break and Leak Before Break (LBB). The auxiliary line breaks include:

- Accumulator line (ACC),
- Residual Heat Remove line (RHR),
- Pressuerizer line (PRZ), etc.

The major coolant line breaks include:

- Reactor Vessel Inlet Nozzle (RVIN),
- Reactor Vessel Outlet Nozzle (RVON).
- Reactor Coolant Pump Outlet (RCPON)

For some power plants, the analysis results indicated that a few deformed grids were predicted at periphery of reactor cores with severe seismic or LOCA or combination of both. See Figure 4.

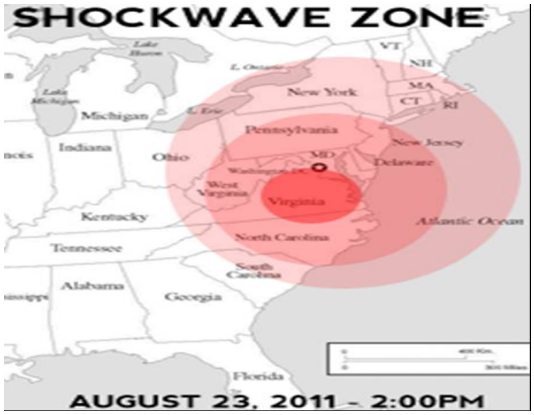

Figure 3. Earthquake in Eastern Coast, US

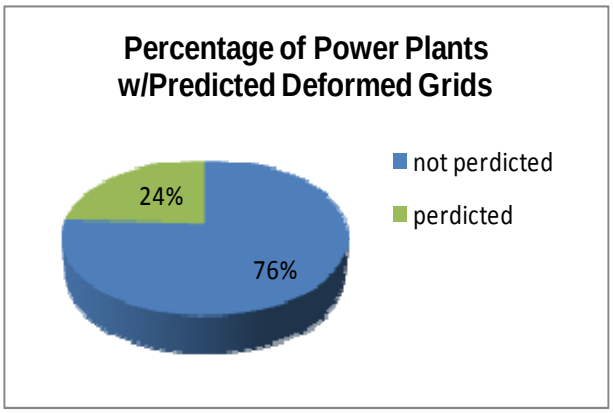

Figure 4. Plants w/Predicted Deformed Grids

The nuclear plants with predicted deformed grids could occur in different types of reactors (2, 3 or 4 loop plants). Predicted deformed grids could be different types of fuel assemblies. The distributions of deformed grids for different types of Fuel Assembly (FA) and reactor power plants are given in Table 1.

Table 1. Distributions of Deformed Grids for Different Types of Fuel Designs and Power Plants

Reactor type	2 loop		3 loop		4 loop	
fuel type	14x14	16x16	15x15	17x17	15x15	17x17
# of plants	2		6		2	
# plants/fuel type	2	0	2	4	0	2

Predicted deformed grids may be induced by severe seismic or LOCA or combined both. Only extremely long term seismic resulted in deformed grids for the 4-loop plants. The distribution of deformed grids for different seismic and LOCA loads and fuel assembly types are given in Table 2.

Table 2. Distributions of Deformed Grids for Seismic or LOCA and Different Types of Fuels

Load type	seismic			LOCA		
Fuel type	14x14	15x15	17x17	14x14	15x15	17x17
# of plants	0	0	2	2	2	4

3. Westinghouse Seismic/LOCA Methodology Overview

The general analytical procedure used for evaluating Seismic/LOCA (Loss of Coolant Accident) loads, fuel deflections, grid impact forces and induced stresses is shown in Figure 5.

The FA design criteria are established based on NRC SRP (Standard Review Plan 4.2) requirements:

- Fuel rod should be no fragmentation
- Meet Control rod insertability
- Meet Coolable geometry

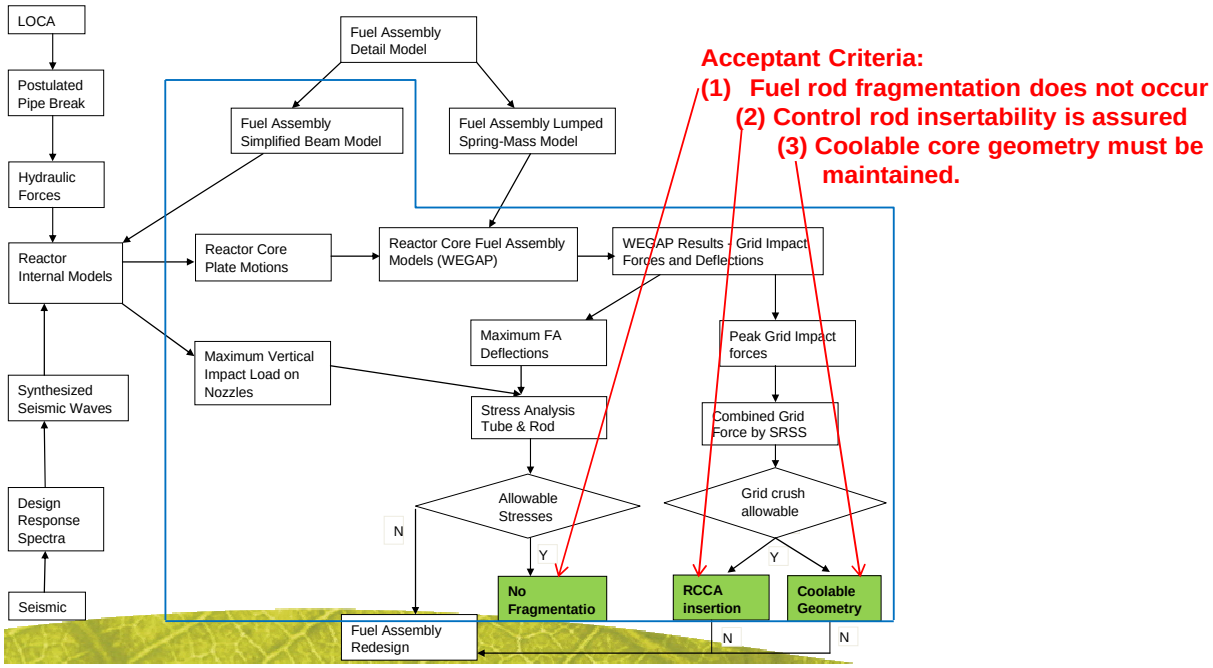

Figure 5. Seismic/LOCA Analysis Procedure Flow Chart

Seismic and LOCA analyses use direct integration method. The input loads are time history of core plate and barrel motions. A typical core plate and barrel motions are given in Figure 6.

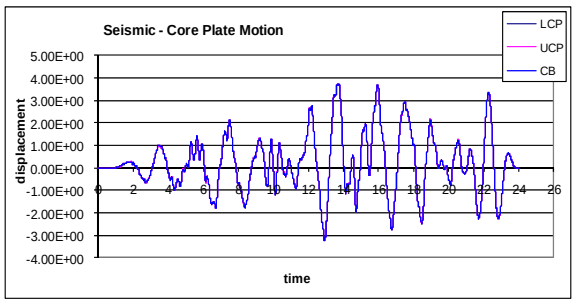

Figure 6. A typical Seismic Core Plate Motions

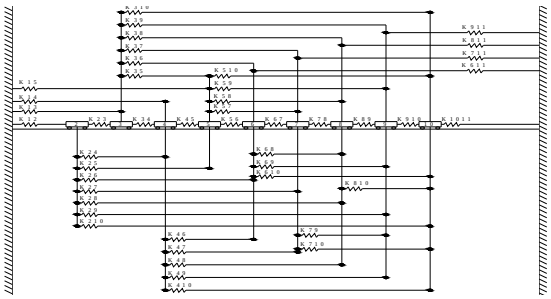

Figure 7. Simplified FA Lumped Mass-Spring Model

FA and reactor core modeling starts with the FA detailed model which was built based on the geometries of FA components and material properties, etc. The detailed model gives the FA dynamic characteristics of frequencies and mode shapes which will be benchmarked by the mechanical tests. The detailed model consists of a large number of dynamic degrees-of-freedom and requires large data capacities for performing a complex analysis. To effectively analyze the FA responses under a transient condition, the FA model is further simplified using discrete masses and linear spring-viscous damper elements. The mechanical constants of simplified FA model, including spring stiffness and damping coefficient, were determined based on the mass distributions, natural frequencies, mode shapes, and tested damping. A typical simplified lumped mass-spring model is given in Figure 7.

The dynamic features of simplified lumped mass-spring models were checked and compared with the detail model. Typical mode shape comparisons of simplified and detailed model are given in Figure 8.

Combined with the reactor fuel gaps and the grid dynamic impact characteristics, the simplified lumped mass-spring models were used to generate the reactor internal models with full core of fuel assemblies. The full core FA models include:

- Homogenous core
- Mixed transient cores

Typical full core FA model is in Figure 9.

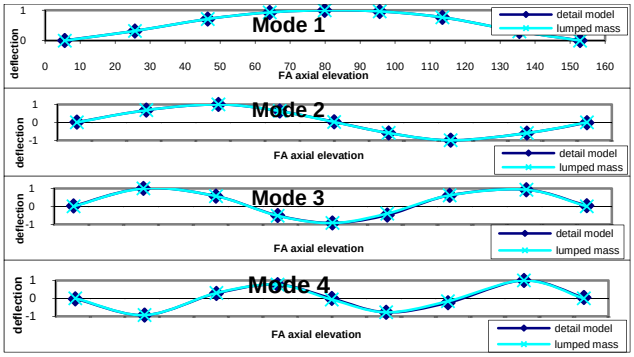

Figure 8. Mode shape comparisons

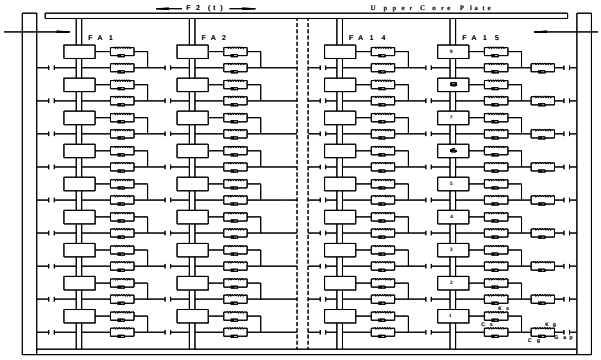

Figure 9. Full Core FA Model

The grid impact forces resulting from seismic and LOCA are combined using SRSS (Square Root of Sum of Square) method. The deformed grid crush strength is established based on the 95% confidence level on the true mean of the test data at operating temperature.

4. 8/23/2011 Post Seismic Activities

Initial **W** actions are issued Engineering Impact Evaluation Sheets and filed NF 9.5 by procedures. To support the customer's Root Cause Analysis, **W** performed the seismic analyses to check how the FA responded in the first second. 15 FA row lateral deflection responses in the first second are given in Figure 10.

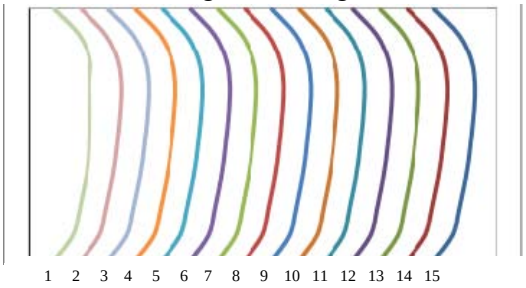

Figure 10. Typical 15 FA Row Lateral Deflections in First Second

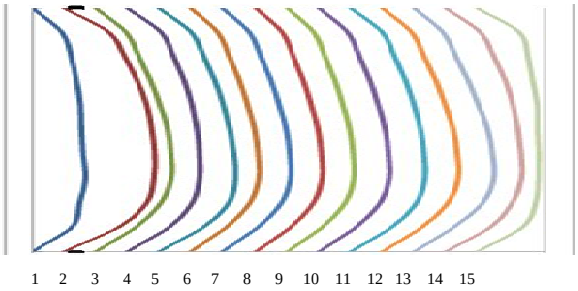

Figure 11. Typical Lateral Deflections of Periphery Fuel Impacted Baffle

Continued evaluations for the FA assumed that LOCA occurred with 8/23 earthquake. **W** performed post 8/23 seismic analysis as the DBE condition and combined with plant specific worst LOCA analysis results to support the Utilities FSAR (fuel safety analysis report).

To support Utilities continued operation, the 8/23 core plate motions were considered as OBE load and new analyses were performed. The results show that the maximum grid impact force increased significantly in the North-South direction, but it is still well below the limits. Figure 11 show typical lateral deflections when periphery fuel impacted the baffle.

The particular transient cores of power plants with specified fuel loading maps were analyzed for future core reload conditions. Typical grid impact force history of FA next to baffle is given in Figure 12.

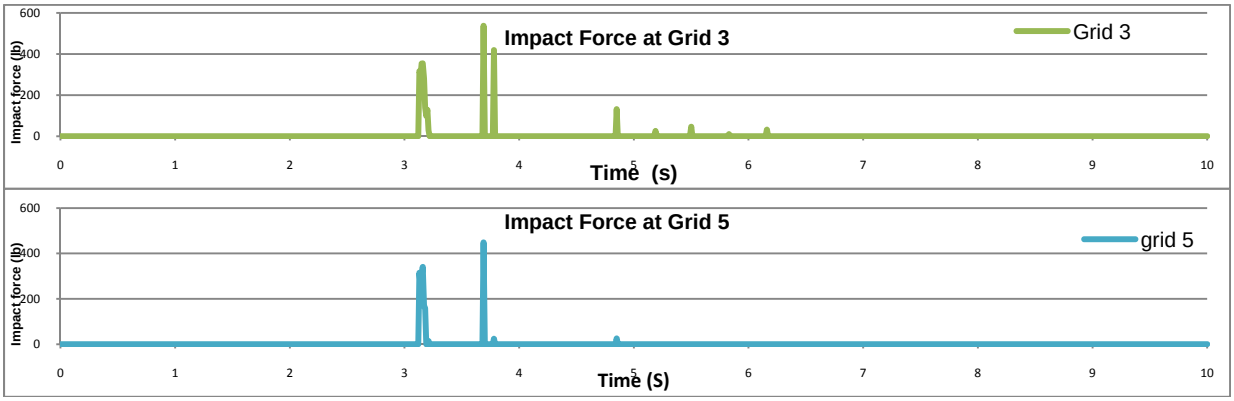

Figure 12. Typical grid impact force history of FA next to the baffle at grid 3 and grid 5 elevations

5. Potential Increased Seismic and LOCA Impacts

New earthquake computer model will help regulators assess U.S. reactor risks [1]. Research suggests the risks posed to the nation's nuclear reactors may have been underestimated and therefore could be worse than the power plants were designed to withstand [2] [3].

- For the potential new level seismic, OBE and DBE/SSE, new core plate motions are needed and new analyses should be performed.
- The new potential DBE/SSE results will be combined with the plant most limiting LOCA load using SRSS method
- Determine the incremental percentage of grid impact forces and determine how many deformed grids and where located (periphery or inboard of core, grid elevations, RCCA locations, etc.)
- If the deformed grids appear at the location which and not covered by the current coolable analysis methodology, a new coolable analysis methodology has to be created to satisfy the design criteria.
- Finally to review, update the FSARs and support the licensing of impacted plants.

6. Summary

After Fukushima Daiichi reactor accident, nuclear plant safety has been elevated on the world stage. Recently the 8/23/2011 earthquake which occurred in Eastern United States brings more attention especially that the earthquake exceeded some plant operating and design limits. The current Seismic and LOCA analyses margin were reviewed for US Plant. Some of the plants seismic/LOCA margins are tight. Evaluation of post seismic for FA with and without LOCA event showed that design criteria are satisfied. The new analysis was performed for post 8/23 seismic to support the continued operation of utilities. For potential increased seismic and future impacts, the actions and risks were evaluated.

Overall, reactor safety during normal operation and seismic/LOCA events are extremely important for the entire nuclear industry and mankind. **W** engineers will continue to comply to the our highest nuclear safety standards using approved methodologies and ensure **W** fuel designs meet current and future seismic standards and conditions.

7. References:

[1] Environment & Energy Publishing, Peter Behr and ClimateWire, January 31, 2012.
[2] **NEI SmartBrief** NRC, industry officials to discuss nuclear plant seismic risks. Feb. 2012.
[3] **NEI SmartBrief** Industry Plans Alternative Approach To Seismic Hazard Re-Evaluations, March 1, 2012

FISSION GAS RELEASE OF MOX IRRADIATED TO HIGH BURNUP

N. NAKAE, H. MIURA, H. AKIYAMA, T. BABA, K. KAMIMURA
Nuclear Energy System Safety Division, Japan Nuclear Energy Safety Organization
Toranomon Towers Office, 4-1-26, Toranomon, Minato-ku, Tokyo, 105-0001, Japan

S. KUREMATSU, Y. KOSAKA
Nuclear Fuel and Core Research & Development Department, Nuclear Development Corporation
622-12, Funaishikawa, Tokai-mura, Ibaraki, 319-1111, Japan

A. YOSHINO, T. KITAGAWA
Fuel Design Department, Mitsubishi Nuclear Fuel Co., LTD.
12-1, Yurakucho 1-Chome, Chiyoda-ku, Tokyo, 100-0006, Japan

ABSTRACT

Japan Nuclear Energy Safety Organization (JNES) has conducted high burnup MOX irradiation experiment which is called as Instrumented Fuel Assembly (IFA) 702.MOX fuels are fabricated by Short Binderless Route (SBR) and Micronized Master blend (MIMAS) methods. The specification of MOX fuel used in this study corresponds to that of 17x17 PWR type fuel. Irradiation was carried out in Halden Boiling Water Reactor (HBWR) in Norway. Fuel centerline temperature and plenum gas pressure were measured in situ during irradiation. The maximum pellet peak burnups achieved are 74.4 and 73.8GWd/t for SBR-MOX and MINAS-MOX, respectively. PIE was carried out in Kjellar of Institute for Energy Technology (IFE), Norway and in Cadarashe Center of Commissariat à l'énergie atomique (CEA), France. In order to examine fission gas release behavior Electron Probe Micro Analysis (EPMA) and Secondary Ion-microprobe Mass Spectrometry (SIMS) have been done at different radial positions of fuel pellet. Fission gas release rate (FGR) was measured by puncture test. The test result showed that FGR at end of IFA 702 irradiation were 15.0 (SBR)/16.5 (MIMAS) %, respectively. EPMA and SIMS results showed that fission gases tend to be released in the region from pellet center to mid radius where temperature is relatively high and to be still kept in the pellet outer region. The behavior and mechanism of FGR were examined and discussed in detail by use of the results of EPMA and SIMS in this paper.

1. Introduction

The plutonium utilization in thermal reactors (Light Water Reactors, LWR) is now actively promoted in some European countries. We call it as "pluthermal". A lot of Mixed Oxide (MOX) irradiation tests have been performed in some countries including Japan. [1-8] It is considered that one of the important issues in pluthermal is to clarify the irradiation behavior of MOX fuel. Japan Nuclear Energy Safety Organization (JNES) started to examine the irradiation behavior of such kinds of MOX fuels from 2007 for five years. The irradiation test results on the MOX of high plutonium content of 14.3 wt% have been published in the previous conference

(TOPFUEL 2009) [9] and will be presented in this conference (TopFuel 2012). [10] The irradiation test program of MOX fuel with high burnup has also been conducted by JNES and it is called as Instrumented Fuel Assembly (IFA) 702. IFA 702 irradiation rig consists of two MOX rods and one UO_2 rod. These fuel rods were selected and taken out from twelve fuel rods composed of IFA 626. IFA 626 was irradiated in IFA 609 at early stage of irradiation. Since trouble of instrumentation of IFA 609 occurred, the fuel rods were re-installed to IFA 626. The irradiation tests of IFA 609 and IFA 626 were carried out by Japanese Pressurized Water Reactor (PWR) group. [11] Three fuel rods of IFA 626 were transferred to JNES and irradiation extension and post irradiation examination (PIE) were carried out by JNES as IFA 702. The thermal and fission gas release (FGR) behaviors were examined by comparison between the in situ measurements and analytical code calculations. The results have already been presented in the previous conference (TopFuel 2010). [12]

2. Experiment

2.1 Fuel specification

Fuel specification of fuel rods used in IFA-702 is shown in Tab. 1. As shown in this table the specification is almost corresponded to that of the current 17x17 PWR fuel rod. Some of fuel pellets are taken out from upper part of the original fuel stack of IFA-626 when IFA-702 is re-fabricated and re-instrumented.

	SBR-MOX	MIMAS-MOX	UO_2
FUEL PELLET			
Fabricator	BNFL	CEA	IFE
Fabrication method	SBR*1	MIMAS*2	-
Puf *3 content (wt%)	6.12	6.12	-
Put *3 content (wt%)	8.4	8.4	-
^{235}U enrichment (wt%)	depleted	depleted	8.0
Diameter (mm)	8.19	8.05	8.19
Density (%TD)	95	95	95
CLADDING			
Material	Zry-4	Zry-4	Zry-4
Outer/inner diameter (mm)	9.50/8.36	9.50/8.22	9.50/8.36
FUEL ROD			
Stack length (mm)	244(300)*4	243(300)*4	245(300)*4
Filled gas	He	He	He
Gas pressure (bar)	5	5	5

*1: Short Binderless Route
*2: Micronized Master Blend
*3: Puf and Put mean fissile plutonium and total plutonium, respectively.
*4: The numbers blanketed represent the values of IFA-609/626. Some pellets are taken out.

Tab. 1 Fuel specification of IFA-702

2.2 Irradiation condition

Irradiation condition of IFA-609/626 (Base irradiation) and IFA-702 (Extension irradiation) is shown in Tab. 2. The mean linear heat rate (MLHR) represents the axially averaged LHR and

peak burnup represents the pellet peak burnup. The burnup at the beginning of IFA-702 is higher than that at the end of IFA-626 because some pellets are taken out.

		SBR-MOX	MIMAS-MOX	UO_2
BASE IRRADIATION (IFA-609/626)				
MLHR[*1] (kW/m)	BOL	25	25	25
MLHR (kW/m)	EOL	15	15	15
Averaged BU[*2] (GWd/t)		63.6(65.3)[*3]	63.3(65.0)[*3]	63.1(65.0)[*3]
Peak BU (GWd/t)		70.9	70.4	70.8
EXTENSION IRRADIATION (IFA-702)				
MLHR (kW/m)	BOL	26	23	22
MLHR (kW/m)	EOL	20	20	19
Averaged BU (GWd/t)		70.0[*4]	69.4[*4]	69.1[*4]
Peak BU (GWd/t)		74.4[*4]	73.8[*4]	73.5[*4]

*1: Mean Linear Heat Rate
*2: Burnup
*3: The numbers blanketed correspond to the burnups of beginning of IFA-702.
*4: The burnup numbers correspond to the sum of base and extension irradiations.

Tab. 2 Irradiation condition of IFA-626 and IFA-702

3. Results and Discussion

3.1 Fission gas release rate

Fission gas release rates are measured by puncture test after base (IFA-626) and extension (IFA-702) irradiations, respectively. The total fission gas release rate is also evaluated based on these data by taking into account of the change of fuel stack length in IFA-626 and IFA-702. The three fission gas release rates are shown in Tab. 3. The fission gas release rate of MIMAS-MOX is highest after base irradiation among the three rods even if the histories of linear heat rate (LHR) are almost same. The highest fission gas release rate during extension irradiation is obtained with SBR-MOX because the LHR of SBR-MOX is highest as shown in Fig. 1 which shows the time histories of in-situ measured internal gas pressure and mean (averaged) LHR. As shown in Fig. 1 fission gas release rate of UO_2 is higher than that of MIMAS-MOX although the LHR of MIMAS-MOX is higher than that of UO_2. The reason is not clear now. However, the thermal conductivity is evaluated in this experiment based on the in-situ measurement of pellet centerline temperature, and the result shows that thermal conductivity of UO_2 might be lower than that of MOX at high burnup more than 70 GWd/t. The total fission gas release rate of MIMAS-MOX is highest.

	SBR-MOX	MIMAS-MOX	UO_2
IFA-626 (base only)	3.6 %	9.2 %	3.2 %
IFA-702 (extension only)	11.6 %	7.9 %	10.6 %
IFA-626/702 (base and extension)	15.0 %	16.5 %	13.6 %

Tab. 3 Fission gas release rates after base and extension irradiation

Since UO_2 pellet used in this experiment was fabricated by dry mixing of two kinds of UO_2 powders having high enriched U-235 and low enriched U-235, UO_2 pellet contained U-235 high content zone (U-235 spot). The relative high FGR (13.6 %) obtained with UO_2 as compared with FGR of normal UO_2 having no U-235 spot might be due to the U-235 spot.

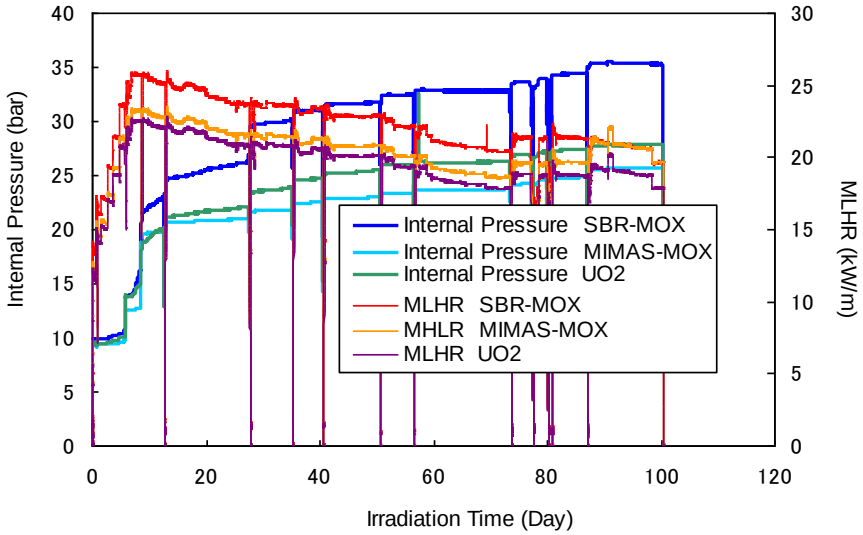

Fig. 1 Histories of in-situ measured internal gas pressure and MLHR

3.2 Xe distribution measured by EPMA and SIMS

SIMS (Secondary Ion-micro Mass Spectrometry) which sputters the pellet surface by oxygen ion beam can give two kinds of data which are “residual total Xe” and “retained Xe”, since SIMS can give several thousands of data showing information of from surface to inside (2 - 6μm in depth) of pellet. Here, “residual total Xe” represents total amount of Xe remaining in fuel pellet without release and these Xe exist mainly in form of fission gas bubble and/or in form of isolated single atom in intragranular matrix, and “retained Xe” represents the Xe existing in intragranular matrix. EPMA (Electron Probe Micro Analyzer), on the other hand, can give only the data limited on surface (about 1μm in depth) of pellet. Thus, EPMA data might correspond to the data of “retained Xe” by SIMS. It is well known that MIMAS-MOX has plutonium high content zone so called as “Pu spot or Pu agglomerate”. There are mainly three regions of Pu spot zone and non-Pu spot zone which is composed of intermediate zone (plutonium low content zone) and uranium high content zone. The fractions of each zone in MIMAS-MOX used in this irradiation test are estimated to be 10, 50 and 40%, respectively. The burnup fractions of each zone are estimated to be 20, 60 and 20% based on fraction of zone and corresponding fissile enrichments. SIMS analysis are carried out with both Pu spot and non-Pu spot.

Radial distribution of Xe concentration measured by using both EPMA and SIMS is shown in Figs. 2 and 3 with SBR-MOX and MIMAS-MOX, respectively. Vertical axis of Xe concentration shown in Figs. 2 and 3 is the weight fraction of measured element to related sample. Total amount of Xe generated by fission at each radial position can be computed by multiplying Nd concentration by ratio of Xe to Nd at the position where no Xe can be released. It corresponds to the red line in Fig. 2. Green line in Fig. 2 is obtained by averaging adjacent 5 data points of EPMA. “Matrix” in Fig. 3 corresponds to non-Pu spot. The difference between red symbol

(residual total Xe) and blue symbol (retained Xe) corresponds to Xe in form of bubble. Fission gas bubble can be observed at both intergranular and intragranular regions. It might be considered that fission gas atom escaping to grain boundary can be easily trapped in intergranular as-fabricated pore and it becomes intergranular bubble. Fission gas atom trapping in intragranular as-fabricated pore becomes intragranular bubble. When ion beam of SIMS comes across a fission gas bubble, a large amount of Xe confined in bubble can be detected and peak of Xe concentration is seen in SIMS observation.

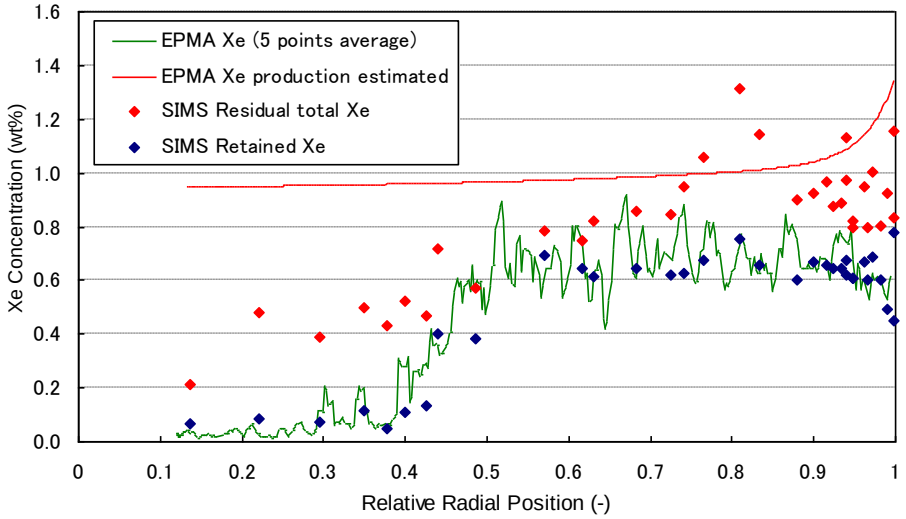

Fig. 2 Radial distribution of Xe concentration of SBR-MOX by EPMA and SIMS

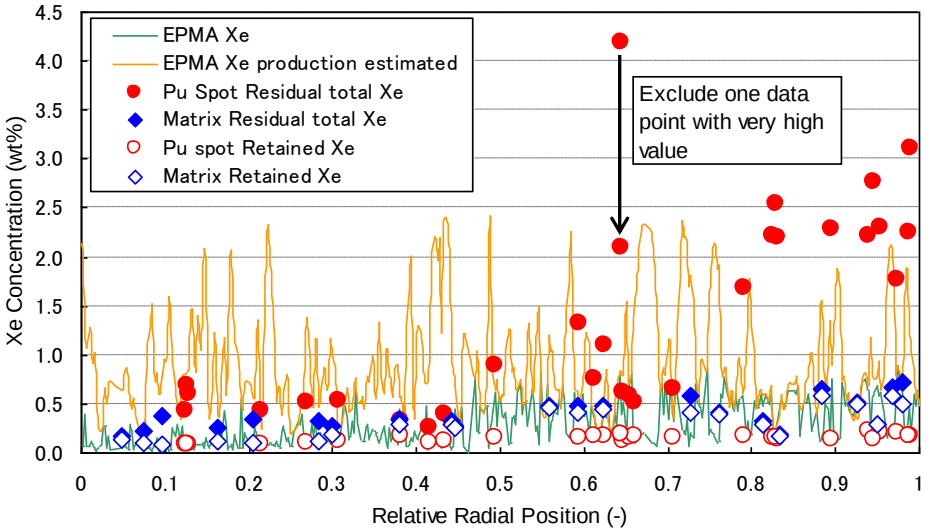

Fig. 3 Radial distribution of Xe concentration of MIMAS-MOX by EPMA and SIMS

In SBR-MOX, EPMA result shows that Xe concentration decreases in the radial region from 0.5R (representing middle of pellet radius, intermediate region) to pellet center, and that almost of all Xe releases in the region from 0.4R to center. SIMS result, on the other hand,

shows that residual total Xe concentration still remains in pellet outer region from 0.8R to surface, and that it gradually decreases in the region from 0.7R to center. Residual total Xe concentration in inner region is roughly 5times as compared with retained Xe concentration. Some amount of Xe is trapped in bubble in both inner and outer regions of pellet. The fission gas release rate is estimated to be 16.2% from Fig. 2 and the value roughly corresponds to that obtained by puncture test (15.0 %).
In MIMAS-MOX, SIMS result for matrix shows that Xe release behavior is relatively well corresponded to that obtained with SBR-MOX. SIMS result for Pu spot shows that residual total Xe concentration abruptly decreases from 0.6R to center, and that retained Xe concentration is very low from surface to center of pellet. This means that almost of all Xe is trapped in bubble from 0.6R to surface, and that small amount of Xe is trapped in bubble from 0.6R to center. The fission gas release rates are estimated to be 38 and 16% for Pu spot and non-Pu spot, respectively from Fig. 3. Since very few of Xe release is considered from uranium high content zone, total Xe release for MIMAS-MOX is estimated to be 17.2% by taking account of burnup fractions, which are 20 % in Pu spot zone and 60 % in intermediate zone indicated in page 4, (38x0.2+16x0.6=7.6+9.6=17.2 %) and the value roughly corresponds to that obtained by puncture test (16.5 %). About 40% (7.6/17.2=0.44) of Xe release occurs from Pu spot zone.

A fission gas release mechanism has been presented in the international conference of ICAPP 2011. [13] The fission gas release mechanism for relatively homogenized micro structure such as SBR-MOX and non-Pu spot zone is as follows. Fission gas atom is generated by fission and it migrates to grain boundary. Gas atom can move easily on grain boundary if there is no gas trapping site such as intergranular pore. Gas atom is usually trapped in intergranular pore and formed fission gas bubble on grain boundary. Fission gas release might occur if the pressure of gas bubble exceeds the hydrostatic stress due to plenum gas pressure and/or pellet cladding mechanical interaction (PCMI). The mechanism for not well homogenized micro structure such as Pu-spot zone, on the other hand, is as follows. A large amount of fission gas atoms is generated in Pu spot zone and fission gas atoms are trapped within intergranular pores and formed into gas bubble. Even if the pressure of the gas bubble becomes high, fission gas might not release until Pu spot zone disappears by inter-diffusion of plutonium and uranium at the surface of Pu-spot zone due to high temperature as indicated by another paper presented in TopFuel 2012. [10] It might be speculated that gas atom escaped from a gas bubble in the Pu spot zone can easily be trapped in an intergranular pore in non-Pu spot zone where there are not a lot of fissions as plutonium content is relatively low. The fission gas release behavior shown in Figs. 2 and 3 can support the fission gas release mechanism mentioned above.

4. Conclusion

MOX irradiation test has been carried out up to high burnup of more than 70 GWd/t as pellet peak using Halden reactor. A lot of important results concerning fission gas release in MOX are obtained. These results are summarized as follows;

- A large amount of fission gas release occurs for both MOX and UO_2 under high linear power irradiation at high burnup stage. The release rates are in the range from 13.6 to 16.5%.
- SIMS analysis can give us important information of fission gas release behavior. The data obtained by SIMA can distinguish the fission gases which exist in intragranular matrix and

bubble.

- The fission gas release rate estimated from SIMS result roughly corresponds to that obtained by puncture test. This shows that SIMS can detect almost of all fission gases retained in fuel pellet.
- Fission gas release behavior is much affected by MOX pellet microstructure on which MOX pellet fabrication method has much influence. A clear difference in fission gas release mechanism is observed with pellet having different micro structures of well and poor homogenized.
- The fraction of Xe release from Pu spot zone is reached to be about 40%. Thus the influence of Pu spot on FGR should be carefully considered in fuel design and safety evaluation.

5. References

[1] R. J. WHITE, et al., “Measurement and analysis of fission gas release from BNFL’s SBR MOX fuel,” J. Nucl. Mater. 288, 43-56 (2001).

[2] P. COOK, et al., “PIE OF BNFL’s FIRST COMMERCIALLY IRRADIATED SBR MOX FUEL,” IAEA Symposium ‘MOX Fuel Cycle Technologies for Medium and Long Term Deployment,’ p.233, IAEA, Vienna, Austria (1999).

[3] C. T. WALKER, et al., “MOX FUEL IRRADIATION BEHAVIOR: RESULTS FROM X=RAY MICROBEAM ANALYSIS,’ IAEA TCN ‘recycling of Plutonium and uranium in water reactor fuel,’ p. 301, Windermere, UK (1995). IAEA-TECDOC-941

[4] Y. GUERIN, et al., “Microstructure Evolution and In-reactor Behavior of MOX Fuel,” Proc. of the 2000 International Meeting on LWR Fuel Performance, Park City, USA (2000).

[5] S. A. HODGE, et al., “Irradiation Test of Mixed-Oxide Fuel Prepared with Weapons-derived plutonium,” Proc. of the 2004 International Meeting on LWR Fuel Performance, p. 285, Orlando, USA (2004).

[6] D. BOULANGER, et al., “High Burnup PWR and BWR MOX fuel performance: a review of BELGONUCLEAIRE Recent Experimental programs,” Proc. of the 2004 International Meeting on LWR Fuel Performance, p. 273, Orlando, USA (2004).

[7] F. LEMOINE, “Estimation of the grain boundary gas inventory in MIMAS/AUC MOX fuel and consistency with REP-Na test results,” Proc. of the 2005 International Meeting on LWR Fuel Performance, p. 623, Kyoto, Japan (2005).

[8] P. BLANPAIN, et al., “MOX Fuel performance and Development,” Top Fuel 2001, 4A-2, Stockholm, Sweden (2001).

[9] N. NAKAE, et al., “Trend in Plutonium Content of MOX in Thermal Reactor Use and Irradiation Behavior of MOX with High Plutonium Content”, 2009 LWR Fuel Performance Meeting, TOP FUEL 2009, 7-9, September, 2009, Paris , France.

[10] N. NAKAE, et al., “CHANGES OF PLUTONIUM DISTRIBUTION AND FISSION GAS RELEASE IN IRRADIATED MOX FUEL,” to be published in TopFuel 2012.

[11] H. FUJII, et al., “Final Assessment of MOX Fuel Performance Experiment with Japanese PWR Specification Fuel in HBWR,” Proceeding of the 2007 International LWR Fuel Performance Meeting, San Francisco, California, USA, September 30 – October 3, 2007 Paper 1043 (2007).

[12] N. NAKAE, et al., “Irradiation Behavior of MOX Fuel under High Burnup,” Proceedings of 2010 LWR Fuel Performance/TopFuel/WRFPM, Orlando, Florida, USA, September 26-29, 2010, Paper 007.

ANALYSIS OF FISSION GAS IN ADVANCED GAS COOLED REACTOR FUEL

M.A.BARKER, N.RUTHERFORD, M.S.ADAM, A.FOSTER, S.MORGAN, M.GONZALES, N.GRAVES, I.ROBINSON
National Nuclear Laboratory Ltd
Sellafield, Seascale, CA20 1PG – United Kingdom

J.BALL, M.LEVY
EDF Energy Nuclear Generation Ltd
Barnwood, Gloucester, GL4 3RS – United Kingdom

ABSTRACT

Results are presented from the analysis of fission gas sampled from Advanced Gas Cooled Reactor (AGR) fuel pins. The measurements cover the full range of burnups experienced in the current operation of these reactors, with fuel pin burnups ranging up to 40MWd/kgU. Trends in fission gas release (FGR) with burnup for AGR pins are presented and comparison made with FGR in light water reactors (LWR).
In addition to the fission gasses xenon and krypton, volatile elements such as caesium and iodine are sensitive to relocation in the fuel matrix at elevated temperatures and burnups. Axial gamma scan observations are used to reveal the occurrence of caesium release. Quantitative measurement of caesium relocation using axial gamma scans is presented and compared with FGR results. The relationship between caesium release and FGR is considered and demonstrated to have a strong trend with FGR.

1 Introduction

Advanced Gas-cooled Reactor (AGR) power stations are the UK's second generation gas-cooled commercial nuclear power plants, developed in the 1960s to 1980s. There are currently seven commercial AGR power stations operating in the UK. Typically, the fuel consists of 64 uranium-dioxide pellets with a central bore, encased in helium-filled stainless steel cladding to form a fuel pin. A fuel element is comprised of 36 such pins held together in a stainless steel support grid surrounded by a graphite sleeve which acts as a structural support and a moderator. The uranium is enriched in ^{235}U to levels of several percent, dependent on fuel design and target burn-up.
Eight fuel elements are stacked on top of each other to make a *stringer*. Stringers are loaded vertically into the core of the AGR. In the reactor, fuel reaches a clad temperature of around 750°C at the top of the core, whilst at the bottom of the core the coolant gas enters at a temperature of around 350°C.
Mean assembly discharge burnups have risen from the mid-1990's value of 27 MWd/kgU particularly with the recent introduction of a new robust fuel design with an increased pellet bore diameter, higher fuel enrichments and in some cases revised grid/brace designs.
Fission gas expertise at NNL includes the development of a mechanistic model of fission gas release (FGR) implemented in the ENIGMA fuel performance code, detailed analysis of bubble interlinkage in MOX and UO_2 fuels [2][3], and analysis of fission gas composition in MOX [5][6] and UO_2 fuels. The experimental fission gas programme is also supported by ceramography of fuel samples [1], in part to evaluate the porosity distribution.

2 Measuring fission gas at NNL

Analysis of the composition of AGR fission gas was performed on a recently commissioned magnetic sector mass spectrometer, with a custom designed batch inlet. Commissioning tests on the mass spectrometer were extensive, with the specific intention of assuring accurate isotopic determination across a wide range of He/Xe/Kr mixtures. Particular features of the instrument are:

- A specially designed inlet leak method, in order to control the pressure dependence of measurements.
- Three certified gas mixtures simultaneously connected to the batch inlet allowing frequent cross-comparison, providing quality assurance of measurements from Kr levels of a few parts per million up to tens of percent.
- Utility attachment port, allowing production of multiple aliquots of gas for testing purposes.
- Tungsten shielding to reduce operator dose.

The results of the commissioning indicate that the NNL mass spectrometer produces measurements of percentage Xe and Kr with an uncertainty of better than 3%. This uncertainty level covers a gas composition ranging from that expected for fuels with low levels of FGR (1000 ppm Kr, 0.5% Xe in He) to the compositions typical of samples from fuel that has experienced extremely high FGR (5% Kr , 50% Xe and above).

3 Analysis of fission gas release

3.1 Overview of FGR in AGR fuels

At low burnups, fission gas release in AGR fuel is dominated by athermal mechanisms, the rod average fission gas release fraction is low, at less than 1%, and is approximately proportional to burnup: this is similar to the behaviour of LWR fuel. As burnup increases, interlinkage occurs in the inner, hot regions of the fuel pellets where diffusion is fastest, and the release fraction rapidly increases above 1%. Where interlinkage has occurred, further more moderate increases in the release fraction continue as irradiation proceeds and more of the fuel volume undergoes interlinkage.

The amount of fission gas that diffuses to the grain boundaries is strongly dependent upon the fuel temperature and fuel grain size. AGR fuel is manufactured with a well controlled grain size, specifically to control FGR. Since the diffusion rate is exponentially dependent on temperature, it is temperature which is the dominating observable influence on measured data. As with LWR fuel, the rod average burnup at which 1% fission gas release occurs is strongly correlated with the fuel centreline temperature similar to the Halden or Vitanza threshold [8].

Although phenomenologically the same, there are two important differences between the factors affecting fission gas release in AGRs and LWRs:

(i) The cladding temperature of AGR fuel is, by design, greater than LWR fuel. Furthermore, as a result of the coolant chemistry, layers of carbonaceous deposit may build-up on AGR fuel pins. The resulting heat transfer impairment can enhance fission gas release.

(ii) The relatively low hydrostatic stress imposed upon AGR fuel pellets throughout life leads to low rates of morphological relaxation of grain face bubbles. In contrast, the hard pellet-clad contact which occurs in LWR fuel after approximately two years of irradiation gives high hydrostatic stresses and therefore high morphological relaxation of grain face bubbles [3].

Despite the above differences, a plot of AGR fission gas release as a function of burnup (Figure 1(a)) appears similar in shape to what is expected for LWR fuel, with a linear trend with burnup for FGR less than 1% (and burnups of up to ~30MWd/kgU), and more rapid increases above this level. Excursions to higher FGR at intermediate burnups, such as that seen for a sample of pins at ~20MWd/kgU, are generally due to unusually high carbonaceous deposit rates.

3.2 Analysis of isotopic composition

A range of stable isotopes of Kr and Xe are produced in fission of U-235 and Pu-239, with the relative yields depending on the parent nucleus as well as the neutron spectrum. As a result, the ratio Kr-86/Xe-134 is strongly dependent on the fissile isotope and neutron spectrum. Thermal fission of U-235 produces a ratio of ~0.25, thermal Pu-239 has a ratio of ~0.1 and fast U-238 has a value of ~0.17. Similarly, ratios of isotopes within a specific element provide an indication of whether the isotopic content is as expected. Figure 1(b) shows isotopic ratios for recent results from AGR stations. The figure shows both a Xe-isotopes ratio (black points) and a Kr-isotopes ratio (red points) as a function of the inter-elemental ratio Kr-86/Xe-134. For comparison, results from MOX fuel [5] are also shown, demonstrating the isotopic composition of gas which is released when a substantial fraction of products arise from thermal fission of Pu-239.

While the majority of AGR fission gas measurements lie on the expected trends for isotopic composition, the isotopic results are seen to lie in two main groups. Firstly, a group of pins with a Kr86/Xe134 ratio of below 0.200 and secondly the main group of results with values greater than 0.200. The group with lower Kr86/Xe134 values are from pins which, despite having a high burnup, show only moderate levels of low fission gas release. These pins with low Kr86/Xe134 are shown in red on figure 1(a). The remaining pins, with Kr86/Xe134 greater than 0.200, have either more moderate burnups (with a range of FGR) or have tended to show high fission gas release above ~30MWd/kgU; these pins with high Kr86/Xe134 are shown in green on figure 1(a).

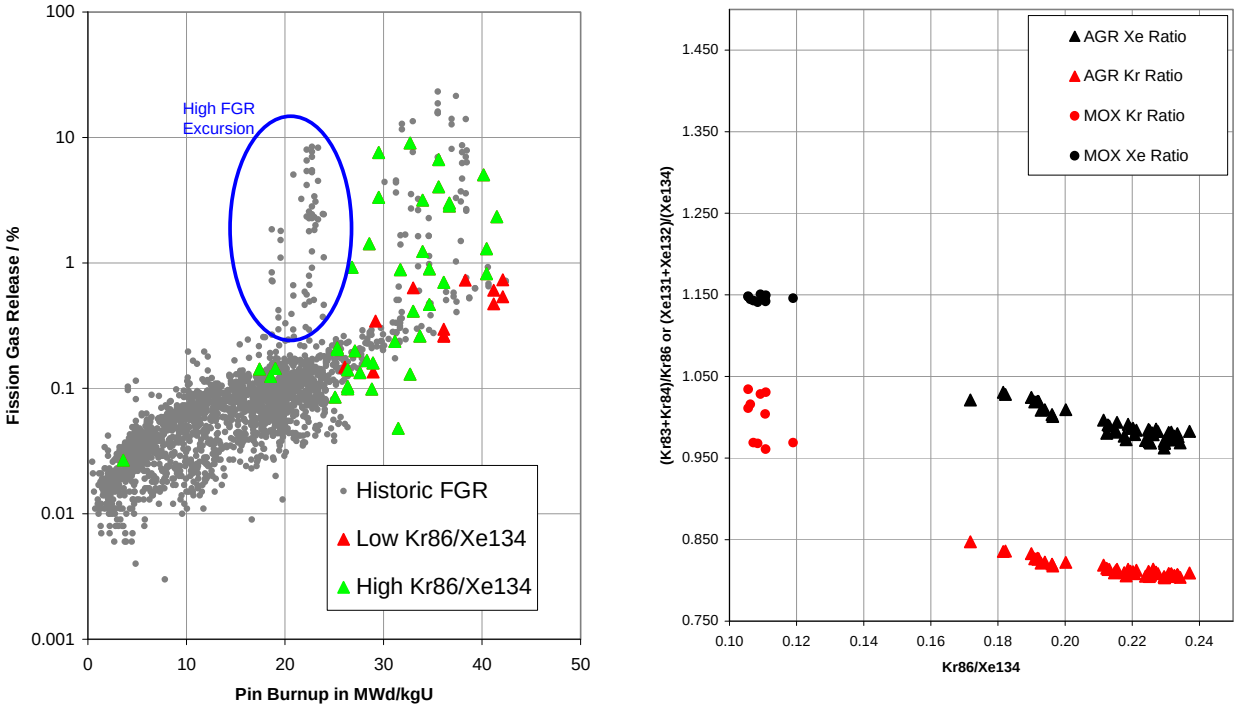

(a) (b)

Figure 1 (a) Measured fission gas release for historic data and recent measurements.(b) Isotopic Composition of AGR Fission Gas with MOX fuel as comparison.

4 Comparison of Xe and Kr release with volatile release

In addition to the fission gasses Xe and Kr, volatile elements such as Cs and I are sensitive to relocation in the fuel matrix at elevated temperatures and burnups. The vapour pressure of Cs is ~1 atmosphere at 690°C and the dissociation temperature of its oxides is less than ~700°C. Previous studies of LWR fuel, conducted by Walker [7] have found Cs to migrate through the fuel in a similar way to fission gas. The relatively high yield of Cs means that, with the occurrence of FGR, substantial partial pressures of Cs may develop, and these vapours may condense in cool regions of the fuel pin. Cs is transported by gas-phase diffusion to surfaces that are cold enough to reduce the Cs vapour pressure below the local partial pressure, leading to condensation and accumulation of Cs on colder surfaces in the pin.

Gamma scan observations reveal the occurrence of Cs deposition at the ends of the fuel stack and also at pellet-pellet interfaces. Figure 2(a) shows an example gamma scan, with an illustrative x-ray of a pin placed adjacent. Puncture measurements reveal the gamma-scanned pin to have experienced a relatively high FGR of greater than 10%. At both ends of the pin, enhancements to the gamma intensity from localised Cs deposition are seen. The detailed structure of the gamma scan profile in the bottom region of the pin shows a rise in Co-60 coincident with the end cap (labelled end cap) and a broader, lower rise coincident with a thickening of the clad wall (labelled collar). In this region the Cs-137 intensity profile displays a major reduction due to the absence of fuel at the alumina insulator end pellet, which thermally protects the pin end cap from the fuel stack. The insulator pellet is bounded by two local maxima in the Cs-137 gamma intensity, each of the maxima correspond to areas of Cs deposition. The local enhancements either side of the alumina insulator pellet result from the reduced temperature in this area combined with available free volume for deposition. Cs is also responsible for the major fraction of the gamma intensity along the alumina pellet, depending on the available free volume for deposition in this region, and some form of diffusion process appears to lead to a reduction in Cs intensity moving along the insulator pellet.

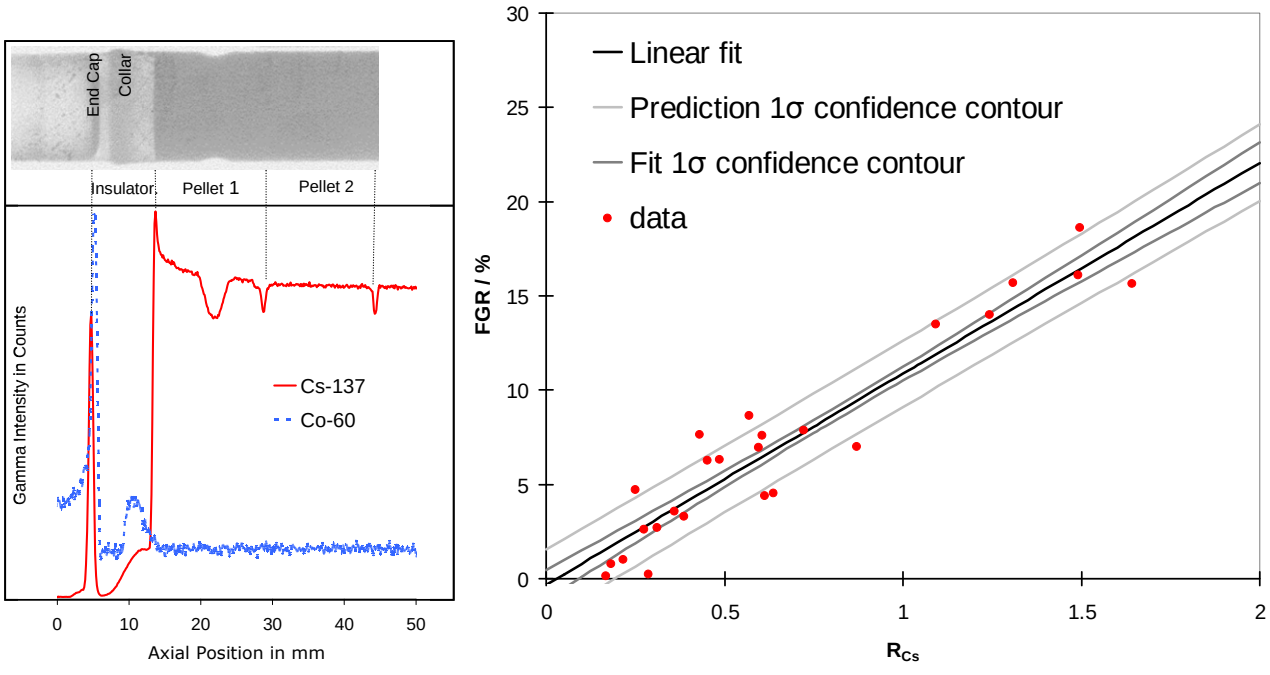

Figure 2: (a) Occurrence of Cs deposition regions at the bottom of an AGR fuel pin, either side of the insulator pellet. (b) Linear relationship between FGR and the relocation of Cs.

A total of 27 pins for which the FGR was measured by pin puncture were gamma scanned and the intensity of the end cap Cs measured. The intensity values are compared to fission gas release in Figure 2(b). A linear fit is applied to the data; the relationship between the calculated gamma scan based parameter and the pin puncture measurements of FGR is sufficient to permit prediction of puncture FGR using gamma scan profiles. As an example, the technique predicts FGR of 10 % with a 1σ confidence level of ±1.8 % absolute. This accuracy deteriorates rapidly for FGR of less than 5%, due to factors other than FGR and Cs deposition having a significant influence on the observed gamma intensity in the regions of Cs deposition.

5 Conclusions

The National Nuclear Laboratory continues to perform a successful range of studies on fission gas across a range of fuel types. Fission gas release in AGR fuel is expected to be dominated by the same mechanisms as for LWR fuel and this is manifested in the overall features of the presented measurements.

Isotopic analysis is a useful tool for examining fission gas and this continues to be an area of research at NNL, particularly as higher burnups are reached in AGR fuel. Current results demonstrate how the isotopic mixture of released gas changes with fuel burnup while also being closely linked to the degree of post-interlinkage release of gas from the central regions of the fuel.

The lack of a plenum in AGR fuel pins means that use of Kr-85 to determine fission gas release by gamma scanning is not possible. However, the end cap structure and end cap insulator pellet leads to a complex Cs-137 gamma-intensity profile at the end of the fuel stack. Cs levels in the end cap region have been shown to be proportional to FGR in the pin. Measurements of Cs in the end cap region, by gamma spectroscopy, are able to provide indicative measurements of FGR.

References

[1] S.Morgan, et al. *these proceedings*

[2] M.A.Barker & C.P.Chatwin, *Fuel Performance Activities at Sellafield Ltd and the UK's National Nuclear Laboratory,* in Water Reactor Fuel Performance Meeting 2008, October 2008, Seoul, Republic of Korea

[3] M.A.Barker, C.Chatwin & S.Owens, *Experimental and Computational Analysis of the Development of Intergranular Bubbles in Oxide Fuels,* in TopFuel 2009, Paris, France

[4] R.J.White, J.Nucl.Mater. **325** (2004) 61-77

[5] M.A.Barker et al., *The manufacture and performance of homogeneous microstructure MOX fuel*, in Proceedings of the ANS 2007 International Meeting on Fuel Performance, San-Francisco, USA

[6] M.A.Barker et al., *PIE of High Burnup SBR MOX Fuel* in TopFuel 2006, Salamanca, Spain

[7] C.T.Walker, C.Bagger & M.Mogensen, J.Nucl.Mater. **240** (1996), 32-42

[8] C.Vitanza, E.Kolstad & U.Graziani, *Fission gas release from UO_2 pellet fuel at high burn-up*, ANS meeting, Portland, USA, April 1979

STUDY OF FISSION GAS BEHAVIOUR AND FUEL RESTRUCTURATION IN IRRADIATED (U,Gd)O_2 FUEL

R. DELORME, Ch. VALOT, L. FAYETTE, X. PUJOL, I. AUBRUN, J. LAMONTAGNE, T. BLAY, B. PASQUET, P. BIENVENU, I. ROURE, C. POZO, G. CARLOT, C. SABATHIER, P. MARTIN
CEA, DEN, Département d'Etudes des Combustibles
F-13108 Saint Paul lez Durance, France

G. TRILLON
AREVA/NP SAS, 10 rue Juliette Recamier, 69456 Lyon cedex 06, France

V. AURET
EDF-DIN/SEPTEN, 12-14 avenue Dutriévoz, 69628 Villeurbanne cedex, France

S. BOUFFARD
CIMAP, CEA-CNRS-ENSICAEN-Université de Caen, 6 boulevard du Maréchal Juin, 14050 Caen cedex 4, France

ABSTRACT

Gadolinium is a burnable absorber which provides a negative moderator coefficient at the beginning of life of fuel assemblies and therefore helps shape core power distributions. ^{155}Gd and ^{157}Gd isotopes have high macroscopic neutron absorption cross sections. Solid solutions of the (U,Gd)O_2 type containing in our study 8 wt% of Gd_2O_3 can be easily formed by classical fuel fabrication route.
The understanding of fuel behaviour under irradiation is of major importance for nuclear reactor performances and safety in operation. For example, the release of fission gas from the pellet to the free volume of the rod increases the internal pressure.
The main objective of the present work is to study in-pile (U,Gd)O_2 fuel modifications and more specially to investigate possible gadolinium impact on fission gas behaviour. According to our knowledge, the fine characterization of irradiated (U,Gd)O_2 fuel and particularly the SEM[1]/EPMA[2]/SIMS[3] coupled quantitative analysis of xenon is first reported in this study.
The (U,Gd)O_2 fuel considered in this study had an initial enrichment in ^{235}U of 2.5 wt%. The characterized sample was taken from a fuel rod with M5® cladding irradiated 3 cycles in a French PWR (rod average burn-up : 39.2 GWd/t_U). Volumetric analysis gave a fraction of fission gas released out of the fuel of 0.51 %.The local burn-up calculated at the sampling position was 43.7 GWd/t_U.
Comparisons of EPMA Xe mapping between (U,Gd)O_2 matrix and remaining free UO_2 clusters located at same radial positions (i.e. close local burn-up) clearly indicate that gadolinium local content influences Xe precipitation and fuel restructuration.

1. Introduction

Due to high macroscopic neutron absorption cross sections of ^{155}Gd and ^{157}Gd isotopes the gadolinium burning step occurs first at the outer region of the pellet while the inner fuel is shielded from thermal neutrons. With the burn-up increase, the interface between burned and unburned gadolinium moves toward the pellet centre. This effect influences the power radial distribution and therefore the radial creation of fission products [1].
The introduction of trivalent Gd cation in substitution of U cation into the fluorite structure has been widely studied [2-3] and affects notably the oxygen vacancy content and U cations electronic configuration. To maintain lattice electrical neutrality a population of U^{5+} and U^{6+}

[1] Scanning Electron Microscopy
[2] Electron Probe Micro-Analysis
[3] Secondary Ion Mass Spectroscopy
M5® is a registered trademark of AREVA

ions can coexist with oxygen vacancies depending on oxygen potential of the sintering atmosphere [4]. Consequences of gadolinium introduction on fuel properties are numerous. For example in [1] it has been demonstrated that effective diffusion coefficient of fission gas is lowered by gadolinium addition. Furthermore, many authors [5-8] have pointed out a lower thermal conductivity for $(U,Gd)O_2$ than for UO_2.
For all the reasons forequoted the fission gas behaviour may be affected by the introduction of gadolinium into UO_2 fuel. The understanding of rare gas behaviour is of main importance for nuclear fuel performances and safety in operation and during incidental or accidental events. The objective of the present work is to study in-pile $(U,Gd)O_2$ fuel evolution and particularly fission gas behaviour and microstructural evolution.

2. Experimental

The $(U,Gd)O_2$ fuel considered in this study contained 8 wt% of Gd_2O_3 and had an initial enrichment in ^{235}U of 2.5 wt%. The residual presence of free UO_2 grains clusters is observed notably by EPMA and has been already mentioned in other studies [9](Fig 2.a) and [10].
The sample characterized in this work has been taken from the high power region of a fuel rod with M5® cladding irradiated 3 cycles in a French PWR (average rod burn-up 39.2 GWd/t_U). Volumetric analysis after rod puncturing gave a fraction of gas released out of the fuel equal to 0.51 % of the creation. The selected sample was embedded in a low melting point metallic alloy to ensure good electrical conductivity and polished on one side perpendicular to the rod axis. The local burn-up calculated at the sampling position is 43.7 GWd/t_U.
The same sample was examined by SEM, EPMA and SIMS; all devices are located in the LECA-STAR hot laboratory of CEA Cadarache (France). SEM observations were done using a shielded XL 30 model (PHILIPS) with Centaurus KE BSE detector. EPMA analyses were performed with a shielded SX-100R (CAMECA). Quantitative analyses and maps were done with an incident beam current of 200 nA at respectively 20 kV and 30 kV. SIMS measurements were performed with a shielded IMS 6f (CAMECA) with a 20 nA defocussed oxygen $^{16}O_2^+$ primary beam at +15 kV. Quantification of total xenon concentration was performed using methodology described in [11-14].

3. Results

3.1 Radial distribution of Xe

Fig 1. shows some typical SEM images of the sample at different radial locations. At pellet centre (Fig 1.a) and in the mid-radius region (Fig 1.b) no bubbles are clearly observed. At pellet periphery (Fig 1.c) a high density of bubbles is highlighted indicating the occurrence of extensive fission gas precipitation. This specific microstructure evolution at pellet periphery is one feature of a High Burn-Up Structure (HBS) which is usually observed in highly UO_2 PWR irradiated fuels (local burn-up above 60 GWd/t_U), for example in [15].

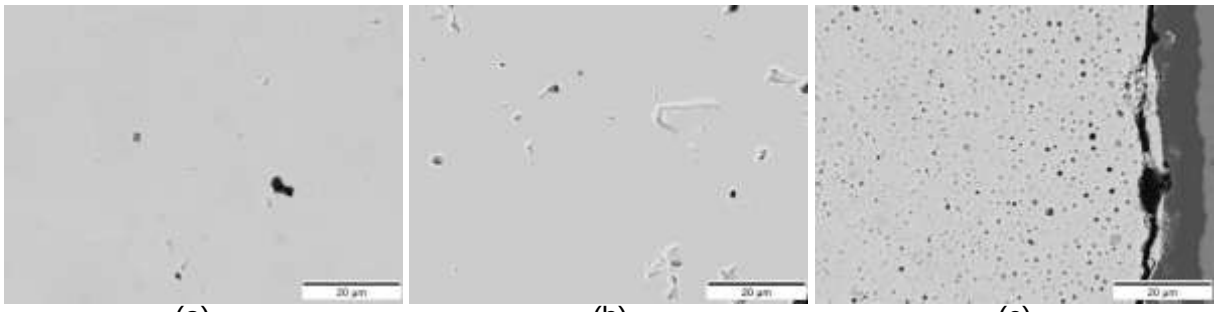

(a) (b) (c)

Fig 1. Backscattered electron images at different radial positions: r/R=0 (a), r/R=0.5 (b) and r/R=1 (c)

The absence of simultaneous local decrease of both EPMA signal and SIMS signals (Fig 2) indicates that thermally activated precipitation and/or release at pellet centre did not occur. Due to extensive gas precipitation, a sharp fall in Xe content measured by EPMA is observed

at pellet periphery (starting between 120 and 180 µm from the pellet edge). This local decrease in Xe content arises mainly from surface bubbles opened during sample preparation. The occurrence of gas precipitation within bubbles at pellet periphery is also highlighted by ^{132}Xe depth profiles measured by SIMS (Fig 3). Otherwhile, SIMS total inventory is very close to the creation profile. This is fully consistent with a low in-pile gas release (i.e. 0.51% of the creation). Moreover, gas precipitation at pellet periphery does not seem to have furthered any particular gas release.

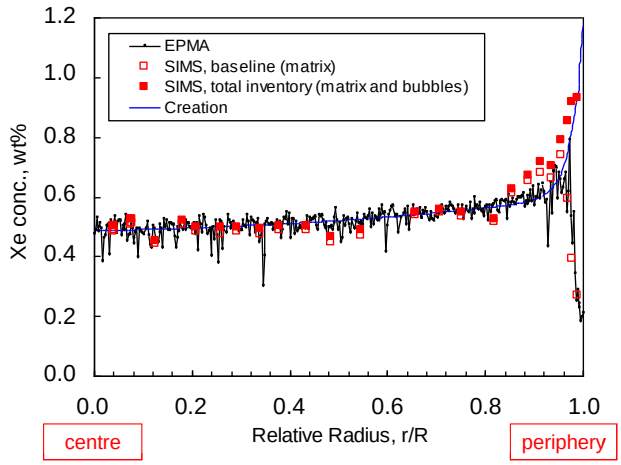

Fig 2. Radial distribution of Xe measured by EPMA and SIMS and comparison with creation

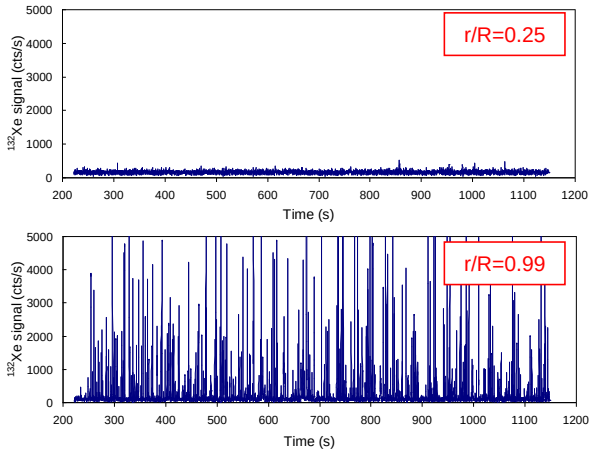

Fig 3. Depth profiles of ^{132}Xe at different radial positions

3.2 Detailed study of pellet periphery

Fig 4. shows U, Gd and Xe EPMA maps of pellet periphery. Bright spots are observable on Gd map indicating Gd_2O_3 particles which were already present before irradiation [17].

Fission gas bubbles formation is evidenced on Xe X-ray map by bright and black dots corresponding respectively to gas filled bubbles located just beneath the surface and opened bubbles during sample preparation. At pellet edge the Xe map is characteristic of micro-bubbles as observed in restructured fuel. Furthermore, no distinction can be made between free UO_2 clusters and the $(U,Gd)O_2$ matrix in this area. On contrary, at 60 µm from the pellet edge, the Xe content appears to be higher in the free UO_2 cluster (brighter area) than in the $(U,Gd)O_2$ matrix. This point will be discussed further (i.e. § 4.2.).

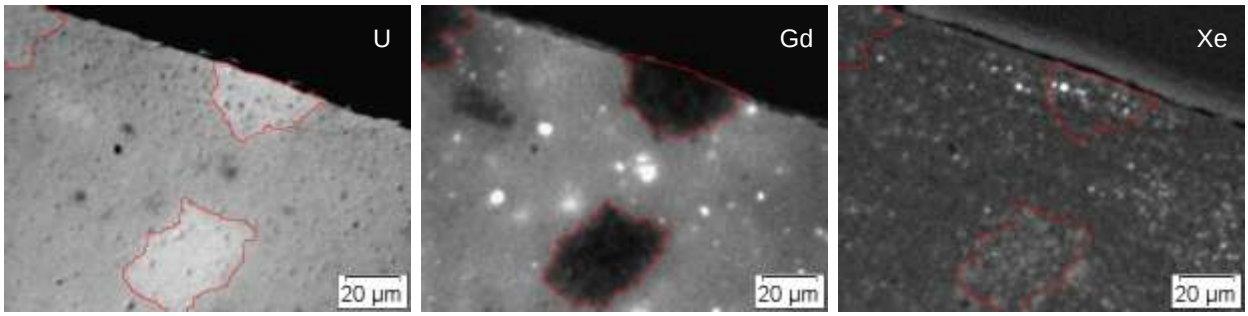

Fig 4. X-ray maps (U, Gd, Xe) located at pellet periphery

Optical images of pellet periphery after chemical etching are given on Fig 5. A generalized fission gas precipitation is observed at pellet edge (Fig 5.a), while two distinct microstructure evolutions are highlighted at 100µm from pellet periphery (Fig 5.b). In this latter region, UO_2 clusters exhibit high content of planar defects while $(U,Gd)O_2$ matrix shows intragranular HBS type restructuration.

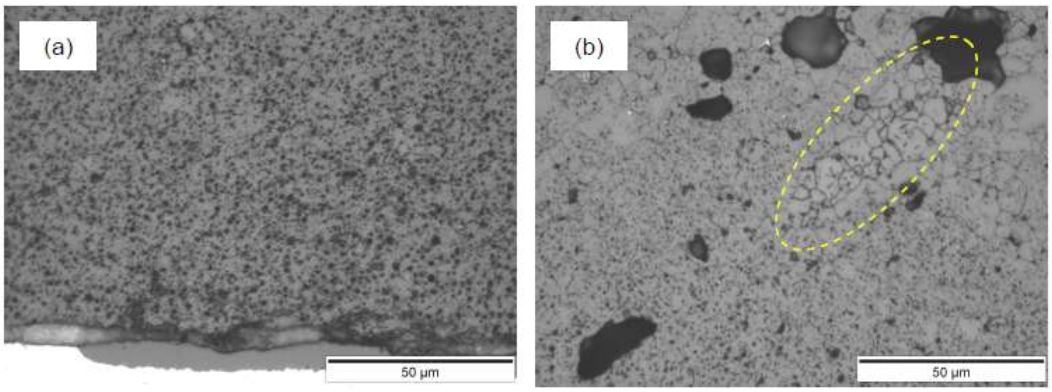

Fig 5. Optical images after chemical etching of pellet edge (a) and of a region located at 100 µm from pellet periphery (b)

4. Discussions

4.1. Fission gas behaviour

Fission gas release measurements after rod puncturing and quantitative analysis of Xe both indicate a low value of in-pile release. The determined release is in the range of reported data for PWR irradiated UO_2 at similar burn-up level, though in case of UO_2 fuel higher operating power is reached due to higher initial enrichment [16].

Radial evolution of Xe content and microstructural observations both highlight the non-occurrence of thermally activated precipitation or release from the centre to 180 µm from the pellet periphery. In this area, comparison between free UO_2 clusters and $(U,Gd)O_2$ matrix [17] indicates a similar behaviour for both considered phases. This result means that operating temperatures were too low to induce fission gas precipitation into both free UO_2 clusters and $(U,Gd)O_2$ matrix. At these levels of temperature and local burn-up no distinct behaviour can be attributed to the presence of gadolinium, in spite of its consequences on fuel properties (i.e. gas diffusion coefficient [1], thermal conductivity [5-8]…).

At pellet periphery (0 to 180 µm from the edge), a differential fission gas precipitation is observed in the free UO_2 clusters and in the $(U,Gd)O_2$ matrix. This has been shown to be correlated with a differential occurrence of HBS formation. This topic is therefore discussed in the following section.

4.2. Fuel restructuration

Optical microscopy, SEM observations, EPMA maps and Xe quantitative analyses have demonstrated the occurrence of gas precipitation in bubbles at pellet periphery. Further observations by SEM [17] have highlighted the presence of grains subdivision, polyhedral sub-grains and round sub-grains surrounding bubbles which are characteristic of fuel restructuration. Generalized HBS formation at r/R=1 (0 to 50 µm from the pellet periphery) indicates that the local burn-up is sufficiently high (above 70 GWd/t_U) to induce restructuration of both UO_2 free clusters and $(U,Gd)O_2$ matrix. The Nd content in this region ranges between 0.61 and 0.81 wt%. Outside the fully restructured periphery a transition region (extended between 50 and 180 µm from the pellet periphery) is observed where $(U,Gd)O_2$ matrix is restructured whereas UO_2 clusters are not (Fig 4 and Fig 5.b). The Nd content in this region evolves between 0.44 and 0.61 wt%. According to our knowledge, such a large HBS zone has never been reported for this range of rod average burn-up (39.2 GWd/t_U) neither for these values of local Nd content in PWR irradiated UO_2 fuel. Comparison of our results and reported data for various UO_2 fuel is not always relevant though, as many existent differences lie in between considered objects (i.e. initial enrichment in ^{235}U, irradiation conditions, fission gas diffusion coefficient…). Still, comparison of UO_2 clusters and $(U,Gd)O_2$ matrix within the fuel remains pertinent because initial ^{235}U enrichment and irradiation parameters are similar into both considered regions.

Potential causes of enhanced HBS formation into $(U,Gd)O_2$ are now discussed :

- Temperature effect has to be rejected since it is assumed that operating temperature is similar into UO_2 clusters and neighbouring $(U,Gd)O_2$ matrix for a given radial position (due to small size of free UO_2 clusters).

- Specific neutronic behaviour of $(U,Gd)O_2$ rod (i.e. gadolinium burning step) is not the key parameter since it has been demonstrated that at a particular radial position with the same neutron flux UO_2 cluster are not restructured while $(U,Gd)O_2$ matrix is (i.e. Fig 5.b).
- Presence of plutonium does not seem to have an impact since no significant difference of Pu content in UO_2 clusters and $(U,Gd)O_2$ was found using quantitative analysis by EPMA at various radial positions [17].
- Therefore, the 'chemical effect' of gadolinium seems to be the key parameter in the enhanced HBS formation into $(U,Gd)O_2$. Here, the 'chemical effect' term bring together all the consequences of charge compensation mechanism (i.e. O vacancies and U^{5+}/U^{6+} cations).

Two major hypotheses on the role of gadolinium on the HBS apparition can be suggested:
- The introduction of Gd cation in the fluorite lattice increases the oxygen vacancy content. These vacancies could act as traps for fission gas atoms [1]. An increased number of bubbles for a given value of created fission gas atoms can lead to an early grain subdivision; by a stress-induced mechanism as described in [18].
- A fuel restructuration mechanism induced by point defects (interstitials and vacancies) has been reported in [19]. The grain subdivision is a result of interstitials, dislocations and dislocations loops. In the other hand, bubbles are formed by vacancies and fission gas atoms. Despite recombination effect, increased initial point defect content due to gadolinium introduction into the fluorite cell could lead to an anticipated HBS formation.

5. Conclusions

According to results reported in this paper and the discussion proposed above two major conclusions can be drawn regarding the effect of Gd addition on fission gas behaviour in fuel during irradiation:
- Fuel sample temperature in operation has been too low to induce fission gas precipitation or release from the pellet centre until the rim region (180 μm from the pellet edge). At these levels of operating power, local temperature and local burn-up, the fission gas behaviour may not been modified by the presence of gadolinium.
- The HBS formation is enhanced by the presence of gadolinium but this does not seem to induce any additional fission gas release. The local burn-up threshold for HBS formation may be lowered by the 'chemical effect' of gadolinium.

Additional observations notably at higher burn-up levels are however needed to confirm and refine the interpretation of observed phenomena.

6. References

[1] A.R. Massih *et al.*, J. Nucl. Mater. 188 (1992) 323.
[2] R.J. Beals *et al.*, J. Am. Ceram. Soc. 48 (5) (1965) 271.
[3] A.G. Leyva *et al.*, J. Nucl. Mater. 303 (2002) 29.
[4] S.M. Ho *et al.*, Nucl. Techn. 73 (1986) 350.
[5] K. Minato *et al.*, J. Nucl. Mater. 288 (2001) 57.
[6] S. Fukushima *et al.*, J. Nucl. Mater. 105 (1982) 201.
[7] M. Hirai, J. Nucl. Mater. 173 (1990) 247.
[8] M. Amaya *et al.*, J. Nucl. Mater. 231 (1996) 29.
[9] T. Cardinaels *et al.*, J. Nucl. Mater. (2012), doi: 10.1016/j.jnucmat.2012.02.014.
[10] L. Pagano Jr. *et al.*, J. Nucl. Mater. 378 (2008) 25.
[11] L. Desgranges *et al.*, Nucl. Instrum. Methods B215 (2004) 545.
[12] J. Lamontagne *et al.*, Microchim. Acta 145 (2004) 91.
[13] J. Lamontagne *et al.*, Microchim. Acta 155 (2006) 183.
[14] L. Desgranges *et al.*, Nucl. Instrum. Methods B266 (2008) 147.
[15] J. Noirot *et al.*, J. Nucl. Mater. 372 (2008) 318.
[16] J. Noirot *et al.*, Fission Gas Behaviour in Water Reactor Fuels, Seminar Proceedings, NEA/OECD, NEA #03053, Cadarache, France (2000) 223.
[17] R. Delorme *et al.*, To be published (2012).
[18] J. Spino *et al.*, J. Nucl. Mater. 256 (1998) 189.
[19] K. Nogita *et al.*, J. Nucl. Mater. 226 (1995) 302.

[13] N. NAKAE, et al., “KINETICS OF GASEOUS ATOMS IN URANIUM PLUTONIUM MIXED OXIDE,” Proceedings of ICAPP 2011, Nice, France, May 2-5, 2011, Paper 11442.

AREVA PRODUCT EXPERIENCE IN SUPPORT OF EPR™ FUEL DESIGN

G. GENTET[1], C. HINTERGRÄBER[2], P-H. LOUF[1], N. TEBOUL[1], C. WILTZ[3]

[1]AREVA, AREVA NP SAS
10 Rue Juliette Récamier
69456 Lyon Cedex 06
France

[2]AREVA, AREVA NP GmbH
Paul-Gossen Strasse, 100
91052 Erlangen
Germany

[3]AREVA, AREVA NP Inc
2101 Horn Rapids Road
99354 Richland WA
USA

ABSTRACT

Through its engineering and manufacturing operations in the USA and Europe, AREVA supplies nuclear fuel assemblies and associated core components to pressurized water reactors worldwide, representing today more than 120,000 fuel assemblies. AREVA is keeping active its two main historical PWR fuel technologies: the HTP™ and the AFA®. These technologies have provided proven performance and are currently operated in more than 70 plants in total. Both have undergone continuous improvement over the years, to ensure the highest fuel assembly reliability, robustness and performance in meeting utility expectations.

AREVA has the largest manufacturing and operating experience in the world with long bundles, through HTP™ supplied in German plants and AFA 3G® in French 1300 MW and N4 plants. PWR fuel assembly designs offered today to AREVA customers benefit from all the experience feedback AREVA has built up for years and from a continuous improvement approach. With respect to this approach, AREVA's worldwide teams are organized to run a very systematic process for collecting experience feedback and performing global analyses. This process drives understanding and modeling of phenomena. It is supported by R&D programs to continuously refine the phenomenological approaches in support of upgrading the prediction of the fuel assembly overall behavior and its validation on a huge experience feedback. Prediction tools also support the identification and development of hardware solutions.

EPR™ fuel is benefiting from all AREVA's global knowledge and experience with long bundles. The fuel assembly/reactor interface of the plants has been carefully designed in order to minimize potential risks. In particular, design measures have been taken to homogenize the flow in the core and reduce its incidence on adverse fuel assembly behavior. Capitalizing on its experience, AREVA has developed the latest version of its technologies for long bundles to further increase its performance with regard to fuel assembly straightness: AFA3 G®-I and HTP™-I, which are under deployment for the 13ft and 14ft installed base plants. "I" designs consist of a package of features to increase robustness and dimensional stability, such as the optimized hold down system, Q12 guide tube material with enlarged wall thickness and stiffening the spacer to guide tube connection. Those features to further reinforce long bundle fuel assembly designs will be deployed on EPR™ fuel reloads to upgrade first cores designs that were fixed as reference fuel for licensing studies some years ago.

1. INTRODUCTION

AREVA has built the largest manufacturing and operating experience in the world with regard to long bundles, through AFA 3G® in French 1300 MW and N4 plants and HTP™ supplied in German plants. PWR fuel assembly designs currently offered to AREVA customers benefit from the experience feedback AREVA has built up for years. Through its engineering and manufacturing operations in the USA and Europe, AREVA supplies nuclear fuel assemblies and associated core components to pressurized water reactors worldwide, representing today more than 120,000 fuel assemblies.

AREVA is maintaining active its two main historical PWR fuel technologies: the HTP™ and the AFA®. These technologies are both proven and currently operated in more than 70 plants in total. Both have undergone continuous improvement over the years, to ensure the highest fuel

assembly reliability, robustness and performance in meeting utility expectations for installed base and new builds.

2. UPGRADED FUEL ASSEMBLIES

AREVA technologies have grown based on huge experience feedback and a continuous improvement approach. AREVA's worldwide teams are organized to run a very systematic process for collecting experience feedback and performing global analyses. This process drives the worldwide deployment of best proven features and components, as well as common progress in understanding and modeling of phenomena. Understanding and modeling are supported by R&D programs to continuously refine the phenomenological approaches in support of upgrading the prediction of the fuel assembly overall behavior. The performance and quality of the predictive tools, and any test setups required are keys to adequately support the fuel assembly design development and behavior assessment. Their validation requires on a huge experience feedback.

2.1 PROVEN COMPONENTS

AREVA has continuously reinforced its technologies for long bundle fuel assembly designs by selecting and deploying the best components, while continuing to develop and implement new features and resulting in improved performance, robustness and reliability.

2.1.1 MONOBLOC™ guide tube

A greater resistance to fuel assembly bow has been achieved with the introduction of the MONOBLOC® guide tube design. The outside diameter of these enlarged, thick guide tubes is constant over the length of the tube. In contrast to other solutions in the industry, the MONOBLOC™ guide tube is made from one piece, including the reinforced dashpot zone (Fig. 1). The first fuel assemblies featuring MONOBLOC® guide tubes were made of Zircaloy-4 and inserted in 1998 in Belgium and Sweden. As of May 2012, the operational experience with MONOBLOC® guide tubes includes more than 26,500 assemblies with a 17x17 array irradiated in 69 plants, 12,500 of them with an active core height of 12ft and 14,000 with an active core height of 14ft. Additionally, more than 2,650 assemblies featuring an all-M5® MONOBLOC® guide tube have been manufactured and irradiated. A maximum assembly average burnup of 58 MWd/kgU has been achieved with Zircaloy-4 and 63 MWd/kgU has been achieved with M5®.

Fig. 1: MONOBLOC® guide tube

2.1.2 AFA 3G® Improved Grid

This grid is the advanced version of the existing AFA 3G® spacer and includes implementation of design adjustments to reduce the risk of hang up with neighboring fuel assemblies during loading/unloading operations, and to facilitate fuel-assembly handling (Fig. 2). Compared to the first generation of the AFA 3G® spacer, the outer-strap geometry and the grid corners have been re-designed. The outer straps feature guide vanes and are bent back to form a rounded corner gusset, with the straps welded together on the lateral face by seam welds. Pressure balancing holes have also been implemented to reduce the lateral hydraulic loads and thereby contributing to resistance against fuel assembly distortion. All improvements have been implemented without impact on the excellent critical heat flux and T/H performance of the AFA 3G® grid.

Fig. 2: AFA 3G® Improved Grid

The Improved AFA 3G® grid was first introduced in the 14ft reactors and later harmonized for all 12 and 14ft AFA 3G® assembly applications. At the end of April 2012, the operational experience with the improved AFA 3G® grid includes more than 2,300 AFA 3G® 14ft assemblies in 20 plants with at least one irradiation cycle and no observation of grid tearing being reported for adjacent assemblies, neither those equipped with the AFA 3G® improved grid or the neighboring fuel assemblies.

2.1.3 AFA 3G® bottom end grid: the Twin Grid

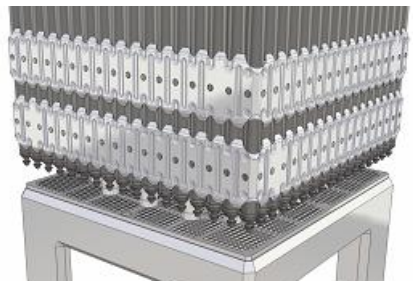

Fig. 3: Twin-grid

Due to the high hydraulic loads existing in the 14 ft – 4 loops reactor (higher F.A. flow rate, higher peaking factors), some fretting occurred in these reactors in the 2000's, as the margins decreased with burn-up increase, at the bottom grid level. At that time all the designs implemented in the14 ft - 4 loop reactors were affected. An enhanced resistance against grid-to-rod fretting was achieved through implementation of a second grid at the lowermost position. This solution, the twin-grid concept (Fig. 3), was validated through hydraulic and endurance tests in CEA's HERMES T and HERMES P flow loops before its introduction in core and adaptation to all the 14ft AFA 3G® fuel assemblies. From 2003, date of its first introduction in core, no observation of failure due to grid-to-rod fretting in the lowermost position has been reported on the AFA 3G® 14ft assemblies. As of May 2012, the operational experience with the twin-grid at lowermost position includes more than 8,300 AFA 3G® 14ft assemblies irradiated in 23 plants. A maximum assembly average burn-up of 63 MWd/kgU has been achieved.

2.1.4 TRAPPER® anti-debris bottom nozzle for AFA technology

The TRAPPER® bottom nozzle was developed to further enhance the protection of the bundle against the debris, while featuring a very low pressure drop. Compared to the previous generation of anti-debris bottom nozzle used in the AFA 2G® design, the main evolution consists in a ribbed structure fitted with 4 legs and topped with a thick anti-debris device.

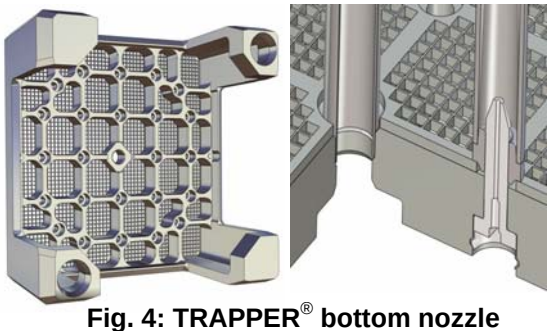

Fig. 4: TRAPPER® bottom nozzle

The ribbed structure provides a very low flow resistance, while ensuring a very high mechanical strength of the bottom nozzle. It supports and protects the anti-debris device and provides an outer enclosure compatible with handling requirements. The peripheral rib forms a chamfered "skirt", which contributes to the nozzle reinforcement and prevents any debris from being carried back to the flow stream. The anti-debris device consists in a thick plate with a 3.3 mm mesh size, which provides a superior protection of the fuel assembly against debris (Fig. 4). Between 1998 and May 2012, more than 25,700 AFA 3G® 17x17 assemblies equipped with the TRAPPER® bottom nozzle had been inserted into 64 plants worldwide.

2.1.5 Robust FUELGUARD™ bottom nozzle for HTP technology

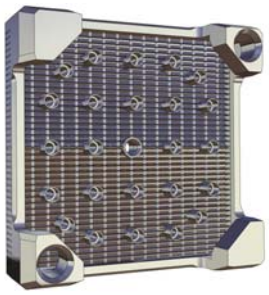

Fig. 5: Robust FUELGUARD™ bottom nozzle

FUELGUARD™ has been in use since 1988. This concept provides a "no-line-of-sight" flow path for the coolant, very effective at trapping debris.

The Robust FUELGUARD™ (Fig. 5) is a proven solution included in the HTP™ technology eliminating debris-related fuel failures. The bottom nozzle design has shown a level of robustness making it resistant to impact damage by large pieces of debris. In total, FUELGUARD and Robust FUELGUARD™ have been supplied as part of over 13,700 PWR assemblies to date.

2.2 Analytical means and modelling to support continuous development and upgrades

AREVA has developed advanced predictive tools to help in finding hardware solutions and to accompany the definition and improvements of its products. Advanced calculation codes and methods, improved modeling tools and test facilities, mainly contribute to reinforce reliability,

robustness, thermal-hydraulic performance and maneuverability of nuclear fuel under ever more demanding operational conditions.

2.2.1 Improvement of resistance to grid-to-rod fretting thanks to analytical and experimental means

In this domain, key for fuel reliability, the goal is to enhance the understanding of the phenomenon of flow excitation of the fuel assemblies in the reactor in order to improve the design in a way that guarantees the highest robustness against fretting phenomena. To reach this goal, AREVA designed and built the Peter Loop (Fig. 6), a very flexible low-pressure loop which allows for simulation of practically all flow configurations, which may occur in the reactor, thus covering different axial and cross-flow situations. The fretting evaluation itself is accomplished after the flow tests by applying experimental methods called “Autoclave Testing”. In the autoclave test setup, a single, shortened test rod is excited electromagnetically in a way that reproduces exactly the excitations measured for the simulated flow in the Peter Loop and the fretting behavior of the rod is studied over several hundreds of hours. Before insertion in core, a final fretting evaluation is performed through a 1000 hour endurance test on a full size mockup, fully representative of the fuel assembly design, in the HERMES P loop (CEA test facility), which reproduces PWR operating core conditions.

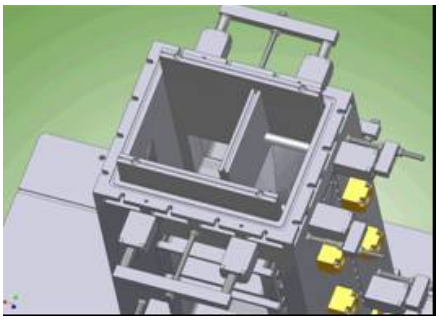

Fig. 6: Peter loop (adjustable walls)

2.2.2 Development of tools to identify solutions to improve fuel assembly resistance to lateral deformation

AREVA has developed an advanced methodology to predict and evaluate fuel assembly bow that combines analytical and experimental methods [1]. Fuel assembly distortion is a creep related phenomenon due to the influence of external forces on the fuel assembly: both hydraulic forces between fuel assemblies and mechanical axial (e.g. axial hold-down forces) and lateral interactions between fuel assemblies and core internals. Measurements from reactors show that fuel assembly distortion does not occur randomly but shows typical structured bow patterns. It is also influenced by reactor specific inlet and outlet conditions, by shuffling strategy and also by fuel assembly design but has no strong correlation with the temperature and flux distributions. These observations lead to the conclusion that fuel assembly distortion must be treated by a mechanically-hydraulically coupled model with Fluid Structure Interaction (FSI).

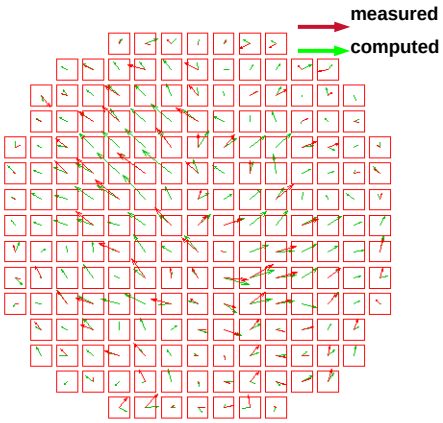

Fig. 7: Example of bow pattern prediction at EOC (no interaction between FAs)

The methodology accounts for FSI effects acting between neighbored fuel assemblies, which have been recognized to play an important role in the fuel assembly creep bow, together with the classical mechanisms like hold-down forces, temperature and power gradients. The model applied is a mechanically / hydraulically coupled FSI model in which the mechanical model is a finite element model.

The method is based on a two step approach. The first step consists of determining the hydraulic “bow characteristics” of a given fuel assembly design in a given reactor, either through application of CFD or obtained through a specific test on a full scale fuel assembly surrounded by two neighboring fuel assemblies in the GLASSTRAN tests setup. In the second step, the hydraulic parameters derived from the first step are then used to build a simulation model able to represent full rows of fuel assemblies or a full core. The core inlet and outlet flows, generating lateral forces acting on the lower and upper regions of the fuel assemblies, are modeled using

the results from the first step. Simulation of the evolution of the fuel assembly bow throughout one or several reactor cycles is then performed stepwise over time to account for the creep effect. At each calculation step, the pressure determined by the hydraulic network model defines the outer loads for the finite element model, while, concurrently, any bow of the fuel assembly is accounted for hydraulically to determine the FSI coupling conditions.

Validation of the network model has been obtained through the re-calculation benchmarking of in-core fuel assembly bow as measured for different fuel assembly design and cores. Fig. 7 presents one example of those benchmarks between measured and computed bow at end of cycle. This methodology is now in use to assess the impact of designs changes on the behavior of the fuel assembly with regards to lateral deformation.

2.2.3 Use of CFD to support development of improved designs

Thanks to its capacity to calculate flow and pressure fields around the fuel rods, Computational Fluid Dynamics (CFD) is used to define appropriate geometries, which minimize downstream flow heterogeneity that reduces the excitation sources of vibration regimes. This helps the designer get access to local flow vectors, which are difficult to measure and need to be known to avoid excessive vibrations of the fuel assembly. As an example, this approach has been successfully used to orientate the development of GRIP bottom nozzle (see Section 3.2.2).

In the area of fuel performance, CFD codes are also used to assess the effect of the detailed geometry of mixing grids. They help the designers evaluate the impact of the grid cell geometry and mixing vanes, including their bend angle, on grid pressure drop and reactor coolant flow. Thus, the influence of each geometric element of a grid can be assessed with CFD and parametric studies performed to choose the optimized geometry, reducing the pressure drop while increasing the DNB performance.

2.3 AREVA “I” designs : a further improved design for long bundles

Capitalizing on its operating feedback in long cores which is supporting validation of its advanced methodology to predict in-reactor bow (as described in Section 2.1.2), AREVA has developed the latest version of its technologies for long bundles. These upgrades target further increase performance with regard to fuel straightness. The network model has been used to define appropriate design modifications, to predict their efficiency and identify parameters influencing the distortion behavior. Generic parameter studies were performed to investigate the effect of certain design modifications or boundary conditions like core management or flow profiles at core inlet/outlet. From the design perspective parameters identified were mainly hold-down (HD) forces, fuel assembly stiffness and guide tube creep behavior.

On this basis AREVA proposed a package of measures to increase fuel assembly straightness called “I”-features. The evolution lies in a combination of key features to further improve robustness and dimensional stability.

These newest versions of AFA 3G® and HTP™ technologies called AFA 3G®-I and HTP™-I and applied combinations of those features are under deployment for the 13ft and 14ft installed base plants.

2.3.1 Optimization of the HD forces

The reduction of the excess HD forces and consequently the stresses in the guide tubes is seen as an effective measure to reduce the fuel assembly distortion. The efficiency is confirmed by the experience feedback as shown as an example on Fig. 8.

“I” designs are designed with an optimized HD device allowing the more appropriate reduced HD forces: A so-called “stepped” HD device was developed for Siemens reactor type fuel where number of leaves was reduced at the same time as fuel

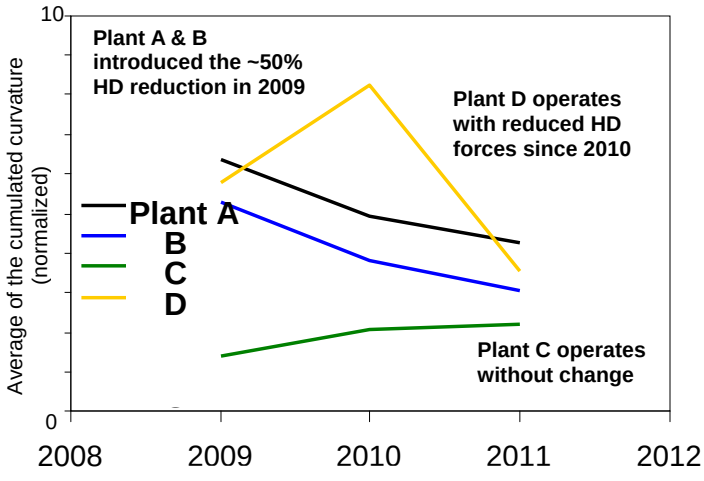

Fig. 8: Effect of HD forces reduction on average cumulated curvature

assembly length was fine tuned for 17x17 14ft fuel.

2.3.2 Fuel assembly resistance against lateral deformation

Increasing fuel assembly resistance against lateral deformation targets a reduction in the response of the fuel assembly to external forces which may result in fuel assembly distortion. Specific “I” features were developed in this respect:

- Reinforcement of guide tube geometry : thick guide tube with enlarged cross section increasing lateral stiffness while reducing creep response by reducing stresses in the guide tubes
- Additional enhancement of guide tube creep resistance by the deployment of so-called Q12 material (Zr1Nb0.5Sn0.1Fe Ultra Low Tin Quaternary alloy) [5]
- Further increase in lateral stiffness by rigidifying spacer to guide tubes connections.

Globally, the gain in fuel assembly stiffness for combination of “I” features is estimated up 30%.

3. FUEL FOR EPR™

3.1 The EPR™ Core specificity

The EPR™ development was based on the latest PWR product lines N4 and Konvoi, of former Framatome and Siemens respectively. Table 1 provides a comparison of the main core characteristics from these reactors.

Type of power plant	EPR™	N4	Konvoi
Thermal Power (MW)	4250 to 4900	4250	3850
Number of F.A.	241	205	193
Number of Absorber rods	89	73	61
Fissile height (cm)	420	427	390
Number of fuel rod per assembly	265	264	300
Average Linear power (W/cm)	155 to 179	180	167

Table 1: Core characteristics

The main characteristics of the core are derived from a set of objectives, namely minimization of cycle cost, a plutonium recycling capability (MOX fuel assemblies up to 100% of the core), the desired flexibility in respect to cycle length (from 12 to 24 months) and fuel management strategies (out/in and in/out). The fuel assembly design allows for small reload quantities (number of assemblies), corresponding to high discharge burnup (average burnup of fuel assemblies on unloading) of more than 60 GWd/t. The implementation of the incore instrumentation is similar to that of Konvoi reactors as it penetrates through the reactor vessel head, eliminating penetrations through the vessel bottom. The instrumentation “fingers” are inserted into one of the guide tubes of some fuel assemblies. This feature allows for the addition of one fuel rod, contributing to a decrease in heat generation rate. For a thermal output equivalent to that of a N4 reactor, the linear power is roughly 13% lower. This allows for more margins in safety analyses or higher burnup potential.

The main differences of EPR^{TM} fuel design, compared to existing 17x17 - 14 ft designs are:

- the fuel assembly consists of 265 fuel rods with a lower plenum and, as mentioned; the instrumentation system is introduced from the top of the fuel assembly (hence the instrumentation tube is eliminated and the top nozzle adapted),
- the bottom nozzle height is the same as for the 12-foot fuel assemblies although it is a 14ft design. This change allows having more room for the fuel rod and particularly the fission gas

plenum; it provides more margins with regard to all phenomena driven by internal rod pressure.

- the fissile height is reduced by 70 mm while the total rod length is slightly increased

Based on the analysis of AREVA's operating experience of the long bundle fuel products in the 13ft and 14ft reactors, the fuel designers have formulated specific requirements for designers of new reactors, and particularly the EPR™, in order to reduce the hydraulic loads, as they explain an important part of the difference of 12ft and 14ft fuel assembly behaviors. To fulfill such requirement, the EPR™ lower internals have been optimized to reduce the core inlet flow peaking factor to a value similar to that of the 12ft reactors.

3.2 AREVA fuel for EPR™

3.2.1 First cores

Two AREVA PWR fuel technologies were used for EPR™ reactors as reference fuel for licensing and first cores. HTP™ and the AFA 3G® designs were adapted to the specific requirements of EPR™ cores:

- HTP™LE (HTP reference fuel for EPR™ reactor) providing the best design features resulting from AREVA's global applications. The design of each component is well proven and validated by a large irradiation experience of several types of fuel assemblies, the majority of them being 17x17 fuel assemblies.
- AFA 3G®LE (AFA 3G® reference fuel for EPR™ reactor) is the EPR™ version of the design AREVA's most worldwide supplied for 14 ft existing reactors. First implemented in reload quantities in 2002, with Zy4, as structural and cladding alloy, the fuel assembly design has been supplied with M5® from beginning in 2004.

Both fuel assembly technologies offer fuel of high quality, reliability and performance and fulfil the EPR™ technical requirements.

The main features of the HTP™ LE and AFA 3G®LE are respectively described in Table 2.

	HTP™LE	AFA 3G®LE
Bottom nozzle	Robust FUELGUARD™	TRAPPER®
Fuels rods	265 M5®-clad fuel rods	265 M5®-clad fuel rods
Bottom end grid/ Top end grid	Alloy 718 HMP /Alloy 718 HMP	AFA 3G® Twin-Grid /AFA 3G® grid
Mixing spacers	8 M5®-HTP™	8 M5® AFA 3G®
Guide tubes	24 M5® -MONOBLOC®	24 M5® -MONOBLOC®
Upper connection	24 Quick-Disconnect connections	24 Quick-Disconnect connections

Table 2: Main features of EPR™ first cores fuel

3.2.2 Further reloads

As a result of capitalization on its experience, AREVA has developed the latest version of its technologies for long bundles to further increase its performance with regard to fuel assembly straightness: AFA3G®-I and HTP™ -I, which are under deployment for the 13ft and 14ft installed base plants. "I" designs features (described in § 2.3) to further reinforce long bundle fuel assembly designs will be deployed on EPR™ fuel reloads to upgrade first cores designs that were mostly fixed as reference fuel for licensing studies some years ago.

AREVA's next generation fuel assembly design for 17x17 applications, so-called GAIA, is also being considered as fuel for EPR™ cores, first as Lead Use Assemblies irradiation programs. The GAIA fuel assembly design is the result of a worldwide AREVA R&D project, which focused on fuel performance requirements such as reliability, robustness and thermal margin.

The GAIA fuel assembly main attributes are:

- GRIP™ bottom nozzle assembly which provides improved performance regarding flow induced fuel rod vibration, while ensuring low pressure drop and high level of filtering efficiency. The GRIP™ is combined with an Alloy 718 HMP lower end grid to provide superior resistance to grid to rod fretting thanks to enhanced fluid homogenization obtained (see Fig. 9).

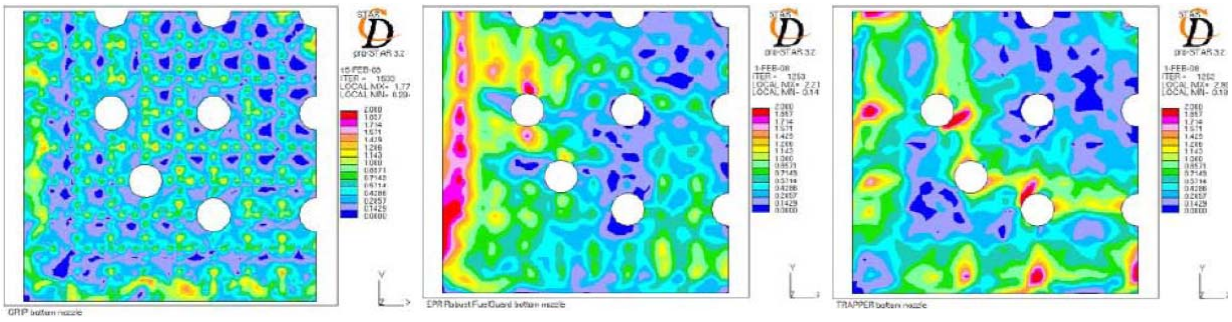

GRIP™ FUELGUARD™ TRAPPER®

Fig. 9: Examples of horizontal transverse velocity fields calculated by CFD (evaluation at a same axial elevation between nozzles and rod bundles under identical boundary conditions)

- GAIA mixing vane spacer grid, which combines improved critical heat flux and mechanical performances, including high grid-to-rod fretting resistance and low handling risks (Fig. 10),

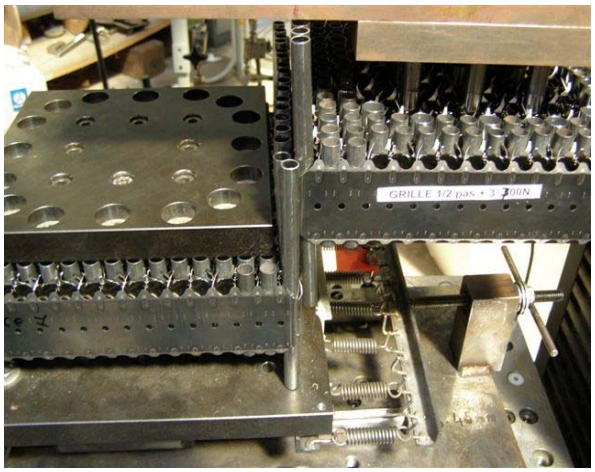

Fig. 10: Handling Tests

- MONOBLOC® thick guide tubes using Q12 material and a reinforced connection with the GAIA mixing spacers to enhance fuel assembly distortion resistance. The further increase of guide tube outer diameter improves the fuel assembly lateral stiffness and a supplementary reinforcement of guide tube to grid connections allows doubling this benefit, yielding more than 15% increase.
- GAIA optimized fuel rod [2].

4. Conclusion

During the 25 past years AREVA has continuously reinforced its fuel assembly designs based on its extensive experience feedback, the largest in the world for long bundles, and its huge investment in developing advanced tools to use in establishing unique hardware solutions and accompany the definition of its products. Obviously, EPR™ fuel assembly designs benefit from extensive AREVA knowledge and experience, best proven components and other features that have been implemented in the designs. Additional improved features will be implemented for the EPR™ fuel assembly design in further reload supplies upgrading the reference fuel used for licensing and first cores. So far, EPR™ fuel will benefit of the latest features to improve performance, robustness and/or reliability as those developed for the newest versions of AFA®

and HTP™ technologies called AFA3G®-I and HTP™ -I, which are today under deployment for long bundle installed base plants. AREVA's next generation fuel assembly design for 17x17 applications, so-called GAIA, is also considered as LUAs part of first reloads.

Acknowledgments

The authors wish to thank all the participating organizations and customers involved within AREVA's fuel developments and irradiation programs. Their support and contributions to the project are gratefully acknowledged.

References

[1] J. STABEL and al. "Advanced methodology to predict in-reactor bow of pwr fuel assemblies for efficient design optimization: Background, Validation, Examples" Light Water Reactor Fuel Performance Meeting, Chengdu, China, September 11-14, 2011

[2] S.E. COLE, C. DELAFOY, R.F. GRAEBERT, P-H. LOUF, N. TEBOUL "AREVA Optimization of fuel rod design for LWRs" Light Water Reactor Fuel Performance Meeting, Manchester UK, September 2012

[3] J-P. MARDON and al. "M5® a breakthrough in Zr alloy", Light Water Reactor Fuel Performance Meeting, (Proc. ANS Con. Orlando, 2010) Paper 0697)

[4] V. GARAT, D. DEUBLE, B. DUNN, J.P. MARDON "Quantification of the margins provided by M5® cladding in accidental conditions" Light Water Reactor Fuel Performance Meeting, Manchester UK, September 2012

[5] S.TRAPP-PRITSCHING, V.CHABRETOU, C.P.SCOTT, H-J.SELL "Ultra Low Tin Zr1NbSnFe Quaternary Alloys – Perspectives for structural components in PWR Fuel Assemblies" Light Water Reactor Fuel Performance Meeting, Manchester UK, September 2012

ATOMIC DIFFUSIVITY MEASUREMENT OF XENON GAS IN VARIOUS TYPES OF FUEL WITH LOW BURNUP BY POST-IRRADIATION ANNEALING TEST.

Heemoon Kim, Keon-Sik Kim, Sang-Ho Na, Kweon Ho Kang, Dong-Joo Kim, Jae-Won Lee, Sang-Bok Ahn

PIE & Radwaste division, Korea Atomic Energy Research Institute
150 Deokjin-Dong, Yuseong, Daejeon 305-353, Republic Korea

Kwangheon Park

** Dept. of Nuclear Eng., Kyunghee University*
Kiheong, Yongin, Kunggi, Republic Korea

ABSTRACT

To observe the xenon diffusion behavior in fuel, post irradiation annealing tests were performed with various types of fuel samples. The samples were made using natural uranium, and the shapes were single-grained powder, cubes, and disks. These contents were pure UO_2, $(Th,U)O_2$, SIMFUELs, UN, UO_2+additives(+3, +4 and +5), and different grain sized UO_2. The weights of these samples were below 0.3g, and the samples were contained in an irradiation capsule. A 16 minute irradiation period(0.1 MWd/t-U) was carried out. Each sample was loaded into a furnace and annealed at 1400 ^oC~ 1600 ^oC for oxide fuel and 1200 ^oC ~1400 ^oC for nitride fuel. Under an oxygen potential condition, The oxygen potential had a higher Xe-133 release rate in UO_2 due to a higher uranium vacancy concentration. The xenon diffusivity of $(Th,U)O_2$ was lower than UO_2, and that of UN was similar to UO_2. The additive effect showed a different diffusivity; a valence of +3 was lower while that of +5 was higher, than pure UO_2. These experiments were performed for 10 years, and over 60 samples were used. Some of the data showed an abnormal trend, and this issue will be studied in detail from other viewpoints.

1. Introduction

The fission gas release has been studied to estimate fuel rod sustainability during reactor operation. Many models were developed and applied to the fuel performance codes[1,2]. Most models are based on the diffusion equation and diffusion coefficient of fission gas[3,4]. In particular, the diffusion coefficient is an important factor obtained experimentally. Xe-133 is a dominant isotope of fission gases and can be a good gamma tracer. Here, diffusivity measurements of Xe-133 have been performed using nuclear fuel through a post-irradiation annealing test. The Booth model, a governing equation in this study, was applied with several assumptions: a spherical coordinate with an equivalent surface area of fuel, with no sink, no trap, no bubble, and only atom mobility in the matrix[5]. Therefore, To observe the atomic diffusion in a matrix, fuel samples were irradiated slightly without fission bubble generation[6]. In this study, a Xe-133 diffusion behavior in UO_2 must be observed by temperature, burnup, additive valence, and stoichiometry, as well as in other fuels(thorium mixed fuel and nitride). To obtain a fractional release(f) by gamma detection, the methodology was not published in detail. Thus, our own technique is developed and applied in every PIA test following the suggestion of (squared f) in Matzke[7].

$(Th,U)O_2$ and UN are studied as fuel or blanket materials in a fast reactor. For $(Th,U)O_2$, the diffusion data were sufficient, but a few data were found from India in which the research of thorium oxide has been performed[8]. For UN, it has a NaCl structure which is different with UO_2[9]. However, the data was too few. In this study, xenon diffusion was observed with various conditions via a PIA test.

2. Experimental

2.1 Sample preparations

To observe the Xe-133 diffusion behavior, many samples were made, irradiated, and annealed since 2000, as shown in table 1. Most samples were made with 0.3g and natural enrichment. Initially, UO_2 single grain powders were made, and all following samples were poly-crystals. In fig.1, the cubic and disk shapes were available to calculate the volume and surface area. A BET measurement was carried out in some samples, but it was not reasonable. $(U,Th)O_2$ samples were made with 35% of ThO_2 and 65% of UO_2. SIMFUEL was made with natural elements based on a 27,500 MWd/t-U, as shown in table 2. In 2008, Nitride fuel samples(green pellet) were made into disk type and high porosity to compare with oxide fuel. To observe the valence effect of additives, Nd_2O_3, CeO_2, and Nb_2O_5 were mixed with pure UO_2 in 2010. Moreover, two different grain sizes of UO_2 were made, and currently, four additional different grain sizes were added.

Year	Samples	No.	Grain size(μm)	TD(%)	Enrichment
2000	UO_2(powder)	1	23	N/A	Natural U
2001	UO_2(powder)	4	23	N/A	
2002	[a]UO_2, [b]$(Th,U)O_2$ (powder, 3cubes)	13	[a]8.1±0.5 [b]7.5±0.5	95~97	
2003	SIMFUEL(3cubes)	1	10±2	95~97	
2004	SIMFUEL(3cubes)	12	10±2	95~97	
2006	SIMFUEL(3cubes)	2	10±2	95~97	
2007	SIMFUEL(3cubes)	4	10±2	95~97	
2008	UN(disk)	4	N/A	45.2	
	UO_2(disk)	2	N/A	47.6	
2010	UO_2+additives(disk)	11	9~17	95~97	
2011	UO_2(four grain size)	12	6, 15, 25, 40	92~97	

Tab 1: Ceramic sample summary for PIA test

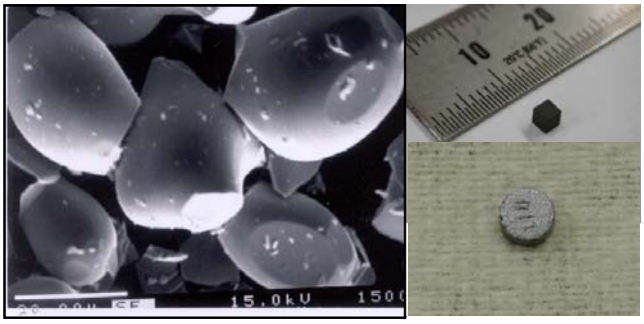

FIG. 1. Sample shapes(left: powder, right(top) : cube, right(bottom) : disk)

Contents	mg	Contents	mg
Rb	0.095	PdO	0.34
SrO	0.171	TeO_2	0.126
Y_2O_3	0.12	$BaCO_3$	0.57
ZrO_2	1.04	La_2O_3	0.42
MoO_3	1.055	CeO_2	1.99
RuO_2	0.825	Nd_2O_3	1.46
Rh_2O_3	0.11	UO_2	300
Total	308.35		

Tab 2: Contents of SIMFUEL

2.2 Irradiation

The samples were contained in a quarts tube initially, but was changed to a zry-4 tube for safety. The container was filled with 1.2 bar of helium and inserted in 3 irradiation capsules as shown in fig. 2. The capsules were placed in the IP4(C) hole in the HANARO research reactor for irradiation. 20 minutes of irradiation time was available for a 24 MW power of the reactor, but the irradiation time was reduced to 16 minutes for 30 MW of operation power, which was equivalent to the same burnup.

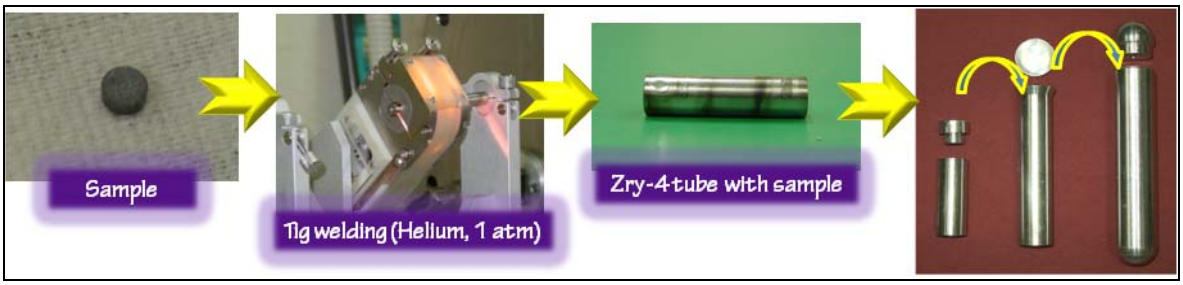

FIG. 2. Sample container(welding) for irradiation

2.3 Annealing test

For the annealing test, the system was designed as shown in fig. 3. It consisted of a furnace, filtration, and gamma detection. The furnace was an electric resistance type(super kanthal), and can be heated up to 1600 ^{o}C. The chamber and internal structures were made of pure alumina. A B-type thermocouple was installed to measure the sample temperature. An oxygen sensor, a ZrO_2 tube, measured the oxygen partial pressure in the chamber. Helium gas was flowed with 100 ml/min. as a carrier.
The filtration was designed as a cryogenic trap system to catch the gaseous xenon by solidification. The filter media was charcoal with a glass casing. It was placed into a liquid nitrogen. The helium, as a carrier, remained as gas during filtration. The gamma detector was a semi-conductor type with a high pure germanium crystal(HPGe). It was installed in the filtration and activated to obtain gamma-rays of Xe-133 released from the sample.
After the irradiation and cooling time(7 days), a sample contained in an alumina crucible following the capsule was dismantled. The gamma detection for 3,600 sec was carried out for the sample in a crucible to obtain the radioactivity of Xe-133 generated before the annealing.
After the sample was loaded into the furnace chamber, the temperature was controlled incrementally at 1400 ^{o}C, 1500 ^{o}C, and 1600 ^{o}C for UO_2, $(Th,U)O_2$, and SIMFUEL at 1200 ^{o}C, 1300 ^{o}C, and 1400 ^{o}C for UN. The annealing time for each temperature was decided according to the amount of xenon release.

Generally, a disk sample with 95% TD would be kept for 15 hours, 9 hours, and 6 hours, respectively, but a shorter annealing time was applied in the case of an oxidation atmosphere or low TD of the sample. During annealing, gamma detection of Xe-133 accumulated in the filtration system was activated for every 3,600 sec. After annealing, sample gamma detection for 3,600 sec was performed again before disposal.

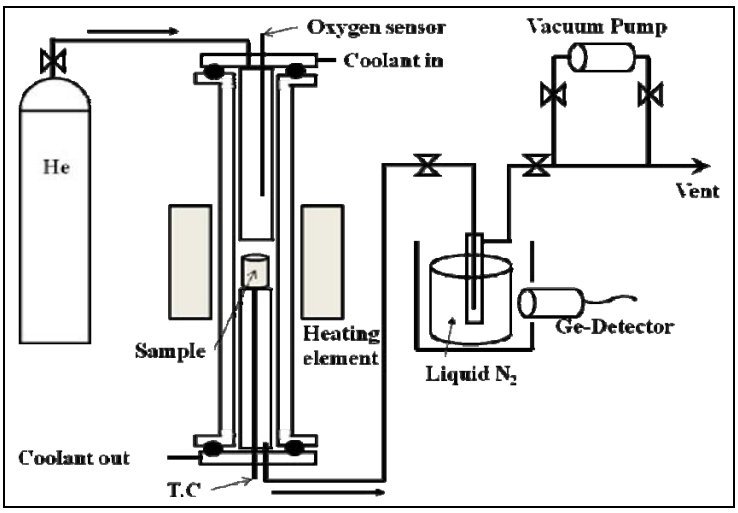

FIG. 3. Diagram of the annealing system

2.4 Theoretical approach

To obtain the diffusion coefficient, a Booth model is applicable with several assumptions: a sphere shape without defects(trap, sink, etc) in the matrix, and only diffusion controlled as shown in eq.1[5].

$$f^2 = \frac{\pi D}{36a^2} t \quad \text{if } f < 0.3 \qquad (1)$$

where 'f' is the fractional release, 'a' is the equivalent radius, 't' is the annealing time, and 'D' is the diffusion coefficient. Thus, the linear slope at each temperature in the plot of f^2 .vs. t is equal to $\pi D/36a^2$. Thus, if 'a' is determined, 'D' is obtained[7]. To obtain 'f' in the plot, gamma peaks of Xe-133 generated in the sample and released can be converted into radioactivity(Ci). Then, Ba-133(81keV and 356keV), the reference source, is detected to compare with Xe-133 at the same as geometry due to the same gamma energy(81 keV). But unfortunately, the generation amount of Xe-133 was not obtained using Ba-133 directly due to the peak burial in a low energy region. However, an I-131 peak(364 keV) was chosen as a substitute and compared to 356 keV of Ba-133. An ORIGEN-2 code was used to obtain Xe-133 generation through calculation with the radioactivity of I-131[10]. In this case, 8 keV of energy difference was ignored.

3. Results and discussion

Using data from gamma detection for Xe-133 released and generated, a plot(f^2.vs. t) was obtained at various temperatures. Single-grained powder UO_2 was performed at first to verify the system and compared to the reference[11]. Following good agreement with those data, polycrystal UO_2 samples were used to observe difference. The fractional release of polycrystal samples was higher than single grained powder because of the grain boundary effect. Fig.4 shows the difference between UO_2 and

$(Th,U)O_2$, and the xenon diffusion in $(Th,U)O_2$ was lower than UO_2 due to the high bonding energy of thorium oxide[11,12]. To observe burnup effect, SIMFUELs were used, and those data, e.g. are shown in fig.5[13]. The oxygen potential effect and the SIMFUEL behavior are shown in fig.6.

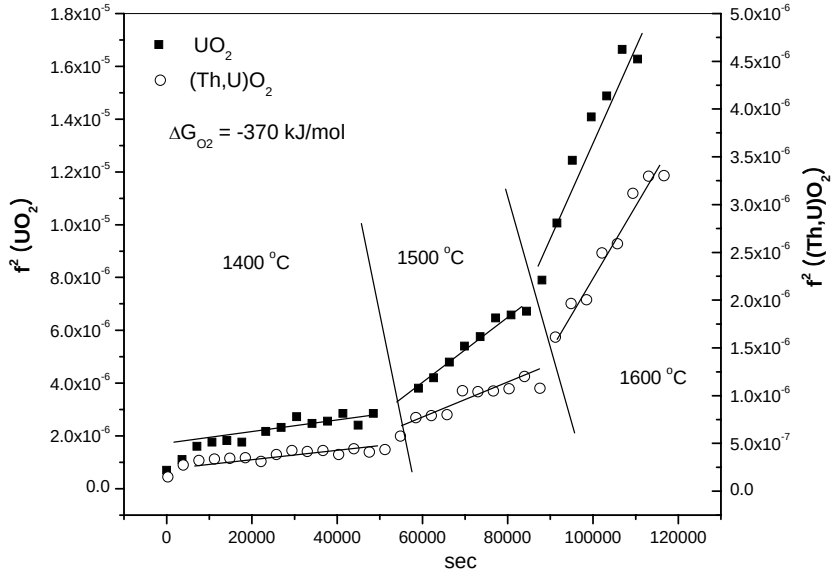

FIG. 4. Fractional release of Xe-133 in UO_2 and $(Th_{0.35},U_{0.65})O_2$

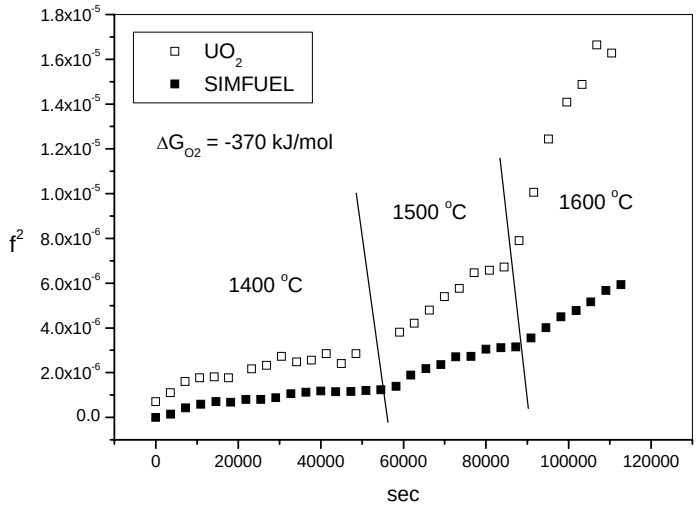

FIG. 5. Fractional release of Xe-133 in UO_2 and SIMFUEL

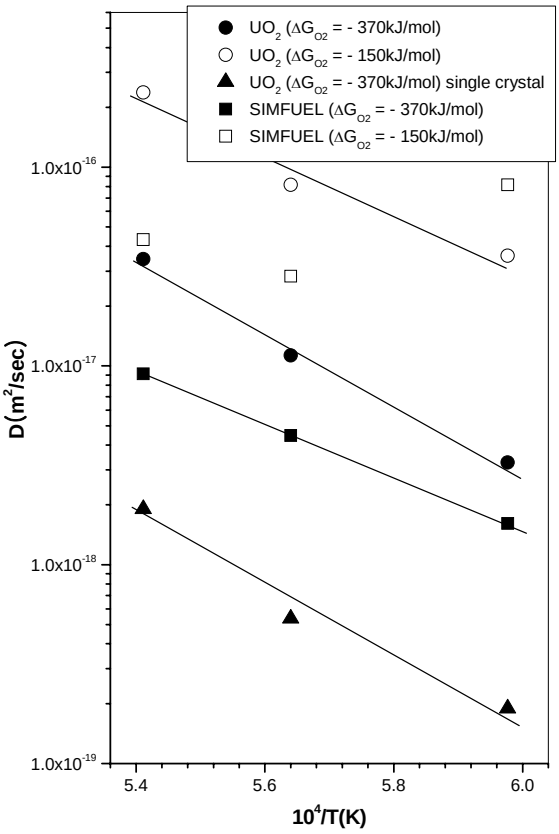

FIG. 6. Xe-133 diffusion coefficients in UO_2 and SIMFUEL with oxygen potential(1400^oC, 1500 ^oC, 1600 ^oC)

To observe the effect of additive valence, +3, +4, and +5 additives were used as shown in fig. 7. The higher valence of additives in UO_2 were a higher diffusivity. However, an independence of content for diffusion was observed. It seemed to be beyond the saturation content, the effect of which was shown.

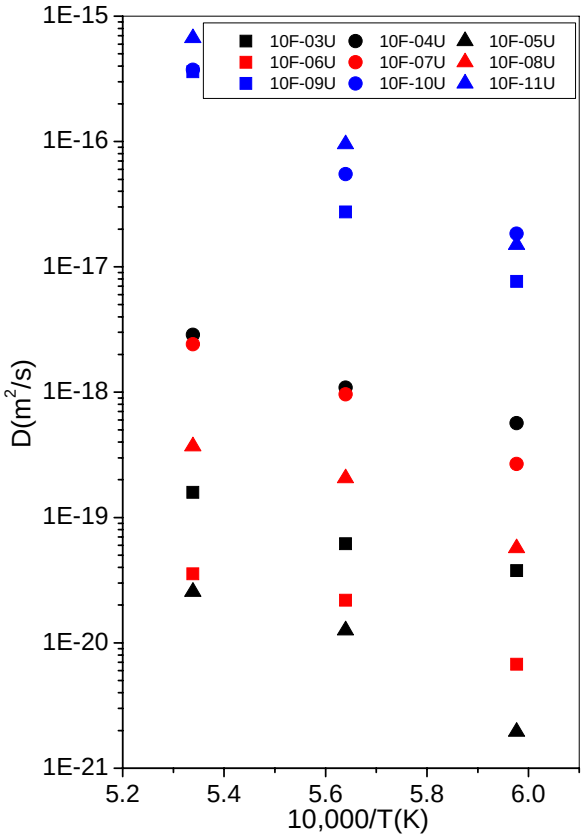

FIG. 7. Xe-133 diffusion coefficients in UO_2 with additives(▲●■ : Nb_2O_5, ▲●■ : CeO_2, ▲●■ : Nd_2O_3)

The Xe-133 diffusion in uranium nitride(UN) was measured and compared to other data and UO_2 as shown in fig.8[9]. UN has a NaCl structure, however the diffusion behavior was almost similar to UO_2, at least in the temperature range(1200 ^oC ~ 1400^oC), however, the diffusion mechanism has not been known yet. Fig.9 shows the xenon diffusion with the grain size. Generally, larger grained UO_2 has a lower diffusivity, but samples with 25μm and 40μm were higher than that with 15μm. It seemed that many open pores on the surface of the sample may cause a higher release rate.

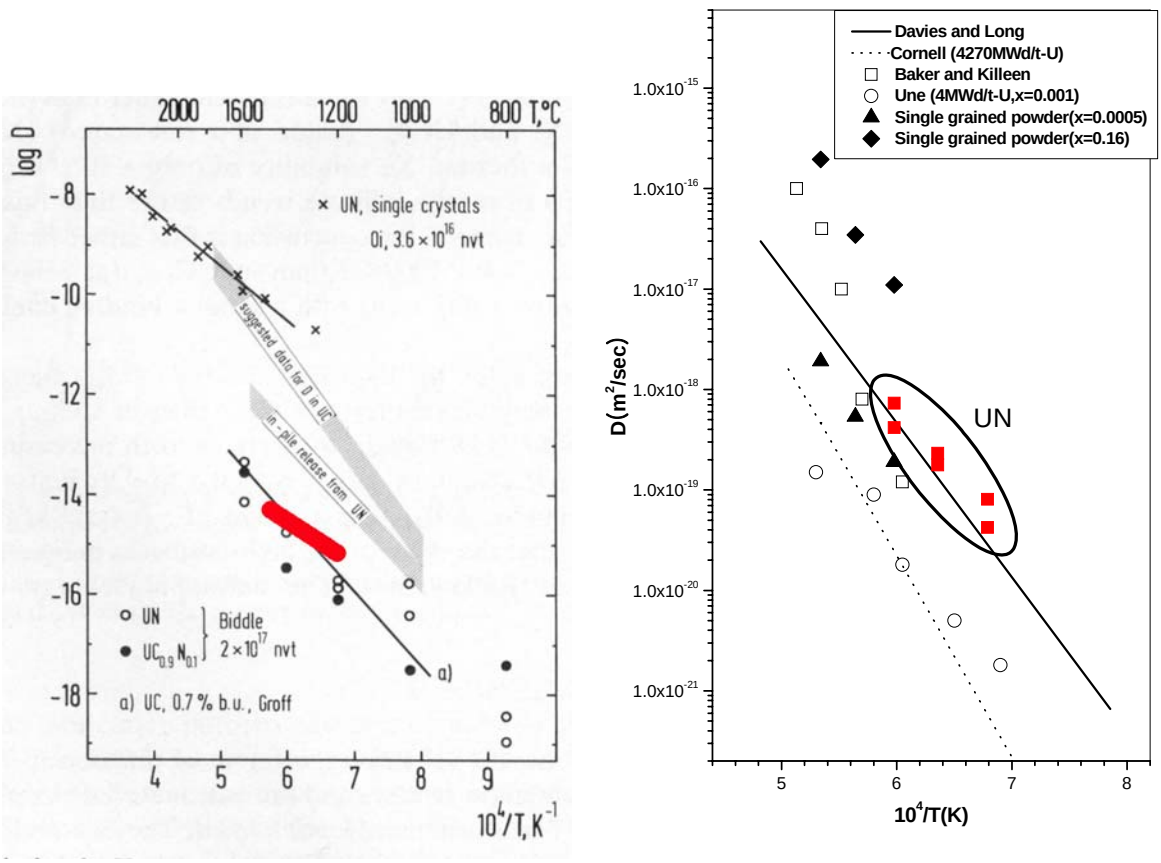

FIG. 8. Xe-133 diffusion coefficients in UN and comparison with UO_2

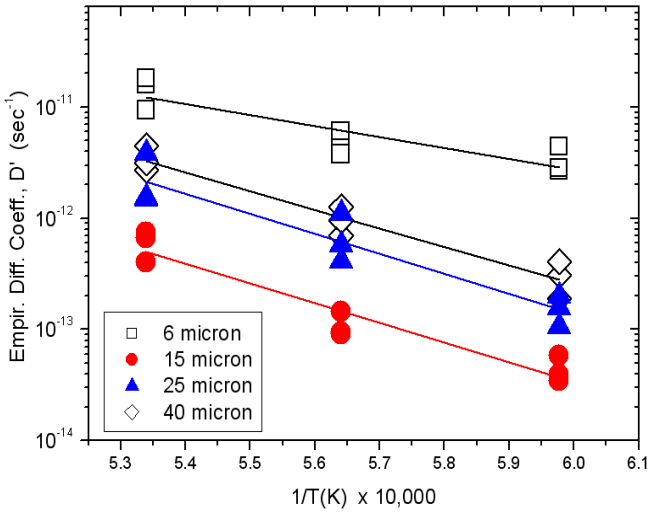

FIG. 9. Xe-133 diffusion coefficients in UO_2 with various grain sizes

4. Conclusions

Many samples with various conditions were used to observe Xe-133 diffusion for over 10 years. A PIA test was good for measuring the xenon diffusion. The xenon diffusion showed a different behavior with the temperature, oxygen potential, additives, grain size, and different fuel type. Generally, xenon diffusion in UO_2 was higher with higher oxygen potential and valence of additive, and a thorium oxide reduced the xenon diffusivity based on higher bonding energy. Nitride sample showed similar behavior of UO_2 even though different structure. The xenon gas release in larger grained UO_2 was smaller, but data of some samples were observed with abnormal trend. It will be studied with porosity effect.

Even though the surface area measurement was not applied and single crystal samples were not prepared, most results were reasonable except a few, which will be studied continuously. It will be possible to study a disk coordinate instead of the Booth theory(spherical coordinate) for a fractional release because most samples were disk shaped. With this experience, the PIA for metallic fuel(U-Zr) will be performed to observe xenon mobility.

5. References

[1] H.H.Wong, 'ELESTRES.M9C User's manual and Code Description', CWAPD-347 (1980)
[2] D.D.Lanning, C.E.Beyer, C.L.Painter, 'FRAPCON-3 : Modifications to Fuel Rod Material Properties and Performance Models for High-Burnup Application', NUREC/CR-6534(1997)
[3] C.S.Rim, C.E.Beyer,'Background and derivation of ANS 5.4 standard fission product release model', NUREG/CR-2507(1982)
[4] K.Forsberg, A.R.Massih,'Diffusion theory of fission gas migration in irradiated nuclear fuel UO_2.', J.Nucl.Mater 135(1985)140
[5] A.H.Booth, 'A Method of Calculating Fission Gas Diffusion from UO_2 Fuel and Its Application to The x-2-f Loop Test.', CRDC-721 (1957)
[6] J. R. MacEwan and W. H. Stevens, J. Nucl. Mater., 11 (1964) 77
[7] Hj.Matzke, 'Gas release mechanisms in UO_2-A critical review.', Radiation Effects, 53 (1980) 219-242
[8] K.Shiba, A.Itoh, M.Ugajin, 'Fission xenon release from lightly irradiated (Th,U)O_2 powders.', J.Nucl.Mater. 96 (1981) 255
[9] Hj. Matzke, 1986, Science of Advanced LMFBR Fuels", North-Holland.
[10] A.G.Croff, " A user manual for the ORIGEN2 computer code", ORNL/TM-7175(1980)
[11] H.Kim, et al,"Xenon Diffusivity in Thoria-Urania Fuel.", Nuclear Technology, 147, pp.149, 2004
[12] K.Bakker, E.H.P.Cordfunke, R.J.M.Konings, R.P.C.Schram,'Critical evaluation of the thermal properties of ThO_2 and $Th_{1-y}U_yO_2$ and survey of the literature on $Th_{1-y}Pu_yO_2$.', J.Nucl.Mater. 250 (1997)
[13] H.Kim, K.Park, et. al., 'Diffusion Coefficient of Xe-133 in a SIMFUEL with a low Burnup', Annals of Nuclear Energy, vol.34 (2007) 153-158

POST-IRRADIATION EXAMINATION OF HIGH BURNUP FUEL RODS FROM VANDELLOS II

IGNACIO ARANA, CRISTINA MUÑOZ-REJA,
ENUSA Industrias Avanzadas, S.A
Santiago Rusiñol, 12. 28040 Madrid. Spain

FRANCISCO CULEBRAS
Asociación Nuclear Ascó-Vandellós II
Edificio Sede L´Hospitalet de l´Infant 43890 Tarragona. Spain

ABSTRACT *-As the nuclear power generating industry has matured there has been an increase in core operating fuel duties. To support these conditions the fuel designs have been continuously improving in several areas. In the continuing evolution of fuel and more specifically pellets, to provide performance margin and support higher fuel duty designs, ENUSA and ANAV conducted a High Burnup Irradiation Program that consisted on irradiating four assemblies in C.N. Vandellós II up to an approximate fuel assembly burnup of 70 MWd/kgU in four eighteen month cycles. Material from this program has been extensively used in several research programs all over the world.*

Eight rods from the High Burnup Program with discharge burnup in the range 64.0-74.5 MWd/kgU were selected to be characterized in a Post Irradiation Examination (PIE). The PIE program was completed with four additional fuel rods irradiated in C.N. Vandellós II. These standard rods were irradiated two eighteen month cycles at high power with discharge burnup up to 52 MWd/kgU.

Thus, the characterized fuel has been operated under high duty conditions, as high power and high burnup. Moreover, the selection of the twelve fuel rods intends to cover several fuel features as different pellet densities from standard to high densities, and a wide range of gadolinia concentrations from the 0% of the UO_2 fuel rods till 2% and 8%.

The paper will present the bases for the definition of this extensive test matrix focused on the improvement of the knowledge on two of the main key performance characteristics of pellets, as densification and fission gas released of high density and variable concentrations of gadolinia fuels. It will also describe how the results of the program will be used to adjust the fuel rod design models by reducing the uncertainties at high fuel power and burnup.

1. Introduction

In the year 2000, the PWR utility Asociación Nuclear Ascó-Vandellós II (ANAV) and ENUSA Industrias Avanzadas jointly launched the High Burnup Irradiation Program (Programa de Alto Quemado, PAQ) in order to understand the margin available at high burnups and high residence times.

The PAQ is part of a more ambitious program conducted by ENUSA and the PWR Spanish utilities to achieve the highest level of fuel reliability in the Spanish PWR plants fueled by ENUSA, the Coordinated Research Program (Programa de Investigación Coordinada, PIC), which objectives are to surveillance product changes and monitor the effect on the fuel of the changes in the plant operating conditions such as power or chemistry.

During the development of these programs, ENUSA in collaboration with technological partners and customers has presented the main results and conclusions at international congresses. A good overview of the PIC program results is given in [1]. The results of the fuel assembly performance at high burnup from the PAQ program have been released in [2].

In this frame, eight rods from the PAQ with discharge burnup in the range 64.0-74.5 MWd/kgU were selected to be characterized in a Post Irradiation Examination (PIE). The PIE program was completed with four additional fuel rods coming from the PIC irradiated in C.N. Vandellós II. These standard rods were irradiated two eighteen month cycles at high power with discharge burnup up to 52.0 MWd/kgU.

2. Objective

The main objective of the PIE of fuel rods irradiated in C.N. Vandellós II is to extend the database on fission gas released and net fuel swelling by including standard and high density fuel results and variable concentrations of gadolinia data, irradiated under high duty conditions. The main features of the fuel rods characterized in hot cells are as follows:

- Low gadolinia concentration pellets irradiated at high power
- High gadolinia concentration pellets irradiated at high burnup
- Standard density UO_2 pellets irradiated at high power
- High density UO_2 pellets irradiated at high burnup

Additionally, the hot cell program is completed with other examinations such as rod visual inspection, clad corrosion and hydriding measurements, clad metallographies and fuel rod growth. All the information generated will be incorporated to the ENUSA databases on fuel behavior and will be used to feed back the fuel performance models used to design and license fuel operation.

3. Material tested in the hot cell pogram

The material selected for the hot cell program comprised 8 fuel rods coming from the PAQ and 4 from the PIC. These rods were extracted from the fuel, inspected in-site and transported to the Studsvik Nuclear AB laboratory in Sweden. Table I describes the main characteristics of the fuel rods hot cell examined.

# rods	Description. Fuel type and irradiation conditions	Gad conc., %	Nominal density, % T.D.	Irradiation cycles	Rod burnup, MWd/kgU
2	Low gadolinia concentration and high power	2	95.5	14-15	49.6-50.9
1	High gadolinia concentration and high burnup	8	96.0	12-15	54.4
2	UO_2 standard density at high power	---	95.5	14-15	51.4-51.9
5	UO_2 standard density at high burnup	---	96.0	12-15	64.0-73.8
2	UO_2 high density at high burnup	---	97.0	12-15	64.2-64.4

Table I. Fuel rod characteristics

4. Test matrix

To reach the main objective of extending the experimental database on fission gas released and net fuel swelling, the test matrix was designed as follows:

- Fission gas release on 100% of the fuel rods
- Net fuel swelling. 2 samples on each of the 12 fuel rods.

5. Results and discussion

The hot cell characterization program was developed according to the initial plan without any incident. This section provides the test results and discusses its conclusions. To complete the analysis, it has been compared the PIE results with the performance models used by ENUSA for design and licensing purposes.

For both type of characteristics, the measurements have been performed in accordance to standard laboratory techniques.

5.1. Fission gas released

Figure I depicts the fission gas release of the fuel rods taking part in the program. The results obtained in the rods that have operated at high power show a similar performance compared to the current experience. In addition to experience a higher fission gas release at higher burnups, it is also observed an enhanced gas release for the rods that have operated at higher power levels. This response is consistent with the experience and the accepted theories which consider the fuel temperature as a major contributor to the fission gas release, and the fuel temperature in turn depends basically on the rod power.

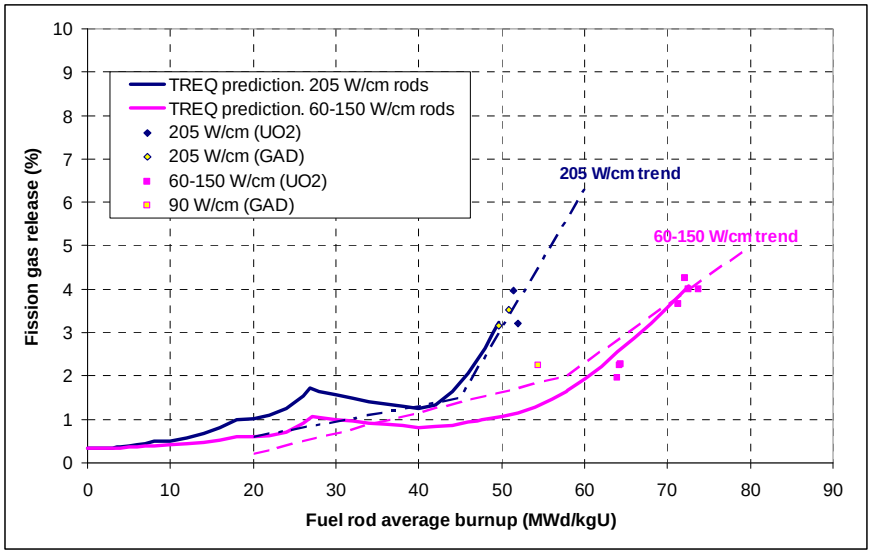

Fig. I Fission gas release results and its prediction with code TREQ

The measurements plotted in Figure I and the fission gas release trends as a function of burnup and final rod average power indicate that the athermal component is predominant at rod powers below 150 W/cm and that the thermal fission gas released is activated for rod powers above 150-200 W/cm. Figure I also provides the predictions with the fuel rod thermal-mechanical code TREQ used by ENUSA, and that accounts for fuel thermal conductivity degradation. It can be observed the high prediction accuracy of the fission gas release model incorporated to TREQ under high duty conditions as high burnup and high power during irradiation. This prediction capability is valid for several fuel features as pellet density and gadolinia concentration variation.

5.2. Net swelling

The results obtained in the laboratory were properly corrected to account for the clad and oxide volumes and masses.

Based on the density values before and after operation, it is calculated the volumetric increment of the pellet due to net fuel swelling and swelling during irradiation. Figure II plots the fuel volume increment as a function of local burnup.

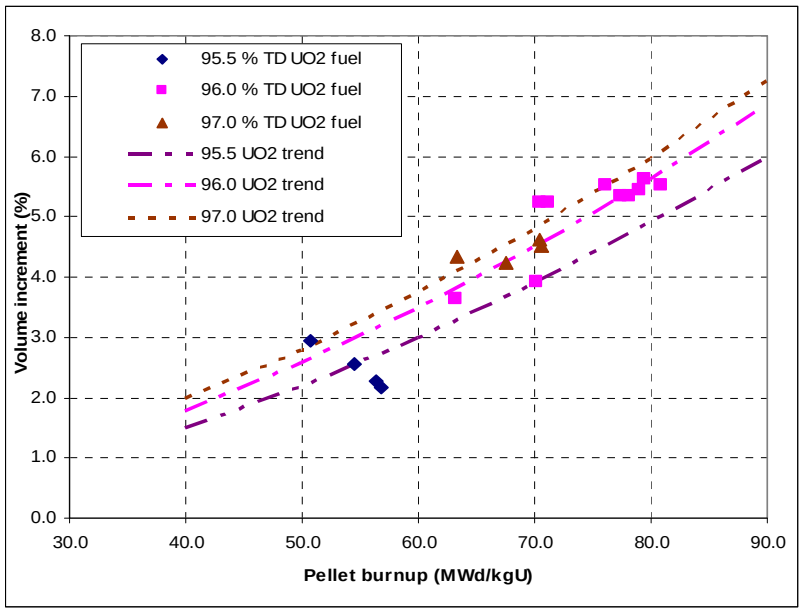

Figure II. Volume increment

It is observed that at discharge burnups between 50 and 60 MWd/kgU, the volume increase is close to 3% of the initial volume. These results are consistent with the experience.

Compared to fuel with burnup between 50 and 60 MWd/kgU, the high burnup fuel has experienced more swelling mainly due to the higher burnup. In accordance to this trend, it can be concluded that high burnups favor the fuel swelling but up to average rod burnups of 75 MWd/kgU (≈ 80 MWd/kgU local burnups), the net fuel swelling is not accelerated.

To a lesser extent, the higher initial density, 96.0-97.0 % T.D respect to 95.5 % T.D (the standard fuel currently manufactured), increases the net fuel swelling at end of life. This performance is attributable to the lower densification at beginning of life driven by the lower fine porosity volume in the high density fuel. In any case, the difference in net fuel swelling as a function of initial density is not as significant as the influence of the fuel burnup.

Additionally, at discharge burnups around 50.0-60.0 MWd/kgU, it is observed that the net swelling of the gadolinia fuel is very similar to the observed in the UO_2 fuel.

In regards of the predictions on net fuel swelling, the analysis conducted preliminary concludes that the design model captures properly the densification and swelling response of the UO_2 pellets as a function of fuel density and burnup. For the gadolinia fuel, the first evaluation determines that the densification and swelling models tend to underpredict the net fuel volume.

6. Future programs

The hot cell program conducted on the fuel rods irradiated in C.N.Vandellós II is the kernel of international collaboration programs. Currently, ENUSA participates in several international investigation programs where additional material coming from the hot cell program will be tested. Two of them will further investigate on the pellet characteristics and performance.

The first is the Halden IFA-720 project which objective is to research into gadolinia pellet characteristics such as thermal conductivity and to investigate deeper on key performance phenomena like fission gas release and swelling. The remaining program will be held in the frame of the SCIP-II project, that among other analyses, will study the influence of the pellet characteristics on the fuel rod failure mechanism due to Pellet clad mechanical interaction, PCMI.

7. Conclusions

The PWR utility Asociación Nuclear Ascó-Vandellós II (ANAV) and ENUSA Industrias Avanzadas jointly launched the High Burnup Irradiation Program (Programa de Alto Quemado, PAQ) in order to understand the margin available at high burnups and residence times. The PAQ is part of a more ambitious program conducted by ENUSA and the PWR Spanish utilities to achieve the highest level of fuel reliability in the Spanish PWR plants fueled by ENUSA, the Coordinated Research Program (Programa de Investigación Coordinada, PIC), which objectives are to surveillance product changes and monitor the effect on the fuel of changes in the plant operating conditions such as power or chemistry. Once the fuel operation concluded, it was decided to perform a Post Irradiation Examination (PIE) in order to understand the margin available at high burnups and high residence times.

The main objective of the PIE of fuel rods irradiated in C.N. Vandellós II was to extend the database on fission gas release and fuel net fuel swelling by including high density fuel and variable concentrations of gadolinia data, irradiated under high duty conditions. The material selected for the hot cell program comprised 8 fuel rods coming from the PAQ with discharge burnup ≈ 64.0-74.5 MWd/kgU and 4 additional rods of burnup ≈ 52.0 MWd/kgU.

The main conclusions from the PIE can be summarized as follows.

Fission gas released.

- The results obtained in the rods that have operated at high duty show a consistent performance compared to the database.
- In addition to experience a higher fission gas release at high burnups, it is also observed an enhanced gas release for the rods that have operated at higher power levels.
- The fuel rod thermal-mechanical code TREQ used by ENUSA, and that accounts for fuel thermal conductivity degradation predicts with a high accuracy level the gas release under high duty conditions as high burnup and high power during steady state operation.

Net fuel swelling.

- The volume increase of the UO_2 rods with discharge burnups between 50 and 60 MWd/kgU is consistently with the experience, close to 3% of the initial volume.
- The high burnup fuel has experienced more swelling mainly due to the higher burnup, but up to average rod burnups of 75 MWd/kgU, the net fuel swelling is not accelerated.
- At discharge burnups around 50.0-60.0 MWd/kgU, it is observed that the net swelling of the gadolinia fuel is very similar to the observed in the UO_2 fuel.

8. References

1. C. Muñoz-Reja, M. Quecedo, J.A.Gago and M. Novo. PWR fuel surveillance in Spain: a decade of fuel examinations, Top fuel meeting, Orlando, Florida, USA (Sept 2010)

2. M. Aulló, J.M. García-Infanta, D. Chapin, J.L. Gago, A. Pontejo, J. Sanchez. Post irradiation examination of high burnup assemblies in Vandellòs II, Top fuel meeting, Orlando, Florida, USA (Sept 2010)

SUCCESSFUL HIGH BURNUP IRRADIATION CAMPAIGN OF THE GE14 LUAS AT TVO'S OL1 REACTOR: INSPECTION RESULTS AND ASSESSMENTS

R. DUNAVANT, M. JAHINGIR, R. SCHNEIDER
Global Nuclear Fuel-Americas
PO Box 780, Wilmington, NC 28402, USA

N. DONCEL, C. MUÑOZ-REJA
ENUSA Industrias Avanzadas
Santiago Rusiñol 12, 28760 Madrid, Spain

ARTTU KNUUTILA, KARI RANTA-PUSKA
Teollisuuden Voima Oyj
Töölönkatu 4, FI-00100, Helsinki, Finland

ABSTRACT

TVO initiated a high burnup irradiation campaign in 2004 primarily to investigate fuel performance phenomena that have the potential to limit fuel discharge burnup. To support TVO's pursuit of higher burnup, GNF/ENUSA Nuclear Fuel, S.A. (GENUSA) fabricated and delivered eight GE14 Lead Use Assemblies (LUAs) to TVO for irradiation in the OL1 reactor. Demanding irradiation conditions were chosen for these LUAs with several of them irradiated for four to five cycles up to a bundle average burnup of ~50 MWd/kgU. In 2006, after 2 cycles of irradiation, cladding oxidation was measured in selected rods. In 2008, fission gas release was non-destructively measured via ^{85}Kr gamma scanning of 20 rods after 3 cycles of irradiation. After the measurements, this LUA was reconstructed and reinserted in the core for one additional cycle of irradiation. In 2010, fission gas release was measured on two high burnup bundles, including 15 rods that were measured in 2008 to determine the incremental fission gas release due to the one additional cycle of irradiation. In addition, cladding oxidation was measured on two high burnup bundles. Cladding oxidation measurements both from the 2006 and 2010 campaigns are as expected for their respective burnups. The fission gas release measurements from the 2008 and 2010 campaigns are well within the GENUSA experience and are conservatively predicted by the GENUSA fuel rod design and licensing methodology, PRIME03. End-of-life rod internal pressures for these rods, as converted from the measured fission gas release, mostly remained below the system pressure, and thus, demonstrated thermal-mechanical margin and supported TVO for licensing higher burnup of 50 MWd/kgU.

1. Introduction

In 2004, TVO initiated a high burnup irradiation campaign to increase the maximum bundle-average discharge burnup to 50-55 MWd/kgU in its reactors. To support the effort, GNF/ENUSA Nuclear Fuel, S.A. (GENUSA) fabricated and delivered eight GE14 Lead Use Assemblies (LUAs) to TVO for an irradiation campaign in the OL1 reactor.

The focus of this LUA campaign was to investigate fuel rod and bundle components dimensional stability, oxidation and fission gas release (FGR) and its impact on fuel rod end of life pressure. There is a special interest in the FGR measurements to understand the fuel rod state at higher burnup and to investigate whether the rod internal pressure requirement in the STUK regulatory guide YVL 6.2 [1] can be fulfilled. Currently, STUK regulatory guide YVL 6.2 implies a very conservative limit for the rod internal pressure, requiring demonstration that the rod internal pressure would not exceed the system pressure at the

end of life (EOL), whereas most other countries apply less demanding “no-lift-off” criteria. Recently, somewhat more relaxed criterion has been accepted by the authority, in which with good confidence 95 % of the rods shall have internal pressure below the system pressure.

Also, cladding oxidation at higher burnup was investigated to assess its impact on fuel rod integrity, as it has the potential to significantly impact cladding dimensional stability and mechanical properties at higher burnup.

In 2006, after 2 cycles of irradiation (bundle average burnup ~27 MWd/kgU), cladding oxidation was measured in selected rods. In 2008, fission gas release was non-destructively measured (^{85}Kr gamma scanning) from 20 rods after 3 cycles of irradiation (bundle average burnup ~40 MWd/kgU). After these measurements, this LUA was reconstructed and reinserted in the core for one additional cycle of irradiation achieving a bundle average burnup of ~48 MWd/kgU. In 2010, cladding oxidation was again measured and most of the rods measured for fission gas release in 2008 were re-measured to determine the incremental fission gas release when moving from "nominal" burnup range to higher EOL burnup range. In addition, ^{85}Kr gamma scanning was performed on another 15 rods from a discharged reload bundle (~44 MWd/kgU). Cladding oxidation was also measured during the 2010 measurement campaign.

The results from the first inspection campaigns performed in the 2005-2006 timeframe, after one and two annual cycles of operation, were reported in [2]. This paper summarizes the operating history, fission gas release, and cladding oxidation data collected from these high burnup GE14 LUAs and also discusses the adequacy of the GE14 design for high burnup application. This paper also briefly discusses the analysis and modelling techniques applied for converting the ^{85}Kr activity measurements to fission gas release and rod internal pressure and will report a comparison of the fission gas release measurements with the GENUSA fuel rod design and licensing methodology, PRIME03 [3].

2. Fuel Design

The Nordic GE14 fuel assembly consists of a fuel bundle and a channel which surrounds it. The fuel bundle contains both fuel rods (full and part-length) and water rod(s) supported in a square array by the upper and lower tie plates and fuel rod spacers. The fuel rod cladding is GENUSA standard barrier cladding, which is comprised of Zircaloy-2 tubes with a metallurgically bonded inner zirconium layer. The GE14 LUAs nuclear design is derived from the GE14 bundle design for an equilibrium cycle, modified to accommodate the available enrichments and gadolinia contents at the time of manufacturing. The eight LUAs have the same design with some rods containing 4 wt% Gd_2O_3 and enrichments ranged from 2.0 to 4.9 wt% ^{235}U.

3. Operational Information

Demanding irradiation conditions were chosen for these LUAs with several of them irradiated for four cycles as shown in Table 1. The inspected LUA with four irradiation cycles had high power ratings during the last two cycles, reaching a bundle average discharge burnup of 48.7 MWd/kgU, above the licensing limit of 45 MWd/kgU that existed at that time. The maximum rod burnup at end of life, from the measured rods, is around 55 MWd/kgU.

Table 1. Operational history for the inspected GE14 LUAs

OL1 Cycle	Bundle Avg. Burnup MWd/kgU	Cycle Average LHGR kW/m
26	14.4	24 – 29
27	27.5	22 – 25
28	40.0	19 – 21
30	48.7	13 – 17

During each campaign a selected number of rods have been inspected, with consideration for minimizing disturbances in the reload activities while providing enough information for the surveillance of the bundles.

4. Measurement Methods and Equipment

The fuel visual inspections were performed using a TVO supplied high-resolution colour underwater TV camera installed in the fuel storage pool, with DVD recording. The fuel rod oxide liftoff and the fuel rod profilometry (diameter) measurements were performed with the SICOM-ROD, equipment provided by GENUSA and TECNATOM. Fission gas release was determined non-destructively by measurements of gamma activity in the selected rods at the OL1 storage pool. Measurement of ^{85}Kr activity in the plenums of individual fuel rods was performed using the Water Submersible Gamma Scanner (WSGS) equipment, provided by GENUSA.

5. Data Evaluation

5.1. Visual Inspection, Dimensional Stability and Oxide Thickness

One bundle and its channel were inspected visually on all four sides during the 2005 outage. After one annual cycle of operation, the channel, bundle, and the fuel rods were in good condition as expected.

In 2006, after two annual cycles, the bundle was visually inspected and rod oxide thickness measurements were made on the selected rods. The oxide thickness for these rods was generally 5 to 15 μm, which is a typical range for rods irradiated for two annual cycles; the profiles were consistent among different circumferential orientations [2].

During the 2010 inspection, after four cycles of irradiation, detailed bundle peripheral component inspections were performed to assure the assemblies are performing as designed. As shown in Figure 1, the fit-up at the top of the bundle is as expected: e.g., no unusual responses in rod growth, expansion spring compression, tie rod nut capture, etc. was observed. Rod-to-rod spacing is normal, within GNF's design limits. There was very light crud deposition on the lower and upper tie plate. The debris filter lower tie plate (DFLTP) showed no build-up of crud in the flow holes and was viewed from all possible angles to include all the holes. Spacer structural integrity is maintained. It should be noted that after five cycles of irradiation, and burnups ~53 MWd/kgU, some difficulties were encountered while trying to lift the bundle out of the channel, believed to be due to Zry-2 spacer growth. Rather than risk handling damage, it was decided to not remove these bundles.

Visual inspection of the peripheral rods shows a typical, stable surface oxide layer, maintaining its integrity (no spalling). Overall crud deposition was considered moderate, and diminished on the cladding at elevations above the top spacer. The spacers were properly positioned and had negligible crud deposition.

Ten rods were removed and measured by SICOM-ROD for oxide thickness and profilometry using LVDT. The profilometry data indicated no observable increase in clad diameter.

The oxide thickness data indicates liftoff values consistent with the visual observations during the inspection. These oxide results have been compared within GNF's historic corrosion database; results are well within the experience base for GENUSA fuel at these burnups.

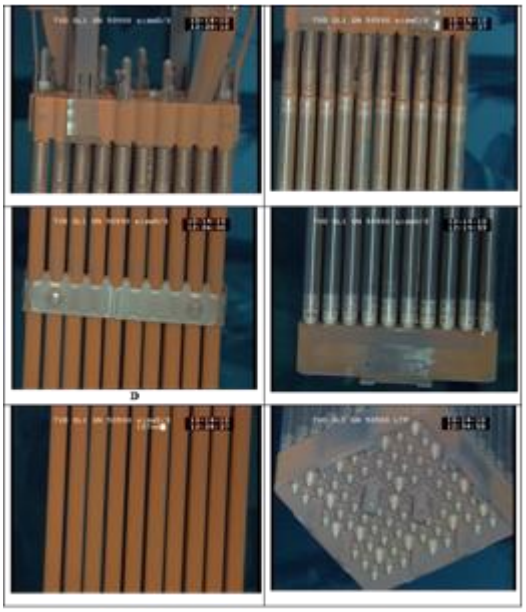

Figure 1. Pictures of Nordic GE14 LUA after four cycles of irradiation

5.2. Gamma Scanning

The 2008 gamma scanning campaign consisted of 20 rods from LUA bundle 50500. The 2010 gamma scanning campaign consisted of gamma scanning of rods from two bundles, LUA bundle 50500 and reload bundle 50519. Fifteen rods were measured from each of the bundles. The enrichment of the measured rods range from 1.6 to 4.9 wt% ^{235}U; four of the rods, two from each bundle, also contain 4 wt% Gd. The measured rods from LUA bundle 50500 were also previously measured in 2008. At the time of the 2008 gamma scanning, bundle 50500 had undergone 3 irradiation cycles and the burnup for the 15 re-measured rods ranged from 34 to 45 MWd/kgU. In 2010, after the fourth irradiation cycle of bundle 50500, measured rods covered a wide range of average burnups, i.e., from 37 to 55 MWd/kgU.

The core location and general irradiation history of the LUA bundle that underwent gamma scanning in 2008 and 2010 for each irradiation cycle is indicated in Figures 2 and 3. Like the rod burnups, there were large rod to rod variations in rod powers depending on the location in the bundle. Gamma scanning is a non-destructive method to determine the relative fission product inventory in nuclear fuel. It measures several aspects of the fuel, determined by the isotope measured and the scanner configuration. The goal of the 2008 and 2010 gamma scanning campaigns was to determine the ^{85}Kr concentration in the subject rods. The measured concentration of ^{85}Kr combined with total cold void volume, calculated by the GENUSA thermal-mechanical code PRIME03, determines the total amount of ^{85}Kr released to the rod void volume. The total amount of ^{85}Kr in each rod at the time of the measurement is then calculated using ORIGEN. Combining these results, the measured FGR was calculated as the ratio of the ^{85}Kr measured in the rod void volume to the total amount of ^{85}Kr present in the rod from ORIGEN. Rod internal pressures at operating conditions were also determined based on the measured FGR. Rod internal pressure was determined from the rod void volume and temperature distribution combined with the total amount of gas present in the rod. The total moles of gas present in the rod are calculated by adding the measured FGR to the amount of helium present in the rod (from helium pre-pressurization and PRIME03 predicted helium generation). PRIME03 is also utilized to determine the temperature distribution of the gas in the rod void at reactor operating conditions. The predicted temperature distribution, void volume, and the total moles of gas in the rod are used to calculate rod internal pressure via the ideal gas law. FGR fractions and rod internal pressure measurement results are summarized in Figure 4 and are grouped by campaign.

The FGR is highest in rods with highest burnups. The ratios of PRIME03 predicted/measured FGR as a function of burnup are shown in Figure 5.

In addition to ^{85}Kr measurements, some of the rods were measured for the ^{137}Cs activity along the active length of the fuel rod to determine the relative axial burnup profile. An example of such measurement for one rod from bundle 50500 is shown in Figure 6. The Figure shows also a comparison to the calculated result by the SIMULATE-3 reactor simulator that used for core tracking at TVO.

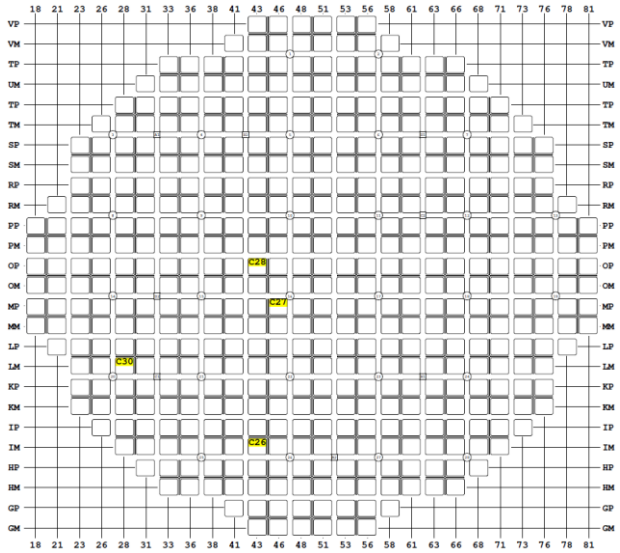

Figure 2. LUA Bundle 50500 Core Locations

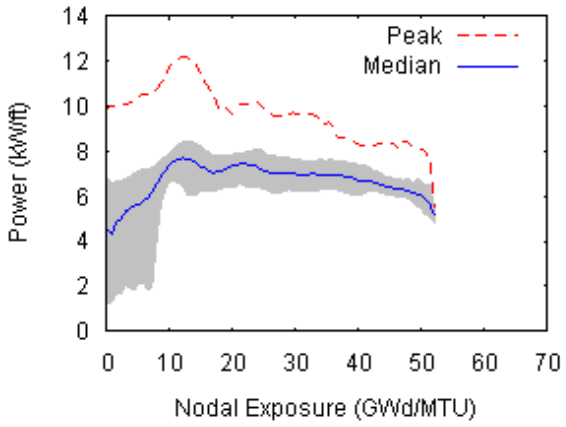

Figure 3. LUA Bundle 50500 Irradiation History

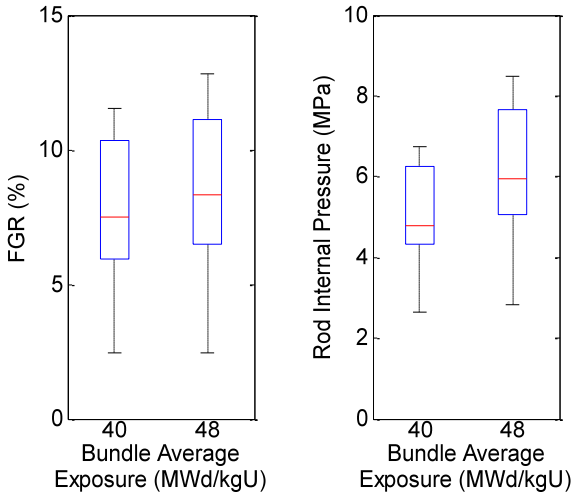

Figure 4. LUA Bundle 50500 Summary of Fission Gas Release and Rod Internal Pressure Measurements

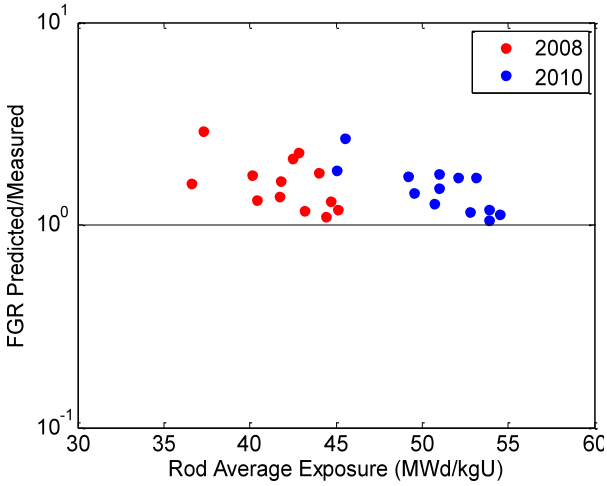

Figure 5. PRIME03 Predicted/Measured FGR

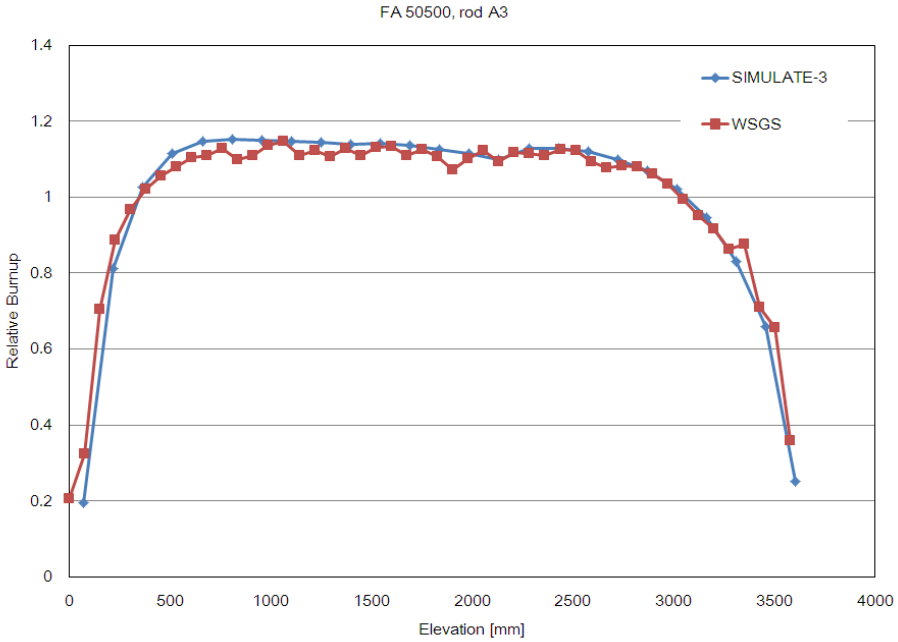

Figure 6. Calculated and measured axial relative burnup profile

6. Conclusions

The GE14 high burnup LUA campaign at OL1 has been successfully completed. Several key fuel performance data were collected during the 2006, 2008 and 2010 measurement campaigns, including visuals, oxidation, FGR, etc. All visible fuel bundle components performed as expected for their respective burnup, with normal rod-to-rod spacing, no hardware items bent or out of place, and no difficulties in exchanging fuel rods. Visual inspection of the peripheral rods shows very minimal to no oxide spalling and as-expected oxide and crud depositions. The shape of both, oxide thickness and profilometry traces, are consistent across a large number of rods/traces. Therefore, there is no indication of any strong axial or azimuthal variation indicative of unusual crud or corrosion. The observed liftoff values are well within the experience base for GENUSA fuel at this burnup range.

The ^{85}Kr gamma scanning campaigns provided valuable data for high burnup fuel rods. Additionally, the campaigns resulted in a unique set of fission gas release measurement data for identical rods from 2008 and 2010 (after an additional cycle of irradiation). These measurement data are well within the GENUSA experience. A comparison of PRIME03 predicted to measured FGR shows that PRIME03 is nominally conservative and predicts fission gas release well at higher burnups. Rod internal pressures for these rods, as determined from the measured fission gas release, mostly remained below the system pressure, and thus, demonstrated thermal-mechanical margin and supported TVO for licensing higher burnup of 50 MWd/kgU in 2010.

7. References

1. STUK regulatory guides, “YVL 6.2 Design bases and general design criteria for nuclear fuel”. Nov. 1999.
2. K. Ranta-Puska et al; “TVO’s Measurement Campaign for GE14 Lead Use Assemblies. Pursuing Higher Burnup”. Proceedings of the 2006 International Meeting on LWR Fuel Performance, Salamanca (2006).
3. Jahingir, M., et al., “High Burnup Fuel Behaviour Modelling,” Paper 1062, 2007 International LWR Fuel Performance Meeting San Francisco, California, September 30 – October 3, 2007.

IN-CORE FUEL MANAGEMENT WITH MIXED FUEL ASSEMBLIES FOR BELGIAN NUCLEAR POWER PLANTS

HUBERT DRUENNE, JINZHAO ZHANG
Nuclear Department, Tractebel Engineering (GDF SUEZ)
Avenue Ariane 7, B-1200 Brussels, Belgium
Phone: +32.2.7739843, Fax:+ 32.2.7738900,
E-mail: hubert.druenne@gdfsuez.com, jinzhao.zhang@gdfsuez.com

FEMKE FLACHET
Nuclear Fuel Management, ELECTRABEL (GDF SUEZ)
Avenue Ariane 7, B-1200 Brussels, Belgium
Phone: +32.2. 505.07.46, Fax:+ 32.2. 505.07.90, E-mail: femke.flachet@electrabel.com

ABSTRACT

In this paper, the definition, principle and technical bases of the ICFM with mixed fuel assemblies are first described, followed by the applicability and limitations of the approach. The next sections present the concepts of reference fuel and reference core as they are used in the safety analysis performed and licensed in Belgium, and how the reload safety evaluation is handled, both for a new fuel and for new loading patterns. The additional aspects for treatment of the transition mixed core are then discussed in the following section, and the last section gives an insight of the Belgian experience with mixed cores.

1. Introduction

In Belgium, fuel supply and manufacture for the existing 7 nuclear power plants are subject to open competition. As a consequence, in-core fuel management (ICFM) with mixed fuel assemblies becomes a normal practice. Therefore, a practical approach has been developed for the final safety analysis report (FSAR) accident analysis and the reload safety evaluation, consistent with the requirements of the Belgian Safety Authorities (BSA) [1-2].

This safety demonstration is based on a decoupled approach between the analyses performed by various disciplines: neutronics, core thermal-hydraulics, system thermal-hydraulics, fuel rod thermal-mechanics and assembly mechanics. In this framework, the compatibility of a new fuel design with the FSAR on the one hand is possible through the verification of a limited number of interface parameters and specific calculations; and on the other hand, its compatibility with other co-resident fuel in the core requires some complementary verification. This approach is possible through allocation of margins in the reference core and fuel used in the FSAR accident analysis.

In this paper, the definition, principle and technical bases of the ICFM with mixed fuel assemblies are first described, followed by the applicability and limitations of the approach. The next sections present the concepts of reference fuel and reference core as they are used in the safety analysis performed and licensed in Belgium, and how the reload safety evaluation is handled, both for a new fuel and for new loading patterns. The additional aspects for treatment of the transition mixed core are then discussed in the following section, and the last section gives an insight of the Belgian experience with mixed cores.

2. Principle and technical bases

In the standard safety analyses, the main disciplines are decoupled from each other, and the links between each are insured by a limited number of physical interface parameters. The standard safety analyses are usually based on a *reference fuel* and a *reference core.* For these analyses to remain bounding of fuel design or loading pattern changes, adequate *design provisions* are applied in the analyses. The compatibility of a new fuel design can be limited to the verification of the bounding character of the interface parameters.

2.1. Principle of margin allocation

In the reference safety analysis, a *safety margin* must always be kept between the *safety limit* and the acceptance *safety criterion* (Figure 1); but other margins are considered as well.

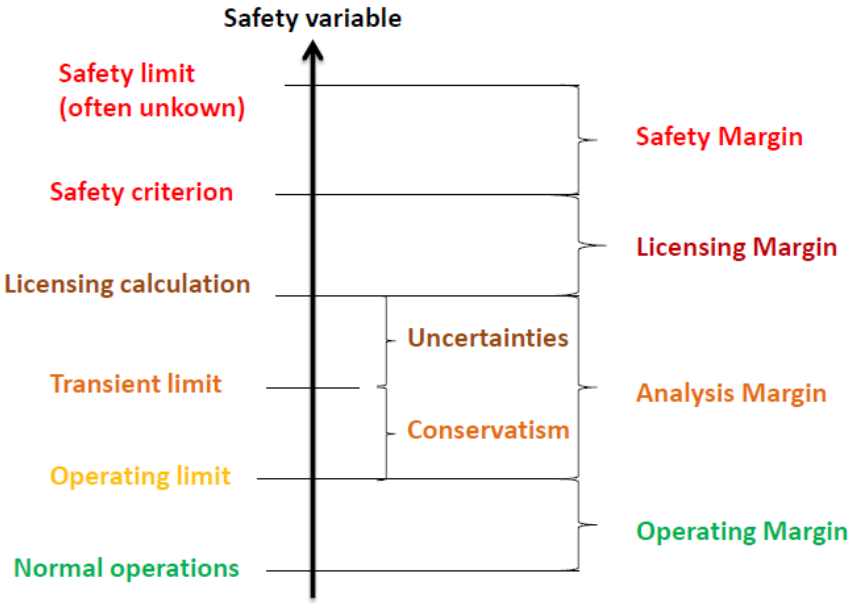

Figure 1: Margins in reference safety analysis.

The licensing margin is the difference between the maximal value calculated for the related physical parameter during the analyzed transient and the acceptance safety criterion; the analysis margin is the difference between the operating limit and the maximal value calculated for the related physical parameter during the analyzed transient. The operating margin has to be provided to ensure plant operation flexibility and reliability.

The *analysis margin* consists of the *conservatism* on the following assumptions:

- physical data which characterize the *reference core* and *reference fuel* (*design provision*);
- the performance of the plant safety related systems (in particular, the protection systems and the safeguard systems) which are involved in the analyzed transient;
- the values of the parameters which characterize the operating point at the beginning of the transient: these values shall be the envelope of all the initial conditions of normal operations

and the *uncertainties* related to the analysis:

- individual modelling or overall code uncertainties;
- representation uncertainties, numerical inadequacies;
- user effects, computer / compiler effects; and
- data uncertainties on the analysis of an individual event

which shall be determined either by conservative calculation or by best-estimate calculation plus uncertainty evaluation. An improvement of the codes and a quantification of the uncertainties can be made through extensive code verification and validation, which will again allow increasing the design provision or operating limit.

The *design provisions* on physical data of the core and fuel are allocated for later justification of different core and fuel designs.

2.2. Principle of decoupling in the reference safety analyses

2.2.1. Standard safety analyses

The plant transient behaviours during accidents are modelled with system T/H code. In such a code, the core protection is accurately modelled, but the core is usually represented by a simplified model (point kinetic or 1 dimensional axial kinetic model, and simplified Departure from Nucleate Boiling or DNB correlation).

The neutronic data (the Nuclear Key Safety Parameters - NKSP), which are necessary to feed the simplified core model, are calculated with full core neutronic model of the *reference core*. The same core model is also used to provide the power distributions (peaking factors and fuel census in various configurations) and power histories for fuel rod design and residual heat evaluation.

The *reference core* is an equilibrium ICFM scheme representative of the expected operation. This reference core aims to prove the ability of this operation to meet the main neutronic limits, and to provide the nuclear parameters for accident analyses. Adequate *design provisions* are applied to cope with limited future changes in the ICFM.

The core protection set points are derived from the core thermal limits (CTL) which are calculated for the *reference fuel.* The same thermal hydraulic (T/H) model applied to the *reference fuel* is also used at the end of the process for the safety criterion verification at the reference state point of the accident.

The *reference fuel* is a proven design from the vendor who is in charge of the *FSAR* analyses. The aim is to prove that a proven design does exist on the market which is able to withstand the operating conditions. Adequate *design provisions* are applied on some design parameters (like pressure drop differences, rod internal pressure for Loss-Of-Coolant-Accident or LOCA analyses, or gap thermal resistance in fuel rod thermal evaluations in the non OTDT accidents,...) in the safety demonstrations in order to have margin for future minor design changes in fuel designs and for mixed core configurations. In that sense, the *reference fuel* is a “virtual fuel”.

The fuel rod analyses cover the following aspects:

- Fuel rod design verification of the thermal mechanical (T/M) design criteria;
- Fuel rod safety limits for non-LOCA accidents;
- Fuel rod safety limits for LOCA.

The Figure 2 represents the main links between the various disciplines in reference safety analysis.

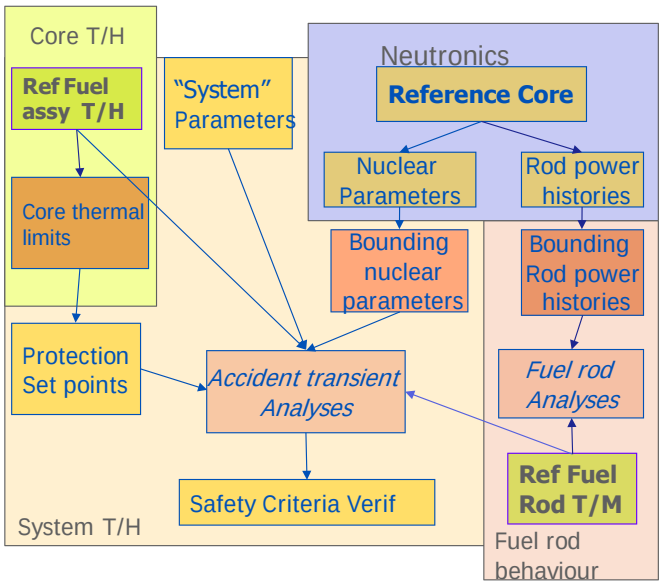

Figure 2: Principle of reference safety analysis.

2.2.1. Advanced safety analysis methods

The recent developments lead to using coupled codes and methods [4], and statistical approach [5]. This raises additional considerations: sensitivity analyses are performed and bounding assumptions are taken to ensure that a limited number of key parameters can be defined, which are sufficiently independent from the loading pattern.

2.3. Principle of the compatibility approach

Any change in the real designs from the reference designs can be justified by a compatibility assessment, depending on the degree of these changes:

- For minor changes from the *FSAR* (e.g.: limited change in fuel assembly pressure losses or feed enrichment), the safety of the new fuel or core design may be justified by the compatibility evaluation with the reference generic safety analysis documented in the existing *FSAR,* as explained in the following chapters.
- For major changes (e.g.: introduction of MOX or change from 12 to 18-month cycle) a full reanalysis of the *FSAR* is required. This new reference safety analysis is performed for the new *reference core* and new *reference fuel* following the process explained above.

The compatibility evaluation of the new design with the existing *FSAR* addresses the T/H compatibility, the fuel rod design compatibility, the LOCA and non-LOCA fuel safety evaluations, and the loading pattern.

If the new design has different *mechanical, hydraulic or thermal-hydraulic* features, some complements may be necessary to justify the compatibility of the new design with the other(s) one(s), in the mixed transition core configurations.

2.3.1. Fuel T/H compatibility

The T/H compatibility of the new fuel design is insured if its specific CTL are bounded by the reference ones, and the DNBR criterion is met at the state point of the most limiting accidents. The new fuel specific CTL are calculated assuming a homogeneous core. Mixed core configurations are treated separately.

2.3.2. Fuel rod design compatibility

- Fuel rod design

  In principle; the conclusions of the fuel rod design remain valid for the reference fuel as long as the rod power histories remain bounding.

  However, T/M properties and behaviour are so dependent of the fuel fabrication process and structure materials that fuel-specific design verification must be performed.

- Non-LOCA accidents

  The thermal properties of the fuel rod do not significantly change from one design to the other; therefore, adequate bounding value can be considered in the safety analyses so as to avoid any future compatibility evaluation.

- LOCA fuel safety evaluation

  Depending on the change the new fuel design has compared to the *reference fuel*, the vendor must perform various levels of fuel rod heat-up analyses on the basis of the transient interface data provided in the NSSS-Fuel Interface File (NFIF), but full LOCA analysis can be avoided [3].

- Fuel mechanical compatibility

  The grid mechanical resistance is verified by a dynamic mechanical resistance of the fuel calculated on the basis of the mechanical NFIF.

2.3.3. Nuclear parameters

The applicability range of the simplified core model is bounded by the NKSPs only; the model has no other link with the loading pattern. The NKSPs are:

- on the one hand reactivity coefficients describing the average neutronic properties of the core; their variation range are often decoupled from each other in the simplified core model (an easy way to insure generic analyses);
- on the other hand peaking factors and axial profiles describing the core power distributions.

The cycle specific loading pattern compatibility is insured if the nuclear parameters are bounded by the reference ones, and if the cycle specific power capability analysis has proven that power distributions are bounded by the reference ones.

3. Applicability and limitations

The approach is validated for the standard *FSAR* accident analysis using decoupled bounding methods. As a general rule, there is a competition between the *design provision* and the *licensing margins.* A high *design provision* allows flexible future reload core and fuel design, but results in small *licensing margin* which may lead to difficulties to license the safety analysis and may lead to possible plant system modifications (hence a reduction of operating margins).

One way to increase both analysis *design provisions* and *licensing margin* is to reduce the *uncertainties* in the reference safety analysis. This can be realized by using best estimate multi-physics codes and uncertainty analysis method [4-5].

If the Vendor in charge of the *FSAR* accident analysis provides such advanced coupled and/or best estimate statistical uncertainty analysis methods, great care should be taken in order to ensure that the safety analysis is compatible with the described approach. Some of the trickiest aspects are the following:

- Physical coupling of the neutronic feed-backs and the application of their uncertainties and provisions;
- Impact of the power distribution on the neutronic feed-backs;
- Power distribution used in the DNBR verification.

Moreover, the licensing efforts of such methodologies should not be neglected.

To accept low *design provisions* and proven decoupled approaches or advanced methods in which decoupled approach is sometimes difficult to implement: it is not possible to fix general rules on that point, but it is a prime condition for later applicability of the compatibility approach. The best equilibrium should be carefully kept between:

- design provisions
- uncertainties associated with the models and methodologies
- the choice of advanced methods for the most limiting accidents and their associated cycle specific applicability.

Experience feed-back has a determining role in these strategic choices which must be done from the early stage of the *FSAR* reference studies. And still more upfront, at the feasibility study and operating point determination, cautious margins shall be kept consistently with the flexibility objectives.

4. Reference core and reference fuel in the FSAR

4.1 Reference fuel

Each discipline is treated separately, therefore it would be more appropriate to refer to T/H reference fuel, T/M reference fuel, mechanics reference fuel and thermal properties range, which is defined with appropriate *design provisions* being allocated to each reference properties in order to cover the expected future changes in the fuel design and mixed core specific configuration.

4.1.1 Fuel assembly thermal-hydraulics

Conservatisms, uncertainties and *licensing margins* are applied at 2 levels on:

- FΔH (*uncertainties* and *conservatisms)* to account for the various parameters which affect the power distributions
- DNBR safety criterion (*licensing margins)*, according to BSA requests, to cover rod bow phenomenon among other things.

The thermal-hydraulic coolant flow taken for these calculations is penalized in order to cover possible future deviations and, to some extent, mixed core specific flow redistribution which can result for example from pressure drop differences between co-resident fuels.

The resulting CTL have reasonable conservatism to confer them a bounding character to cope with future minor changes in the fuel design.

For LOCA analyses, geometrical and thermal-hydraulic parameters (hydraulic diameter, grid spacer shapes, pressure losses and distribution, etc...) are bounded to ensure that the safety analyses remain valid for other fuel designs and mixed core configurations [3].

4.1.2 Fuel rod thermal-mechanics and thermal properties

For the condition II to IV non-LOCA transients limited by fuel cladding or pellets centreline temperature, the thermal properties ranges are taken with *design provisions* which are large enough to cover any burnup and rod power histories, as well as future fuel design changes without fuel specific verification.

For LOCA analysis, bounding fuel rod geometric and thermal mechanical parameters (fuel pellet and cladding parameters, the backfill pressure, etc...) are considered as well, with a view to ensure that the licensing basis analysis remains valid for the other fuel designs [3]. From this reference analysis, a T/H NFIF is issued, which contains all the transient interface data which are necessary for future new fuel vendor to perform fuel heat-up analyses of his own fuel, with the codes and models which are applicable for his own fuel. This approach saves performing full LOCA reanalysis for each new fuel introduction.

4.1.3 Fuel assembly mechanical properties

The verification of the mechanical behaviour of the core internals in case of LOCA and SSE events is performed assuming the core loaded with the *reference fuel*.

The lateral loads on the grid and axial loads on the end pieces which result from this analysis is used to verify the ability of the *reference fuel* to keep coolable geometry. The resistance of the *reference fuel* has previously been determined with adequate tests.

This analysis leads to the issuance of a mechanical NFIF which contains time history core plate motions which can be used for future fuel vendor to evaluate the loads on his own fuel and verify its resistance.

4.2 Reference core

The *design provisions* applied on the neutronic data, the power distributions and the power histories must cover ICFM variations like:

- feed enrichment;
- reload batch size;
- gadolinium product characteristics;
- cycle length and stretch-out length;
- loading pattern scheme and degree of low leakage;
- Calculation chain changes (reference cross section libraries, physical models, methodologies).

These ICFM variations that should be cover in the FSAR are defined in consistence with the flexibility required by the operator, in terms of cycle length variation, and hence in terms of feed size and enrichment.

If various fuel designs with different neutronic parameters are loaded together in the core, the *reference core* is a mixed core: fuel with burnable absorbers mixes with “clean” assemblies, MOX assemblies mixes with UOX assemblies,...

In the safety analyses where coupled methods are used, the *reference core* is explicitly considered. In that case, sensitivity calculations are performed with a view to define bounding neutronic parameters that are sufficiently independent from the loading pattern.

5. Reload safety evaluation

Limited fuel design and ICFM changes do not justify a revision of *FSAR* provided that the compatibility with the *FSAR* is demonstrated.

The compatibility is twofold:

- The fuel compatibility and safety evaluation (FCSE), performed at the first introduction of a new fuel design;

- The cycle specific safety evaluation (CSSE), performed at each cycle: some changes of loading pattern are acceptable, but even if the *reference core* loading pattern is applied, the previous cycle length most often differs from the reference one.

According to the BSA, the FCSE must address the following aspects: neutronic, geometrical and mechanical compatibility, thermal hydraulic compatibility, LOCA compatibility [1-2].

The FCSE is performed by the new fuel vendor with his own codes and methods. They must be fully qualified for the operating range they are expected to cover. The critical heat flux correlation used for the T/H evaluation and its associated DNBR criterion must be supported by experimental data base that cover the range in which it will be used, and the T/M models used must be qualified for the fuel specific characteristics.

The CSSE encompasses NKSP verification, power capability verification, accidents verification and fuel rod power histories.

The CSSE is performed either by Tractebel or by any fuel vendor provided that they have developed their generic safety evaluation files which describe their methodology for safety evaluation in consistence with the *FSAR* methodology. The interface information from the fuel vendor which is necessary for the neutronic evaluations is required in the frame of the fuel supply contract.

5.1 Fuel compatibility and safety evaluation (FCSE)

This section addresses the FCSE content in the new equilibrium core; i.e. after the transient mixed core. If the new equilibrium consists in a mixed core including two different designs from two different vendors, there is no other choice than for each vendor to address his FCSE in a fictitious homogeneous core, and complete it with the additional analyses required to cover mixed core configuration.

The FCSE addresses the aspects listed below.

5.1.1 Neutronic compatibility

This consists in verifying that the fuel neutronic properties and assembly wise power distribution are similar to the *reference fuel* ones.

5.1.2 Geometrical and mechanical compatibility

This addresses the following items:

- the geometrical and mechanical compatibility with the core internals, with the fuel handling components and tools, and with the control rods;
- the fuel structural resistance (grids, guide tubes, end pieces, connexions) under loads resulting from a LOCA combined with an SSE;
- the ability of the hold down springs to prevent assembly lift off under pump over speed.

5.1.3 Thermal-hydraulic compatibility

This consists in verifying that the fuel specific CTL are fully bounded by the reference ones, and, if necessary that fuel specific DNBR at the state point of the most limiting accidents is met. Any insufficient margin should be compensated by a fuel specific FΔH penalty in the same way as it is discussed for the mixed cores

5.1.4 Fuel rod design verification

A fuel rod design and pellet-cladding interaction (PCI) verifications are performed with the same extent as for the reference fuel, but based on power histories which are representative

of the actual ICFM, which can slightly differ from the *reference core*. It is as if the new fuel was replacing the reference fuel in the safety analysis.

5.1.5 LOCA Fuel safety evaluation

The LOCA fuel safety evaluation is performed on the basis of the T/H NFIF [3]. Provided that the geometrical and hydraulic parameters of the new fuel assembly remain within the bounding parameters of the *reference fuel,* the T/H results of the reference LOCA analysis are applicable, and the specific fuel compatibility can be addressed by a heat-up analysis.

The extent of this heat-up analysis depends on the differences between the new fuel and the *reference fuel* on their fuel rod geometrical and thermal mechanical data: they can be a hot rod heat-up or a hot assembly or a core heat up analysis. The necessary NFIF data are less and less extensive, but the models the fuel vendor must rely on are more and more complex, and their qualification more extensive.

5.2 Cycle specific safety evaluation (CSSE)

The first set of the CSSE consists in verifying that the power distributions and all the nuclear key safety parameters remain in the range considered for the *FSAR* analysis taking into account the uncertainties. The verification is done for the whole cycle length and power range.

In a second set, 7 accidents are verified through their specific key safety parameters and dilution accident is explicitly reassessed with the same methodology as for the *FSAR* study.

An extensive power capability analysis is performed with similar methods as for the *FSAR* analysis.

These analyses are performed with 3 dimensional codes which take into account the actual neutronic properties of each individual fuel assembly. These properties can be properly calculated on the basis of fuel compatibility information, which is a contractual set of parameters transmittable form fuel vendor to any other core designer or fuel vendor.

6. Specific treatment of mixed core

The compatibility of the new fuel design is usually performed in homogeneous core with a view to demonstrate the compatibility with the *FSAR*. This section addresses the necessary complements to demonstrate the compatibility of the new fuel design with other designs in mixed core.

Mixed cores are a concern for the parameter which may be impacted by the interaction of two neighbouring assemblies with different characteristics. The following parameters are concerned:

- Geometrical and mechanical parameters;
- Hydraulic parameters;
- Thermal-hydraulic parameters;
- LOCA aspect;
- Core neutronic aspects.

6.1 Fuel compatibility in mixed cores

6.1.1 Geometrical and mechanical compatibility

The geometrical compatibility in mixed core addresses the mechanical interaction of the new design with co-resident ones: axial locations of the grids (with acceptable deviation to cope with axial growth), radial gaps between grids after irradiation.

Concerning the grid lateral resistance under LOCA loads combined with a SSE, it is a good practice to consider that the homogeneous configuration bounds all the possible mixed core configurations as long as radial gaps between co-resident assembly designs remain comparable.

6.1.2 Hydraulic aspects in mixed core

The main concern is the pressure losses differences between co-resident fuel assemblies. These differences may induce several potential problems associated with cross flows:

- Grid-to-rod fretting caused by cross flows due to either the core inlet flow distribution or pressure loss differences between neighbouring assemblies;
- Assembly lift off: the flow redistribution induces increased coolant flow in the assembly with the lower pressure drop, which increases the lift off force;
- The core average by-pass flow and assembly coolant flow;
- Assembly deformation induced by cross flow hydraulic lateral loads.

6.1.3 Thermal hydraulic aspect in mixed core

Even if the DNB performances of the new fuel design are compatible with the reference CTL in homogeneous core, in some mixed core configurations, the reduced coolant flows can jeopardize its DNB performances. In these cases, for the CTL to remain bounded by the reference CTL, the lack of DNB performance must be compensated by a F△H penalty applied on all the assemblies with the higher pressure losses. Conversely, the other assemblies are not credited for the benefit from the higher coolant flow.

6.1.4 LOCA aspect in mixed core

The reference LOCA safety analysis usually considers a bounding uniform core of the reference fuel with penalized pressure loss coefficients.

The mixed core configuration is addressed through a sensitivity study with maximum pressure loss differences between neighbouring assemblies. As long as the actual pressure losses and their differences remain bounded by the assumption of the reference analysis, the reference LOCA accident analysis remains applicable.

If the mixed core results from the co-residence of fuel assemblies with different active lengths, it is conservatively assumed that the shorter one has a higher average linear heat generation rate, which results in a FQ penalty, as it is assumed that a constant initial local linear heat generation rate (LHGR) would keep the LOCA analysis applicable. So the core FQ limit is unchanged.

6.2 Loading pattern compatibility

As the core calculations are performed with 3D models which take the accurate neutronic parameters of each assemblies into account by fuel specific macroscopic cross section

libraries, the mixed core configuration is explicitly taken into account, provided that the possible FΔH and/or FQ penalties are adequately applied. Therefore, the CSSE remains unchanged for mixed cores.

7. Conclusions

The practical methodology applied for the reload safety evaluation has been developed in order to keep flexibility in the future in-core fuel management in Belgium. The flexibility addresses the cycle length and feed parameter changes, and the ability to move from one fuel vendor to the other or from one design to another for the same fuel vendor without reviewing the full safety analyses.

This methodology is based on a *reference core* and a *reference fuel* which are considered in the safety analyses with adequate *design provisions* to allow this future flexibility. The choice of these *design provisions* results from a trade-off between the operating flexibility target and the licensing need to keep adequate *licensing margins.*

In the frame of a new fuel introduction, the compatibility with the *FSAR* is verified through a limited number of interface parameters and a limited amount of design and safety evaluations. This verification is performed for a new equilibrium core including the new fuel design.

The same principles are extended to verify the compatibility of the new fuel with co-resident fuels in the transition core from the initial core to the new equilibrium core which include the new fuel.

This approach allows the required flexibility for in-core fuel management with mixed core while insuring the safety of the reloads.

8. References

[1] Nadine Hollasky: «Belgium Licensing Requirements: Mixed Cores and Control Rods Insertion Problem Aspects», presented at the OECD CSNI/PWG1 Specialists' Meeting on Nuclear Fuel and Controls Rods: Operating Experience, Design Evaluation and Safety Aspects, Madrid, November 1996.

[2] Nadine Hollasky: «Incore Fuel Management in Belgium: Licensing Aspects», presented at the Advances in Nuclear Fuel Management III (ANFM 2003), Hilton Head Island, South Carolina, USA, October 5-8, 2003.

[3] Jinzhao Zhang, Jean-Paul Dalleur: "Core and Fuel Aspects In LOCA Safety Analysis and Reload Safety Evaluation for Belgian NPPs", Transactions of the 2006 International Meeting on LWR Fuel Performance(TopFuel 2006), Salamanca, Spain, 22-26 October 2006.

[4] J. Zhang and C. R. Schneidesch, "Development, qualification and application of the coupled RELAP5/PANTHER/COBRA code package for integrated PWR accident analysis", IAEA Technical Meeting on Progress in Development and use of coupled Codes for Accident Analysis, Vienna (Austria), 26-28 November, 2003.

[5] Jinzhao Zhang, Jacobo Segurado and Christophe Schneidesch, "Towards an Industrial Application of Statistical Uncertainty Analysis Method to Multi-physical Modelling and Safety Analyses," OECD/CSNI Workshop on Best Estimate Methods and Uncertainty Evaluations, Barcelona, Spain, 16-18 November, 2011.

POST-IRRADIATION EXAMINATIONS ON AGR FUEL PINS IN STUDSVIK

RIKARD KÄLLSTRÖM, JOAKIM K.-H. KARLSSON, HANS JOHANSSON
Studsvik Nuclear AB, SE-611 82, Nyköping, Sweden

MARK LEVY, JANE MINAY
EDF Energy, Barnett Way, Barnwood, Gloucester, GL4 3RS, UK

MATTHEW BARKER, MARK GONZALES
National Nuclear Laboratory, Sellafield, Cumbria, CA20 1PG, UK

ABSTRACT

Fuel pins from advanced gas cooled reactors in the UK have been transported to the Studsvik hot cell facility in Sweden for post-irradiation examinations (PIE). The examination program has included visual inspections and length measurements, axial and rotational gamma scans including burnup determination, pin puncturing and fission gas analysis. The fuel pellet and cladding have also been characterised by microscopy.

This is the first time AGR type fuel pins have been investigated in Studsvik. The paper describes some of the modifications required to the hot cell equipment in order to handle AGR fuel pins. Results from the different measurements performed are presented and analysed. The results are compared to typical light water reactor (LWR) fuel behaviour and the differences due to fuel design and operational characteristics are discussed.

More than 40 fuel pins have been examined from different AGR units. The PIE campaign covered a wide range of burnups and included pins from most axial fuel element positions. Some of the pins have burnups of about 40 GWd/MTU and represent some of the highest discharge burnups currently achieved in AGR reactors.

A new equipment to measure the profile and depth of wear scars on AGR fuel element tie-bars has been developed. This apparatus has also been used for measurements of fretting marks on fuel pins. An example of fretting wear characterisation for an AGR fuel pin is presented in the paper.

1. Introduction

In order to perform PIE on irradiated fuel pins from AGR reactors in the UK, an extensive program has been carried out at Studsvik Nuclear in Sweden. The objective of the program has been to put in place the capability to transport, receive, handle and perform PIE on AGR fuel elements and pins in Studsvik.

An existing storage facility for irradiated fuel was upgraded to handle the 60-ton A2 transport flask for AGR elements. The facility has three deep water pools. One pool is used for the unloading of the A2-flask and storage of fuel elements and cans with individual fuel pins/tie bars. The second pool has recently been furnished with a pool-in-pool system where equipment for visual inspection of fuel elements, element dimensional measurements and extraction of individual fuel pins is available.

The PIE work reported here concerns 46 individual fuel pins transported to Studsvik from the National Nuclear Laboratory (NNL) in June 2009. The fuel elements had originally been

transported to B13 in Sellafield where element measurements were performed and fuel pins extracted and stored pending pin PIE.

2. Pin data and PIE scope

The fuel pins originate from fuel elements irradiated in eight different AGR reactors: Heysham 1 (7), Hinkley Point B R3 (13), Hinkley Point B R4 (2), Torness R2 (7), Dungeness B R21 (1+2), Dungeness B R22 (1), Hunterston B R3 (10) and Hunterston B R4 (8). The values in parenthesis give the number of fuel pins examined for each reactor. The set of pins from each reactor comes from elements in the same fuel stringer, except for Dungeness B R21 where the pins were taken from two different stringers. The stringers were discharged over a number of years from 2001 to 2008. The pins cover a wide range of AGR operating conditions, including burnups from 10 to 40 GWd/MTU and the axial variation of power and temperature in the core.

The PIE program for the fuel pins included the following items:

- Axial and rotational gamma scans including burnup evaluation
- Visual inspection including pin length measurements
- Pin puncturing and fission gas analysis
- Optical microscopy

The main aim of the PIE program was to perform condition monitoring on a representative set of fuel pins. Furthermore, the sets of pins from Hinkley Point B R3 and Hunterston B R3 were of special interest since they have burnups of about 40 GWd/MTU which represent some of the highest discharge burnups currently achieved in AGR reactors. They were also discharged fairly recently in 2008 and 2005 respectively.

3. Pin puncturing and fission gas analysis

In AGR pins the plenum is formed by an annular hole in the fuel pellets, forcing any puncture from the side to puncture into the fuel pellets. The AGR pins also have stainless steel cladding with ribs forming spirals around the outer surface making a gas-tight seal more difficult to achieve. These design features required some modifications to the existing Studsvik puncturing equipment. A new large soft rubber pad was developed to create a gas-tight seal between the puncture hole and the gas collection equipment. A stronger puncture needle was also put in place. Despite one failed puncturing where the pad was misaligned and some gas was lost, the modifications worked successfully for 39 of 40 punctured pins.

The puncturing procedure includes collection of the fission gas in a known volume and measurement of the pressure. After vacuum pumping, the pin is backfilled with a known volume of He by which the free volume of the pin is determined. By analysing the collected gas in a mass spectrometer, the amounts of released fission gas is determined as well as the isotopic composition of the fission gas. The released amount of fission gas compared to the calculated production of fission gas during the irradiation of the pin yields the fission gas release fraction (FGR).

The measured value for the free pin volume is about the same for all pins, approximately 31 cm^3. The initial fill gas pressure in AGR pins is 0.1 MPa at room temperature. The measured pin pressures and evaluated FGR for all pins are shown in Fig 1 as functions of element mean burnup. The figure shows that there is a trend of increasing pin pressure and FGR with increasing burnup. However, there is significant scatter at any given burnup and even at the highest burnup some pins have quite low pin pressure and FGR, while others have high values. Since the fuel temperature is very important for the gas release, it is inferred that the scatter in part can be explained by studying the trend of FGR with fuel temperature at different axial locations in the core.

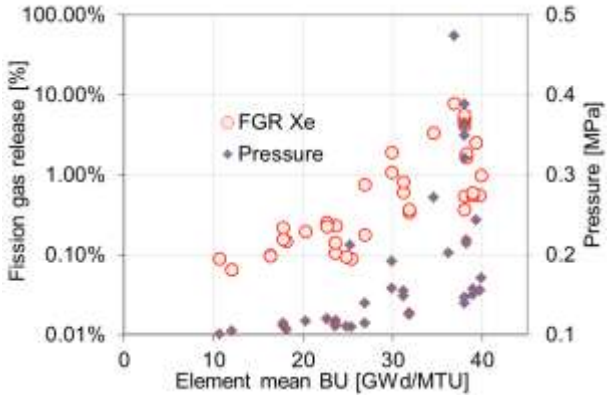

Fig 1. Fission gas release fraction and pin pressure for all analyzed AGR pins.

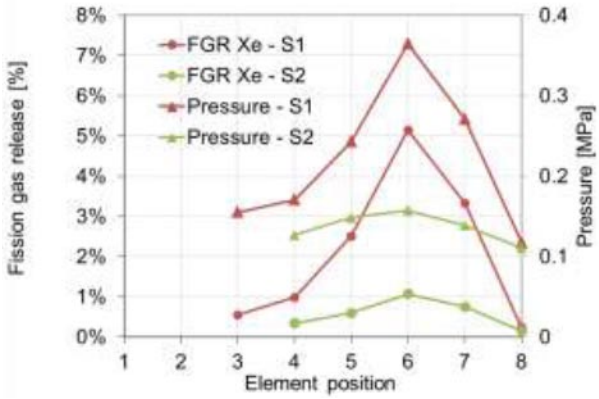

Fig 2. Fission gas release as a function of element position for two fuel stringers.

In Fig 2 the FGR and pin pressure are given as a function of the element position for pins from two individual stringers, S1 and S2. The figure shows that the FGR is highest at element six, where the highest fuel temperature is also expected. It is clear that the scatter that was observed in the previous figure can at least in part be explained by differences in fuel temperature.

The experimental measurements of pin pressure and fission gas release at hot cells give important data to support model predictions of gas release in AGR fuel pins. The cladding temperatures in AGRs are quite high and a large gas release causing a positive pressure differential across the cladding, for example in a hypothetical fault, would pose a risk of overpressure failure of the cladding. Thus, the incentive to keep the pin pressure down and be able to accurately model the gas release is higher for AGRs than for LWRs.

4. Gamma scan and burnup evaluation

Axial gamma scanning is performed by collecting the pulses from a Ge gamma detector, looking at the pin through a collimator located in the Hot Cell radiation shielding. A multichannel analyser stores the spectrum which is then analysed for the different nuclides, making corrections for dead time losses and decay of the different nuclides since the end of the irradiation. The scan is repeated in axial steps along the whole pin. The collected data for each isotope can then be plotted and further analysed.

An example of the measured Cs-137 and Co-60 activity profiles at the bottom of a pin are illustrated in Fig 3. The long-lived fission products such as Cs-137 show the variation of the burnup along the pin. The Co-60 profile shows the activity of the steel cladding. The start and end positions of the cladding and pellet stack can easily be determined from the activity profiles. This is illustrated by vertical lines in Fig 3 at the starting positions of the cladding and pellet stack. The scan also gives a good possibility to detect any changes or flaws along the pellet stack. Fig 3 clearly shows the drops in the Cs-137 curve at the pellet-pellet interfaces and larger drops at the anti-stacking grooves (ASGs), where there is less fuel present. The profile also shows the end effect with an increase in burnup at the end of the fuel stack. If temperature has been high it is possible to detect re-distribution of fission products. This is true for the particular pin in Fig 3 where the Cs-137 activity indicates a peak on the inside of the end cap.

The measured Cs-137 activity profiles are typically quite flat and the burnup can be characterized by the mean Cs-137 activity. Fig 4 shows the mean Cs-137 activity as a function of element mean burnup. The figure illustrates the clear linear build-up of Cs-137 as a function of increasing burnup.

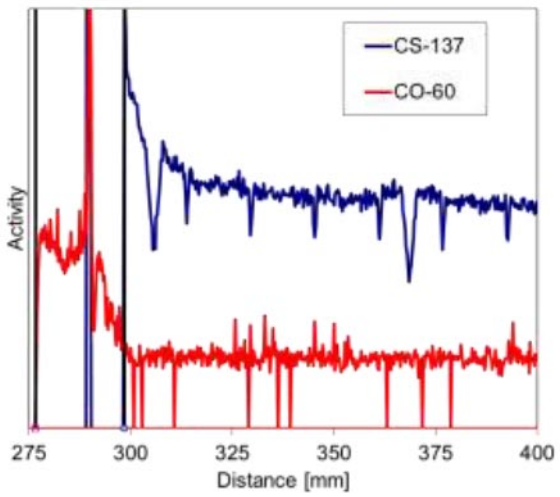

Fig 3. Activity profiles at the bottom end of a fuel pin.

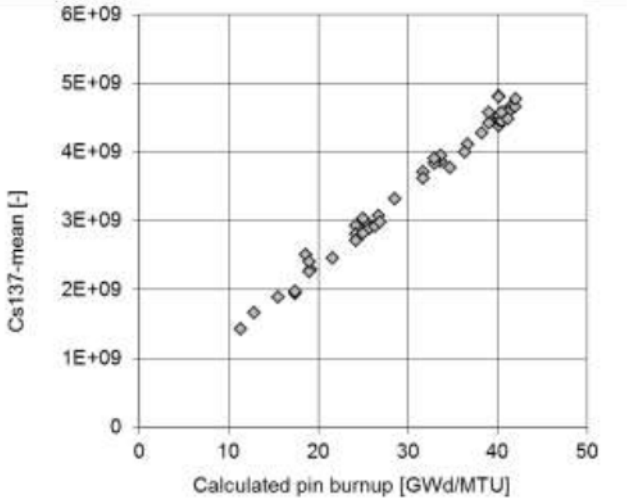

Fig 4. Cs-137 activity as a function of pin burnup.

As indicated by Fig 4 burnup can be evaluated from the Cs-137 activity measured by the axial gamma scanning. To evaluate burnup for a pin, the activity of a reference rod is measured together with the pin. The burnup of the reference rod has been determined by chemical analysis. The burnup is obtained by applying correction factors on the Cs-137 activity data. In particular the irradiation and cooling times, as well as fabrication data for the rods are taken into account. Burnup evaluation was performed for a set of 9 pins. The evaluated pin burnups agreed with expected values based on core calculations.

5. Visual inspection including pin length measurements

Eight pins were selected for detailed visual inspection. All interesting features were photographed and documented. Observations included intact and spalled carbon deposits, fretting, wear and corrosion. Pin lengths and bending were determined by optical measurements. Pin growth was found to increase with burnup and the pins with highest burnup had a growth of about 8 mm. The growth values were found to be in agreement with the experience database.

One pin showed fretting with rib damage due to pin brace interaction (PBI) at the top brace. The fretting damage is shown in Fig 5. The fretting damage has been further characterized using a newly developed machine for surface profilometry. The machine uses a contact measurement probe to scan the surface of a solid rod or tube specimen. The machine operates like a sewing machine taking one measurement per second. The machine has very good resolution in axial and angular position and in the determination of wear scar depths. By using an undamaged area of the specimen as a reference for zero, both wear depths and protruding features can be determined. By measuring the fretting damage on the fuel pin in Fig 5 a detailed map of the surface profile was obtained in Fig 6. The unit for the colour bar is mm and positive values indicate wear depth into the cladding, while negative values protrude out from the surface. The map clearly shows the ribs and the fretting damage to the ribs and cladding.

Fig 5. Photograph of a PBI fretting wear.

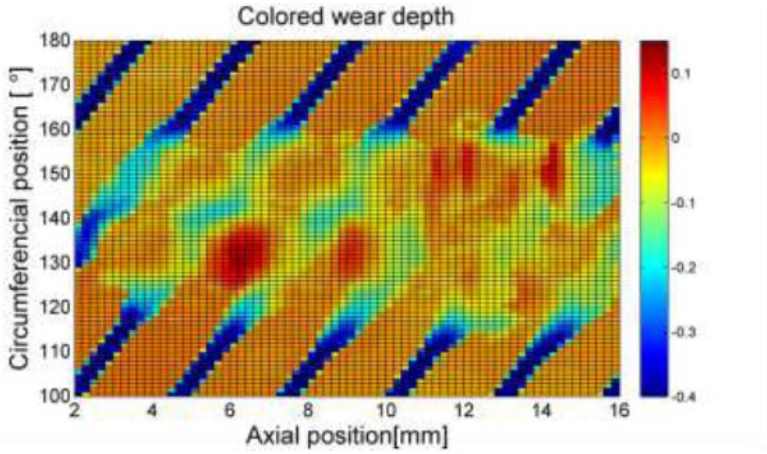

Fig 6. Map of measured wear depth for the PBI damage in Fig 5.

6. Optical microscopy

An extensive scope of microscopy was performed on two samples; both samples were taken from pins irradiated in Hunterston B R4. Both pins had high element burnups of about 40 GWd/MTU. One of the pins was selected because it had the highest peak power and the other was selected because it had the highest FGR. The etched cross-sections are shown in Fig 7 and Fig 8.

The different sizes of the dark zones clearly indicate the difference in fuel temperature. The dark zones are also off-centre indicating a power gradient across the fuel pins. This is consistent with their location as outer ring pins in the elements. Here, the power gradient is stronger and the dark zone is shifted towards the upper right where the distance to the graphite moderator is shorter and the power and temperature are at their peaks. The figures also show a typical fuel crack pattern of AGR pellets with a few larger radial cracks, but also long circumferential cracks forming fuel slivers close to the periphery. The cracks forming the slivers probably occur when the fuel is cooled. Such fuel slivers are not typically observed in light water reactors, where instead circular cooling cracks appear inside the fuel pellet.

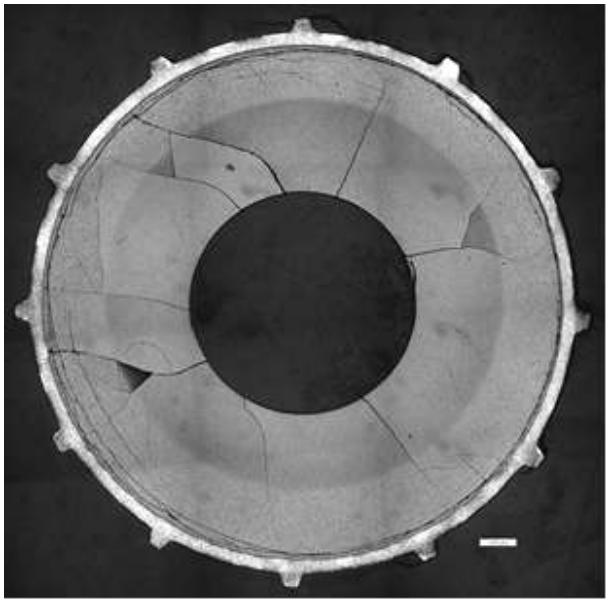

Fig 7. Pin with peak power.

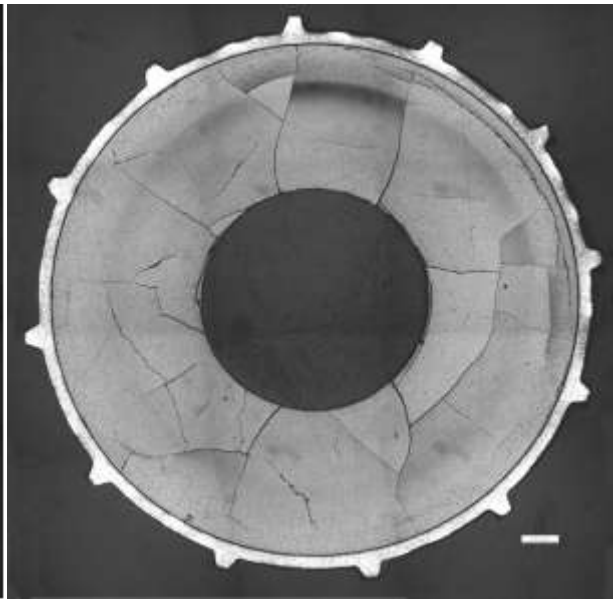

Fig 8. Pin with peak FGR.

7. Summary and conclusions

The first large PIE campaign on AGR fuel pins at Studsvik has been successfully completed. The PIE campaign has included 46 individual fuel pins irradiated in eight different AGR reactors. The examination program has included visual inspections and length measurements, axial and rotational gamma scans including burnup determination, pin puncturing and fission gas analysis. The fuel pellet and cladding have also been characterised by microscopy.

The objective of the PIE program was to perform condition monitoring on a representative set of fuel pins. Furthermore, some pins had burnups of about 40 GWd/MTU which represent some of the highest discharge burnups currently achieved in AGR reactors. In general the pins were found to be in good condition and the data generated lie within the experience database for AGR fuel pins. The high burnup pins showed the characteristics that can be expected for such pins. Some high burnup pins, which have also been operated at high temperature, showed fission gas release fractions above 1%, redistribution of Cs and some evidence of increased grain size and porosity towards the inside of the pellet annulus.

PERFORMANCE OF AN UPDATED CELL FRICTION METHODOLOGY FOR MITIGATING CHANNEL – CONTROL BLADE INTERFERENCE

P.E. CANTONWINE, A.A. KARVE, M.W. THOMAS, AND G.D. GALLOWAY

Fuels Engineering, Global Nuclear Fuel – Americas

3901 Castle Hayne Road, Wilmington, NC 28411 – USA

ABSTRACT

Global Nuclear Fuel initially developed the Cell Friction Methodology in 2005 and updated it in 2007 to mitigate the susceptibility to channel control blade interference in the core design process. Since the last update, interference has continued to occur in cells that were predicted to have a low susceptibility to interference – indicating mispredictions for certain conditions. In addition, GNF has continued to collect channel distortion data. Based on the analysis of the interference observation and the channel-distortion data, GNF has updated the Cell Friction Methodology. Three observations of interference in D-lattice plants were particularly important in driving the update. The conditions where the Cell Friction Methodology mispredicted the susceptibility to interference were related to the low-power density of some D-Lattice plants, the ultra-high Effective Control Blade Exposure (ECBE> 50000 inch-days)) that can occur when a cell with fresh fuel is suppressed because of a failed fuel bundle, and moderately high ECBE (~24000-35000 inch-days) that can occur in certain control strategies. The changes to the model resulted in an improvement in the predictions.

1. Introduction

Observations of channel control-blade interference in GNF designed cores have been occurring since the year 2000 (see Figure 1). In general, interference is observed when a control rod fails to settle into a notch. Interference issues may be observed when the control rod is inserted or scrammed; at the end of an insertion or scram event, the control rod must settle into the intended notch. The first observations between 2000 and 2003 were linked by GNF to shadow corrosion-induced bow, a previously unrecognized channel distortion mechanism. This form of channel bow is a result of shadow corrosion that occurs when 1st-cycle bundles are controlled (i.e., where a control blade is inserted setting up the conditions for shadow corrosion on the channel). The excessive shadow corrosion results in excessive hydrogen on the blade side causing bow toward the blade late in life. This exposure dependence on the accumulation of shadow corrosion-induced bow is likely related to the increase in hydrogen pickup fraction with exposure in Zircaloy-2 [4].

In 2005 GNF introduced the Cell Friction Methodology into the design process to optimize the channel / bundle locations and to minimize the probability of having to declare a control rod inoperable because of channel – control blade interference [1-2]. The Cell Friction Methodology proved successful and observations decreased dramatically by 2007 (see Figure 1). An update to the initial Cell Friction Methodology was released in 2007 [3]. In 2008 there was a significant increase in observations. Although this increase was mainly due to observation in mixed-vendor cores designed with the Cell Friction Methodology where higher uncertainty in predictions are expected, there were a number of surprises in cores with only GNF fuel, especially in D-Lattices plants [5].

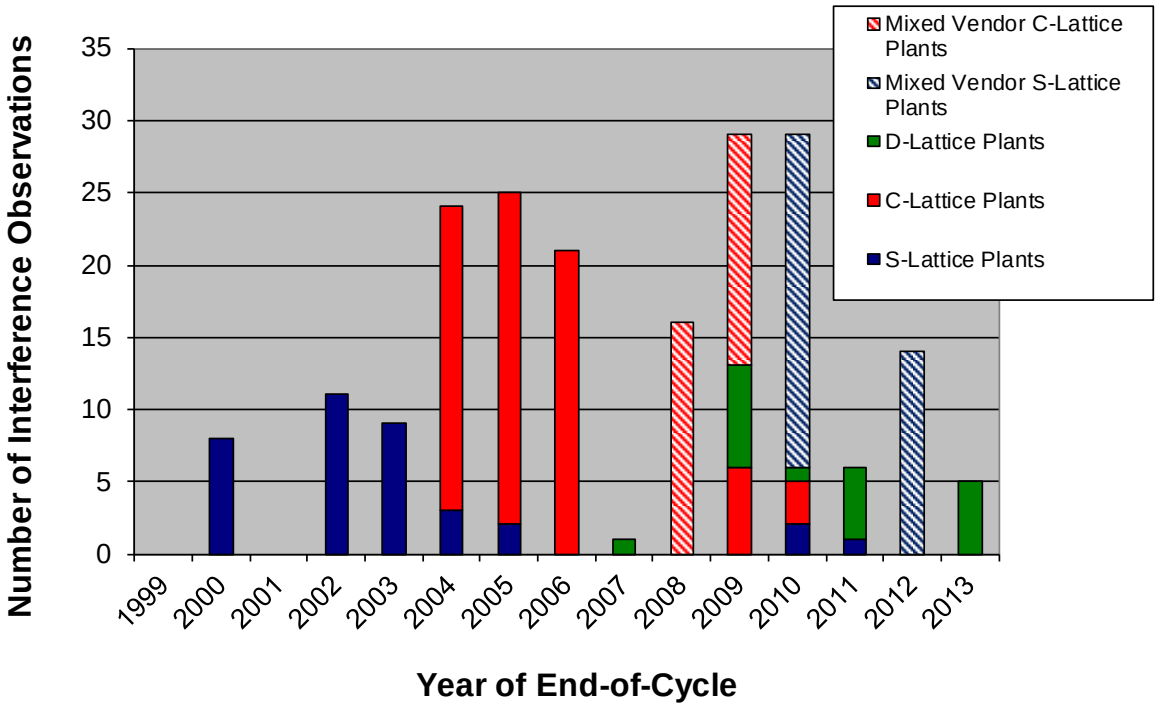

Figure 1 Observations of interference in Boiling Water Reactors with GNF fuel. Interference is observed when the control rod fails to settle into a notch within 30 seconds. The time axis is in terms of the year when the cycle ends rather than in terms of the year when the observations were made.

These more recent observations prompted the industry to form an EPRI-lead working group to evaluate channel distortion [6]. The objective of the EPRI working group is to develop a more fundamental understanding of channel distortion that may result is more effective models of distortion. In parallel, GNF has continued to evaluate the available data and determined that an update to the channel distortion models for Zircaloy-2 in the Cell Friction Methodology was warranted.

The purpose of this paper is to review the observations that initiated the most recent update to the Cell Friction Methodology, released in 2011, and to provide a conservative estimate of the correlation between predicted and observed interference.

The Cell Friction Methodology predicts the susceptibility of interference by calculating a cell friction metric (CFM) that is a function of the predicted channel distortion (channel-type dependent), the gap between the channels (plant-type dependent), and the control blade thickness (plant-type dependent) [1,2]. For the purposes herein, specific CFM values will not be discussed but rather the cells will be characterized using the semi-quantitative categories in Table 1.

2. Review of Observations of Interference

Three specific observations will be reviewed: Monticello Cycle 23, Brunswick 2 C18 and Peach Bottom 3 C17. These three plants had a full core of Zircaloy-2 channels and had been designed before channel distortion was considered a significant issue in D-Lattice plants. The purpose of each review is to highlight a specific change made in the Cell Friction Methodology for Zircaloy-2 channels.

2.1. Monticello Cycle 23

In 2007, the first no-settle observation in a D-Lattice plant occurred at Monticello in cell 42-11 near the end of Cycle 23. The Cell Friction Methodology predicted that the CFM value for this cell was a High Green. The characteristics of the bundles in the cell are given in Table 2.

CFM Level	Relative Probability of Interference
Low Green	Insignificant Probability of Interference
High Green	Very Low Probability of Interference
White	Some Probability of Interference
Yellow	Interference Likely; Inoperability Possible
Red	Inoperability Likely

Table 1 Categories comparing the semi-quantitative descriptions of CFM levels to probabilities of interference

Bundle	Cycle 23 Cell	Cycle	Residence Time (days)	Exposure (MWd/MTU)	ECBE (inch-days)
YJZ708	42-11	3rd	1828	42000	0
YJU378		4th	2401	48400	17795
YJU384		4th	2401	48400	17795
YJU395		4th	2401	45700	712

Table 2 Characteristics of bundles in cell 42-11 at Monticello that experienced interference during cycle 23. Note the exposures reported in Reference [5] have been corrected herein.

There were two characteristics to the observations at Monticello that made them unique. The first was that Monticello was a D-Lattice plant. The D-Lattice plants have the largest gaps between the control blades and the channels and, at that time, were thought to be immune to interference from shadow corrosion-induced bow. The second was that, while the exposure and Effective Control Blade Exposure[1] (ECBE) values were within GNF's experience base, the residence time was approximately 300 days longer than any bundle from an S-Lattice or C-Lattice plant were interference had been previously observed; Cycle 23 was the first two-year cycle at Monticello, which added almost 200 days to the normal residence time of the 4th cycle bundles.

After additional evaluation of the control histories at Monticello, it was determined that the calculation of ECBE for low power-density plants should be modified. Because the exposures at Monticello were within the GNF experience base, the power density (i.e., the average neutron flux) is less than plants where interference had been previously observed. As the in-reactor corrosion rate is known to have a flux dependence (i.e., corrosion thickness is proportional to fluence or exposure), the observations at Monticello indicated that shadow corrosion likely occurs over a longer period of time in low power density plants compared to high power-density plants, which were used to develop the original definition of ECBE.

To account for the Monticello observations in the Cell Friction Methodology, GNF has increased the time over which ECBE accumulates in low power-density plants.

[1] The ECBE metric is a weighted average of the product of insertion length of the control blade (in inches) and the time the control blade is inserted (in days). Thus, the units for ECBE are inch-days.

2.2. Brunswick 2 Cycle 18 and Pilgrim Cycle 18

About two years after the Monticello event there were two other observations of interference in D-Lattice plants that also suggested that updating the Cell Friction Methodology was necessary. The first was at Brunswick 2 in November 2008 discussed in this section. The second was at Peach Bottom 3 in January 2009 discussed in the following section

Near the end of cycle at Brunswick 2, the centre cell (26-27) exhibited a no-settle condition. About a week later after a scram event, a peripheral cell (50-31) also showed signs of channel control blade interference. The interference in 50-31 appeared to be less than observed in 26-27 because the observations were made under cold conditions were friction is known to be greater than under hot conditions[2]. GNF predicted cell 26-27 had a White CFM value while the CFM in cell 50-31 had just become a High Green. Thus, it was not a significant surprise that interference was observed in cell 26-27 while interference in cell 50-31 certainly was unexpected. The characteristics of the bundles in these cells are given in Table 3. The ECBE values of JLE520, JLE511, and JLE611 were well outside the GNF experience base. These ultra-high ECBE values were a result of being in suppressed cells the previous cycle for failed fuel management.

The potential misprediction of shadow corrosion-induced bow at ultra-high ECBE was reinforced about two years later when a similar observation of interference occurred at Pilgrim. In this case, two Low-Green CFM cells containing ultra-high ECBE bundles experienced a no-settle condition. These observations were disconcerting given the expectation that interference was not probably at this CFM level.

To better account for the observations at Brunswick 2 and Pilgrim, GNF has modified the Cell Friction Methodology by increasing the predicted shadow bow at ultra-high ECBE.

Bun. ID	Cycle 18 Cell	Cycles of Operation	Exposure MWd/MTU	ECBE inch-day
JLE520	26-27	3	48459	78106
JLE511		3	47488	78106
JLE606		3	48441	0
JLE700		3	47619	0
JLZ322	50-31	1	18379	9026
JLZ314		1	18817	9026
JLE691		3	43119	0
JLE611		3	40699	87227

Table 3 Characteristics of bundles in cells at Brunswick 2 that experienced interference during cycle 18 [5].

2.3. Peach Bottom 3 Cycle 17

The observations of interference at Peach Bottom 3 during Cycle 17 were more significant than the observations at Monticello and Brunswick 2 because they occurred approximately nine months prior to the end-of-cycle (EOC) and because there were four observations rather than only one or two. At the time of the observations, GNF predicted the CFM values in all four cells were High Green; however the corresponding CFM values at EOC were High White, which indicates some probability of interference. The characteristics of two of the cells (14-55 and 18-55) are provided in Table 4. The ECBE values were on the high side but not outside the GNF experience base.

[2] The channel stiffness increases as the temperature decreases increasing friction from interference.

Bundle ID	Cell	Cycles of Operation	Exposure (MWd/MTU)	ECBE (inch-days)
JLH523	14-55	3	49489	0
JLH483		3	47503	0
JLH539		3	51145	2783
JLH547		3	48788	32335
JLH611	18-55	3	47048	0
JLU245		2	37124	22642
JLH507		3	48252	24388
JLU189		2	38198	25182

Table 4 Characteristics of bundles in two cells at Peach Bottom 3 that experienced interference during cycle 17 [5].

Once the observations were made, friction testing was performed according to Reference [7]. When it became apparent that two of the control rods (18-55 and 42-55) might reach the inoperability limit during the summer, the control rods were proactively inserted to decrease the friction in the cell [4]. This technique for decreasing friction from interference was first developed at LaSalle [8]. The CFM values were White at the time the cells were projected to become inoperable when the preferred prediction was Yellow. This indicated possible under-prediction of shadow bow in the 24000 – 35000 inch-days range. In truth, the measured channel distortion from these bundles was unusually large compared to channels with similar characteristics. This observation was further indication that shadow corrosion induced bow of Zircaloy-2 channels is highly variable.

However for conservatism, GNF decided to modify the Cell Friction Methodology to predict cells 18-55 and 42-55 as Yellow at the time when were projected to be inoperable (July 2009), by increasing the predicted shadow bow for moderately high ECBE (24000 – 35000 inch-days).

3. Cell Friction Methodology Update

The Cell Friction Methodology is integrated into the standard GNF three-dimensional (3D) core simulator, PANAC11, used for design and in plant core monitoring. A flow chart of the steps in the methodology is outlined in Figure 3 of Reference [1]. The overall steps in the methodology remained unchanged. The update primarily addressed the bow and bulge prediction in Step 1. The bow and bulge are calculated at each axial elevation on each of the two faces of the channel adjacent to the control blades. To address the observations described in Section 2, the main modifications were in the model for shadow corrosion-induced bow. The most significant changes to the model were for D-lattice plants. For example, ECBE was allowed to accumulate for longer periods of time in low power-density plants compared to the high power-density plants. In addition for all D-Lattice plants, the maximum predicted shadow bow was increased for channels with moderately high ECBE (24000 – 35000 inch-days) and for ultra-high ECBE (>50000 inch-days). Other minor changes were made to the shadow bow models for C-Lattice and S-Lattice plants and the uncertainties in the fluence-bow predictions for all plants, but the effects of these changes will not be discussed herein.

The relative changes in the CFM levels of the D-Lattice cells with interference described in Section 2 are shown in Table 5. In this case only the Pilgrim observations related to performance of ultra-high ECBE bundles are provided; GNF was not able to evaluate

Brunswick 2 Cycle 18 with the updated methodology. The results show a significant improvement in the predicted susceptibility to interference compared to observations.

Plant	Cell	Date of Observation	CFM Level Prior to Update	Updated CFM Level
Monticello	42-11	Jan. 20, 2007	High Green	Yellow
Peach Bottom 3	14-55	Jan. 23, 2009	High Green	White
Peach Bottom 3	18-55	Jan. 23, 2009	High Green	White
Peach Bottom 3	42-55	Jan. 23, 2009	High Green	White
Peach Bottom 3	46-55	Jan. 23, 2009	High Green	White
Peach Bottom 3	42-07	Sept. 9, 2009	High Green	Yellow
Pilgrim	6-39	Oct. 14, 2010	Low Green	White
Pilgrim	46-39	Oct. 14, 2010	Low Green	White

Table 5 Comparison of CFM levels for interference cells in D-Lattice plants prior to and after updating the Cell Friction Methodology. The CFM levels were calculated for the time of the no-settle observation.

When considering the overall changes to the predictions of the fleet, the effect of the update was more subtle. For this purpose the statistical likelihood of observing a no-settle condition as a function of CFM level was determined (see Table 6). The likelihood was calculated as the percentage of no-settle cells in a given CFM level to **all** cells predicted to be in that same CFM level. That is, a probability of a no-settle condition in a cell was calculated as the ratio of the number of no-settle cells to all cells in the fleet for a given CFM level. All the cycles with no-settle observations were included in the statistics but only about 30% of the cycles with no observations of interference were included. Thus, the predicted probabilities are considered conservative (potentially by a factor of 3).

The overall conclusion of these calculations is that the CFM level correlates well with the no-settle observations supporting the descriptions of the CFM Levels in Table 1. The effect of the update was to shift some of the observations in the White level up the Yellow level, increasing the difference in probabilities between the Yellow and White levels. As before there is some small probability of interference in the High-Green level, but with the update, the probability of a no-settle in the Low-Green level is now effectively zero.

4. Summary

The Cell Friction Methodology has been used by GNF since 2005 for design and in-plant core monitoring. The methodology has been updated by modifying the distortion models for Zircaloy-2 channels. The modifications resulted in dramatic changes to the target cells at Monticello Cycle 23, Peach Bottom 3 C17, and Pilgrim C18 but were less dramatic when considering the entire fleet. The estimates of the probability of a no-settle condition provided evidence that the CFM Level is an effective predictor of interference.

CFM Level	Prior to CFM Update Interference Probability	Updated CFM Interference Probability
Yellow/Red	23.08%	26.74%
White	4.37%	3.70%
High Green	0.64%	0.40%
Low Green	0.06%	0.00%

Table 6 Estimated probabilities of interference (a no-settle condition) as a function of CFM Level (includes observations from D-, C-, and S-Lattice plants).

5. References

1. A.A. Karve, G.A. Potts, R.A. Rand, G.M. Latter, and M.A. Dubecky, "A Methodology for Calculating and a Process for Mitigating Channel Distortion and Cell Friction (Part I)," *TopFuel 2006 International Meeting on LWR Fuel Performance*, Salamanca, Spain, European Nuclear Society, (2006).
2. A.A. Karve, M.A. Dubecky, W.C. Cline, A. Enica, J.P. Rea, and J.E. Fawks, "A Methodology for Calculating and a Process for Mitigating Channel Distortion and Cell Friction (Part II)," *TopFuel 2006 International Meeting on LWR Fuel Performance*, Salamanca, Spain, European Nuclear Society, (2006).
3. P. E. Cantonwine, A. A. Karve, Y. P. Lin, S. T. Mahmood, D. W. White, and D. C. Crawford, "GNF Channel Performance and Success in Mitigating Channel Distortion and Cell Friction," *2008 Water Reactor Fuel Performance Meeting (WRFPM 2008)*, Paper No. 8078, October 19-23, 2008, Seoul, Korea (2008).
4. S. T. Mahmood, P. Cantonwine, Y. P. Lin, D. Crawford, K. Edsinger and E.V Mader, "Shadow Corrosion-induced Bow of Zircaloy-2 Channels", 16th International Symposium on Zirconium in the Nuclear Industry,Chengdu, China, ASTM STP 1529, (2010).
5. P. Cantonwine, H. Paustian, G. Hahn, J. Tusar, M. Reitmeyer, and E. Mader, " Channel – Control Blade Interference in GE Boiling Water Reactor, D-Lattice Plants with Zircaloy-2 Channels," 2010 LWR Fuel Performance/TopFuel/WRFPM Conference, Paper No. 079, September 26-29, Orlando, Florida, (2010).
6. E.V. Mader, M. Reitmeyer, P. Garcia Sedano, J. Morris, P. Cantonwine, L. Hallstadius, G. Potts, H.R. Peters, W. Li, "EPRI BWR Channel Distortion Program," 2011 Water Reactor Fuel Performance Meeting, Chengdu, China, Sept. 11-14, Paper #2-001 (2011).
7. SC08-05 Rev. 1, "Updated Surveillance Program for Channel-Control Blade Interference Monitoring," December 17 (2008).
8. P. Cantonwine, D. Crawford, M. Downs, B. Joe, T. Bahensky, J. Reimer, C. del la Hoz, K. Petersen, M. Reitmeyer, J. Morris, A. Zbib, "Channel – Control Blade Interference Management at LaSalle 1 and 2 during 2007 and 2008," *Proc. Of TopFuel 2009*, Paper 2154, p. 6-15, European Nuclear Society, Paris, France (2009).

INVESTIGATION OF BWR CORROSION FAILURES

D. LUTZ
Global Nuclear Fuel - Americas
6705 Vallecitos Road, Sunol, CA 94586 - USA

Y-P. LIN, R. SCHNEIDER, H. YEAGER
Global Nuclear Fuel - Americas
3901 Castle Hayne Road, Wilmington, NC 28402 - USA

A. KUCUK, B. CHENG
Electric Power Research Institute
3412 Hillview Avenue, Palo Alto, CA 94303 - USA

J. LEMONS, K. NESMITH
Tennessee Valley Authority
1101 Market Street, Chatanooga,TN 37402 – USA

ABSTRACT

Fuel rods in 63 fuel assemblies operated in a US BWR failed progressively in late 2001 to 2003 during their second cycle. The fuel failures were investigated by means of fuel examinations in the spent fuel storage pool and two separate hot cell examination campaigns. The primary failure mode was perforation through brittle localized hydrides that formed prior to failure in regions of accelerated corrosion and spalling. Observations of hydride localizations at discontinuities in oxide thickness suggested that corrosion-generated hydrogen localized under the action of local thermal gradients. Although hydrogen is known to have a significant role in light water reactor fuel failures, the specific manifestation of hydrogen in the present corrosion failures is a new, or previously unrecognized, mechanism that has not been identified in the industry.

1. Introduction

1.1 Background

Sixty-three GE13 9X9 fuel assemblies failed by a corrosion-related mechanism in Browns Ferry, Unit 2 (BF-2) during Cycle 12. Failures began in December 2001 approximately seven months after the beginning of Cycle 12. Additional failures in March and early April of 2002 were the first sign that an unusual event was in progress. Failures then continued through the end of the cycle despite efforts to carefully coast down to ~70% of rated power beginning ~ 6 months before the end of the cycle. The acceleration is consistent with other historical corrosion-related events, such as Crud Induced Localized Corrosion (CILC) [Reference 1], which occurred in multiple cycles in all three Browns Ferry units in the early 1980's. Failures also continued through the cycle despite the removal of leaking assemblies during two mid-cycle outages (MCO), in April (MCO 12A) and May of 2002 (MCO 12B), and relocation during the second MCO of bundles considered most susceptible at the time based on exposure and material commonality. Despite these maneuvers, failures were eventually observed in the sixty-three bundles, which included cladding from multiple ingots and lots that were distributed through the core.

The failures and their cause were investigated from 2002 to the present. The investigation included evaluations of materials and manufacturing details, assessments of operating conditions (power/duty and water chemistry), poolside inspections (visual, eddy current lift-off, profilometry, crud scraping), two fuel retrievals and associated hot cell examinations, laboratory measurements and analyses of events and related experience in other plants.

The leaking fuel bundles in BF-2 were identified by sipping. The failed bundles were among second-cycle bundles in BF-2 Reload 10. Among the 63 failed bundles, the failed pin location is known for only one rod in each of 5 bundles: one full-length rod and four part-length rods. A significant part of Reload 10 failed during BF-2 Cycle 12; i.e., ~20% of the bundles. However, none of the Reload 9 or Reload 11 fuel that was in the core during Cycle 12 failed or exhibited accelerated corrosion. A comparison of maximum effective eddy current lift-off measurement results that provide an estimate of the amount of cladding corrosion and highlight the reload discrimination is shown in Figures 1 and 2.

The BF-2 poolside and hotcell examinations were structured to define conditions associated with the fuel failures. Approximately 15 bundles and 75 rods were inspected in detailed poolside inspections, representing failed and sound Reload 10 second-cycle fuel, and sound fuel from prior cycle discharges as well as the sound first and third cycle fuel in Cycle 12. Additional inspections occurred for a similar but smaller event in Browns Ferry Unit 3, during which only three failures occurred. The BF-2 bundles and rods were selected for examination based on the results of in-core sipping, reviews of fabrication and operational records, and to explore the apparent effects of cladding composition, power/duty, time or exposure, and crud deposits on the failure process. Evaluation of the failures supported by the poolside inspection results established the following:

- Failures were caused by a complex interaction of cladding material, power/duty, and water chemistry; however, despite gaining considerable knowledge of the event's causal factors it is still not completely understood;
- Leading highest power bundles failed first;
- Failures occurred throughout the core;
- Most of Reload 10 exhibited accelerated corrosion and surface spallation to varying degrees;
- Corrosion was discriminated by reload such that earlier and later reloads operating at the same time did not experience accelerated corrosion;
- Axially double-peaked corrosion was exhibited;
- The greatest spalling, corrosion, and failure occurred at upper elevations, e.g., near 90-100 inches for part-length rods and slightly higher on full-length rods;
- Heavy spalling occurred in regions of accelerated corrosion;
- Corrosion was relatively unaffected directly beneath the ferrule spacers;
- Azimuthal corrosion variation; i.e., where the sides of fuel rods facing the bundle OD (channel) or central water rods exhibited dramatically reduced corrosion;
- Corrosion behavior was sensitive to alloying content, primarily iron and tin;
- Multiple ingots were affected;
- Ingots supplied by two different vendors were affected;
- The failures have not recurred.

The failure investigation and root cause assessment were discussed in 2004 based only on available poolside inspection results [Reference 2]. Since that time, seven fuel rods have

been examined in the hotcell in two campaigns to gain further insight and characterization of the failure mechanism. Results of these hotcell investigations are discussed in this paper.

1.2 Fuel Description

All of the Reload 10 failures were of the GE13 design that consists of a 9X9 rod lattice with 74 full-length fuel rods, 8 part-length rods, 2 water rods, 8 spacers distributed with varying axial separation along the length of the fuel rods and tie plates at both ends. The fuel pellets are contained in heat-treated, recrystallized Zircaloy-2 tubes with a zirconium liner on their inner surface. The rods are filled with helium and sealed with Zircaloy-2 end plugs.

Cladding from all retrieved fuel rods was produced with the same cladding manufacturing process that was used in about 3 million fuel rods produced by GNF from 1994 through 2004. This same fuel operated to end of life exposures, with normal corrosion, at all other reactors supplied by GNF.

1.3 Rod Retrieval and Operating History

Seven GE13 fuel rods were selected from five bundles for retrieval and hotcell examination in two different campaigns. Examination results for three exemplary rods discussed presently are summarized in Table 1. The rods include one sound part-length rod (YJS614 G9) that was relatively undamaged, one sound full-length rod that was near failure (YJS616 B8), and one failed part-length rod (YJS734 H2). All rods are from second-cycle Reload 10 bundles.

The irradiation history of the retrieved rods is also summarized in Table 1. The Reload 10 fuel had operated for a total of 906 days and had reached ~30 GWd/MTU bundle average exposure at the time of the first failure in Cycle 12. Sound Reload 10 rod YJS616 B8 and sound Reload 10 rod YJS614 G9 operated from BOC 11 until MCO 12A when they were discharged on April 23, 2002.

The failed Reload 10 Rod YJS734 H2 operated from BOC11 and was discharged at EOC 12B on 10/19/2002. This bundle was sipped and found to be sound during MCO 12A, which occurred between April 23, and April 30, 2002. Bundle YJS734 was identified as failed by sipping during MCO 12B. Plant failure indications suggest that it failed between 9/14/2002 and 10/19/2002, thus YJS734 H2 operated in the failed condition for at most ~35 days, but possibly as few as 1-2 days.

2. Hotcell Examinations

2.1 Hotcell Examination Objectives and Tasks

The objectives of the hotcell examination were to 1) to characterize the fuel rod conditions associated with failure, 2) to the extent possible, identify the fuel failure mechanism. The hotcell examination included a full complement of characterization activities to meet these objectives including visual examination, gamma scanning, fission gas analysis, burnup analysis, neutron radiography, leak testing, optical microscopy/metallography, hydrogen analysis, scanning and transmission electron microscopy, chemical analysis, SIMS analysis, and corrosion testing. Selected characterization results are discussed further below.

2.2 Identification and Characterization of Primary Failure Location in Failed Rod YJS734 H2

The primary objective of the YJS734 H2 rod examination was to identify the primary failure location. The rod exhibited heavy spallation and corrosion in the upper enriched half of the rod that was typical of the event.

Two leaking locations at 52.7 and 93 inches were identified by basic visual examination (Figure 3). To find other possible primary failure locations, the ends of rod sub-sections

were sealed and then the sections were pressurized with He. The pressurized sections were placed in a water trough to identify leak locations with escaping He bubbles. Three perforations were identified by this method at 95.9, 97, and 103.6 inches. None of these perforations had obvious visual indications of through-wall corrosion localization (i.e. corrosion “pit”). All five perforated locations required further detailed metallographic investigation to identify the primary failure location among them. Up to 26 closely spaced grinding/polishing planes were examined in some samples.

The characteristics observed for two adjacent samples from near 93 inches are consistent with a perforation being present at that location during operation because crack faces were oxidized. However, through-wall localized corrosion was not the cause of that perforation. Rather, the perforation was caused by OD-initiated cracks through a locally hydrided region. The three perforations located at 52.7 97.0, and 106.3 inches also contained cracks associated with hydride localizations but none contained significant metal thinning, a through-wall localized corrosion pit or a through-wall crack with well-oxidized faces on the outer and inner surfaces that would be indicative of a primary corrosion failure location.

The 95.9 inch sample contains an extensive, multi-branch crack network within a large hydride localization that spans the cladding width (Figure 4). Some cracks originate on the outer surface and some on the inner surface. Many cracks have well-oxidized faces, indicating that the crack was present during operation for a substantial amount of time, more so than for the leak near the 93 inch elevation. The outer surface oxide layer thickness varies throughout the sample and is up to 120 microns thick at some planes, which is the thickest oxide observed in the entire examination. The zirconium oxide layer has numerous lateral cracks and delaminations, which are indications of a non-protective oxide. Although most crud had spalled off in this region, there was no crud infiltration into the oxide cracks and a few remaining crud patches were of modest thickness. The remaining metal thickness beneath the 120 micron oxide is consistent with this value, which indicates that the measurement was not significantly affected by spalling.

It was concluded that the 95.9 inch perforation was the most likely primary failure location, with the other observed perforations likely secondary failure sites. This conclusion is supported by the well-oxidized crack faces at the 95.9 inch elevation at both cladding surfaces and the lack of similarly well-developed crack face oxide at the four other perforated locations. Although corrosion was high near 95.9 inches, through-wall corrosion did not occur and metal loss was relatively modest. The lack of through-wall corrosion and the presence of cracks only in hydrided locations led to the determination that failure occurred by cracks propagating through hydride embrittled cladding.

2.3 Examination of Sound/Damaged Rod YJS616 B8

Partial-length rod YJS616 B8 was punctured in the hotcell to measure the rod’s internal pressure and to collect fission gas. The rod was fully pressurized, which is an indication of its integrity and classification as an unfailed rod. The YJS616 B8 rod has characteristics similar to the failed H2 rod, with indications of heavy spalling and corrosion with an ~ 90 micron eddy current lift-off peak near 95 inches (Figure 5). The axial eddy current lift-off profile also exhibits a smaller ~ 45 micron corrosion peak near 18 inches. Some shallow pitting exists in the peak corrosion and spalling span. There is an abrupt drop in spalling and corrosion directly beneath the fifth spacer location near 99-100 inches. Despite the advanced corrosion condition, there are no visible perforations or through wall corrosion pits.

Nine metallographic samples were examined from the sound YJS616 B8 rod between 15 and 104 inches. Residual outer surface oxide thicknesses range from 1.9 to 58.2 microns and have moderate circumferential variation (Figure 6). Cross-sectional photomicrographs reveal a laterally cracked oxide along the entire rod length, without crud infiltration, and modest metal loss (Figure 6).

Hydriding characteristics vary along the length of the rod as shown by cross-section average hydrogen measurement results and radiography indications summarized in Figure 5. Below 65 inches the cladding metal hydrogen content is between 40 and 266 ppm with no visible hydride localizations in the radiography. Moving upward axially, beginning near the 85 inch elevation, the hydrogen and quantity of hydrides increases, and despite the lack of visible hydride localizations in the radiography at that elevation several hydride localizations are visible metallographically on the cladding outer surface (Figure 6). Some localizations are best described as hydride rims, both thick and thin. The highest cross-section average hydrogen content (~850 ppm) and the largest hydride localization occur at 95 inches, which is in the peak corrosion and spalling zone. The localization penetrates a little more than half the cladding thickness to the inner surface (Figure 7). One common hydriding feature observed in the examination is that many of the smaller hydride localizations were located directly between two converging oxide fronts that created a small well between them (Figure 8). The oxide was thin directly above the hydride, and the well was filled with crud.

A longitudinal sample from 98.9 inches was examined based on the neutron radiography that highlighted a circumferential hydride band that formed beneath the bottom of the fifth spacer and corresponding to an abrupt drop in corrosion and spallation (Figure 9). This band was investigated in an approximately 0.8-inch-long longitudinal clamshell metallography sample that straddles the transition into the bottom end of the spacer. Characterization of this sample clearly shows a step change in oxide thickness consistent with the visual appearance and eddy current lift-off profile, and a shallow outer surface hydride rim corresponding to the radiographic indication.

2.4 Examination of Sound Rod YJS614 G9

The sound full-length YJS614 G9 rod was examined in detail from the lower endplug tip to the upper endplug tip. Eddy current lift-off measurement of this rod identified a broad ~40-50 micron corrosion peak near 120 inches. The rod has moderate corrosion and crud deposition levels, but there is very little spalling and little indication of damage that the other two rods experienced. The type and amount of corrosion is not well defined by visual appearance alone, but discrete oxide nodules, that seem to be coalesced at lower elevations, become visible above about 136 inches (Figure 10). The presence of nodular corrosion is unusual for GNF heat treated cladding.

Two metallography samples were examined from the sound Reload 10 YJS614 G9 rod at 96.0 and 118.5 inches. The oxide characteristics are similar at both elevations as the other two rods but less thick and less variable. Oxide thicknesses range from very thin up to 46.6 microns, and crud thicknesses range up to 21 microns. Cross-sectional photomicrographs reveal a laterally delaminated, cracked oxide with nodular-like characteristics.

Axial variation of cladding hydrogen content is less than about 55 ppm (Figure 11). Due to the very low hydrogen content, the hydrides are short speckles distributed throughout the cladding cross-section. No hydride localizations were observed.

3.0 Discussion

Hotcell examination results showed that cladding oxidation did not lead to deep pits or gross wall thinning that perforated the cladding. Rather, localized hydrides that were present prior to failure (in the areas with maximum corrosion) were the sites of the initial cladding perforations. Some of the non-primary perforations in the failed rod may be due to secondary hydriding, in particular the lowest 52.7 inch one on the YJS734 H2 rod, however it is difficult to discern between pre-failure and post-failure hydrides.

Fuel rod nodal power histories were evaluated in detail using GNF's thermal-mechanical fuel rod codes. It was found that the onset of relatively modest tensile hoop stresses in the cladding, at the elevations where the maximum corrosion and hydride localizations were

found, occurred at about the same time in the cycle as the failures occurred. This is consistent with a mechanism involving cracking of a hydrogen-embrittled region.

The contrast in hydriding between the sound YJS616 B8 rod and the sound YJS614 G9 rod is evident. There is a clear correlation between hydride localization and the degree of corrosion, hydriding, and spalling. Based on this observation, it is likely that hydrogen and localization in the B8 rod did not increase dramatically until after large-scale spalling of oxide began to occur. However, the exact timing is not clear from the available data.

It is well established that thermal gradients can provide a driving force for diffusion and concentration of hydrogen at cold spots in zirconium alloys. For example, thermal gradient effects have caused lenticular shaped hydrogen localizations to form beneath a localized spallation of 160 micron thick oxide in PWRs [Reference 3] and on the cladding side directly opposite an accelerated corrosion feature [Reference 4]. Leger et al. conducted a laboratory study that caused the formation of a localized hydride lens in CANDU pressure tube material [Reference 5]. In that study, a stream of cold air was directed onto the surface of a heated sample that contained 100 ppm uniform hydrogen. The local temperature gradients that developed caused migration and concentration of the bulk hydrogen into a very large lens directly beneath the impinging air stream. Thermal gradients may have similarly affected hydride localization in damaged BF-2 rods.

Local temperature gradients are postulated to exist in the BF-2 rods due to local variations in heat transfer that are in turn caused by local variations in oxide thickness due to spalling and local variations in the oxidation rate. The small localized hydrides that formed directly beneath thin oxide layer in the plateau wells that were formed by converging oxide fronts supports this. The thin oxide would provide less thermal resistance and would be slightly cooler than the adjacent regions that have thicker oxide. The local temperature disturbance around the well could then draw hydrogen into the well. Likewise, the step change in oxide thickness beneath the fifth spacer in the YJS616 B8 rod would cause a local temperature gradient that would promote the migration and concentration of hydrogen beneath the spacer.

The primary alloying constituents of the YJS734 H2 and YJS614 G9 rods were measured on small pieces obtained from their plenum regions. Both rods had similar, normal alloying contents, e.g. approximately 0.17 wt% Fe and 1.3 wt% Sn, and yet they performed quite differently. As indicated in Table 1, the G9 rod was removed 171 days earlier than the failed YJS734 H2 rod, which partially explains its performance difference for an equivalent alloying content. The YJS616 B8 and YJS614 G9 rods were removed at the same time in MCO 12A and also exhibited different behavior. The rod-specific alloying content of the B8 rod was not measured, so alloying contents cannot be compared directly for these two rods. Both rods had similar peak nodal power levels, which suggests that there may be an in-specification alloying difference between these two rods, consistent with an in-specification alloying sensitivity that was observed in broader poolside inspection measurements. Still, the H2/G9 comparison suggests that the G9 rod would have eventually advanced with further irradiation to the same damaged state as the H2 rod provided that comparable power levels were maintained.

Hydrogen has played a significant role in light water reactor fuel failures; however the specific manifestation of hydrogen is different in the BF-2 failures than in other published corrosion-related hydride failures. For example, corrosion-generated hydrogen is absorbed and forms large localizations under the action of thermal gradients in “classic” BWR CILC failures that required crud infiltration into the oxide, but failure was ultimately thought to ultimately occur by autocatalytic progression of through-wall corrosion [Reference 4]. In a second failure mechanism, outside-in cracking of BWR fuel rods can occur under power ramp conditions that promote radial hydride formation on the outer surface with modest bulk cladding hydrogen levels [Reference 6]. In a third mechanism, small, multiple hydride localizations formed during operation from corrosion-generated hydrogen in high burnup PWR cladding [Reference 7]. These localizations are somewhat similar to the BF-2 case

and promoted failure under severe burst test conditions, but not during normal operation. The present corrosion failures are a new, or previously unrecognized, mechanism that has not been identified in the industry.

A broad investigation into the failures determined that they were caused by a complex interaction of cladding material, power/duty, and water chemistry [Reference 2]. Although some important underlying aspect of the failure event has not yet been determined, corrective measures were taken to the extent possible to provide some margin against recurrence. Actions by GNF led to the 2004 introduction of cladding that has tighter specification limits for Zircaloy-2 alloying elements and a modified heat treatment. The cladding is expected to provide additional resistance to nodular corrosion in challenging water chemistry environments. Actions were also taken to better control water chemistry, which included controlling feedwater zinc injection to < 0.4 ppb, installation of higher efficiency filter elements to reduce feedwater iron concentrations, installation of improved filter connection hardware to improve condensate demineralizer operations, and expanded reactor water monitoring. Periodic fuel inspections at BF-2 since the failure event have shown no signs of recurrence.

4.0 Summary

Hotcell investigations advanced the state of knowledge of a significant corrosion-related BWR fuel failure event. The investigation established that the BF-2 Reload 10 fuel failed by accelerated cladding nodular corrosion that resulted in the absorption of corrosion generated hydrogen. Localization of hydrides is postulated to have resulted from local thermal gradients that are caused by local differences in oxide growth and spalling of oxide. Massively hydrided regions then fractured under tensile loading that arose with accumulation of exposure during the course of normal operation. The specific manifestation of hydrogen and its localization in the BF-2 corrosion failures is a new, or previously unrecognized, BWR failure mechanism that has not been published in the industry.

5.0 References

1. Marlow, M.O., Armijo, J.S., Cheng, B., Adamson, R.B., “Nuclear Fuel Cladding Localized Corrosion,” American Nuclear Society International Topical Meeting on Light Water Reactor Fuel Performance, April 21-24, 1985, Orlando, FL.
2. Schardt, J., Keys, T.A., Lemons, J.F, Ottenfeld, C., “Fuel Corrosion Failures in the Browns Ferry Nuclear Plant,” Proceedings of the 2004 International Meeting on LWR Fuel Performance, Orlando, FL, September 19-22, 2004, Paper 1036.
3. Garde, A.M., Smith, G.P., and Pirek, R.C., “Effects of Hydride Precipitate Localization and Neutron Fluence on the Ductility of Irradiated Zircaloy-4,” Zirconium in the Nuclear Industry: Eleventh International Symposium, ASTM STP 1295, E. R. Bradley and G. P. Sabol, Eds., American Society for Testing and Materials, 1996, pp. 407-430.
4. Ogata, et al, International Topical Meeting on Light Water Reactor Fuel Performance, West Palm Beach, Florida, April 17-21, 1994.
5. Leger, M., Moan, G. D., Wallace, A. C., and Watson, N. J., “Growth, Fracture, and Nondestructive Evaluation of Hydride Blisters in Zr-2.5 Nb Pressure Tubes,” Zirconium in the Nuclear Industry: Eighth International Symposium, ASTM STP 1023, L. F. P. Van Swam and C. M. Eucken, Eds., American Society for Testing and Materials, Philadelphia, 1989, pp. 50-65.
6. Shimada, S., Etoh, E., Hayashi, H, Tukuta, Y., “A Metallographic Study of Outside-in Cracking Caused by Power Ramp Tests,” Journal of Nuclear Materials, Volume 327, 2004, pp. 97-113.

7. Hermann, A., Yagnik, S., Gavillet, D., “Effect of Local Hydride Accumulation on Zircaloy Cladding Mechanical Properties,” Zirconium in the Nuclear Industry: Fifteenth International Symposium, ASTM STP 1505, Bruce Kammenzind and Magnus Limback, editors, 2009, pp. 141-162.

	Cycle 11	Cycle 11	Cycle 12A	Cycle 12A	Cycle 12B	Cycle 12B		
Bundle/Rod	BOC	EOC	BOC	EOC	BOC	EOC	Irradiation Time (days)	Rod Average Exposure (GWd/MTU)
YJS614 G9	05/10/99	03/09/01	04/17/01	04/23/02	N/A	N/A	1040	34.477
YJS734 H2	05/10/99	03/09/01	04/17/01	04/23/02	05/01/02	10/19/02	1211	47.262
YJS616 B8	05/10/99	03/09/01	04/17/01	04/23/02	N/A	N/A	1040	41.105

Table 1: Irradiation history of BF-2 Reload 10 GE13 fuel rods examined in hotcell

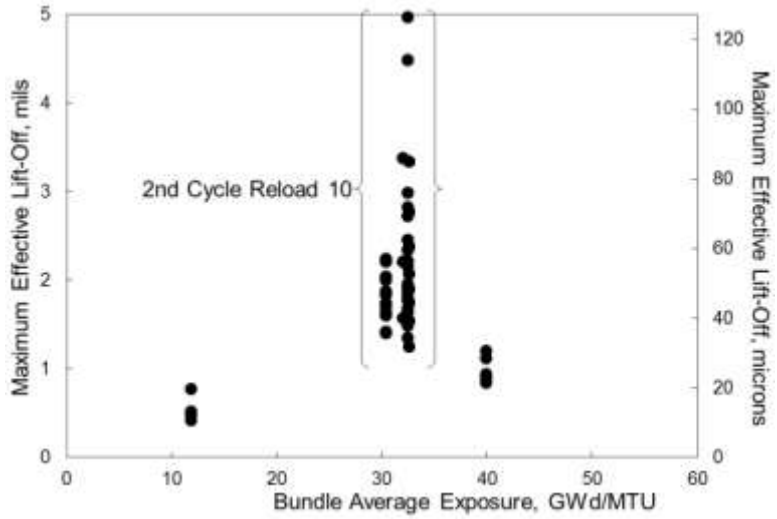

Figure 1: BF-2 Lift-Off vs. Exposure Showing Affected Reload 10 Fuel Rods Compared to Normal Performance of Earlier (Reload 9) and Later (Reload 11) Reloads

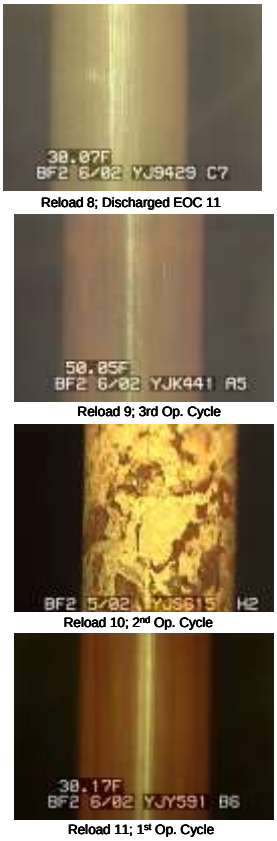

Figure 2: Visual Appearance of Fuel Rods in BF-2 Reloads 8, 9, 10 and 11

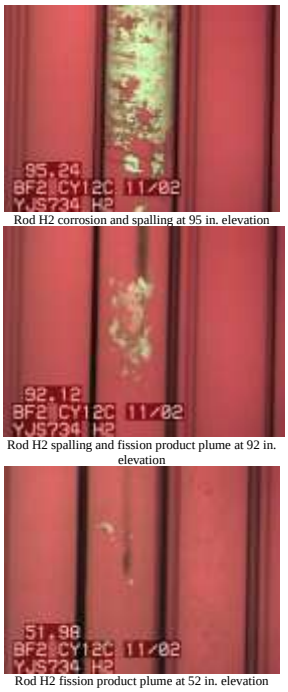

Figure 3: Visual Appearance of Failed BF-2 Reload 10 H2 Rod In Place in Bundle YJS734; Leaking Locations Near 52 and 92 inches and Heavy Spalling Starting Near 95 inches are Shown

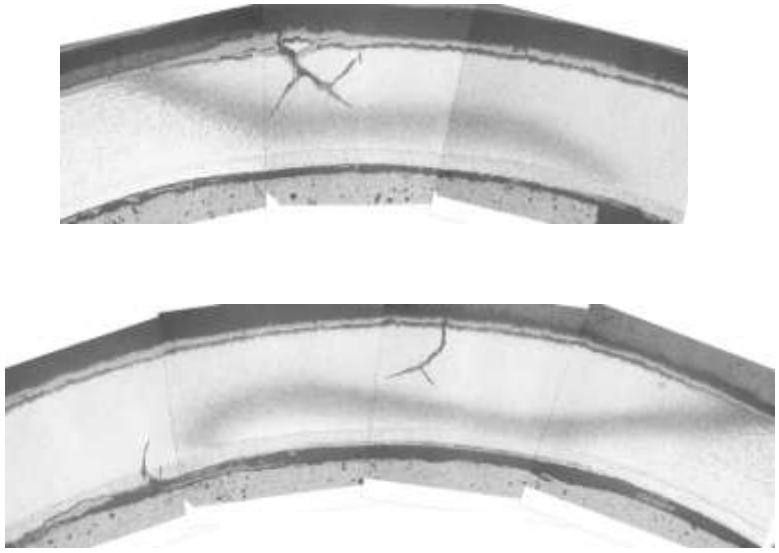

Figure 4: Etched Cladding Cross-section from Failed BF-2 Reload 10 Rod YJS734 H2 at 95.9 inches Showing Cracks Within Massive Hydride Localization near Primary Failure Location

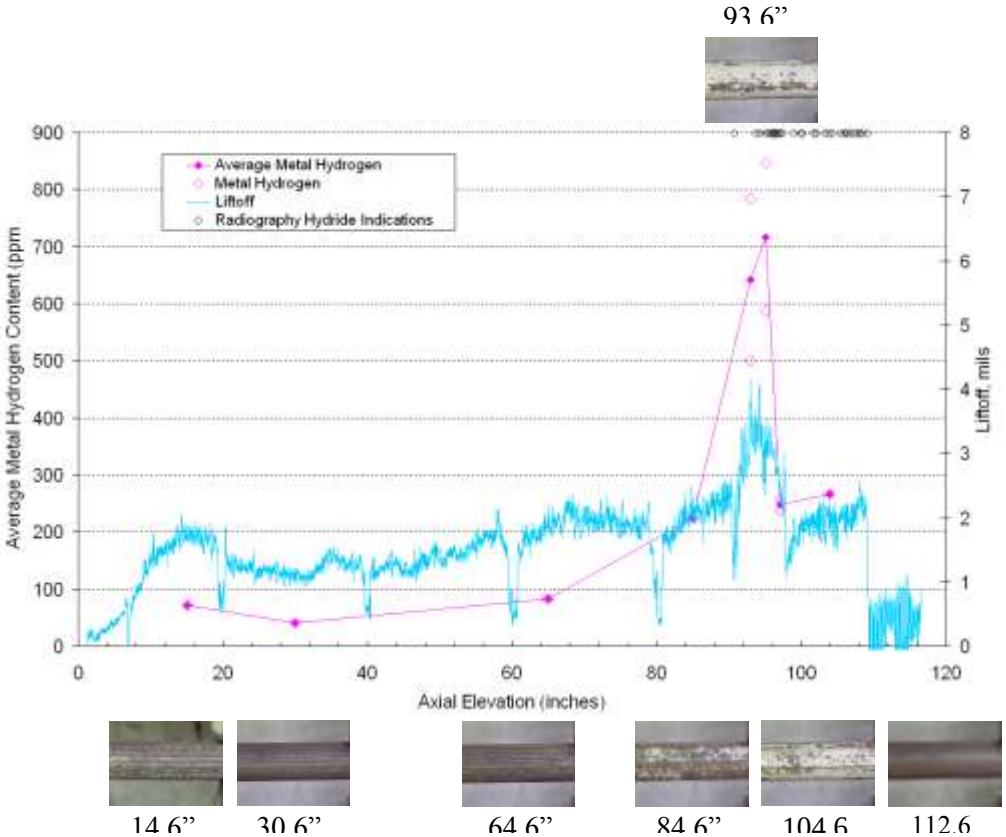

Figure 5: Variation of Visual Appearance, Lift-off, Cladding Metal Hydrogen Content, and Radiography Hydride Localization Indications in Sound BF-2 Reload 10 YJS616 B8 Rod

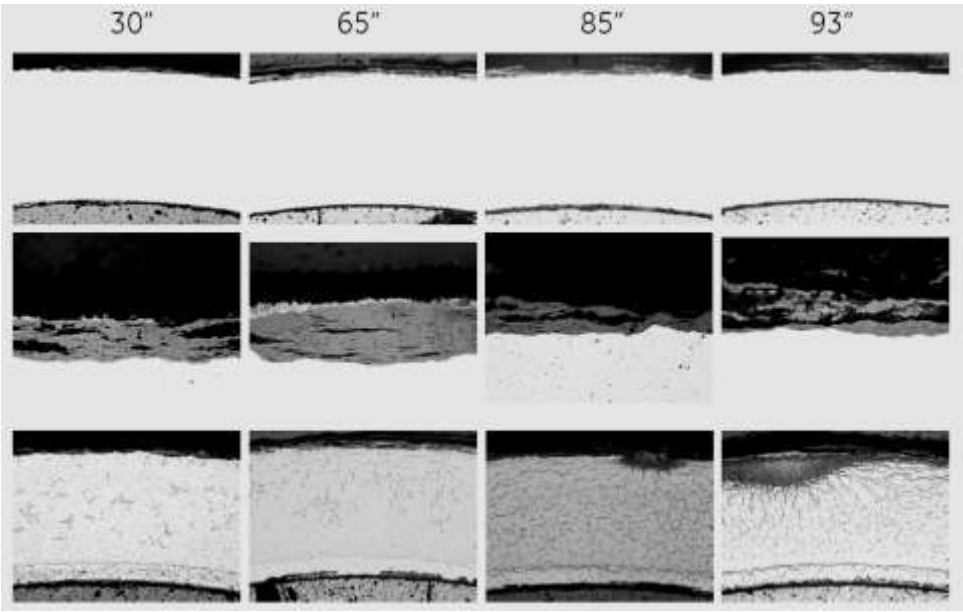

Figure 6: Polished and Etched Metallographic Cross-sections at 30-93 inch elevations for Sound BF-2 Reload 10 YJS616 B8 rod; Low Magnification Cross-sections Show Relative Residual Cladding Thickness (upper row, whole cladding thickness), High Magnification of Cladding Outer Surface Showing Residual Oxide thickness, Crud thickness, and Oxide Morphology (middle row), and Hydrides (bottom row)

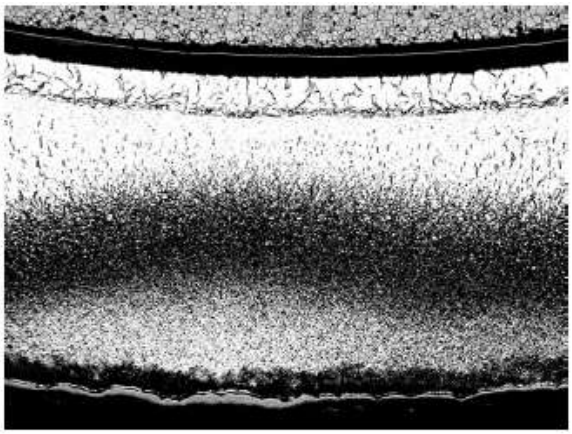

Figure 7: Etched Metallographic Cross-section at 95.1 inches for Sound BF-2 Reload 10 YJS616 B8 rod; Cross-section Shows Massive Pre-Failure Hydride Localization

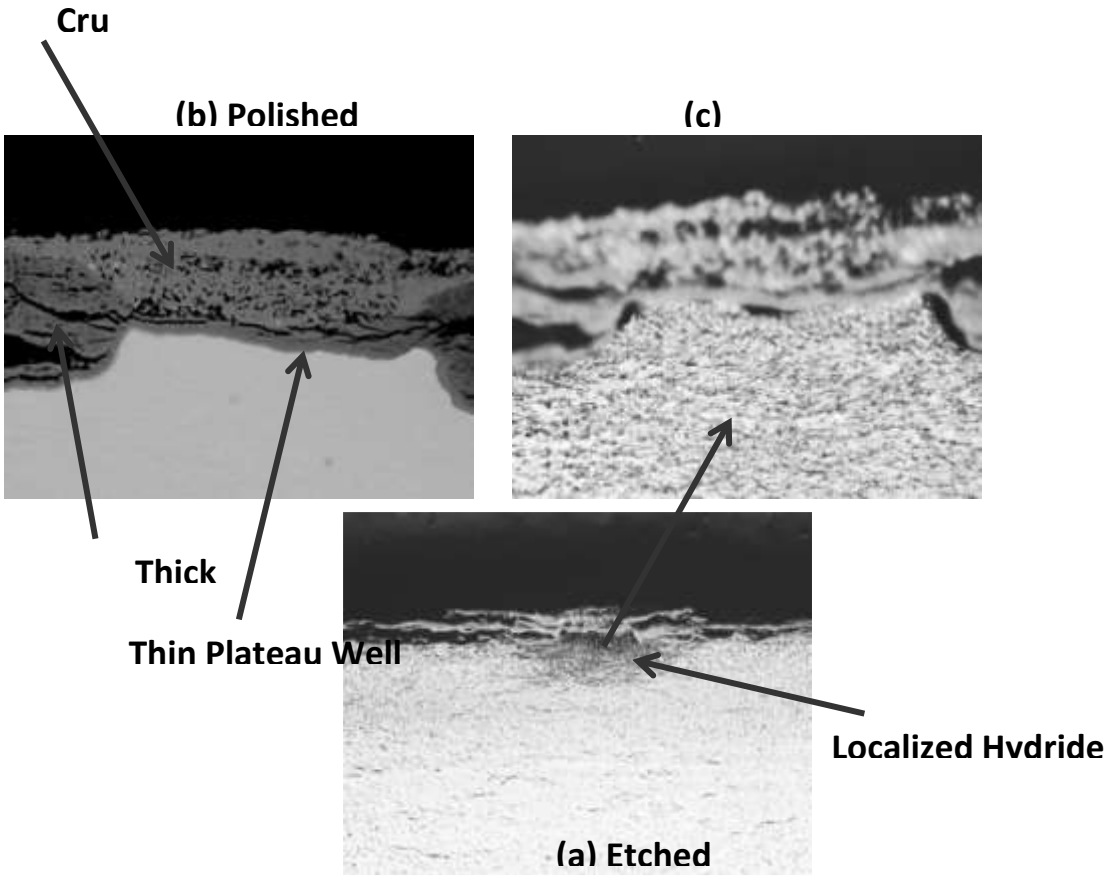

Figure 8: Polished and Etched Cross-sections of Sound BF-2 Reload 10 Rod Showing Localized Hydride Formation Beneath Oxide “Well”

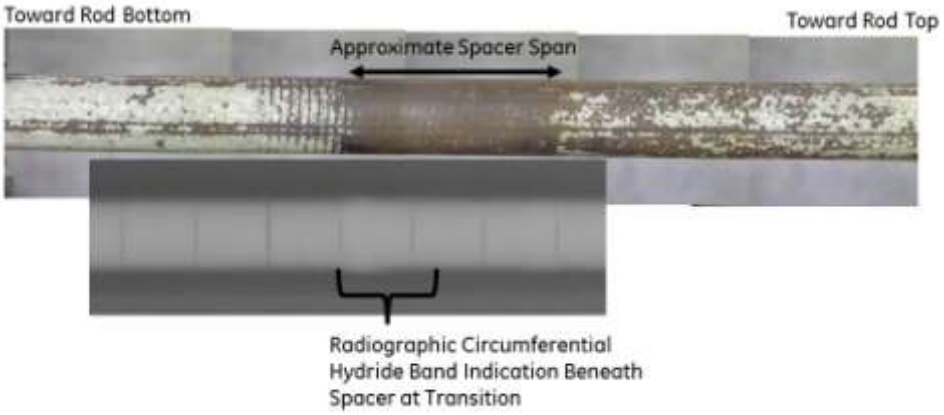

Figure 9: Visual Appearance of Region Containing Fifth Spacer Near 99-100 inch Elevation of Sound BF-2 YJS616 B8 Rod Showing Step Change in Corrosion and Spalling Directly Beneath Spacer Location ; Radiographic Circumferential Hydride Band Indication Aligns with Transition to Fifth Spacer

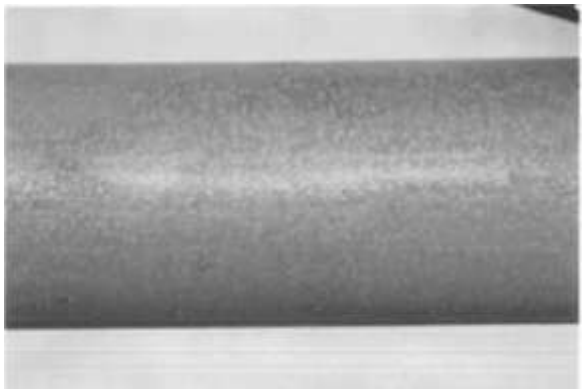

Figure 10: Nodular Corrosion on Upper Elevation (136 inches) of Sound BF-2 Reload 10 YJS614 G9 Rod

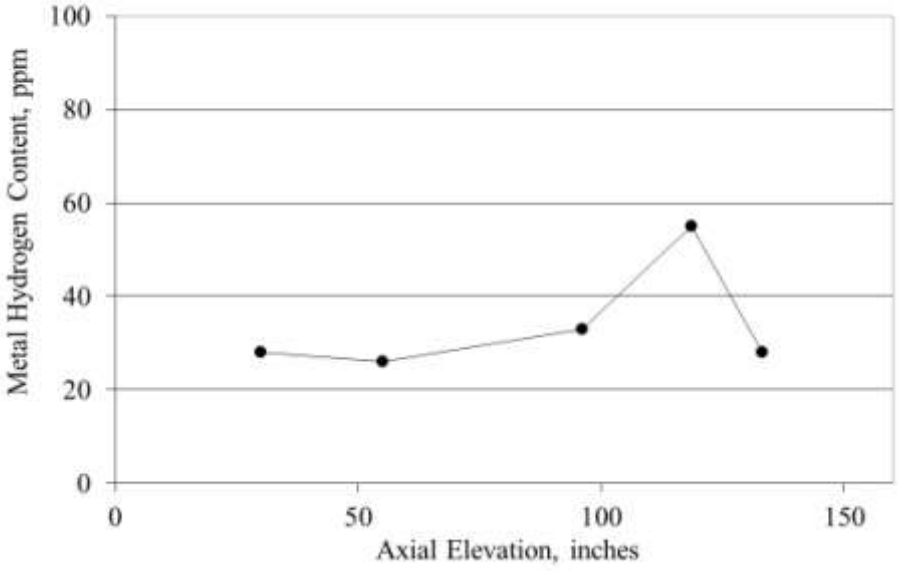

Figure 11: Axial Variation of Metal Hydrogen Content in Sound BF-2 Reload 10 YJS614 G9 Rod

REVISED INDUSTRY GUIDANCE ON LIGHT WATER REACTOR FUEL SURVEILLANCE AND INSPECTION

R. DAUM, K. YUEH, E. MADER
Electric Power Research Institute
3420 Hillview Avenue, 94304 Palo Alto, California - USA

E. ARMSTRONG
Finetech Inc.
959 U.S. Highway 46 East, 07054 Parsippany, New Jersey - USA

F. SMITH
Entergy Corporation
1340 Echelon Parkway, 39213 Jackson, Mississippi - USA

ABSTRACT

The Electric Power Research Institute has revised guidance for performing nuclear fuel assessments and inspections. The revision provides technical guidance on the scope and frequency of fuel performance assessments and inspections to support the industry goal of zero fuel failures and operational issues. To achieve this goal, both failed and healthy fuel must be inspected. Such inspections advance understanding of fuel failure mechanisms and unit-specific fuel margins, leading to more robust fuel designs and enhanced operating guidance. Moreover, the revision maintains an emphasis on monitoring of margins following significant changes or anomalous operating events that affect fuel performance. In doing so, this guidance promotes coordination and sharing of inspections among utilities to optimize industry-wide resources while still maintaining focus on margin determination.

Revision 1 to the *Fuel Surveillance and Inspection Guidelines* implements lessons learned from fuel inspections conducted since issuance of the original guideline in early 2008 – primarily from inspections of "Priority 1 plants" as designated by the major fuel suppliers. The revision includes two main changes: (1) A switch in the inspection strategy from priority-based "baseline" fuel inspections for all U.S. plants to one in which the need for baseline inspections is determined via a technical evaluation process. The technical assessment can be based on plant-specific fuel inspections or a combination of applicable industry inspections, including ones conducted on bounding or sister plants. This change should reduce the number of plants that will require extensive baseline fuel inspections yet permit sufficient cost-efficient margin determinations. (2) Addition of non-intrusive visual fuel inspection programs to monitor for margin impact of cumulative small changes and to help ensure applicable margins are maintained. The scope of the *recommended inspections* has been increased to address not only fuel failures from clad perforation, but also fuel performance issues that can have a significant impact on unit operations (e.g., PWR fuel assembly distortion).

1. Introduction

The Fuel Reliability Program (FRP) of the Electric Power Research Institute (EPRI) has revised the Fuel Reliability Guidelines: Fuel Surveillance and Inspection. This revision was envisioned when the initial Fuel Surveillance and Inspection Guideline (FSIG) was developed and issued in early 2008. It provides an overall new direction to determine when baseline fuel inspections are

needed to assess margins to operational limits and fuel failure. This new direction utilizes a formal, technical assessment process rather than mandated baseline inspections at all plants. The originally mandated baseline inspections were prioritized for the US fleet (Priority 1, 2 and 3 plants) and served as the starting point in the original FSIG. This new direction is based upon fuel inspection efforts and results completed over the past few years - mostly from completed Priority 1 plant baseline inspections and documented in EPRI reports by three fuel suppliers [1,2,3]. The overall results of these inspections have indicated that it is possible to determine margins to fuel failure at some plants based upon industry inspections rather than plant specific inspections. This revision also addresses use of fuel inspections to aid the industry in detecting fuel anomalies at an early stage to help prevent major operational impacts (e.g., PWR assembly top end fitting hold down spring issues). Background information that led up to the original FSIG and this update follows.

In response to industry's goal of zero fuel failures by 2010, U.S. Chief Nuclear Officers backed a new Fuel Integrity Initiative in 2006 that placed a significant emphasis on the development of fuel reliability guidelines. The first step in the guidelines process was to support the Institute of Nuclear Power Operations (INPO) in developing a series of fuel integrity excellence guidance documents. These documents summarized current industry information to assist utilities in improving their programs, and hence, fuel integrity and performance. Following issuance of more technically in-depth EPRI Fuel Reliability Guidelines (FRGs) discussed below, directly related INPO guide documents were withdrawn in favor of the more detailed FRGs. At the time of issuance of this revision to the FSIG, the top level INPO 2010 document on fuel reliability [4] and one of the area-specific INPO fuel integrity improvement documents on fuel fabrication [5] remained in place. The FRP developed three technical guidelines that were in key fuel failure areas, and one guideline, the FSIG, in fuel inspection. The goal of this effort was to capture the industry's state-of-the-art knowledge in these areas and offer, where possible, specific guidance and good practices to assist utilities with avoiding fuel failures by the specific failure mechanism. The key technical areas addressed by the FRP are:

- Pellet Cladding Interaction (PCI) (BWR and PWR)
- Corrosion and Crud (BWR and PWR)
- Grid-to-Rod Fretting (GTRF) (PWR)
- Fuel Surveillance and Inspection (BWR and PWR)

Failure by debris fretting is another common fuel failure mechanism and it is addressed by the EPRI Nuclear Maintenance Application Center (NMAC) through the Foreign Material Exclusion Guidelines [6]. Although not directly under the Fuel Reliability Program, both maintenance and FRP fuel personnel work together to address the challenges of debris control often referred to as Foreign Material Exclusion (FME).

The Corrosion and Crud for BWR [7] and PWR [8], respectively, and the PWR GTRF [9] Guidelines also contain guidance on fuel inspections - sometimes referring to the FSIG and sometimes providing stand alone guidance. This FSIG revision provides general guidance on integrating the FRG's in the area of fuel margin assessment and inspection realizing that they are not perfectly aligned since each of the FRG's are on different revision schedules. The Fuel Reliability Program: Fuel Design Evaluation Handbook [10] is another source of information on fuel components that are addressed in Chapter 2 and also contains information on irradiated fuel inspections for demonstration of certain design features.

The FSIG is heavily oriented towards inspections associated with baseline margins for corrosion and crud on both PWRs and BWRs and GTRF on PWRs. PWR fuel assembly distortion (FAD)

has also been added in this revision. Note that although the PCI failure mode is not stressed in the FSIG, poolside inspections such as fuel rod profilometry may provide some insight on margin. BWR channel distortion is only touched upon in this revision since the BWR Channel Distortion Program at EPRI is managing this issue. Lastly, Lead Fuel Assembly (LFA) inspections are briefly addressed but a future revision of the FSIG may provide more detailed guidance.

In summary the thrust of this guideline revision is as follows:

- a change from mandated baseline fuel inspections for determining baseline margins to fuel failure to a formal, technical evaluation process to determine when such inspections are needed and mandating such determination at a minimum frequency of every ten years;
- a continuation of the change management process in the original FSIG with enhanced guidance on determining when fuel inspections are needed to monitor the impact on margins of changes to fuel designs and manufacturing, reactor operations, chemistry and plant modifications;
- a continuation of the original FSIG direction to determine when fuel inspections are needed to monitor the impact on margins of anomalous operating conditions (e.g. chemistry excursions, incomplete control rod insertion, and fuel handling issues);
- implementation of a non-intrusive visual inspection process to maintain a closer awareness of overall fuel performance on a qualitative basis;
- an addition to the program to reduce or eliminate major operational issues from anomalous fuel performance that are not necessarily related to actual clad perforation; and
- optimization of industry-wide resources for coordinating and sharing inspections, while maintaining focus on margin determination.

2. Fuel Assessment, Inspection and Surveillance

Fuel assessment, inspection and surveillance activities are an essential part of ensuring that adequate margins exist. They also ensure that fuel and plant changes do not lead to unexpected challenges to fuel integrity or fuel performance issues that impact plant operations. Such inspections provide information to support the causal analysis of failed fuel rods or other anomalous fuel performance conditions. Proper controls and monitoring of fuel integrity and overall performance need to be established to assess the design and operating margins.

While fuel performance information from plants operating under similar conditions can be valuable, it is recognized that fuel reliability is a complex, multi-dimensional issue. Factors that influence fuel performance include the fuel design, fuel manufacturing processes, materials, water chemistry, and operating strategy. These parameters and the interactions between them make each operating unit unique in some way. Our ability to predict such differences and their impact of fuel reliability is improving, but the most comprehensive way to assess fuel performance in a given unit continues to be performing measurements directly in that unit.

However, based upon the results of completed Priority 1 plant baseline fuel examinations, this revision endorses a formal technical assessment process to determine the need for future baseline examinations at a particular plant for baseline margin determination. This process includes an assessment of a plant's fuel design(s), operating environment, inspection data from bounding or "sister" plants, industry LFA programs and failed fuel inspections that often also include healthy fuel inspections for comparison. The process is further supported by a periodic non intrusive fuel inspection on the unit being evaluated. It is important to note that this baseline

margin assessment may lead to additional inspections in the industry or at the plant being evaluated to supplement the existing inspection data base. However, it is not expected that extensive, baseline inspections will be needed at all plants following implementation of the assessment process.

This revision continues to rely on "change management" examinations for determination of future performance following significant changes to fuel design, fabrication, operations or the operating environment. It must be noted that past failure-free performance does not guarantee similar performance in the future. Hence, utilities need to adopt proactive fuel surveillance and inspection programs to quantify current margins to fuel failure or performance issues and verify that subsequent changes do not jeopardize fuel integrity or performance. Baseline and change management process flow charts and a number of assessment checklists are included in addition to tables as aids to utilities in developing this proactive program of fuel inspections.

The intended audience of this revised guideline is fuel engineering personnel, reactor engineering management, operations management, outage planning management, plant managers, INPO site evaluation teams, and fuel suppliers. Utilities need to set up a formal fuel assessment, inspection and surveillance program for each nuclear unit. The program will determine baseline margins to operational criteria and fuel failure and provide a basis for monitoring margins following significant changes or anomalous operating events. This guideline provides a detailed outline of what such a program should entail. This program is to be technically based. For baseline margin determination it should include an evaluation from one or more of the following: unit-specific fuel inspections, unit-specific past fuel performance, fuel inspections at sister or bounding plants, LFA and failed fuel inspections. If warranted, the assessment should recommend additional fuel inspections either at the plant being evaluated or at one or more sister or bounding plants to permit a complete determination of margins to failure.

Use of change management is then implemented to determine if a significant change in fuel design, fabrication, operations and / or operating environment triggers an inspection depending upon the magnitude of available margin. Determination of fuel inspections following anomalous operations such as chemistry excursions is to be included. Periodic non-intrusive visuals are to be a part of the program and will serve as a means for qualitative monitoring of fuel performance.

The key baseline surveillance data should include visual inspections and measurement of corrosion and crud for BWRs, and visual examinations, measurement of corrosion and crud, clad fretting wear and fuel assembly distortion measurements for PWRs. Although unit-specific measurements are the best way to assess current performance, the database from the recently completed baseline inspections at Priority 1 plants and other applicable industry inspections will serve as the basis for some plants to determine baseline margins through the new assessment process. This process will allow inspection resources to be focused on plants where margins may not be well understood. It will allow plants with good performance and substantial industry inspection data that is applicable to their fuel design, operating strategy and environment to avoid large scale baseline inspection campaigns.

It is essential to this approach for fuel suppliers to establish and maintain adequate resources to support utility needs for both technical assessments and fuel inspections. It is also essential that fuel suppliers work with the utilities to ensure optimal prioritization of such resources across the industry. Adequate sharing of inspection results by fuel suppliers is encouraged to facilitate comparisons.

An important part of achieving the overall goal of operations without fuel defects is to understand the cause of failures and to prevent re-insertion of failures. Guidance is provided on failed fuel issues including timely root cause determination and means to identify defects and prevent re-insertion. Such failed fuel inspections take top priority.

The key recommendations of this guideline are given in Table 1. This document adheres to the same implementation protocol set forth in NEI 03-08, Materials Initiative Guidance [11]. All recommendations, identified as either Mandatory, Needed or Good Practice, are presented in this paper along with supporting information related to the recommendation.

Implementation Category	Recommendation
Mandatory	Each utility shall establish a unit-specific assessment, inspection and surveillance program for non-failed fuel
	Each utility shall establish a program to prevent the re-insertion of failed fuel
	Utilities shall perform causal analysis for fuel failure events
Needed	Perform Baseline assessments and / or inspections to establish unit-specific margins at a frequency of ≤ 10 years
	Following a significant change or anomalous event, conduct a utility / vendor assessment to determine the need for targeted inspections
	Establish a non-intrusive visual inspection program to provide periodic qualitative feedback of general fuel condition at a frequency of ≤ 6 years
	Enter performed inspection scope into EPRI's Fuel Reliability Database (FRED)
	Utilities shall report annually to EPRI the status of their non-failed fuel assessment and inspection program
Good Practice	Inspect fuel on a cycle basis for general or qualitative fuel condition

Tab 1: Key Recommendations

In 2004, utility executives charged EPRI's FRP with establishing a fuel reliability database from which fuel performance could be monitored and trended. The Fuel REliability Database (FRED) is a web-based program containing data entries for cycle operational information, fuel design and features, core components, water chemistry, fuel inspection, damaged fuel, undamaged discharged fuel, radiochemistry and other performance issues, such as axial offset anomaly (AOA) in PWRs and channel deformation in BWRs. The purpose of the industry-wide fuel reliability database is to provide timely information and trends on fuel performance and reliability, as well as to guide research and development (R&D) efforts. Users can also upload root cause and fuel surveillance reports directly into FRED for other participants to view. Organizations that have access to FRED are participating U.S. and international utilities, fuel suppliers, INPO and EPRI. FRED now accepts information about the scope of surveillance campaigns as well as key results to help utilities know what inspections have been performed and what was learned. FRED is a key database for capturing actual inspections and key results generated as part of this Guideline.

3. Non-Failed Fuel Surveillance

The revised guideline recommends a program for non-failed (healthy) fuel surveillance to establish baseline performance margins and to provide guidance on monitoring this performance during future changes. The main objectives are to provide guidance on:

- obtaining and using unit specific fuel inspection data or performing an assessment of sister plant inspection data for baseline performance determination, and
- type and magnitude of changes or anomalous operating events that could impact performance and the type of fuel inspections that might be warranted.

The objective of the technical assessment, inspection and surveillance activities for non-failed (healthy) fuel is to use actual fuel inspection data to first establish a *baseline* of performance for fuel operating under unit-specific conditions and, second, to provide the technical basis against which future performance can be compared. As such, the data collected as part of these inspections and / or surveillances (a) have the best chance to identify precursor conditions that could lead to fuel failure or serious performance issues, and (b) enables quantitative comparison to assess subsequent changes in fuel design, manufacture or operation. These objectives may be accomplished through a formal process for use of industry wide inspection data directly applicable to the plant under evaluation rather than necessitate baseline fuel inspections at each plant. This will permit appropriate utilization of industry resources in targeting detailed inspections and data evaluations where most useful. Resource optimization includes utility and fuel supplier engineering staff time for assessments, and in the area of inspections, the number of inspection field teams, outage impact, overall cost and dose considerations. Figure 1 is included to serve as an example of a *baseline* process.

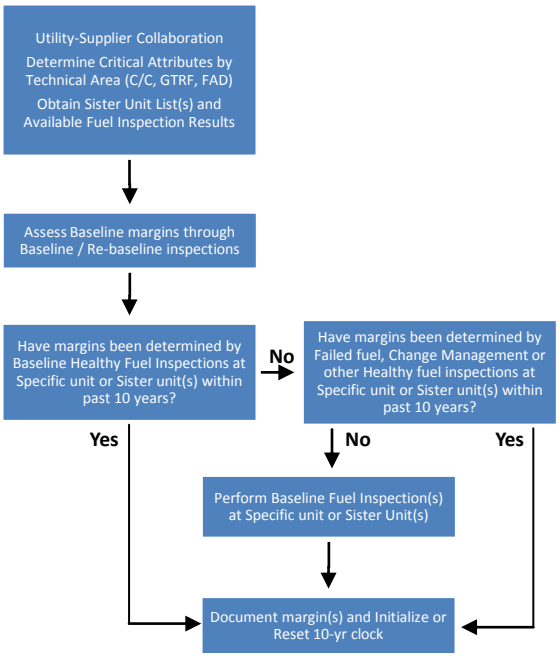

Fig 1. Baseline assessment / inspection process flow chart

Furthermore, Table 2 describes sensitive attributes in the following fuel reliability areas for *baseline* margins assessments and inspection needs:

- BWR/PWR Corrosion/Crud (C/C),

- PWR Grid-to-Rod Fretting (GTRF), and
- PWR Fuel Assembly Distortion (FAD).

This material will assist utilities and fuel suppliers in evaluating where to focus baseline assessments and, if warranted, inspection activities when determining baseline performance margins; particularly, with those plants with bounding sensitive attributes within a group of sister units.

Area	Attribute
BWR Corrosion / Crud	Past history of corrosion / crud failures
	High feed water (FW) iron concentration
	High FW zinc concentration
	High reactor water (RW) copper concentration
	High Noble Chemical deposition
	High RW conductivity
	High potentially detrimental (Si, Li, …) impurity concentration
	High fuel duty
PWR Corrosion / Crud	Past history of corrosion / crud failures
	Low pH
	High lithium concentration
	High zinc concentration
	High steaming rate
	High outlet temperature or highest fuel duty index
	High potentially detrimental (Si, …) impurity concentrations
	Core-wide AO >4 percent or local AO >6 percent
PWR Grid-To-Rod Fretting	Past GTRF experience with currently deployed fuel design
	Past GTRF experience suggestive of challenging plant conditions
	Assembly residence time on periphery
	Flow velocity
	Potential for cross-flow (e.g., mixed fuel design cores)
	Lowest burnup / power ratio between successive cycles
PWR Fuel Assembly Distortion	Past history of fuel assembly distortion
	Incomplete rod insertion related to fuel
	Slow rod insertion time related to fuel
	High drag forces due to fuel
	Core load / unload issues due to fuel
	Grid damage from distortion
	Distortion/bow measurements

Tab 2: Sensitive Attributes for Fuel Reliability Areas

Once baseline margins are established, a *change management* process is implemented. Following *significant* changes in fuel design, water chemistry, core design or operating strategy, utility personnel for each unit should consult with their fuel supplier(s) and evaluate the need for targeted inspections to verify acceptable margin. Other changes, such as plant modifications, or significant anomalous operational events, including severe chemical intrusions and fuel handling

issues resulting from fuel performance, may also require inspections depending on the risk to fuel integrity. Figure 2 is included to serve as an example of a *change management* process.

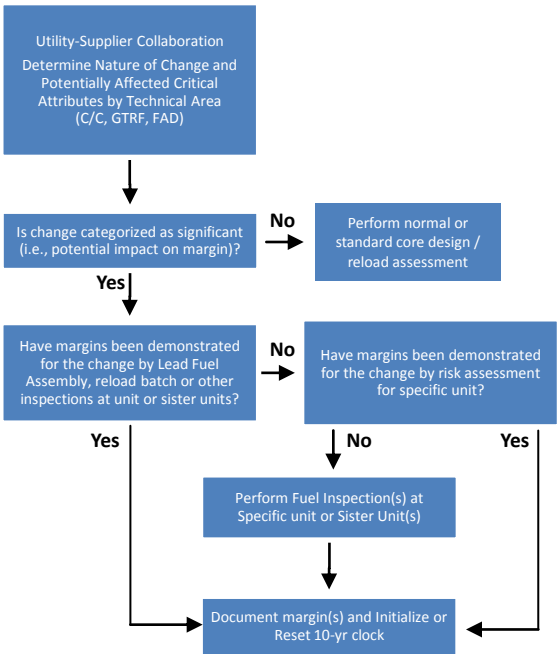

Fig 2. Change Management assessment / inspection process flow chart

The revised FSIG includes example checklists for each of the fuel reliability areas to again assist utilities and fuel suppliers in determining if additional fuel inspections are needed as a result of a change. The first step in this evaluation is to determine if the change is categorized as *significant* such that it could impact fuel performance margins.

It is realized that subtle changes may occur or cumulative effects of small changes may add up over time to impact margins. To help in achieving the overall objective, it is necessary to monitor for such effects as well as to re-affirm baseline margins remain intact even in the absence of known change. This is accomplished through implementation of periodic (≤ 6 years) non intrusive visual examinations to qualitatively identify fuel performance issues that may then require more refined inspections. This program is implemented as part of the *Needed* recommendations (see Table 1). Beyond this formal visual inspection program, a Good Practice has also been identified to inspect fuel on a cycle basis. Such frequent inspections would provide additional input into subtle changes from cumulative effects of small changes or unexpected issues.

4. Failed Fuel Inspection

All cases of fuel failure should be resolved as to the cause of failure to enable mitigating actions to prevent the recurrence of failure and re-loading of failed fuel into the core. Causal analyses should identify the apparent cause of failure and attempt to resolve inconsistencies that do not support the identified failure mechanism. More-detailed hot cell examinations may be required if a failure mechanism cannot be identified.

Fuel failure actions leading to establishment of the cause of failure should take precedence over non-failed fuel surveillance. Once identification and removal of all failed fuel is achieved and apparent cause evaluations are initiated, non-failed fuel surveillance and inspection programs should be evaluated with respect to the apparent failure mechanisms. If deficiencies are identified, additional inspections should be considered.

The EPRI Fuel Reliability Monitoring and Failure Evaluation Handbook (2010) (hereafter referred to as the FRMFE handbook [12]) is a primary reference document for fuel integrity monitoring and failed fuel inspection practices. Utilities should consider the guidance given in the FRMFE handbook when developing fuel integrity monitoring programs and failed fuel inspection practices, and the utility experience should demonstrate that the developed programs and practices are effective. Sections of the revised FSIG provide additional amplifying information on existing guidance provided in the FRMFE handbook in the specific areas of:

- fuel integrity monitoring program data collection;
- evaluation and assessment of fuel integrity monitoring program data;
- actions to assess and effectively manage the failed fuel;
- identification of failed fuel; and
- causal analysis.

Fuel monitoring and inspection activities are an essential part of confirming the causes of fuel failures and ensuring that fuel and plant changes are not causing unexpected challenges to fuel reliability. Experience has shown that a failed fuel action plan is needed to ensure fuel failures are appropriately managed to reduce plant impacts and to preserve evidence to establish the root cause. Identification and disposition of the failed fuel are also essential to (a) ensure that failed fuel is not reloaded into the core, and (b) to identify failure mechanisms to ensure that appropriate remedies can be implemented. It is therefore recommended that each utility should establish a program to prevent the reinsertion of failed fuel and perform causal analysis to identify the most likely failure mechanism(s) for all fuel failure events.

When the cause of a fuel cladding failure cannot be determined, the utility works with the fuel supplier to establish a program to perform a more-detailed causal analysis. This may include (a) additional fuel inspections to obtain more supporting information for failure analysis, (b) the use of hot cell examinations, and (c) leveraging of existing industry programs, such as the EPRI Fuel Reliability Program, to obtain needed resources to determine the root cause and to broaden the industry experience base.

5. SUMMARY

The Fuel Reliability Program (FRP) of the Electric Power Research Institute has revised the Fuel Reliability Guidelines: Fuel Surveillance and Inspection. The purpose of this revision is to provide guidance to nuclear plant operators for developing proactive fuel assessment, inspection and surveillance programs that will:

- identify baseline margins in key fuel performance areas for operating fuel designs with particular emphasis on BWR and PWR corrosion and crud, PWR grid-to-rod fretting, and PWR fuel assembly distortion;
- assess margins following changes in fuel design, manufacture and operation;
- assess margins following anomalous operating events; and
- provide guidance on failed fuel action planning.

The ultimate goal of a successful fuel assessment, inspection and surveillance program is to

ensure acceptable fuel performance to prevent fuel failures and other major operational impacts from anomalous fuel performance issues. The information collected during non-failed fuel inspections (also referred to as healthy fuel inspections) should aid fuel failure root cause analyses and evaluation of other non-failure performance issues, while encouraging coordination and sharing of inspections among utilities to optimize industry-wide resources.

The authors would like to acknowledge the participation and contributions of representatives from EPRI utility members and the three major fuel suppliers during the development of this guideline and its revision. Their expert advice, active support, and repeated encouragement in the revision of this guideline document through the Charlotte and Annapolis workshops, the numerous conference calls / web casts and reviews of the various draft versions is greatly appreciated and highly valued. It is noted that this was a challenging document to develop. This guideline has sought to achieve a reasonable consensus of the industry, generally erring on the side expected to improve fuel reliability.

6. References

[1] Fuel Reliability Program: Global Nuclear Fuel Priority 1 Fuel Inspections Results Assessment Report: Inspections 2007 to 2009. EPRI, Palo Alto, CA: 2011. 1022890.

[2] Fuel Reliability Program: AREVA Priority 1 Fuel Inspections Results Assessment Report. EPRI, Palo Alto, CA: 2011. 1022892.

[3] Fuel Reliability Program: Westinghouse Priority 1 Fuel Inspections Results Assessment Report. EPRI, Palo Alto, CA: 2012. 1022891.

[4] INPO 07-004 Rev 1, "Guidelines for Achieving Excellence in Nuclear Fuel Performance," March 2009.

[5] INPO Fuel Integrity Excellence, "Fuel Fabrication Oversight - Methods for Ensuring Fuel Integrity," May 2007.

[6] Nuclear Maintenance Application Center: Foreign Material Exclusion Guidelines. EPRI, Palo Alto, CA: 2008. 1016315.

[7] Fuel Reliability Guidelines: BWR Fuel Cladding Corrosion and Crud, EPRI, Palo Alto, CA: 2008. 1015451.

[8] Fuel Reliability Guidelines: PWR Fuel Cladding Corrosion and Crud, EPRI, Palo Alto, CA: 2008. 1015449.

[9] Fuel Reliability Guidelines: Grid to Rod Fretting, EPRI, Palo Alto, CA: 2008. 1015452.

[10] Fuel Reliability Program: Fuel Design Evaluation Handbook, EPRI, Palo Alto, CA: 2011. 1022424.

[11] “Material Initiative Guidance – Addenda to NEI 03-08 Guidelines for the Management of Materials Issues”, Nuclear Energy Institute, April 2007.

[12] Fuel Reliability Monitoring and Failure Evaluation Handbook (2010), Revision 2, EPRI, Palo Alto, CA: 2010. 1019107.

FUEL INSPECTIONS AT TEMELÍN NPP AND THE ROOT CAUSES STUDY

M. MALA, M. MIKLOS
Reactor Services Division, CV Rez Ltd.
Husinec-Rez 130, 250 68 Rez – Czech Rebublic

ABSTRACT

The post irradiation inspections of fuel assemblies are associated to the reactor operation, nuclear safety and radiation protection as well. The inspections are mostly provided in western countries, but the implementation of high duty cores brings other needs of fuel inspections during reactor operation worldwide.
The role of fuel inspections in the Czech Republic became more important after the Temelín NPP started the operation in 2002. NPP Temelín (two units) is the first VVER-1000 reactor, where the Russian design meets the American one. Main problems and successes with fuel operation and handling are presented in the paper.
One of the root causes for the possible fuel failure is non-uniform power distribution through the core. Results of some benchmark type experiments performed on light water, zero-power research reactor together with the real data from the post irradiation inspection at NPP Temelín were used for investigation of the above phenomenon and are presented in the paper. Obtained information can be used for a code validation and subsequently for the fuel failure occurrence investigation.

1. Introduction

The post irradiation inspections of fuel assemblies are associated to the reactor operation, nuclear safety and radiation protection as well. The inspections are mostly provided in western countries, but the implementation of high duty cores brings other needs of fuel inspections during reactor operation worldwide.
The role of fuel inspections in the Czech Republic became more important after the Temelín NPP started the operation in 2002. NPP Temelín (two units) is the first VVER-1000 reactor, where the Russian design meets the American one. Since the first load, VVantage-6 fuel assemblies made in the Westinghouse Electric Corporation LLC (WEC) have been used at both units. The reason of the inspections has been the mixture of a western design of fuel and an eastern type of reactor design and water chemistry. During past ten years, Temelín has got a lot of operational experience as well as experience with the fuel repair and inspections. NPP Temelín together with the fuel vendor has performed a post irradiation inspection on the fuel assemblies. Main problems and successes with the Westinghouse fuel operation and handling are presented in the paper.
At first, the inspections have been provided by a fuel vendor (WEC), and they are still carried out by means of the Fuel Repair and Inspection Equipment (FRIE) during the reactor outage. During these ten years of operation the fuel design had been modified and four construction modifications had been used. In 2010 the fuel vendor changed to JSC TVEL. The new type of fuel is TVSA-T and has got a reinforced construction with angles and a debris filter in the bottom nozzle.
In 2009 the CV Rez joined as an independent fuel inspector and since 2011 it has provided the same measurements and visual inspections as the fuel vendor in parallel. But all activities in the frame of the fuel monitoring are covered by the current fuel vendor TVEL. However, CV Rez participates on the fuel inspections and measurements in the frame of the Post-Irradiation Inspection Program (PIIP) to support the independent long-term monitoring and evaluation of fuel behavior at Temelín NPP. These measurements will be used for the codes validation and also as a main basis for the future experiments for fuel failure behavior study under normal and abnormal conditions.
The root causes of a fuel assembly (FA) growth and bowing leading to local limitation of coolant flow, reduction of heat transfer, magnifying cladding corrosion and pellet-cladding interaction (PCI) could be represented by material texture, neutron flux non-uniformity,

gradients of the temperature and neutron current. Such situation can be expected near by some core heterogeneities and construction materials of the reactor´s internals. The root cause is unknown in many cases. This is in accordance with results concerning examination of 7 VVER-1000 FAs at zero power reactor in CV Rez. Main causes of fuel failures are debris fretting, local overheating and grid-to-rod fretting, but almost in one quarter of all cases the cause of failure is unknown [1]. Further, at Loviisa NPP during operational life of U1 and U2 (1978-2008) an estimation of the fuel failure causes shows that 35 % is unknown [2]. And finally, according to IAEA Review [3], 25.1 % of the fuel failure causes for PWR (worldwide during 1994-2006) is unknown. That is why the investigation of the fuel failure occurrence concerns also power distribution changes through the core. Whereas sometimes the needed data cannot be obtained from an NPP´s operation, results of experiments performed on research reactors are used to determine the root causes of fuel failures. [1]

2. Nuclear Fuel at Temelín NPP

Since the first reload in 2002 at Unit 1 (U1) and in 2003 at Unit 2 (U2), fuel assemblies from American fuel vendor WEC VVantage-6 have been used (at U1 till August 2010, at U2 till May 2011). VVantage-6 (VV-6) design (see Fig. 1) is a Westinghouse assembly with hexagonal shape, which became from the square design VVantage-5. Westinghouse fuel assemblies for PWR reactors have undergone significant evolutionary changes, from the early standard fuel assembly with Inconel spacer grids to the VVantage-5. VVantage-5 PWR fuel already included state-of-the-art features such as removable top nozzle (RTN), debris filter bottom nozzles, low-pressure-drop Zircaloy structural grids, Zircaloy intermediate flow mixing grids, optimized fuel rods, In-Fuel Burnable Absorbers (IFBAs) and increased burnup capability to region average values of 48,000 MWd/MtU. These advanced product features have been adapted for the VVER reactors in order to update VVER fuel and provide increased fuel reliability, more efficient uranium utilization and enhanced performance margins. [4]

The VVantage-6 fuel rod design already incorporates significant irradiation and operational experience, including the rod outer diameter, cladding thickness, pellet diameter, and pellet-to-cladding gap. The cladding thickness was selected to maximize uranium utilization and reduce fuel cycle cost while providing reliable performance for high discharge burnups. Cladding material properties have been selected to obtain optimum corrosion performance and accommodate high burnup levels. [5]

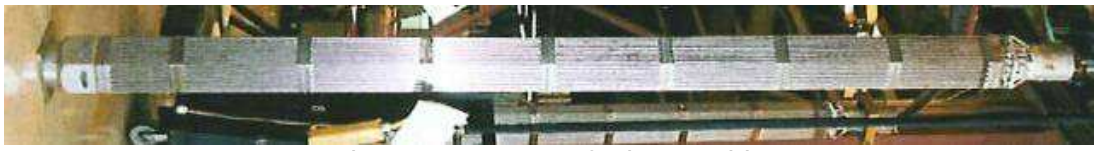

Fig. 1 VVantage-6 fuel assembly

In 2006 CEZ, as the fuel operator, signed contract with new fuel vendor TVEL for the fuel delivery from 2010/2011. The fuel assemblies TVSA-T (Fig. 2) were designed and built by MSZ Elektrostal. The main differences between VVantage6 and TVSA-T are: different construction of the top nozzle (also removable, but under different processes), 6 corner plates (angles - for better stiffness of whole assembly), different grids design (to minimize grid-to-rod fretting (GFR)), debris filter in the bottom nozzle (to avoid any debris fretting), and main materials of the whole fuel assembly are E110 and E635 (instead of Zircaloy or ZIRLO^{TM} and Inconel used for VV-6).

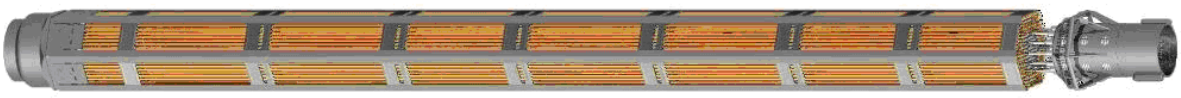

Fig. 2 TVSA-T fuel assembly

3. Post Irradiation Inspection Program at Temelín NPP

NPP operator (ČEZ) together with the fuel vendor (WEC) has performed the Post-Irradiation Inspection Program (PIIP) on the fuel assemblies using the Fuel Repair and Inspection Equipment (FRIE). There were several reasons for using this equipment like additional proof of PWR materials compatibility in VVER water chemistry, analytical method support and verification, overall thermo-mechanical performance demonstration, independent check of the fuel system in-core behavior, root causes examination of an eventual fuel rod (FR) and fuel assembly failure or unexpected deformation; and fuel assembly repair.

After the fuel assembly is placed into the FRIE, several procedures can be done: FA measurement (visual inspection, bow and twist measurements, overall FA length measurements, peripheral FR corrosion inspection, grid cell geometry measurements), single FR measurements (visual inspection, corrosion measurements, profilometry measurements), RCCA inspections (measurements of total wear of the tube cross section, the distribution of the wear around the circumference of the rodlet).

To avoid any fuel problems during future operation with TVSA-T, the large PIIP has been set as well. Therefore, during the unit outage several fuel assemblies are chosen and inspected on the FRIE. The main operations that have been set up to present, with the FAs at FRIE are: inspections - visual inspection of FA, extracted FRs, and RCCA, ultrasonic testing (to detect leaking FR); measurements - FA and rod bow and twist, FA/FR length measurement (growth); and FAs repair.

4. Operational experience at Temelín NPP

By means of the inspections in a frame of PIIP, the root causes of fuel deformation and failures were identified and minimized by the changes in fuel assembly design. During 10 years of operation with VV-6 FAs four different types of FAs were used at Temelín site. The first one called VVantage6 T1 design was the first prototype of VVantage6 fuel assembly for VVER-1000 reactors and was used only for the first batch at the unit 1. The second design VVantage6 T2 was used at both units till 2006 and according to T1 design only small changes in the fuel assembly design were made. The bigger changes were made in 2005-2006, where the VVantage6-Phase0 and in 2007 VVantage-Phase1X were designed. The main design changes were [6],[7]: tube-in-tube dashpot design and top nozzle modifications (Phase 0), fuel rod loading equipment alignments, new structural materials of FR cladding (Zry-4 was changed into ZIRLO^{TM}) and other FA components (Phase 1X).

After these design changes, the fuel assembly bow&twist and the GRF was minimized on the as low as achievable level. The Unit 1 is a proof of these successes, where no leakers were occurred during the last cycle with Westinghouse fuel VV-6.

The new fuel has passed meantime 1 cycle at U1, so meantime there are only few results from the PIIP carried out on TVSA-T [8]. The next PIIP continues in May 2012 at U2 and in August 2012 at U1. The first year of operation at U1 gives good results. No significant twist&bow or growth was found. Also no significant oxide layers were found. Three fuel assemblies with leakers were identified by in mast sipping and two of them were confirmed by the UT system on FRIE. No UT was performed on the third leaking fuel assembly. All three leaking FAs were on the periphery of the core. The authors assume that the reason of the leakage could be a manufacturing failure. However, the root cause of all leakages is still unknown. Hydridation on the upper weld was indentified in one case.

5. Root causes study at CV Rez

Not all data can be obtained in the real operation. Some of them come from the experiments on research reactors and complete the real data. An influence of the fuel rods containing gadolinium burnable absorber (Gd FRs) on power distribution was investigated at 0 g/kg boron acid concentration in a VVER-1000 type core with a model of 7 FAs at CV Rez Ltd. Each FA contained 312 FRs with 4.4% enrichment of ^{253}U. Central FA was different; it contained 18 FRs with 3.6 % enrichment containing 2 % Gd_2O_3. Power distribution was

determined in all FRs of the 30-degree symmetry sector of CFA which contained 3 Gd FRs. The results illustrated a power release decrease in Gd FRs, given by the ratio of the values in Gd FR and average value in 6 FRs around Gd FR with average decrease of about 27 %. [1]
Several VVER-1000 mock-up experiments of benchmark type have been realized for power distribution measurements, too, the main reason of these experiments was to support the reactor pressure vessel dosimetry metodology qualification. For this study two VVER-1000 mock-ups at 6.37 and 4.6 g/kg boron acid concentration in moderator and corresponding VVER-1000 geometry sectors ~60° from the core perip hery area, radial shielding heterogeneities to the biological shielding were modelled with core loading enrichment specifications. The mock-ups were not only azimuthally but also axially shortened due to the 1250 mm LR-0 FR active length. [1]
An influence of the baffle on the power distribution was investigated with both mock-ups by means of measurements carried out in 4 neighbouring FAs in selected FRs to estimate the decrease in power distribution given by the ratio of the mean values corresponding 2 opposite FR rows to- and outwards baffle. In one case the power distribution decreased to 51 %, 44 %, 32 % and 57 %, resp., for 4.4 % enrichment, and in second case: 29 %, 34 %, 19 %, and 35 %, resp. for 2.0 % enrichment. [1]

6. Conclusion

Post Irradiation Inspection Program was specified, and different inspections have been done at Temelín NPP to get large amount of data from the bow, twist and growth measurements. In several years many data have been measured, root causes have been found, and many recommendations for new fuel design have been applied.
All the fuel changes and PIIP led to the successful operation with VV-6 fuel assemblies at Temelín NPP. The fuel assembly bow and twist were reduced by involvement of new FA design, as well as the leaking FAs due to GRF. These fuel operational problems have made a big lesson, and this experience can by used by the NPP stuff and CV Rez on ongoing fuel inspections and repairs. [9]
Presented results have limited information relevance, because they were determined by means of experiments realized on zero power research reactor during 1988 - 2002 at special conditions. Therefore they can differ from values concerning real power reactors because of dependence on enrichment and dimensions of the (Gd) FRs, Gd_2O_3 contents, FR pitch, Gd FRs number and positions in FAs, boron acid concentration in moderator, temperature, pressure, etc. Further less influence of the baffle, core blanket and dummy steel assembly can be expected in case of real VVER-1000 and low leakage type cores because of less dimensions of the LR-0 cores used in mock-ups.
Influence of gadolinium containing fuel rods in fuel assemblies, further baffle, core blanket and dummy steel assembly simulators on power distribution was investigated for VVER-1000 type cores on the bases of experiments performed on zero power reactor LR-0 in CV Rez. Detailed data of this type cannot be obtained from real power reactors; however, the data coming from the experiments complete the real data from power plants. The experiments show that fuel failures can be expected close to some heterogeneities and construction materials, for example at the periphery of the core, where the power distribution is more variable. Often the fuel failure occurs after the FA is placed at first at the periphery of the core and then somewhere else. This means that the failure sometimes does not occur during the cycle when the FA is placed at the periphery, but the failure shows up during the next cycle. In this case it does not matter on the FA position in the core so much, because the failure has begun during previous cycle.
Therefore the experiments are necessary to amend the real data. Results of presented measurements can be used for code validation, as well as the data from PIIP, and subsequently for fuel failure occurrence investigation. [1]

7. References

[1] Mikus J.M.: Influence of Heterogeneities on Power Distribution in WWER-440 and WWER-1000 Type Cores and Fuel Failure Root Causes. Proceedings of 2010 LWR Fuel Performance/TopFuel/WRFPM, Orlando, Florida, USA, September 26-29, 2010, paper 057.

[2] Teräsvirta R., „Operational Experience of Nuclear Fuel in Finnish Nuclear Power Plants (with Emphasis on WWER Fuel)", Proceedings of the 8th International Conference on WWER Fuel Performance, Modelling and Experimental Support, Burgas, Bulgaria, 16 September - 4 October, 2009.

[3] Killeen J., Basak U.: IAEA Programme on Nuclear Fuel Performance and Technology, http://www.iaea.org/NuclearPower/Downloads/Technology/meetings/2011-Jul-26-28-TWG-LWR-HWR/Session-II/TWG-FPT-(Basak).pdf (downloaded 3 May 2012).

[4] Mikloš M., Malá M., Ernst D.: The role of CVR in the fuel inspection at Temelín NPP. Prezentation at the IAEA Technical Meeting on Hot Cell Post-Irradiation Examination and Pool-Side Inspection of Nuclear Fuel, Smolenice, Slovakia, 23-27 May, 2011.

[5] Ernst R., Ernst D., Milisdorfer L. a kol.: Palivo Westinghouse – R. 2000 až 2010, Bezpečnost jaderné energie, 18(56), 2010 č. 11/12, in Czech language.

[6] Ernst D., Milisdorfer L.: 10 years of experience with Westinghouse fuel at NPP Temelín, VVER 2010, Prague: 2010.

[7] Hlavinka V.: International Cooperation in Development and Supply of Nuclear Fuel for Czech NPPs. Presentation at ATOMEXPO 2009, 2009.

[8] Mecir V., Milisdorfer L., Durdak Z.: WWER fuel performance TVSA-T implementation and operational experience at Temelin NPP, presentation, 9th International Conference on WWER Fuel Performance, Modelling and Experimental Support, Burgas, Bulgaria, 17-24 September, 2011.

[9] Mala M., Miklos M., Ernst D.: Fuel inspections and failures at NPP Temelin, ENYGF 2011 – Extended Abstracts, European Nuclear Young Generation Forum 2011, Prague, Czech Republic.

New cores on base coated particles for power water reactors (PWR-CP)

E.I. GRISHANIN, P. N. ALEKSEEV, N.E. KOUKHARKIN
National Research Center "Kurchatov institute", Akademika Kurchatova pl., 1
Moscow, 123182, Russia

ABSTRACT

Proposed is an innovative decision–core on base coated particle for power water reactor (PWR-CP) with particle-bedded fuel implementing the core with lateral flow fuel assemblies. The concept is shown to provide: perfect confinement of fission products within the limits of fuel coating boundaries in practically any design basis and severe accidents, extremely low level of heat energy and potential chemical energy in the core, high degree of self-control in reactivity accidents.
National Research Center "Kurchatov institute", VNIIAM and "LUCH" have carry out a research, which confirms the ability of CP to keep radioactivity in normal and the conditions imitating of serious accidents.
Developed are conceptual design schemes for fuel element, fuel assembly, core and safety systems. The features proposed for further development are targeted to provide the simplicity of design and operation, high degree of passive safety and economic efficiency of an NPP with PWR-CP. Performed are computational evaluations of PWR-CP thermahydraulic and neutron characteristics, coated particle fuel strength characteristics and accident performance.

1. Introduction

Aim of this innovation is create fuel assembly for nuclear power plants, which excludes fission products release during any serious accidents and any terrorist actions.
The reason for vulnerability of nuclear power plants is usage of uranium fuel element covered by zirconium alloy. Zirconium alloy is very good for balancing neutrons inside core, but it loses its strength at any accidental regimes at high temperatures, and fission products releases. The ceramic cladding technologies have been developed in nuclear engineering. These claddings effectively keep accumulated activity at temperature of about 1600°C. Such technology was applied in gas cooled high-temperature reactors. It is interesting to consider the synthesis of high-temperature reactor technology and technology of PWR. Application of coated particles (CP) for PWR, BWR will make possible to design really effective system for retaining fission products in any conditions of severe accidents. The general engineering background for this design is as follows [1, 2].
First, multi-layer coatings of graphite (PyC) and silicon carbide remain and even slightly enhance the strength on temperature rising above 1600°C. At such temperature heat is removed at the expense of natural convection processes, heat conduction and radiation with no active devices used.
Second, the CP, having rather small size (of 1-2 mm) and cooled directly with water coolant-moderator, ensure rapid (0.03 s) compensation of practically any positive reactivity at the expense of temperature and density effects of reactivity of water coolant-moderator. It helps to keep radioactivity in CP at any accidents and any terroristic actions.
Thus, application of CP in PWR type reactors as well as in BWR makes possible to develop the actual safety inherent system on the deterministic level.
Therefore, there is an aspiration to approach NPP safety to the level, when the fission product leakage is not possible, i.e. to make an "all-forgiving" reactor design (error of staff, designers and etc.).
May be unification of CP fuel assembly and conventional fuel assembly as to their dimensions, attachment components, hydraulic and neutron-physical parameter.

2. General base

All existing types of reactors wherein zirconium alloys (PWR, BWR, CANDU, RBMK) are used as fuel element cladding material were not designed for effective retaining of accumulated fission products within fuel elements under severe accident conditions. That was the main reason to provide the containment thereat made of iron-concrete. That was the main reason to provide the containment thereat made of iron-concrete. The fuel itself, the fuel element cladding, in most cases made of zirconium alloys, the coolant circuit material and the containment of iron-concrete are assigned to be the barriers. For PWR-type reactors the design basis accident with breakdown of the maximum diameter pipeline results in temperature rise of zirconium alloy cladding beyond 1000^{0}C. The major part of fuel elements having zirconium alloy cladding loses its leak tightness at this temperature and high activity releases into the space in the containment. Thus, with respect to one initiating event, i.e. pipeline breakdown, 3 out of 4 barriers became ineffective just at once. There remains the only barrier, the containment. Discussions about the multiple barriers and defense-in-depth appear to be the word-wasting practice! Application of CP for PWR, BWR will make possible to design really effective system for retaining fission products in any conditions of severe accidents. The general engineering background for this design is as follows.

First, multi-layer coatings of pyrolytic graphite (PyC) and silicon carbide remain and even slightly enhance the strength on temperature rising above 1600^{0}C. At such temperature heat is removed at the expense of natural convection processes, heat conduction and radiation with no active devices used.

Second, the CP, having rather small size (of 1-2 mm) and cooled directly with water coolant-moderator, ensure rapid compensation of practically any positive reactivity at the expense of temperature and density effects of reactivity of water coolant-moderator.

Thus, application of CP in PWR type reactors as well as in BWR makes possible to develop the actual safety inherent system on the deterministic level [1].

3. Engineering base

The engineering design base is intended is follow:

-direct cooling of free pebble bed CP by water coolant in the fuel assembly with cross coolant flow;
-the CP outside coating of silicon carbide being corrosion resistant to water coolant (water chemistry of and PWR) having parameters of 16.0 MPa and 350^{0}C during long term operation within the reactor, for example, of not less 30 000 hours;
-the outside coating of SiC, resistant under severe accident conditions, as well, for example, in air-steam environment at temperature of 1300^{0}C, pressure of 0.6 MPa during several hours;
-SiC outside coating chemically compatible when there is the contact with structural materials CrNi alloy;
-excluding of zirconium alloys from the core;
-immovability of the pebble bed within the fuel assembly;
-unification of CP fuel assembly and conventional design fuel assembly as to their dimensions, attachment components, hydraulic and neutron-physical parameters

National Research Center "Kurchatov institute", VNIIAM and "LUCH" have conducted a research, which confirms the ability of CP to keep radioactivity in normal and the conditions imitating of serious accidents [3, 4]:

-research of corrosion stability CP in a water coolant at nominal parameters (350^{0}C, 19MPa) over 18 months;
-of corrosion stability CP in a superheated steam (550^{0}C, 10 MPa), 15 months;
-the est CP in a superheated steam (950^{0}C, 10 MPa) 14 days;
-the test CP in gas flame at temperature 1600^{0}C (CP kept hermetic);

This research demonstrated, that: the mass loss of o CP tested in water environment 18 months has made 3-4 10^{-2} %, the mass loss of CP tested in superheated steam has made 0, 4 %. The test CP in gas flame demonstrated, that CP destroyed absence at temperature >1600^{0}C, but 25% CP destroyed after test at temperature 1670^{0}C (see Fig 1 b). That temperature of 1600^{0}C is design limit. The test complex of research demonstrated, that CP for water reactor with core on base CP provide reality inherent safety.

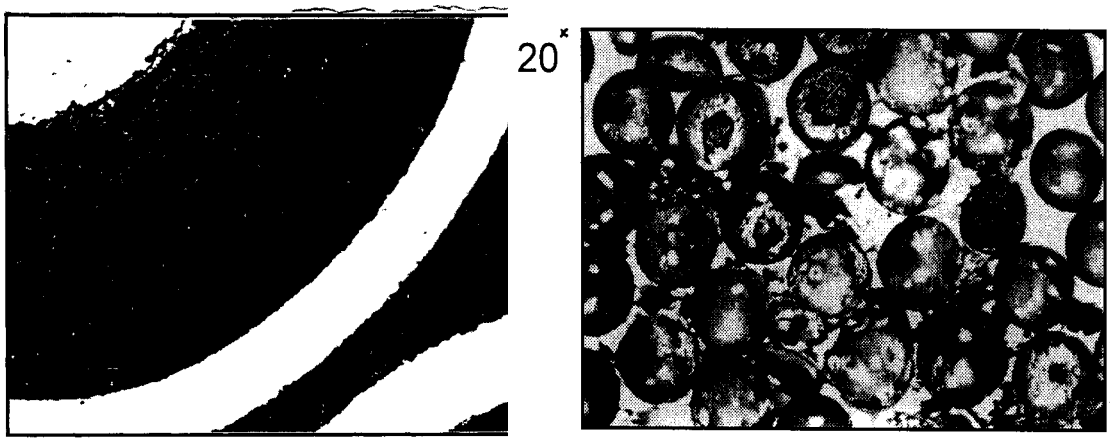

a) **(b)**

Fig.1. The coated particle after tests in a gas flame at a temperature of 1600^{0}C **(a)** and temperature 1670^{0}C **(b)**

4. Coated particle design

The design scheme of CP developed in ap plication to the conditions of operation in a core with light water coolant and moderator is shown in Fig. 2. CP is realized as a sphere of 1.8 mm diameter with kernel of uranium dioxide and the three-layer coating of high-temperature ceramic materials. The kernel has a diameter of 1.4 mm. The next to kernel coating is made of porous pyro-carbon (PyC) with the density of about 1 g/cm^3. The thickness of this layer is ~ 90 μm. The second layer is made of dense PyC (with the density of about 1.8 g/cm^3). The thickness of this layer is ~ 5 μm. The third, outer layer is made of silicon carbide. The thickness of this layer is ~ 105 μm. Table.1 gives a comparative data on the parameters of CP of HTGR and the PWR-PB proposed.

The calculation of stress-strain state PWR-CP demonstrated, that mechanical failure is not predicted, even with account of the conservative assumptions adopted above. These calculations are performed on base methodic developed in paper [5, 6].

Table 1. Comparison of technical characteristics and conditions of operation of fuel elements for HTGR, PWR-1000 and PWR-CP

Parameter	HTGR	PWR-CP	PWR -1000
1. Fuel material	UO_2	UO_2	UO_2
2. Design burn-up fraction, %	Up to 15	4	4
3. Kernel diameter/ thickness, mm	0.5/0.25	1.4/0.2	7.6/0.65
4. Coolant	Helium	Water	Water
4.1.Coolant pressure, MPa	4	16	16
4.2. Average heat flux, MW/m^2	0.03	0.07	0.587
5. Max. temperature of cladding/fuel (normal conditions), ^{o}C	1100/1300	350	350/1700
6.Max. temperature of cladding/fuel (accident conditions), ^{o}C: on D= 850 mm pipeline breakdown; on vessel bottom break away	 1600* 1600*	 400* 1000*	 1100* 1000*
7. Carrying over of fuel ("ameba" effect)	> 1400^{o}C	No	-
8. CO partial pressure, MPa	4.0	No	No
9. Fluence, n/cm^2 E >0.2MeV	(1-2)·10^{21}	3·10^{22}	3·10^{22}

* fuel and cladding temperature is practically the same on accident

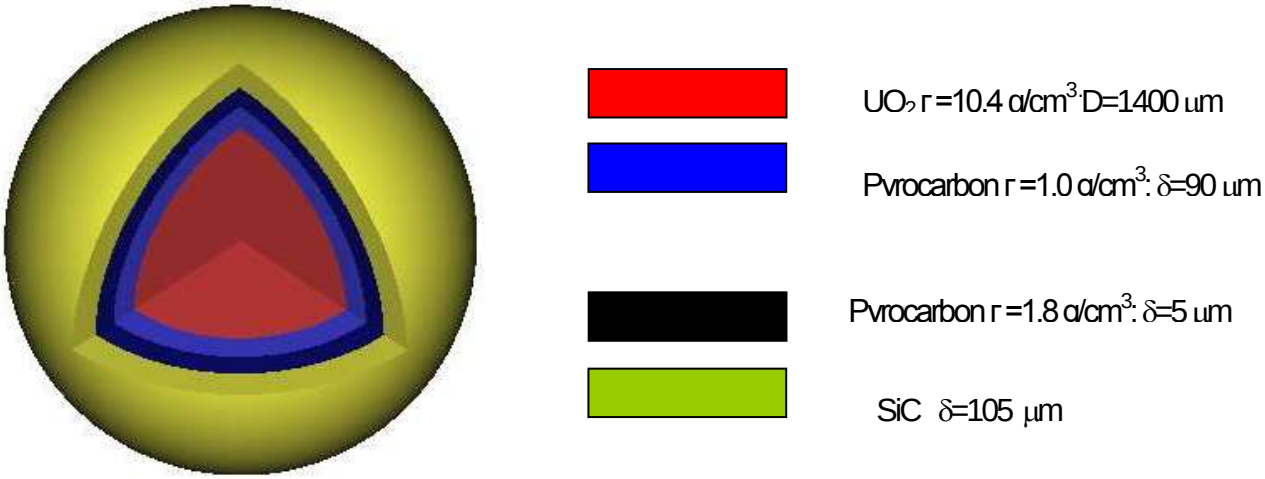

Fig.2. Constructive scheme of CP

5. Fuel assembly design

Fig. 3a. presents the more simple design scheme of fuel assembly with lateral flow of the coolant through CP layer. It has the outer casing with perforated walls, the inlet collector appearing as a cone with its walls perforated also, the layer of CP allocated between them in a particle-bedded mode, the end and head parts. The outlet collector is a gap between neighboring fuel assemblies. To arrange for it, the outer casing is realized as a truncated cone. The guide tubes for control rods are located inside the CP layer. The pattern of these tubes allocation may be the same as in traditional fuel assemblies for PWR reactors. The guide tubes in such fuel assembly act as a main bearing structure of fuel assembly. The outer casing has an option of free movement against other structural elements of fuel assembly. This provides for its reliability in the emergency regimes when its temperature increases up to 1000^{o}C. Outer casing can be equipped by skew reinforcement elements that provide for its necessary stability under the impact of CP backfill weight, and also under the pulse impact of the coolant in its emergency outflow, and under seismic loads. In the current time, the technical features for realization of reinforcement elements have not been finally defined yet, and, hence, the different variants are being considered (grids, ribs, etc.). The thickness of walls of the outer and inner collectors is adopted to be 1 mm. In this, the fraction of stainless steel in the core constitutes about 2.5% of the core volume.

Z-type shape of the collectors with their lateral section converging and diverging along coolant flow path provides a minimum non-uniformity of coolant distribution along the height of CP layer and minimum pressure losses due to the preservation of nearly constant vertical component of coolant velocity in the collectors. A necessary uniformity of coolant enthalpy at the outlet of CP backfill is provided at the expense of variable perforation density in inner collector and outer casing. The selected shape of collectors makes them occupy the minimum volume, as compared to collectors of other types, and provides a maximum volume fraction for the layer of CP in fuel assembly.

Major losses of pressure in fuel assembly of such type are due to the resistance of the collectors, because the resistance of coated particle fuel layer, even at CP diameter of about 1 mm, is rather small.

For a single-collector fuel assembly of large size, like that of PWR-PB, characteristic is the presence of a large water cavity of the inlet collector. Correspondingly, near it observed is a large peak of the thermal neutron flux. In the area of outlet collector such peak is also present, but it is essentially smaller. From the standpoint of CP reliability, the local peak of thermal neutron flux is in the area of inlet collector. This peak is unfavorable, first of all, from the standpoint of non-uniform fuel burn-up along fuel assembly radius. To resolve the problems named above, proposed is the design scheme of fuel assembly with several inlet collectors of a correspondingly smaller size. The design scheme of such fuel assembly is presented in Fig. 3b. It has 7 inlet collectors of cylindrical shape and one outlet collector in the space between fuel assemblies. . Performed are computational evaluations of PWR-PB thermal-hydraulic characteristics by methodic development in paper [7], witch based on experimental research [8].

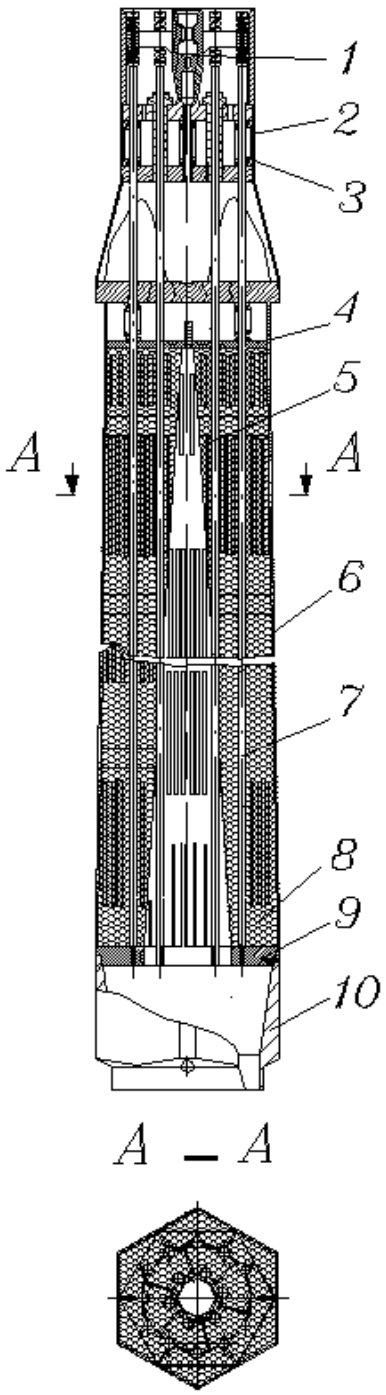

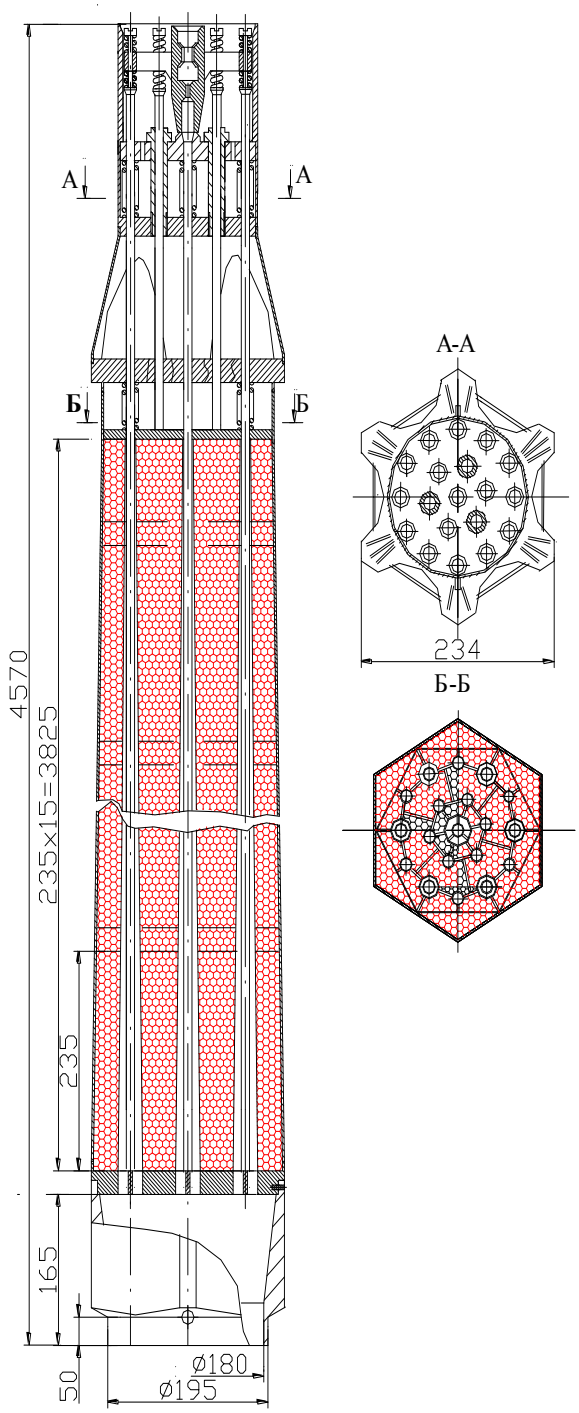

Fig. 3a.Fuel assembly with a single inlet collector

1 – head part; 2 – bushing (shell); 3 - spring;
4 – top head; 5 – inlet collector; 6 - casing;
7 – guide tubes for control rods; 8 – CP fuel;
9 – bottom head;10 – end part

Fig. 3b.Fuel assembly with 7 inlet collector

3. The neutron characteristics

The PWR core with CP has the following distinctive features: practically homogeneous structure of the core and, respectively, significantly greater resonance absorption in U-238, twice as much amount of steel, lesser amount of water, low temperature of fuel.
Increased resonance absorption in U-238 required higher initial enrichment (see Fig.4). This effect is not compensated by higher rate of plutonium. However these negative effects are compensated almost completely at the expense of very low fuel temperature.
Table 2 gives the structural content of PWR-1000 core and PWR-CP. From the Table 2 one can see that CP occupies the greater volume as compared to fuel rods. Amount of steel is 2.2 fold as much and, respectively, the amount of water in the reactor core is for 20% less. The volumetric composition of the reactor core with CP does not essentially differ from traditional one (Table 3).

Table 2. Structural content of the PWR-1000 core and PWR-CP core

Component	PWR-1000	PWR-CP
Fuel elements	0.4207	0.4750
Water	0.5676	0.4994
Steel	0.0117	0.0256

Table 3. Volumetric composition of the core, %

Name	Density, g/cm^3	PWR-1000	PWR-CP
1. UO_2	10.0	28.2	26.3
2. H_2O	0.72	55.5	52.3
3. Zr1%Nb	6.4	11,2	-
4. Steel	7.9	2,4	2.3
5. Graphite	1.6	-	18.0
6. SiC	3.5	-	1.1
7. He	-	2.7	-

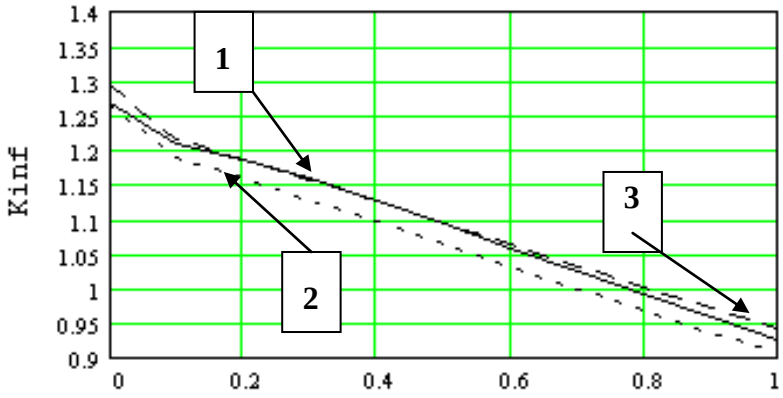

Fig.4. Dependence of Kinf on burn-up (relative unit)

1- PWR-1000 (x=4,4%), **2**- PWR-**C**P (x=4,4%), **3-** PWR-**C**P (x=5%)

5. Characteristics of safety

High strength of multilayer coatings at high temperatures makes it possible to conclude that exceptional radiation safety characteristics might be provided not only in the cases of traditionally considered severe accidents, but also in such hypothetical cases as brittle destruction of reactor vessel, fall-down of a heavy plane, sabotage acts, and even

intentional actions of the sabotage-trained NPP personnel.
This presents results of the preliminary safety assessment performed for 2 characteristic emergency operation occurrence regimes of PWR-CP. The selected regimes (typical of many light water reactors) are:
- rupture of a pipeline of maximum diameter and
- total NPP black-out without scram.
In addition to this, to illustrate potential benefits of coated particle fuel, considered was a hypothetical accident with destruction of reactor vessel bottom and total reactor voiding.

5.1. Pipeline rupture

The results of calculation of the pipeline rupture regime are presented in Fig. 5. It can be seen that CP temperature remains practically constant and equal to the coolant temperature. The reason for this is that in nominal regime the fuel has practically no stored heat. It is obvious that, when coolant temperature goes down because of the vessel flooding by cold water, the CP temperature would go down correspondingly.
For better interpretation of the calculations performed for PWR-PB, Fig. 5 also presents the results of a calculation performed for the accident with the rupture of a pipeline of maximum diameter (DN850) in PWR-1000 reactor.

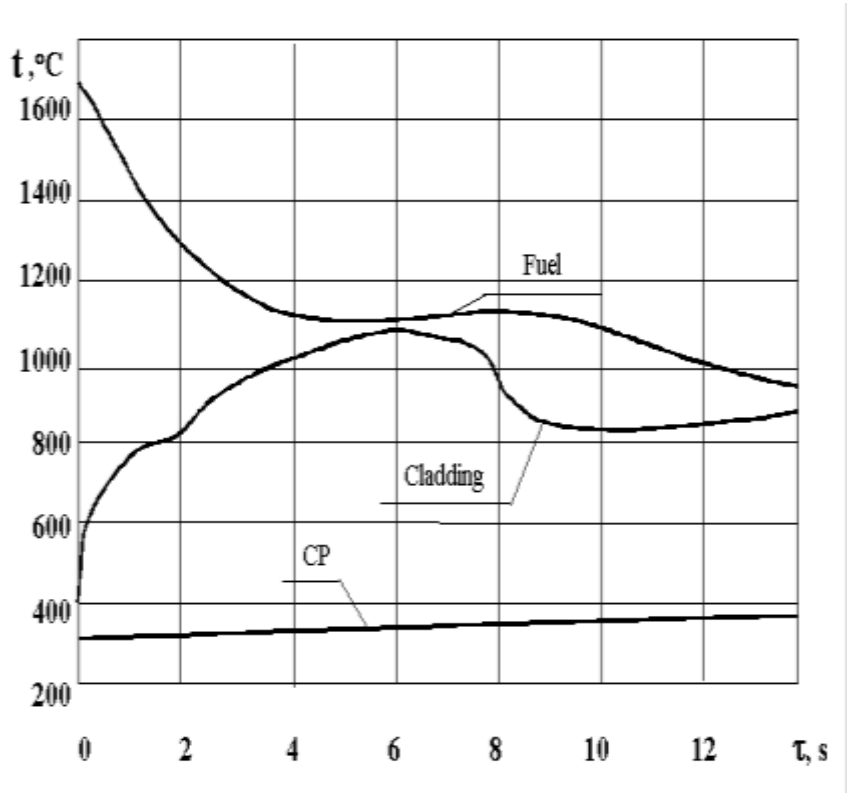

Fig.5. Accident with rupture of a pipeline of maximum diameter.
CP – temperature of coated particles for PWR-CP. Two curves at the top: temperature of fuel and cladding of rod-type fuel elements of PWR.

It can be seen that the course of this accident for the core with CP is essentially different from that in the traditional core. For the traditional core characteristic is fast increase of the temperature of zirconium cladding due to high-temperature heat accumulated in uranium dioxide pellets, and due to heat exchange worsening. In the first seconds of emergency process the core with CP is practically not heated, because the temperatures of coated particle fuel and coolant in nominal regime were different by several degrees only. After that, the temperature of CP is increased in a relatively slow mode due to residual heat. This continues until the start of operation of the emergency core cooling system.

5.2. Total NPP black-out without scram

The results of calculations are shown in Fig. 5. For better interpretation of these results, also presented are the results of calculation of a similar regime for standard PWR-1000 reactor.
It can be seen that the course of this emergency process is radically different for the cores of two types. For standard PWR, the decrease of power takes place very slowly, because released in its course is a positive reactivity due to Doppler-effect of the fuel, which, in nominal regime, is heated up to the temperature of about 1000^{0}C (power effect of reactivity). The chain reaction is terminated after 1000 s, when nearly all primary circuit water had out flown through safety valves. In this, the temperature of zirconium claddings exceeds 1000^{0}C after about 20 s since the accident start. For the core with CP, the accident course is essentially different. Due to the absence of accumulated heat, the CP fuel temperature remains at the level 300^{0}C. The chain reaction is terminated due to density and temperature reactivity effects of coolant-moderator without control rod operation.

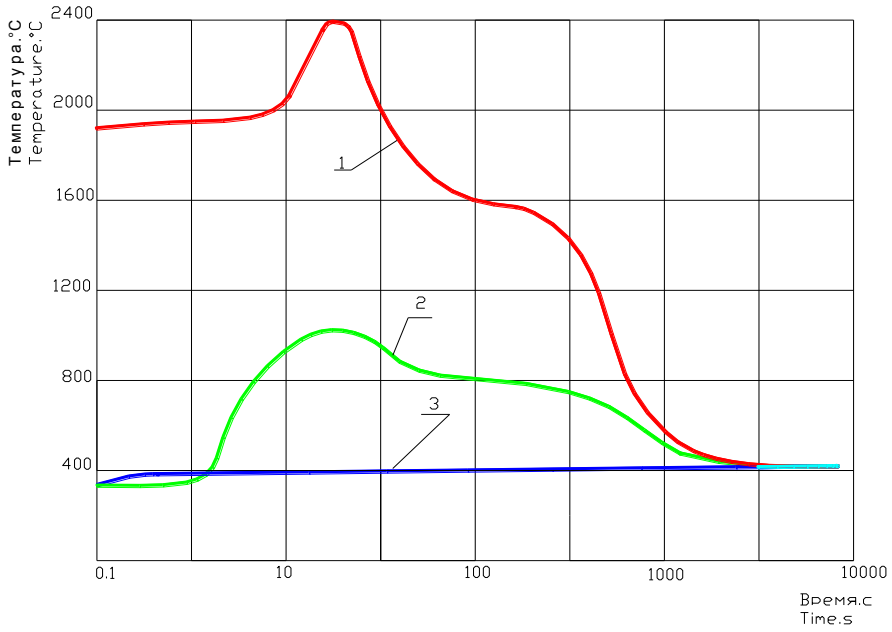

Fig. 5. Accident with total NPP black-out without scram.
1- Maximum temperature of the PWR fuel, 2- cladding temperature of PWR fuel element, 3-temperature of CP.

5.3. Destruction of reactor vessel

This hypothetical accident regime is considered to illustrate the PWR-CP safety potential. The initial event is disruption of the reactor vessel in its bottom part. When primary circuit is dewatered, a highly superheated steam starts flow to steam generators due to natural convection of a steam-air mixture of 6 bar pressure. The cooled-down steam returns to the reactor vessel to the core inlet. A highly superheated steam-air mixture supplied to the steam generators is effectively cooled in them (steam generators have large heat exchange surface) down to the temperature, which is approximately equal to the saturation temperature in secondary circuit (280^{0}C). At high temperatures, an important factor is heat absorption in the reactor internals (the so called “associated” mass), the mass of which is larger than the core mass.
The calculation results are presented in Fig.6.

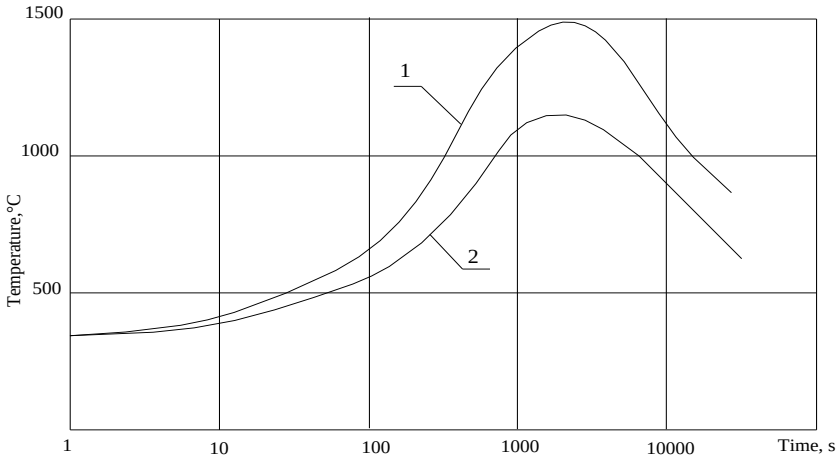

Fig. 6. Hypothetical accident with vessel bottom destruction. Temperature of fuel for maximum-powered fuel assembly (1) and average-powered fuel assembly (2)

At the initial phase, the core temperature increases and reaches its maximum after 2 – 3 hours. Later on, due to residual power decrease, started is a slow cooling-down of the core. The maximum temperature of PWR -1000 fuel in this regime is 1400^0C.

The preliminary analysis performed makes it possible to draw a conclusion on the unconditional advantages provided by the use of CP.

Table 4. Major characteristic of PWR-CP and PWR-1000

Name	PWR-CP	PWR -1000
Thermal power, Mw	3000	3000
Pressure, bar	16	16
Number fuel assembly	163	163
Number fuel element into fuel assembly	$30\cdot10^6$	312
Diameter of CP/UO_2 kernel, mm	1,8/1,4	9,1/7,6
Core high, mm	4000	3500
Fuel element surface, m^2	305	32
Maximum temperature of fuel, °C	350	1600
Pressure drop of fuel assembly, bar	1,5	1,5
Pressure drop of CP pebble bed, bar	0,03	-
Fuel assembly load of uranium dioxide, kg	450	480
Initial enrichment/burn-up, %	4,8/4,9	4,4/4,5
Power effect reactivety, %	≈0	1,0
Number guide tube for control rod	12	19
Diameter guide tube, mm	16x0,8	12,6x0,8
Number inlet collector	7	-
Diameter inlet collector (conical), mm	40	-
Wall thickness of colletor, mm	1	-
Perforation density, %	3-5	

6. Conclusion

NRC "Kurchatov institute" and VNIIAM care out complex research for basing used coated particles in PWR core. This complex demonstrating of the creation possibility of fuel for NPP, witch excluded leakage of fission product at any

accident and terrorist action. The use fuel for NPP provide create of possibility for wide scale development of nuclear power without substantial threats and risks [9].

Acknowledgements

Authors thank of top staff of FRAMATOME at the research finance.

References

1. Н.Н. Пономарев-Степной, Н.Е. Кухаркин, А.Г. Филиппов, Е.И. Гришанин и др. “Перспективы применения микротвэлов в ВВЭР” Атомная энергия, т. **86**, вып. 6, 443 (1999).
(N. Ponomarev-Stepnoy, NE The cook, AG Filippov, E. Grishanin et al, "Prospects for use in VVER microfuel" Atomic Energy”, vol. 86, Issue 6, pp 443 (1999).)
2. Г.А. Филиппов, Н.Е. Кухаркин, Е.И. Гришанин и др. “Перспективы создания корпусного прямоточного реактора с перегревом пара» Атомная энергия, **т. 10**, вып.3, 197 (2006).
(G.A. Filippov, N.E. Koukharkin, E. Grishanin et al, "Prospects for a once-through reactor with a corps superheated steam," Atomic Energy”, Vol 10, Issue.3, 197 (2006).)
3. Г.А. Филиппов, Е.И. Гришанин, М.В. Кондитеров и др. «Исследование коррозионной стойкости оболочек микротвэлов из карбида кремния и пироуглерода применительно к условиям работы легководных реакторов АЭС» Атомная энергия, **т. 10**, вып.4, 270 (2006).
(G.A. Filippov, E. Grishanin, MV Confectioners and others "Study of corrosion resistance microfuel shells of silicon carbide and pyrolytic carbon for the conditions of light-water reactors," Atomic Energy, Vol 10, Issue 4, 270 (2006))
4. Г.А. Филиппов, Е.И. Гришанин, В.М. Трубачев и др. Исследование коррозионной стойкости оболочек микротвэлов из карбида кремния и пироуглерода применительно к условиям работы легководных реакторов АЭС. “Атомная энергия”, т 101, вып. 4, октябрь 2006.
(G.A. Filippov, E.Grishanin, L. Falkowski, B Fonarev, V. Trubachev “Investigation of corrosion resistance microfuel shells of silicon carbide and pyrolytic carbon for the conditions of light-water reactors”. ""Atomic Energy” , Vol 101, Issue 4, 2006)
5.В.С. Еремеев, А.С. Черников и др. "Математическая модель для описания напряжений в микротвэлах". “Атомная энергия”, т. **58**, вып. 3, 15 (1985).
(V.S. Yeremeyev, AS Chernikov et al, "A mathematical model to describe the stress microfuel." ""Atomic Energy” , Vol.58,. Issue 3, pp 15 (1985))
6. M.D. Done, G. Schumacher “Consideration of PyC and SiC coated oxide particles for gas cooled fast reactor application-“J. Nucl. Mater.”, v. **40**, 27 (1971).
7. Е.И. Гришанин Е.И., Е.Е. Денисов, А.Я.. Любин, Л.Н. Фальковский “Разработка математической модели расчета параметров теплоносителя в тепловыделяющей сборке легководного реактора с микротвэлами», Тяжелое машиностроение, № 9, 11 (1995).
(E. Grishanin, E. Denisov, A. Lubin, L. Falkowski, "Development of a mathematical model for calculating the parameters of the coolant in the fuel assembly with a light water reactor microfuel", Heavy Engineering, № 9, 11 (1995)).
8.О.С. Виноградов, И.П. Смирнов, И.П. Тигарев “Гидродинамика кассет с шаровой засыпкой” Труды ЦКТИ, вып.145, Исследование и отработка оборудования АЭС, 107 (1977).
(O. Vinogradov, I. Smirnov, I. Tigarev "Hydrodynamics of the pebble bed assembly" Proceedings of Polzunov Institute Issue.145, Research and development of nuclear power equipment, 107).
9. I. Slessarev, P. Alekseev. New-quality nuclear power without substantial threats and risks:vital risk free fast reactors and fuel cycles. In the Proceedings of the International Conference on Fast Reactors and Related Fuel Cycles: Challenges and Opportunities which will be held from 7-11 December 2009 in Kyoto, Japan.

REDUCTION OF FUEL ASSEMBLY BOW WITH THE RFA FUEL

MIGUEL AULLÓ
Product Engineering, ENUSA Industrias Avanzadas S.A
Santiago Rusiñol, 12. 28040 Madrid - Spain

YURIY ALESHIN
Product Engineering, Westinghouse Electric Company

JULIEN MESSIER
Division Combustible Nucléaire, Electricité de France

ABSTRACT

Fuel assembly bow negatively affects fuel assembly handling, RCCA drop time and plant operational margins. In response to bow issues that appeared in the mid 1990s, Westinghouse and ENUSA developed new fuel designs to help to alleviate the operational problems that occurred. A key element of this understanding of the bow mechanism is the collaboration with the utilities; in this regard EDF collaborates with Westinghouse and ENUSA providing valuable experience feedback.

The Robust Fuel Assembly (RFA) was first introduced in 1997 to improve the bow behaviour of the fuel and is now the standard product provided by ENUSA and Westinghouse for the 17x17 array with 9.50 mm diameter fuel rods. As of 2011, more than 16,000 RFA fuel assemblies have operated in 52 plants in the United States, Europe and South Africa. RFA with Zircaloy-4 structural material was first introduced in EDF 900 MWe and 1300 MWe reactors in 2003. Later on, the transition to ZIRLO® material has been initiated to provide an additional enhancement of fuel assembly distortion resistance and reduce in-core bow.

EDF has developed a bow inspection system called DAMAC which permits to measure the fuel assembly bow of the whole core on-line with the unloading operations. The measurements done with DAMAC in plants loaded with the RFA design have permitted to follow the improvement of the bow of the core since its introduction in EDF reactors. DAMAC is an unparallel source of data that allows to improve the understanding of the bow evolution.

This paper presents the operational experience of the RFA regarding fuel assembly bow including transition from Zircaloy-4 to ZIRLO® structural material. On-site measurements show how cores have been straightened since the introduction of RFA. In plants loaded with RFA hang-ups between fuel assemblies have been practically eliminated, and no RCCA issues related to assembly bow have occurred.

The prediction capability of the fuel assembly bow is also discussed based on the available operation feedback.

1. Introduction

Fuel assembly bow negatively affects fuel assembly handling, RCCA drop time and plant operational margins Fuel Assembly bow mechanisms and remedies have been extensively investigated since the incomplete rod cluster control assembly (RCCA) insertion (IRI) incidents that occurred in mid 1990s.

In response to these incidents Westinghouse and ENUSA introduced the Robust Fuel Assembly (RFA) in 1997. The first reloads of RFA design were introduced in EDF reactors in 2003 (RFA 900 for 900Mwe reactors and RFA 1300 for 1300 MWe reactors) [1]. The RFA 900 and RFA 1300 designs for EDF used Zircaloy-4 material in the cladding and structure. Zircaloy-4 was replaced by ZIRLO® to provide an additional enhancement of fuel assembly distortion resistance and reduce in-core bow in RFA 900 ZIRLO and RFA 1300 ZIRLO designs introduced in EDF plants since 2007.

The introduction of the RFA designs in EDF reactors has been monitored by exhaustive surveillance plans on selected assemblies to confirm that the fuel behaviour is as expected and is consistent with the design models. Typical scope of the surveillance program includes visual inspections, dimensional (bow and growth) measurements, cladding oxide, and fretting wear.

Assembly bow is a core wise phenomenon that cannot be monitored following the behaviour of individual assemblies. EDF has developed a bow inspection system called DAMAC which permits to measure bow (magnitude and shape) of each fuel assembly on-line with the unloading operations. The measurements done with DAMAC in plants loaded with the RFA design have permitted to follow the improvement of the bow of the core since its introduction in EDF reactors.

This paper presents the operational experience of the RFA regarding fuel assembly bow including transition from Zircaloy-4 to ZIRLO® structural material.

2. The RFA design

The RFA design was developed to improve the performance on grid-to-rod fretting, incomplete control rod insertion (IRI), and thermal-hydraulic DNB margin. The features of the RFA design include (Fig. 1):

- Removable top nozzle
- Debris Filter bottom nozzle
- Reduced rod bow Inconel top grid
- Structural RFA-2 mid grids
- High burnup Inconel bottom grid
- Inconel protective bottom grid
- Thicker thimble tubes
- Tube-in-tube dashpot

To reduce fuel assembly bow, the guide thimble and instrument tube wall thickness were increased 25% relative to the previous design by maintaining the inner diameter and increasing the outer diameter of the tube to improve stiffness of the skeleton. The thick guide tubes of uniform section have an independent dashpot tube in a tube-in-tube configuration.

In addition, ZIRLO® material in the guide thimbles (not incorporated in the first designs for EDF) reduces bow due to its superior dimensional stability (lower growth and creep).

The RFA is now the standard product provided by ENUSA and Westinghouse for the 17x17 array with 9.50 mm diameter fuel rods. As of 2011, more than 16,000 RFA fuel assemblies have operated in 52 plants in the United States, Europe and South Africa.

In plants loaded with RFA hang-ups between fuel assemblies have been practically eliminated, and no RCCA issues related to assembly bow have occurred.

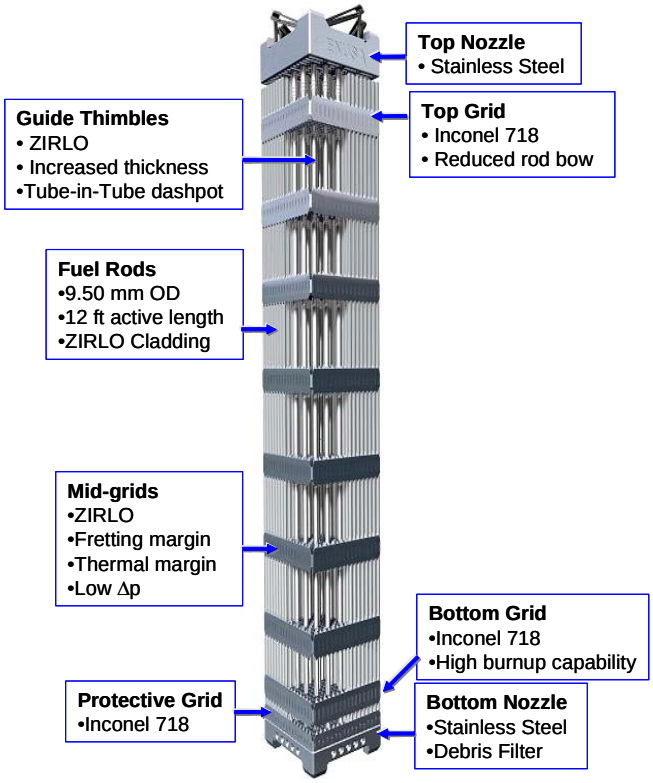

Fig. 1 RFA fuel

3. The DAMAC bow measurement system

DAMAC is a specific device developed by EDF for fuel assembly bow measurement based on the use of an ultrasonic signal to measure the distance between fixed transducers and the grids of a fuel assembly. During core unloading, each fuel assembly is stopped in front of DAMAC where fuel assembly bow is recorded in two directions. This recording device allows for on-line deflection measurement on each grid of each fuel assembly during offload.

This measurement is performed by EDF in order to follow precursor Fuel Assembly behaviour in core and/or to answer Safety Authority requirement regarding RCCA drop time issues. Besides bow amplitude, EDF has defined a “gravity index”. Such parameter combined with bow shape (S, C, W) can be correlated to RCCA drop time T5 and eventually used in order to prevent any Fuel Assembly with excessive bow to be reloaded under a RCCA location.

- The amplitude of the deflection is given by :

$$\rho = \max \sqrt{(Xi - Xj)^2 + (Yi - Yj)^2}, (i; j) \in [1; n]^2$$

  where **X** and **Y** stand for deflection in both directions, and **i** and **j** for grid index.

- The gravity index is related to the potential elastic energy due to this deformation.

  Formulating this energy as : $E = \int_0^h k.x^2(z)\, dz$

  where **h** is the Fuel Assembly height, **k** is related to its stiffness and **x** is the deflection variation between two neighbor grids,

the Gravity index can be written as $I_G = \frac{100}{0.002} . \sum_{i=1}^{n-2} \alpha_i^2$

where α is the angle between two spans, as illustrated here bellow.

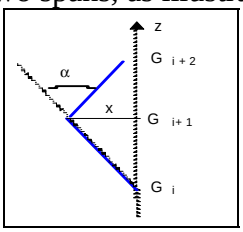

Figure 2 provides a typical fuel assembly bow pattern (maximal amplitude on each Fuel Assembly) obtained with DAMAC in an EDF 1300 MWe reactor loaded with EFG fuel.

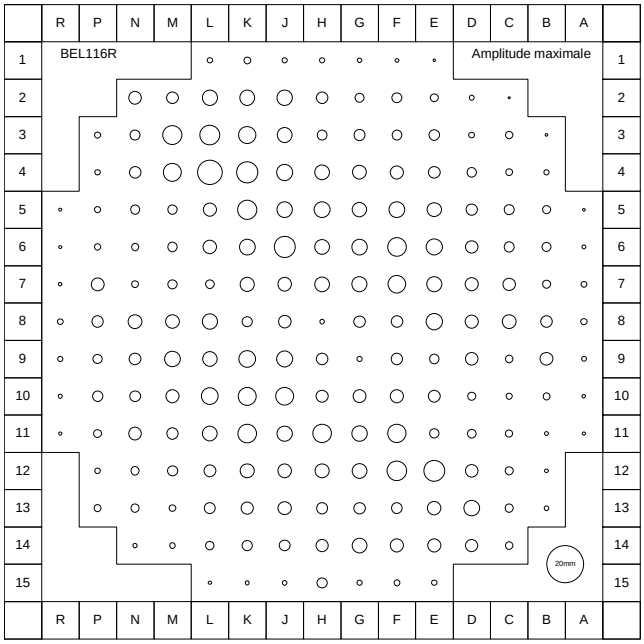

Fig. 2 DAMAC Results

4. Bow evolution in EDF cores loaded with RFA fuel.

The bow behaviour of the RFA fuel has been monitored for the RFA 900 design in Gravelines 6 (Fig. 3) and in Belleville 1 for the RFA 1300

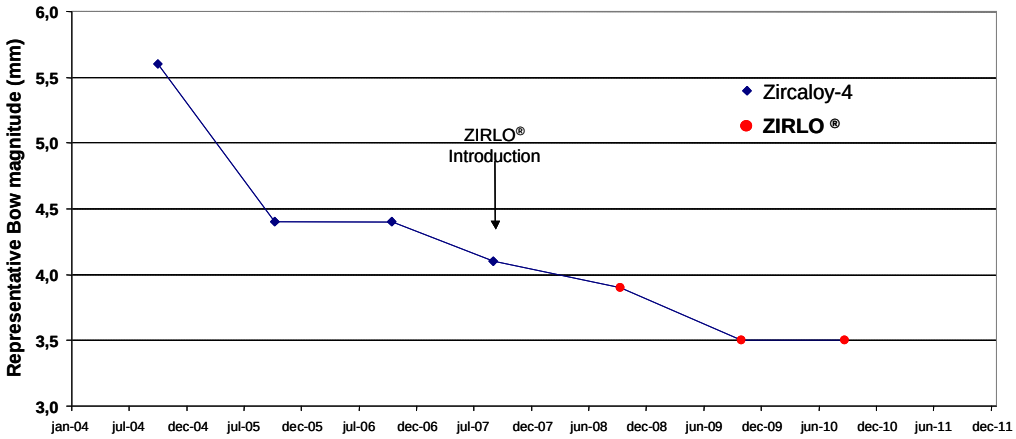

Fig. 3 Bow evolution in Gravelines 6 (RFA 900 and RFA 900 ZIRLO)

The measurements show that these cores have been straightened since the introduction of RFA especially with the implementation of ZIRLO® structural material.

5. Bow Models

Westinghouse and ENUSA in cooperation with KEPCO NF, have developed the computer code SAVAN and the methodology based on the SAVAN to predict the evolution of the bow of the fuel assemblies in core (Fig. 4) [2]. In the other hand, EDF has developed a model to predict in-core bow called MAC3S2 based on the EDF open-source finite element code Code_Aster® (Fig 5) [3].

Fig. 4 SAVAN Output

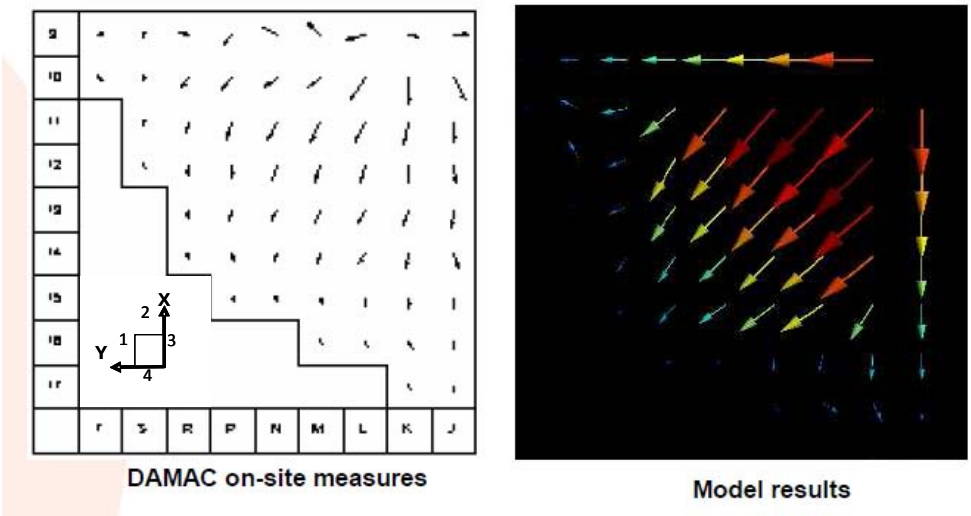

Fig. 5 MAC3S2 results compared with DAMAC measurements

Although both codes have been validated independently with good results, EDF, Westinghouse and ENUSA have jointly recognized that the two programs MAC3S2 and SAVAN have different strengths and limitations. In order to improve their analytical

capabilities, EDF, Westinghouse and ENUSA have agreed on working in a benchmarking program to identify best practices in the use of the codes. Eventually both codes will be validated with DAMAC measurements.

6. Conclusions

Fuel assembly bow negatively affects fuel assembly handling, RCCA drop time, and plant operational margins. The Robust Fuel Assembly (RFA) was introduced in order to improve the bow behaviour of the fuel and is now the standard product provided by ENUSA and Westinghouse for the 17x17 array with 9.50 mm diameter fuel rods.

RFA with Zircaloy-4 structural material was first introduced in EDF 900 MWe and 1300 MWe reactors in 2003. Later on, the transition to ZIRLO® material has been initiated to provide an additional enhancement of fuel assembly distortion resistance and reduce in-core bow.

The measurements done with EDF bow inspection system DAMAC in plants loaded with the RFA design have permitted to follow the improvement of the bow of the core since its introduction in EDF reactors.

EDF, Westinghouse and ENUSA will further collaborate in the development of predictive capabilities. The SAVAN and MAC3S codes used respectively by ENUSA/Westinghouse and EDF to predict the fuel assembly growth and bow will be benchmarked and then validated with DAMAC measurements.

7. References

1. David Chapin, Miguel Aulló, Alberto Cerracín, Göran Boman, “EFG Fuel Designs and Experience in EDF Reactors”, Top Fuel Meeting, Salamanca, Spain (2006)
2. Yuriy Aleshin, Miguel Aulló, Alberto Cerracín, Sang-Youn Jeon, “Methodology to Assess Fuel Assembly Dimension Stability on Design Stage”, Top Fuel, Paris (2009)
3. B. Levasseur, G. Chaigne, R. Fernandes, “3-D Modelling of Fuel Assembly bow for EDF PWRs”, Top Fuel, Paris (2009)

WESTINGHOUSE FUEL DESIGNS AND PERFORMANCE OVERVIEW

JEFFREY L. BRADFUTE, DAVID L. CHAPIN, ADOLFO REPARAZ
Product Engineering, Westinghouse Electric Company
5801 Bluff Rd., Hopkins SC 29061 – USA

MANUEL QUECEDO GUTIÉRREZ, CRISTINA MUÑOZ-REJA RUIZ
Product Engineering, ENUSA Industrias Avanzadas S.A
Santiago Rusiñol, 12. 28040 Madrid – Spain

ABSTRACT

Westinghouse PWR fuel operates in more than 80 reactors of various designs worldwide. This paper summarizes the current fuel designs and performance of Westinghouse fuel. Design improvements have been implemented over the years to improve reliability and eliminate fuel leakage mechanisms and other fuel related issues such as bowing, handling damage, and control rod insert-ability. Healthy Fuel Examinations have been conducted to provide information on in-reactor fuel performance and identify areas for improvement to result in robust fuel designs across all fuel product lines. Typical examinations have included detailed visual inspections, dimensional verification, fuel rod oxide thickness and grid-to-rod fretting (GTRF) wear measurements under a variety of operating conditions.

Design enhancements have been implemented to provide additional margin and resistance to GTRF in fuel products that have been challenged by operating conditions in the core. The main leakage mechanisms observed today have been due to debris or manufacturing-related causes. For debris related leakers, debris resistance enhancements, such as debris filter bottom nozzles, protective grids and oxide coated cladding have been or are being implemented to significantly reduce the probability of debris related leakers. A comprehensive fuel reliability improvement program has been undertaken by Westinghouse and ENUSA to develop and implement manufacturing improvements to mitigate potential leakage mechanisms. Improved materials have been introduced over the years to reduce cladding corrosion and provide good dimensional stability with long cycles and high burnup.

1. Introduction

Westinghouse and ENUSA supply fuel to more than 80 PWR plants worldwide. These plants comprise a number of different reactor types, including Westinghouse-style 14x14, 15x15, and 17x17 designs, Combustion Engineering 16x16 design, and the VVER design. Design improvements have been implemented over the years to enhance reliability and eliminate fuel leakage mechanisms and other fuel related issues such as bowing, handling damage, and control rod insert-ability. In particular, there has been a focus on design enhancements to provide additional margin and resistance to Grid-to-Rod-Fretting (GTRF) in fuel products that have been challenged by high duty operating conditions in the core. Today, GTRF has been significantly reduced or eliminated as a leakage mechanism in Westinghouse fuel using the modern fuel upgraded designs. The main leakage mechanisms observed today have been due to debris and then manufacturing-related causes. For debris related leakers, debris resistance enhancements, such as debris filter bottom nozzles, protective grids and oxide coated cladding have been or are being implemented to significantly reduce the probability of debris related leakers. A comprehensive fuel reliability improvement program, focused on continuous improvement, has been undertaken by Westinghouse and ENUSA to develop and implement design and manufacturing improvements to mitigate potential leakage mechanisms.

2. Robust Fuel Designs

The fuel designs used today include features to improve fuel reliability, enhance margins, and reduce fuel costs. A summary of the basic features of the various designs is shown in Table 1. For the Westinghouse 17x17 fuel type, two main designs designated Robust Fuel Assembly (RFA) or Optimized Fuel Assembly (OFA) are used. The RFA design (ref. 1) was introduced in 1997 and uses a fuel rod diameter of 9.50 mm (0.374 inch) and the RFA-2 mid-grid and operates in 52 plants worldwide. The OFA 17x17 design was introduced in the 1980s and uses a fuel rod diameter of 9.14 mm (0.360 inch) and the OFA mid-grid. The RFA design is used in the USA and Europe, while the OFA design is used at 16 plants in the USA and 1 in Asia. Three Intermediate Flow Mixer (IFM) grids are used in OFA design and in some of the RFA designs. The 15x15 Upgrade product used in 8 plants has a 10.7 mm (0.422 inch) fuel rod diameter with the 15 Upgrade mid-grid and IFMs. The 14x14 422V+ product also uses the 10.7 mm (0.422 inch) fuel rod diameter and operates in 6 plants. The Next Generation Fuel (NGF) design for Combustion Engineering (CE) 16x16 plants uses a rod diameter of 9.50 mm and the NGF mid-grid. The Westinghouse VVER hexagonal design operates in 2 1000 MWe VVER plants in Ukraine.

Fuel Type	W 17x17		W 15x15 Upgrade	W 14x14 422V+	CE 16x16 NGF	VVER
	RFA	OFA				
No. of Plants	52	17	8	6	2	2
Fuel Rod Diameter (mm)	9.50	9.14	10.7	10.7	9.50	9.14
Mid-grid Design	RFA-2	OFA	Upgrade	V+	NGF	VVER
IFMs	Optional	Yes	Yes	No	Yes	No
Top Nozzle	Removable					
Cladding Material	ZIRLO® or Optimized ZIRLO™				Optimized ZIRLO™	ZIRLO®
Debris Protection	DFBN, P-grid, Oxide Coating (US)			DFBN, Oxide Coating	Guardian	No

Table 1. Summary of Westinghouse and ENUSA Fuel Design Types.

ZIRLO® materials are typically used for the cladding and structures (grids and guide tubes) for enhanced corrosion resistance and excellent dimensional stability. Optimized ZIRLO™ cladding (ref. 2) is being introduced in reloads and its use will increase significantly in the future. Optimized ZIRLO™ cladding provides about a 30% reduction in corrosion compared to ZIRLO® cladding and adds margin in fuel rod design for the higher thermal-hydraulic and RCS chemistry duty and longer cycle operation.

Some differences exist among the various designs in the debris protection features. Most of the Westinghouse-type designs have Defense-in-Depth Debris Protection using a multi-layer debris protection as illustrated in Figure 1. The Debris Filter Bottom Nozzle (DFBN) has small holes sizes and is designed to mitigate debris-induced fuel rod fretting failures by preventing debris from entering the assembly. The Protective Grid (P-Grid) is located directly above the bottom nozzle and traps any debris that passes though the DFBN against the elongated solid-fuel-rod-bottom end plug, avoiding penetration of the clad. In US fuel designs, a thin oxide coating is applied over the bottom six inches of each fuel rod to increase the surface hardness, thus increasing wear resistance over uncoated cladding. The 17x17 and 15x15 designs operating in the US use all three levels of debris protection. Fuel designs operating in Europe use the DFBN and P-grid. To increase the level of debris protection, Westinghouse and ENUSA expect to use oxide coating for fuel designs in Europe in the near future.

The CE 16x16 NGF design uses the Guardian Grid to provide debris protection. This design, illustrated in Figure 2, uses a special grid at the bottom of the assembly along with a long end plug to trap debris and prevent it from entering the assembly.

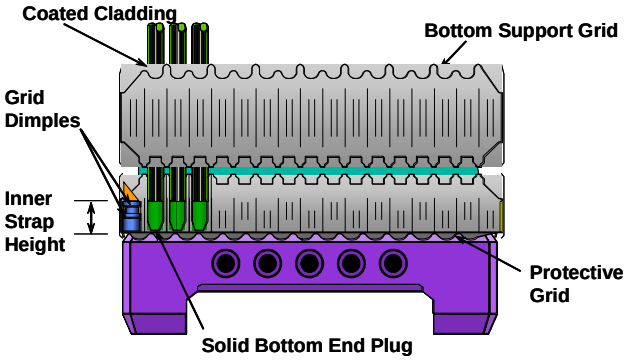

Figure 1. Multiple Levels of Debris Protection on the Westinghouse-type Fuel Designs

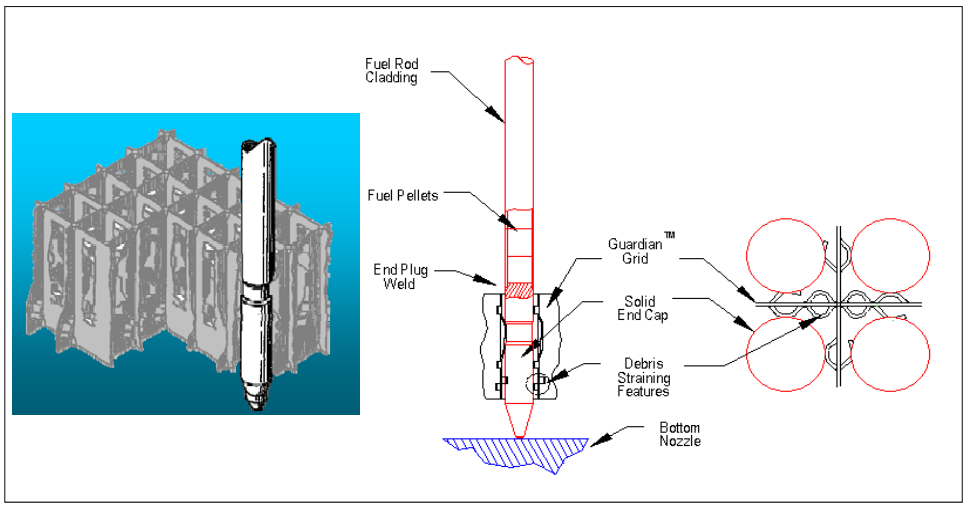

Figure 2. Guardian Grid used in the CE 16x16 NGF Design.

3. Fuel Performance with Improved Fuel Designs

The improved fuel designs summarized in Section 2 above have achieved high levels of fuel reliability as older designs are phased out and eliminated from use. GTRF has been substantially reduced or eliminated for some products as a leakage mechanism. Leaking fuel due to debris has been significantly reduced in recent years. Post irradiation examinations of discharged "healthy fuels" completed in accordance with the EPRI Fuel Surveillance Guideline have confirmed the robust designs have ample margin to known fuel rod leaking mechanisms (Ref 4, 5).

3.1 Grid-to-Rod-Fretting

Some older fuel designs have experienced leaking fuel due to GTRF especially at the mid-grids. The grid designs used in the "modern" robust fuel products have been designed to increase margin to GTRF. For example, the RFA 17x17 and 15x15 Upgrade fuel designs with the P-grid has demonstrated excellent GTRF performance (ref. 3).

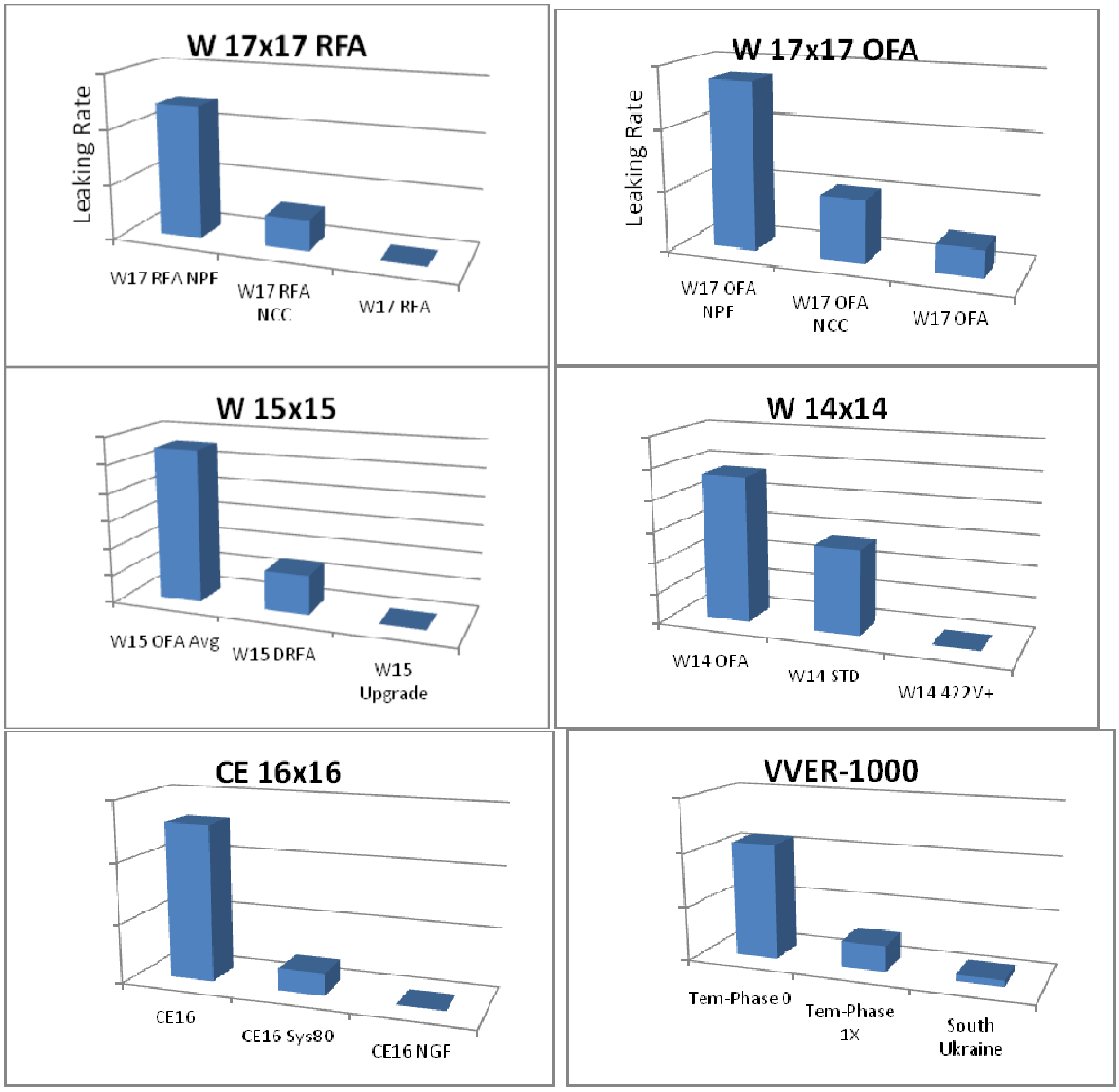

Figure 3. Effect of Robust Designs Implementation in Leaking Rates.

3.2 Debris

As grid-to rod-fretting is being essentially eliminated with the modern Westinghouse robust designs and other leaking mechanisms such as cladding corrosion, particularly crud induced localized corrosion are being addressed by advanced cladding alloys and better coolant chemistry control, debris in the coolant will become the most prevalent fuel leaking mechanism in the near future. Very significant strides are being made by nuclear plant operators to prevent ingress of foreign material in the primary system. Westinghouse continues to improve in the implementation of rigorous foreign material exclusion practices in all its fuel manufacturing sites, as does ENUSA at the fuel manufacturing plant in Juzbado.

For Westinghouse USA plants, the combination of debris filter bottom nozzle, protective grid and coated cladding is the most effective barrier to protect fuel assemblies from harmful debris that could compromise cladding integrity. In Combustion Engineering plants, the use of the Guardian Grid in combination with longer lower end plugs has also proven to be extremely effective.

4. Fuel Performance Improvement Programs

The demonstrated significant improvement in Westinghouse fuel reliability is the consequence of a concerted effort to improve the fuel design and manufacturing process as well as improved monitoring of in reactor performance by a significant increase in the number of pro-active Post Irradiation Examinations (PIEs). The current fuel designs, under the current plant operating conditions, have demonstrated an unsurpassed reliability from a historical perspective. However it is known that the drive to improve fuel utilization will unavoidably require continuous evolutionary design and manufacturing changes. Plant operating conditions, water chemistry, etc. will also change to improve the performance of other plant components and decrease worker dose. These types of changes have been known in the past to challenge fuel reliability in unexpected ways. In order to better understand the potential challenges to fuel reliability and to identify areas for improvement, Westinghouse has implemented a formal process to continuously monitor fuel manufacturing and in reactor performance and to provide feedback to upper management regarding where investments should be considered in order to insure the reliability of the fuel will continue to be excellent in the years to come. Regarding in reactor fuel performance, the process recommended by EPRI in the Fuel Surveillance Guideline is expected to continue to provide very valuable PIE data. A Fuel Performance Team (FPT), with senior fuel designers, material, fuel performance and manufacturing experts is responsible for monitoring the Critical Fuel Reliability Parameters and periodically review manufacturing data and evaluates manufacturing process capability. The FPT also reviews PIE data from baseline inspections (Ref. 4) and the results of root cause analysis of leaking fuel. These reviews may identify existing or emerging issues with the potential for challenging fuel reliability. These findings, along with investment recommendations are presented to the Fuel Reliability Improvement Steering Committee (FRISC) which in turn provides funding and managerial sponsorship and support to the approved projects. This successful process is being extended to the European plants fueled by Westinghouse and ENUSA.

5. Conclusion

Westinghouse and ENUSA have implemented improved, robust fuel designs in recent years for all product lines to improve fuel reliability and provide increased operating margins. GTRF has been greatly reduced or eliminated compared to some prior fuel designs and enhancements in debris resistance have reduced leakage due to debris. Fuel reliability improvement programs have been established to implement design and manufacturing improvements to mitigate potential leakage mechanisms.

6. References

1. P. Loftus and D. Chapin, “17x17 Robust Fuel Assembly: A Decade of Excellent Fuel Reliability and Competitive Fuel Cycle Economics”, 2008 Water Reactor Fuel Performance Meeting, October 2008

2. D. Mitchell, A. Garde, D. Davis, “Optimized ZIRLO Fuel Performance in Westinghouse PWRs”, Proceedings of 2010 LWR Fuel Performance/TopFuel/WRFPM, Orlando Florida, September 2010.

3. M. Aullo, R. Canencia, D. Chapin, R. Lu, W. Rabenstein, “Fretting Performance of the RFA Fuel”, Top Fuel 2009 International Meeting on LWR Fuel Performance, September 2009

4. A. Repáraz, J. L. Bradfute, M. Y. Young, “Baseline Fuel Inspections of Westinghouse Fuel Products”. Proceedings of 2010 LWR Fuel Performance/TopFuel/WRFPM Orlando, Florida, September, 2010.

5. C. Muñoz-Reja et al. “PWR Fuel Surveillance Experience in Spain: a decade of Fuel Examinations”. Proceedings of 2010 LWR Fuel Performance/TopFuel/WRFPM Orlando, Florida, September, 2010

European Nuclear Society
Rue Belliard 65
1040 Brussels, Belgium
Telephone: +32 2 505 30 50 - FAX: +32 2 502 39 02
topfuel2012@euronuclear.org
www.topfuel2012.org